MA/4

REGULATORY INFORMATION DISTRIBUTION SYSTEM (RIDS)

ACCESSION NBR:8006[illegible]102[illegible]2 DOC.DATE: 80/06/09 NOTARIZED: NO DOCKET #
FACIL:50-387 Susquehanna Steam Electric Station, Unit 1, Pennsylva 05000387
50-388 Susquehanna Steam Electric Station, Unit 2, Pennsylva 05000388

AUTH.NAME AUTHOR AFFILIATION
CURTIS,N.W. Pennsylvania Power & Light Co.
RECIP.NAME RECIPIENT AFFILIATION
YOUNGBLOOD,B.J. Licensing Branch 1

SUBJECT: Forwards "Design Assessment Rept,Revision 2," Proprietary version withheld (ref 10CFR2.790).

DISTRIBUTION CODE: P801S COPIES RECEIVED:LTR 1 ENCL 40 SIZE: 2+205
TITLE: Proprietary Info Re PSAR/FSAR

NOTES: SEND I&E 3 CYS FSAR + ALL AMDTS

	RECIPIENT ID CODE/NAME	COPIES LTTR	COPIES ENCL	RECIPIENT ID CODE/NAME	COPIES LTTR	COPIES ENCL	
ACTION:	02 PM MINER	1	1 #3	AD ADILWR	1	0	
	BC LWR#3	1	0	LA LWR#3	1	0	
INTERNAL:	01 REG FILE #1	1	1	03 OPERA LIC BR	1	1	#12
	04 QAB #2	1	1	05 MECH ENG BR	1	1	#13
	06 STRUC ENG BR #4	1	1	07 MATL ENG BR	2	2	#14-15
	09 REAC SYS BR #5	1	1	10 ANL BR	1	1	#16
	11 CORE PERF BR #6	1	1	12 AUX SYS BR	1	1	#17
	13 CONTMNT SYS #7	1	1	14 I&C SYS BR	1	1	#18
	15 PWR SYS BR #8	1	1	16 AD SITE TECH	2	2	#19-20
	18 ACDENT ANL #9	1	1	19 EFLT TRT SYS	1	1	#21
	20 RAD ASMT BR #10	1	1	21 I&E	2	2	#22-23
	23 KIRKWOOD #11	1	1	AD FOR ENG	1	0	
	AD PLANT SYS	1	0	AD SITE ANLYS	1	0	
	AD/CORE & CONT	1	0	DIRECTOR NRR	1	0	
	MPA	1	0	NRC PDR	1	0	
	OELD	1	0				
EXTERNAL:	24 ACRS #24-38	~~16~~	~~16~~ 15	LPDR	1	0	
	LWR#3 LA W/AFF	1	0	NSIC	1	0	

Change : L E
NRC PDR 1 NP Advanced
LPDR 1 NP (L+R)
NSIC 1 NP (L+R)

JUN 13 1980

[redacted]

TOTAL NUMBER OF COPIES REQUIRED: LTTR ~~55~~ 60 ENCL ~~39~~ 42

PP&L

TWO NORTH NINTH STREET, ALLENTOWN, PA. 18101 PHONE: (215) 821-5151

June 9, 1980

Mr. B. J. Youngblood, Chief
Light Water Reactors Branch No. 3
Division of Project Management
U.S. Nuclear Regulatory Commission
Washington, D.C. 20555

SSES DOCKET NOS. 50-387, 50-388
DESIGN ASSESSMENT REPORT, REVISION 2
ER 100450 FILES 172-1, 840-2
PLA-491

Dear Mr. Youngblood:

Transmitted herewith are 40 copies of Revision 2 to the Susquehanna SES Design Assessment Report. Both Volume 1 and the Proprietary Supplement have been revised. Listed below are the major modifications.

1. Revision of Section 4.2, "LOCA Load Definition", to reflect the changes in load methodology required to comply with the October, 1978 NUREG-0487, as well as the addition of Subsection 4.2.3, "Response to NRC Criteria for Loads on Submerged Structure".

2. Update of Section 7.0, "Design Assessment".

3. Preparation of a non-proprietary and proprietary Section 9.0," SSES LOCA Steam Condensation Verification Test GKM-IIM".

4. Completion of Appendix A, "Containment Design Assessment", and Appendix E, "Reactor Building Structural Design Assessment".

5. Update of Appendix D, "Program Verification", to include verification of the KWU computer code VELPOT.

6. Rewrite of Subsection 8.5.4, "Thermal Performance of Quenchers".

B001
1/40
CHANGE: L E
NRC PDR 1 NP
LPDR 1 NP
NSIC 1 NP

8006110222

In addition, a number of editorial and syntactical sentence modifications have been included.

Pursuant to 10 CFR 2.790 and the affidavit submitted with our April 14, 1978 letter (PLA-244), we request that those pages marked proprietary be withheld from public disclosure.

Very truly yours,

N. W. Curtis
Vice President-Engineering & Construction

PAF:JLI

PAF128:3

DOCKET NO. 50-387/388

DATE: 6-13-80

NOTE TO NRC AND/OR LOCAL PUBLIC DOCUMENT ROOMS

The following item submitted with letter dated 6-9-80 from P P+L is being withheld from public disclosure in accordance with Section 2.790.

PROPRIETARY INFORMATION

Rev. #2 TO SES Design Rpt.

Don Laudan

Distribution Service's Branch

UNITED STATES
NUCLEAR REGULATORY COMMISSION
WASHINGTON, D. C. 20555

MEMORANDUM FOR: TERA Corp.

FROM: US NRC/TIDC/Distribution Services Branch

SUBJECT: Special Document Handling Requirements

☐ 1. Please use the following special distribution list for the attached document.

☐ 2. The attached document requires the following special considerations:

☐ Do not send oversize enclosure to the NRC PDR.

☐ Only one oversize enclosure was received - please return for Regulatory File storage.

☑ Proprietary information - send LTR NP ~~affidavit~~ only to the NRC PDR

☐ Other: (specify)

Mike

TIDC/DSB Authorized Signature

cc: DSB Files

EXHIBIT "A"

SECTION 4

TABLES

8006110222

EXHIBIT "A"

4.0 LOAD DEFINITION

4.1 SAFETY RELIEF VALVE (SRV) DISCHARGE LOAD DEFINITION

This section provides a general discussion of the approach used for design of the SSES Safety Relief Valve system (Subsection 4.1.1) as well as the methods used to calculate suppression pool boundary and submerged structure loads. For clarity the loading conditions have been divided into two categories:

a. SRV discharge hydrodynamic loads exerted on the SRV system (pipe, quencher, and support) itself (Subsection 4.1.2)

b. SRV discharge loads on the suppression pool boundary and submerged structures (Subsection 4.1.3).

4.1.1 General Discussion of the SSES Approach

The SRV system used for SSES has been designed based on the following criteria:

a. Reduction to the maximum extent practicable of the wetwell water space dynamic pressures associated with SRV discharge

b. Avoidance of condensation instabilities associated with high mass flux SRV steam discharges in hot (up to 200°F) suppression pools.

To satisfy these criteria, quenchers have been developed specifically for the Pennsylvania Power and Light Company (PP&L) by Kraftwerk Union (KWU). A SSES-unique dynamic load specification has been prepared by KWU for this device and is described in Subsections 4.1.2 and 4.1.3. During an extensive quencher development program (Ref 1), KWU has determined the degree of influence of various SRV system design parameters on the dynamic pressures which result from SRV discharge and has concluded the following:

a. Pool pressure amplitudes decrease with decreasing pool temperature. This is a consequence of the relationship between bubble steam content and saturation conditions.

b. Pool pressure amplitudes decrease with increasing pool free water area. The effect of eccentric SRV discharge locations on pool pressure amplitudes is negligible.

EXHIBIT "A"

c. Pool pressure amplitudes decrease with decreasing quencher exhaust area. For decreasing exhaust areas, the energy input to the oscillating bubble-water system is spread over a longer time, with a corresponding decrease in excitation of the oscillating system.

d. The influence of SRV discharge line length over the range measured by KWU, 9 to 19m (29.5 to 62.3 ft), is insignificant for a constant discharge line air mass. (When two sets of units (English and Metric) are given, the first value is the original one; the second is an approximation provided for convenience.) Detailed information concerning effects due to long discharge lines with numerous bends will be obtained during the Susquehanna unit cell tests described in Chapter 8.

e. Pool pressure amplitudes decrease with decreasing expelled air mass, ie, total energy input to the system decreases with decreasing air volume. However, the air volume in the pipe should not be considered as an absolute quantity of influence, but rather as a relative effect, highly dependent upon the mass of water over which the input energy is distributed and the rate at which energy is added to the system.

f. The following parameters affect pool pressures because of their influence on SRV discharge line clearing pressures, but are less important than those mentioned above: valve opening time, steam mass flux, SRV discharge line temperature, and submergence.

A more complete listing of major and some localized parameters is contained in Table 4-1.

The effects of differences in physical parameters between SSES and KWU BWRs have been accounted for in the quencher design shown on Figure 4-1 and in Table 4-2. To correct primarily for the reduced steam mass flux per SRV and increased line air volumes, the SSES quenchers have been designed with an outlet area approximately 50 percent of that which has been used for German BWRs. This assures that optimum use has been made of the discharge area effect on pressure amplitude reduction. Further decreases in outlet area are not feasible due to the adverse effect on SRV backpressures and SRV discharge line design pressures.

The effect of SRV discharge line length (the longest SSES SRV discharge line is about twice as long as the longest line previously tested by KWU) on pressure amplitude will be studied during the SSES unique testing program, as will the SSES curved

EXHIBIT "A"

pipe arrangement with respect to inhibiting steam-air mixing prior to and during vent clearing.

4.1.1.1 Thermal Performance

One of the keys to the KWU quencher device is its ability to condense stably (without large pressure amplitudes) the steam fraction in exhaust steam-air mixtures as well as pure steam discharges. The most restrictive conditions, which involve high steam mass fluxes and elevated pool temperatures, are of primary importance. Discharge hole patterns are arranged to enable an influx of pool water between adjacent rows under all operating conditions. This arrangement ensures that immediate contact is established between the cooler pool water and the warmer gas discharged.

The optimum quencher hole pattern verified during the GKM quencher development program is used for the SSES design (Figure 4-1 and Table 4-2). The 10 mm discharge holes are spaced 15 mm on centers and are arranged in rows which are separated by 50 mm. The 50 mm center-to-center spacing provides the pathway for supplying water to the steam (see Figure 4-2), thereby enabling the pool to be heated almost to the boiling point without a rise in the pressure amplitudes associated with SRV discharge. Verification of quencher thermal performance may be found in Ref 2 (on Figure 5.13 and page 5-34).

4.1.2 Loads on the SRV System due to SRV Actuation

The loading conditions which are described in the following subsections apply to the SRV piping, quencher body and arms, and quencher support.

4.1.2.1 SRV Line Backpressure Load

The maximum SRV backpressure during steady state blowdown was investigated analytically for the quencher discharge device. The longest line geometry was used in the analysis. It was determined that the maximum SRV discharge line internal pressure is less than 550 psig.

4.1.2.2 SRV System Water Clearing Pressure Load

This subsection summarizes the analytical techniques employed to calculate internal pressures and vertical loads acting on the SRV discharge piping as a result of water slug clearing.

Safety relief valve steam flow was assumed saturated for all calculations. The KWU computer code HOGEM was used to compute the pressure rise in an SRV discharge line throughout the water clearing phase which follows the lifting of an SRV. The code,

EXHIBIT "A"

documented in Ref 1, has been verified with subscale (model) and in-plant test data.

The SSES unique parameters listed in Table 4-3 have been used as input data to the HOGEM computer program.

The flow resistance coefficient for quenchers which had been optimized to parameters unique to KWU-designed plants was found to be = 1.5. When calculating the SSES-unique flow resistance coefficients, particular consideration was given to the SSES-unique quencher. Due to different parameters (compared to KWU plants), approximately one-half the discharge area of earlier KWU designs was required.

Using an area reduction factor of 0.6, the effective discharge area of the Susquehanna quencher is calculated as:

$$Aeff_q = 0.6 \quad Ageom = 0.522 \ m^2 \quad (5.617 \ ft^2)$$

Since the cross-sectional area of an SRV discharge line is:

$$A_D = 0.073 \ m^2$$

the area ratio becomes:

$$\frac{Aeff_q}{A_D} = 0.72$$

The HOGEM code relates the quencher flow resistance coefficient, ξ, to the square of the flow velocity inside the SRV discharge line, necessitating the calculation of a velocity ratio between the quencher discharge and the pipe flow velocities.

$$\frac{W_q}{W_D} = \frac{A_D}{Aeff_q} = \frac{1}{0.72} = 1.39$$

where:

W = flow velocity

For quenchers typical of those used in KWU designed plants, this ratio is equal to one.

As a significant portion of the pressure reduction mechanism is related to the quencher discharge area, an appropriate resistance

EXHIBIT "A"

coefficient was used for the Susquehanna quencher, based on a value which had been previously verified for KWU plants. Consistent with the HOGEM code methodology, the SSES-unique value was calculated by multiplying the KWU value by the square of the SSES velocity ratio.

$$\frac{W^2_q}{W^2_D} = (1.39)^2 = 1.93 \text{ or approximately } 2.$$

Hence, the Susquehanna quencher flow resistance coefficient is:

$$\xi SSES = 2 \times 1.5 = 3. \quad \text{where } 1.5 = \xi \text{ for KWV plants.}$$

The following clearing pressures were calculated for the longest and the shortest SRV discharge lines, respectively, based on the KWU HOGEM analysis:

Length of discharge line	Calculated clearing pressure
48.3 m (158.5 ft)	22.7 bar (314.5 psig)
34.9 m (114.5 ft)	27.1 bar (378.3 psig)

The clearing pressure time histories are shown on Figure 4-3. Subsequent to water clearing, the internal pressure changes to the steady state steam flow condition.

For calculating the vertical load imposed on the quencher due to the directional change in flow velocity within the quencher (vertical SRV discharge line to horizontal quencher arms), a conservative resistance coefficient, $\xi = 0$, was used (rather than the value $\xi = 3.0$ described in the paragraphs above).

The following vertical loads acting on an SRV discharge line result from a change in direction of the water leg during water clearing:

Length of the SRV discharge line	Vertical load
48.3 m	490 kN (110.2 kips)
34.9 m	620 kN (139.4 kips)

The time histories of these vertical loads (with = 0) are shown on Figure 4-4.

EXHIBIT "A"

4.1.2.3 SRV Discharge Line Loads

During water slug clearing, the different pipe runs of the SRV line are subjected to dynamic loads due to flow changes within the pipe (pressure and momentum changes). The piping analysis contained in Section 5.5 includes these loads. Figure 4-5 represents the vertical load on the last pipe run (ending with the quencher). Tables 4-4, 4-5 and 4-6 list the maximum loads experienced by an SRV discharge line during SRV opening, SRV closing and irregular condensation, respectively.

4.1.2.4 Quencher Body Loads

Oscillating bubbles from SRV discharge into the suppression pool produce external loads on the quenchers. An operating quencher is affected by bubbles caused by its own discharge as well as by bubbles from adjacent quenchers. It has been shown experimentally (Ref 23) that the maximum external loading condition on an individual quencher occurs during operation of the quencher itself. The operation of one or more adjacent quenchers does not produce increased loads. External loads on quenchers which are not operating are evaluated using loading conditions described in Subsection 4.1.3 according to their location in the pool.

The loads acting on the quencher body are shown on Figure 4-6. Tables 4-7, 4-8 and 4-9 list the maximum loads experienced by an SSES quencher during SRV opening, SRV closing and irregular condensation, respectively. The load time histories are referenced in the same tables. Seven thousand valve openings, seven thousand valve closings and one million irregular condensation load cycles have been assumed.

4.1.2.5 Quencher Arm Loads

The loads acting on each quencher arm are shown on Figure 4-14.

Tables 4-10, 4-11 and 4-12 list the maximum loads experienced by an SSES quencher arm during SRV opening, SRV closing and irregular condensation, respectively. The load time histories are referenced in the same tables. Seven thousand valve openings, seven thousand valve closings and one million irregular condensation load cycles have been assumed.

4.1.2.6 Quencher Support Loads

The quencher supports have been designed for the following loads:

a. Loads acting on the quencher due to SRV discharge as discussed in Subsections 4.1.2.4 and 4.1.2.5.

EXHIBIT "A"

b. Loads from the SRV discharge line

c. Loads from flow deflection within the discharge line

d. Loads due to oscillating discharge bubbles

4.1.2.7 Quencher Fatigue Loads

Although each clearing event is followed by nearly continuous steam flow, steam condensation does not exhibit a uniform behavior throughout the entire range of steam mass flow rates and wetwell water temperatures. The various regions of condensation behavior are shown on Figure 4-22. The quencher experiences maximum hydrodynamic and thermal fatigue loads during discontinuous flow or irregular condensation (transition region, Figure 4-22). The irregular condensation loads from Table 4-9 are used for fatigue considerations. One million total stress cycles (associated with the irregular condensation are assumed for the analysis.

4.1.3 Loads on Suppression Pool Structures due to SRV Actuation

This subsection describes loads on wetted portions of the suppression pool boundary and submerged structures. Subsections 4.1.3.1 through 4.1.3.3 give the circumferential pressure distributions on the suppression pool boundaries for the various SRV actuation cases.The vertical pressure distribution on the boundaries is discussed in Subsection 4.1.3.4. Subsection 4.1.3.5 gives the pressure time histories used for the analysis.

4.1.3.1 Symmetric Loading Condition (SRV All)

The assumption that all gas bubbles arising from SRV discharge oscillate in phase with the same strength (highest possible) leads to the worst loading case as described for the normalized condition on Figure 4-23. For the entire region (basemat, containment wetted wall, and pedestal wetted wall), the most restrictive pressure time histories as described in Subsection 4.1.3.5 have been used for the analysis to ensure conservatism. In the lower region the amplitude multiplier has been chosen to be consistent with the analysis presented in Subsection 4.1.3.5, while in the upper region the same multiplier decreases linearly to zero at the water surface shown on Figure 4-24.

4.1.3.2 Asymmetric Loading Condition

The most restrictive asymmetrical loading condition occurs when a group of adjacent valves is operating. The analysis was made for the case in which three adjacent valves are operating. The normalized pressure distribution is shown on Figure 4-25.

EXHIBIT "A"

The pressure distribution was defined circumferentially for a 180° segment.On both sides of a 90° range with a constant pressure level, the pressure decreases linearly to zero over 45°. On the other 180° segment of the pool, the pressures were assumed to be zero. The vertical pressure distribution was assumed to be the same as for the symmetrical case. The multiplier described in Subsection 4.1.3.1 is also applied to this case.

4.1.3.2.1 Single Valve Actuation Loading Condition

Asymmetric loading also occurs when a single valve actuates. The normalized pressure distribution for this case is shown on Figure 4-26. The pressure level in the circumferential direction remains constant over a range of 30° and, on both sides of this range, decreases linearly over 47.5° to 20 percent of the maximum value. Outside of this region, the pressure equals 20 percent of the maximum pressure valve. For comparison, a pressure decrease related to the law 1/R is shown on the same figure. The pressure distribution in the radial direction is also included in Figure 4-26.

4.1.3.3 Automatic Depressurization System (ADS) Loading Condition

Assuming that the six ADS valves (for location, see Figure 1-4) are acting in phase, there is no great difference between the symmetric and the ADS loading conditions. Figure 4-27 depicts the normalized pressure distribution used for this case.

4.1.3.4 Vertical Pressure Distribution

Once the gas bubbles have been expelled from a quencher, they coalesce and the resulting bubble agglomeration rises due to buoyancy effects while oscillating. Because of the free surface presence, pressures on containment and pedestal walls near the water surfaces are lower than the pressures on the basemat. For such configurations the observed vertical velocity component is in the order of 2 m/sec. However, the bubble oscillation is nearly damped out after approximately 1 second as can be seen on Figures 4-28 to 4-30. Therefore, the assumed pressure decrease with elevation as shown on FIgure 4-24 is conservative.

4.1.3.5 Pressure Time Histories

The definition of SRV loads on suppression pool wetted boundaries and submerged internals can be limited to loads resulting from gas bubble oscillation following vent clearing, as these loads have been shown to be bounding when compared to those associated with the other phases of SRV discharge (Ref 3). This section contains a discussion of individual pressure time histories as well as spatial effects.

EXHIBIT "A"

Immediately following the lifting of an SRV, a mixture of steam and air is discharged into the suppression pool. The pressure time histories experienced by the suppression pool wetted boundaries and submerged structures differ with respect to amplitude frequency and damping for each actuation event (Ref 21).

To obtain a bounding loading condition for SSES containment analysis, conservatism with respect to frequency, damping, and pressure amplitude is required. The resulting loads are applied to the containment in accordance with the spatial pressure distributions described in Subsections 4.1.3.1 through 4.1.3.4.

In order to obtain a valid frequency spread, measured traces from previous KWU full scale testing programs were selected and analyzed. Approximately 200 runs from various Kraftwerk Union BWR power plants were available. From these, three traces were chosen from the Brunsbuttel non-nuclear hot functional testing program for use in SSES design verification (for conservatism, subsequent actuation cases have been used). The three traces are shown in Figures 4-28, 4-29, and 4-30 and the test conditions are described in Reference 21. Major parameters are listed in Table 4-13.

During the Brunsbuttel testing program, all pressures were measured at a11 wall position adjacent to the operating quencher. Distance to the nearest actuating quencher arm was approximately 1 m (3.28 ft). <u>The measured pressure traces are therefore expected to include all water clearing (water jet) and air bubble oscillation effects</u>.

The traces used were selected not only for their frequency variation but also for their relatively large pressure amplitudes of 0.5 to 0.8 bar (7.25 to 11.6 psia). Figure 4-28 contains the highest pressure amplitude ever measured during in-plant testing following the water slug clearing phase of a KWU quencher equipped safety relief system. While the oscillation shown in Figure 4-28 is damped out rapidly, the other two traces exhibit less damping. A comparison between Figures 4-29 and 4-30 indicates that peak pressure amplitudes can be experienced at different times.

Figures 4-31 to 4-33 contain power spectral density functions for the initial 0.6 sec. of the measured pressure traces. For purposes of comparison it should be mentioned that the traces contain variations in ordinate scaling. In all cases an air bubble oscillation frequency between 6 and 8 cps is dominant. Althoug the pressure amplitude of run #35 has the highest magnitude (refer to Figure 4-28), the magnitude of the power spectral density of the dominant bubble frequency is small (Figure 4-31) when compared to the two other cases (Figures 4-32

EXHIBIT "A"

and 4-33). When the rapid damping of the oscillation as shown in Figure 4-28 is taken into account, a unique bubble oscillation can be presumed to have occurred.

In addition to the most important first 0.6 seconds of each trace, Figures 4-34 to 4-36 show the power spectral density functions during longer periods of the same traces. The bubble frequency remains the dominant frequency even though the pressure amplitudes are in practice damped out before the analyzer trace ends. This prevailing frequency shows that the traces do not contain geometrical effects such as eigenfrequencies of the structure. Therefore, the pressure time histories are used as pure forcing functions. It should be added that the pressure transducers used were fastened to a stiff sandwich wall structure to minimize interaction effects.

In order to obtain a conservative frequency content, the variation in air mass between the Susquehanna SRV discharge lines and those used for Brunsbuttel were taken into consideration. The longest SSES discharge line has a conservatively estimated enclosed air volume of 3.1 m^3 (109.5 ft^3) (refer to Table 1-3) while the Brunsbuttel discharge lines have an enclosed air volume of 1.45 m^3 (51.2 ft^3) (refer to Ref 2). The ratio of these volumes is 2.14 to 1.

Assuming a spherical air bubble, the air bubble frequency is inversely proportional to the cube root of the air volume ratio as can be seen in Ref 4. If a flat bubble with a constant cross sectional area is assumed, the air bubble frequency will be inversely proportional to the square root of the volume ratio as can be seen in Ref 5. This analysis assumes the real bubble shape to be between these two limites, and the resulting frequency shift to be between the two models' prediction of the air-volume ratio proportionality.

In order to obtain a conservative frequency content, the three traces (Figures 4-28 to 4-30) which were used as normalized forcing functions were expanded in time by a factor 1.8 (an expansion) and reduced in time by a factor 0.9 (a contraction). WIthin a given frequency range one of the three traces affects an individual location in the containment structure more adversely than the others.

The Susquehanna SES quenchers were designed to compensate for the fact that some of the Susquehanna parameters were different from those of the Brunsbuttel plant. To adjust for lower values of steam mass flux per SRV, and for the greater initial enclosed air mass, the exit area of the Susquehanna quencher was reduced to approximately one half of that of existing KWU power plants. Any further reduction in quencher discharge area, regardless of its desirability, is unfeasible due to limitations imposed on SRV

EXHIBIT "A"

discharge line internal prssures as well as SRV backpressures. Based on the experience obtained during the subscale testing phase of KWU's quencher development program (refer to Ref 1), it is unlikely the maximum SSES pressure amplitudes will ever exceed a normalized value of 1.5 when applied to the Brunsbuttel pressure amplitudes. Therefore, this evaluation is based on a conservative normalized value of 1.5; this value will be verified during the ~~SSES unique unit~~ cell testing progr... which is explained ~~in~~ Chapter 8, and has been used in co.. junction with pressure-time ~~histories~~. (Figures 4-28 through 4-30) for the suppression ~~pool~~-wall, pedestal, and basemat adequacy assessments.

4.1.3.7 Loads on Submerged Structures due to SRV Actuation

The normalized pressure time histories presented on Figures 4-28, 4-29, and 4-30 (refer to Subsection 4.1.3.5) are also used for the analysis of loads on submerged structures. The vertical pressure distribution of Figure 4-24 is adopted. The loads are calculated using the pressure values and the submerged structure projected area. The computed loads were assumed to be acting in the lateral direction except for the downcomer bracing and the downcomer stiffener ring loads.

The downcomer bracing loads are assumed to be acting in the lateral and vertical directions simultaneously. The lateral load is calculated using the reduced pressure value according to Figure 4-24. The vertical load is calculated using the full pressure value. The downcomer ring plate loads are assumed to be acting in the vertical direction. This vertical load is also calculated using the full pressure value.

Similar to the loads on the suppression pool wetted walls, a multiplier was adopted when applying the normalized pressure time histories to account for differences between SSES and Brunsbuttel quenchers. The value of the multiplier was taken differently depending on the size (diameter) of the submerged structure. Discussions pertaining to the choice of this multiplier are provided below.

For the case of a single spherical oscillating gas bubble, the pressure amplitudes relative to the surrounding water pressure can be calculated by the simple relation:

$$\text{Pressure differential attenuation} = \frac{Ro}{R}$$

where

Ro = bubble radius

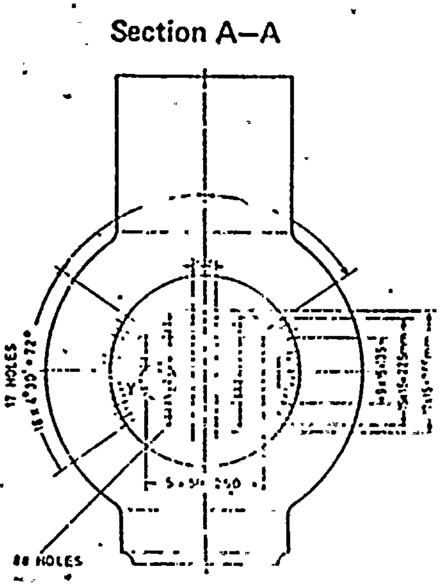

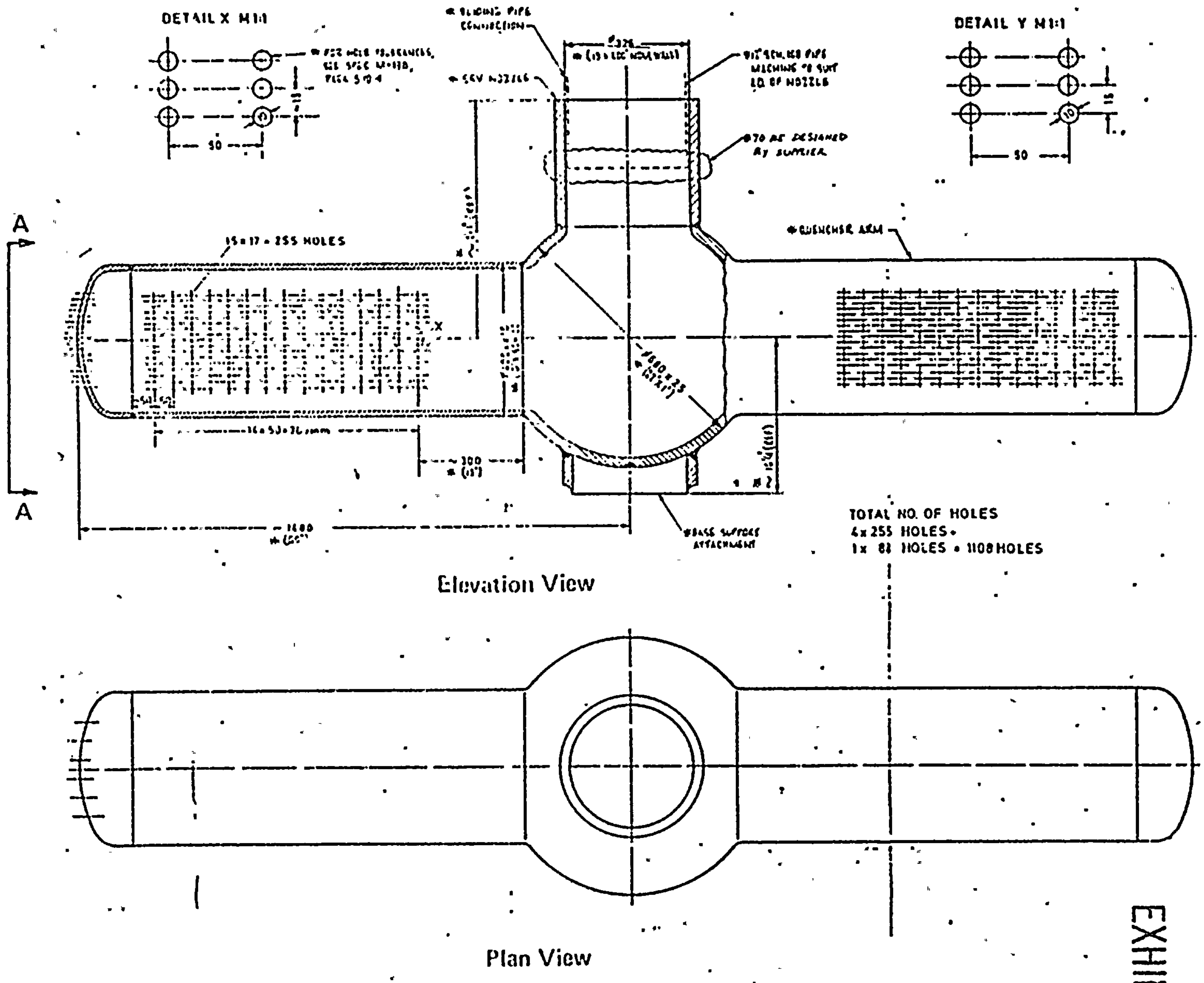

SUSQUEHANNA STEAM ELECTRIC STATION
UNITS 1 AND 2
DESIGN ASSESSMENT REPORT

KWU DESIGNED SSES
UNIQUE QUENCHER

FIGURE 4-1

EXHIBIT "A"

EXHIBIT "A"

TABLE 4-7

TOTAL QUENCHER LOADS DURING SRV OPENING(1)

Load	Maximum Value	Direction	Time History
Internal over pressure	27 bars (377 psig)	-	See Figure 4-7
External load	44 kn(2) (9891 lb)	Simultaneously in the horizontal and vertical quencher planes	See Figure 4-8
Water deflection load inside the quencher	620 kn (139,376 lb)	Vertical	See Figure 4-5
Torque	40 knm (29,501 ft-lb)	In horizontal quencher plane	See Figure 4-9
External load due to bubble oscillation	(See Subsection 4.1.2.4)		

(1) For the case of a sliding joint in the discharge line close to the quencher (Figure 4-10), the pressure inside the pipe acts as an external force. This case is shown in Figure 4.11.

(2) Effects of asymmetric hole arrangement are included.

EXHIBIT "A"

TABLE 4-8

TOTAL QUENCHER LOADS DURING SRV CLOSING

Load	Maximum Value	Direction	Time History
External load	4.5 kn (1012 lb)	Simultaneously in the horizontal and vertical quencher planes	See Figure 4-12
Torque	6 knm (4425 ft-lb)	In horizontal quencher plane	See Figure 4-12

EXHIBIT "A"

TABLE 4-9

TOTAL QUENCHER LOADS DURING IRREGULAR CONDENSATION

Load	Maximum Value	Direction	Time History
External load 3	17.5 kn (3934 lb)	Simultaneously in the horizontal and vertical quencher planes	See Figure 4-13
Torque	19 knm (14,013 ft-lb)	In horizontal quencher plane	See Figure 4-13

EXHIBIT "A"

TABLE 4-11

QUENCHER ARM LOADS DURING SRV CLOSING

Load	Maximum Value	Direction	Time History
Internal over pressure	22 bars (304 psig)	-	See Figure 4-18
External load	4.5 Kn (1012 lb)	Simultaneously in the horizontal and vertical planes	See Figure 4-19
Bending moment on welding seam at intersection between quencher arm and quencher ball	3 Knm (2213 ft-lb)	Simultaneously in the horizontal and vertical planes	See Figure 4-19
Thermal load (Internal temperature)	219°C (426°F)	-	See Figure 4-18

EXHIBIT "A"

TABLE 4-12

QUENCHER ARM LOADS DURING IRREGULAR CONDENSATION

Load	Maximum Value	Direction	Time History
Internal pressure	3.0 bars (28.8 psig)	-	See Figure 4-20
External load	14.5 Kn (6638 ft-lb)	Simultaneously in the horizontal and vertical direction	See Figure 4-21
Bending moment on welding seam at intersection between quencher arm and quencher ball	9 Knm (6638 ft-lb)	Simultaneously in the horizontal and vertical plane	See Figure 4-21
Thermal load (Internal temperature)	133°C (271.4°F)	-	See Figure 4-20

CHAPTER 8
SSES QUENCHER VERIFICATION TEST
TABLE OF CONTENTS

8.2 TEST FACILITY AND INSTRUMENTATION

8.3 TEST PARAMETERS AND MATRIX

8.3.1 Vent Clearing Tests

8.3.2 Condensation Tests

8.4 TEST RESULTS

8.5 DATA ANALYSIS AND VERIFICATION OF LOAD SPECIFICATION

SECTION 8.0

FIGURES

SECTION 8

TABLES

8.0 SSES QUENCHER VERIFICATION TEST

8.1 INTRODUCTION

8.1.1 Purpose of the Tests

The optimized quencher design for SSES and the load specification on the wetted boundaries of the suppression pool, on the submerged structures and on the pressure relief system, are based on parametric model test studies and full scale inplant test results from a similar quencher design. The load specifications for the SSES quencher are described in detail in Section 4.1. In order to verify these load specifications and further verify the quencher's steam condensing characteristics, full scale single cell tests were conducted at the Kraftwerk Union laboratories in Karlstein, West Germany.

8.1.2 Test Concept

The concepts used to design and perform the tests were:

1) Use of a conservatively defined single cell

2) The close simulation of the main safety relief valve system parameters

8.1.2.1 Unit Cell Approach

8.1.2.1.1 Single Cell Theory

For a gas bubble oscillation in a free water space, the water mass coupled to the bubble is alternately accelerated and decelerated. During this process the overpressure and underpressure amplitudes decrease with increasing distance from the bubble. When a solid wall is placed near the oscillating bubble, the water acceleration is restricted in the direction of the wall and the decrease in pressure amplitude in the direction of the wall is less. This effect can be expressed mathematically by replacing the bubble by a potential source and accounting for the wall by the method of images. The effects of the real source and the image source are added for each point of the flow field.

For the case in which a bubble is enclosed in a narrow water space, closely surrounded by solid walls and a solid bottom with a free water surface at the top, the water space below the bubble is for all practical purposes unmoved. Only the water volume above the bubble is free to oscillate. Consequently, the pressure gradient in the lower water space is nearly zero, while the pressure amplitude above the bubble decreases with increasing proximity to the water surface. The pressure amplitudes are zero at the water surface and the method of images applies.

Analytically, the case in which a planar field of uniform strength bubbles are all oscillating in phase is the same as the case in which solid walls exist between each of the individual bubbles. The single cell test configuration used at Karlstein simulates this extremely conservative case of parallel bubbles oscillating in phase with the same source strength. A description of the equivalence of the single cell configurations, using the method of images, is contained in Figures 8.1 and 8.2. For a more detailed evaluation of the Karlstein test tank single cell, see Section 8.5.1.

8.1.2.1.2 Application of Single Cell Approach

The submergence of the quencher in the test tank is equal to the highest value in the plant. As to the water cross-section area the single cell theory described above is used. Figure 8.3 shows a geometrical partition of water space. The water cross-section areas related to the different quenchers are listed below:

	Average Water Surface	Related Water Surface
Quencher A	31.47 m² (338.62 ft²)	21.4 m² (230.26 ft²)
Quencher B	31.47 m²	21.4 m²
Quencher C	31.47 m²	31.3 m² (336.79 ft²)
Quencher D	31.47 m²	42 m² (451.92 ft²)
Quencher E	31.47 m²	31.3 m²
Quencher F	31.47 m²	31.3 m²
Quencher G	31.47 m²	42 m²
Quencher H	31.47 m²	31.3 m²
Quencher J	31.47 m²	31.3 m²
Quencher K	31.47 m²	42 m²
Quencher L	31.47 m²	31.3 m²
Quencher M	31.47 m²	31.3 m²
Quencher N	31.47 m²	21.4 m²
Quencher P	31.47 m²	21.4 m²
Quencher R	31.47 m²	31.3 m²
Quencher S	31.47 m²	42 m²

The smallest water surface (approximately 21.4 m^2) is simulated in the tests. Therefore, the dynamic pressure amplitudes at the walls and the bottom are measured under conservative boundary conditions.

8.1.2.2 Simulation of SSES Parameters

The following section provides a description of those parameters that were simulated in the Karlstein test facility. These parameters are typical of most MK II plants. For more detail on the test facility see Section 8.2

8.1.2.2.1 Primary System Pressure

The reactor operating pressure for SSES is approximately 1000 psig (69 bar) while the highest pressure set point for any SSES Safety Relief valve is 1205 psig (83 bar), which is close to the highest primary pressure that can be simualted in the Karlstein test facility (82 bar). This allowed the test simulation to very closely match the range of initial primary system pressures that can be expected in the operating plant.

8.1.2.2.2 Safety Relief Valve(SRV)

In order to match the characteristics of the Safety Relief Valve, an original Crosby SRV, shipped directly from the plant site, was installed in the test stand and used in all tests.

8.1.2.2.3 Discharge Line

In order to cover the range of discharge line lengths and therefore air volumes that exist in SSES, two vent clearing test series were run; one with a discharge line that simulates the longest SSES discharge line (48 m) and one that simulates the shortest SSES discharge line (35 m). In addition, the number of bends in each line, the inner diameter of the main part of the line (303.9 mm), and the inner diameter of the last vertical run to the quencher (288.9 mm) are closely simulated to that which exists in the SSES plant. (schedule 40 pipe and schedule 80 pipe, respectively). In addition a 24 ft. submergence, corresponding to the highest water level in the suppression pool, was used for all tests.

8.1.2.2.4 Vacuum Breakers

In order to closely simulate the effects of vacuum breaker operation on the tests, two six-inch diameter Crosby vacuum breakers were shipped to Germany and installed in the test stand at the same relative location as planned for the SSES plant.

8.1.2.2.5 Quencher

A full size prototype of the quencher installed in the SSES plant was installed in the test facility and used for all tests. Figure 8.13 shows the quencher with instrumentation for vent clearing tests while figure 8.14 shows the quencher with instrumentation for the condensation tests.

8.2 TEST FACILITY AND INSTRUMENTATION

8.2.1 Test Facility

8.2.1.1 Mechanical Set-up

The test configuration as constructed is typically illustrated diagrammatically in Figure 8.4. The test stand configuration can be divided into:

- the steam boiler,
- the steam accumulator,
- the steam line before the SRV and the buffer tank,
- the SRV,
- the discharge line between the SRV and the water pool with the quencher as pipe termination, and
- the large tank as water pool.

8.2.1.1.1 Steam boiler

The steam boiler is an oil-fired, once-through, forced-flow boiler with an output of approximately 20 MW at a maximum steam pressure of 170 bar (2499 psig) and a maximum steam temperature of 520° C (968° F). The boiler is designed for a closed operating mode in normal operation. A fraction of the boiler's output is recovered from the condensate via the high-pressure cooler. When there is an open loop (i.e., lost condensate), the output is reduced. The steam flow available in this mode is approximately 8 to 9 kg/s (17.6 to 19.8 lbm/s). The lost condensate results in a time limitation on continuous output. The feedwater supply of the boiler is about 20 m^3 (705 ft^3). Once that amount is used up, further steam supply as continuous output is possible only up to the output of the feedwater conditioning system. That amounts to 5 m^3/h (176 ft^3/h). For longer test periods it is necessary to interrupt operation for 4 hours in order to refill the feedwater storage tank.

8.2.1.1.2 Steam Accumulator

As described in 8.2.1.1.1 the amounts of steam supplied continuously by the boiler are too small to test an SRV.

To provide a way to test valves at flow rates of up to approximately 22 kg/s (484 lbm/s), a valve test facility was built using the boiler plant and a pressure vessel connected to it. This vessel is charged with a steam/water mixture by the boiler and is used as a steam accumulator. From this steam accumulator, higher steam flow rates can be delivered for a short period of time. The dimensions of the pressure vessel are 1.5 m diameter and 12 m high, which results in an accumulator volume of approximately 22 m^3.

Adapted to the required steam output, the accumulator is filled with saturated water and saturated steam at the specified ratio.

The steam is drawn downward through a standpipe. The high steam flow to be extracted transiently from the accumulator results in a rapid decrease of pressure and temperature. For strength reasons, the temperature difference between the inside and outside of the accumulator vessel must not exceed a certain value. This limits the maximum pressure drop and thus the available test time.

8.2.1.1.3 Steam Line and Buffer Tank

The connection between the steam accumulator and the valve test stand consists of an ND 250 pipe line. This line contains isolating devices for emergency isolation and a measurement section constructed as a Venturi nozzle. The existing equipment provide for a direct horizontal connection of the valve being studied. This corresponds to the design of the SRVs used in German BWR plants and to their arrangement at the end of a tap line coming from the main steam line.

The steam supply line was rebuilt to match the design features of SSES. The previously described pipe line now ends in a T-piece. In order to simulate the SSES main steam line and to keep the steam supply flow to the valve as uniform as possible, a buffer tank having a volume of 5.2 m^3 was connected to the second horizontal outlet of the T-piece.

The vertical outlet of the above-described T-piece leads to the valve.

8.2.1.1.4 Safety/Relief Valve (SRV)

The SRV used in the tests is the actual version being used for SSES. These valves are arranged vertically, have a steam inlet from below and an outlet to the side. As described in 8.2.1.1.3, the steam supply line was rebuilt in such a way that the same arrangement was possible in the test stand. The valve was mounted on the T-piece, using the same connection dimensions as in the actual plants.

Operation of the valve during the tests requires the connection of power supply lines, control lines and measurement lines. The existing equipment at the valve test facility was used to satisfy most of those requirements. Some modifications became necessary in order to adapt to the construction of the valve. The SRVs in German BWR plants are operated by an electrically actuated pilot valve with its own operating medium. In contrast, the SSES valve used in the test was opened pneumatically. Accordingly, the compressed-air connection was rebuilt so that the opening conditions in the actual plant could be simulated in the test stand.

8.2.1.1.5 Discharge Line and Quencher

The SRV described in 8.2.1.1.4 discharges on the exhaust-steam side into a pipe which represents the SRV discharge line. The length of the SRV discharge line and the number of bends are different for the 16 SRV's for SSES. Two line lengths were used for the tests, corresponding to the longest and shortest lengths of the SRV discharge lines in the plant. Isometric drawings of the two discharge lines are shown in Figure 8.5 (long line) and Figure 8.6 (short line).

Pipe supports and vibration dampers were mounted at the required places. These places were not identical to the corresponding ones in the plant, because the mounting situations and especially the concrete construction of the plant cannot be simulated directly in the test facility.

To prevent the buildup of a large underpressure in the pipe, two actual vacuum breakers were installed in a vertical part of the pipe line, as in the plant.

The quencher forms the termination of the SRV discharge line (see Figure 8.11). The steam is conducted into the water through a large number of holes having a diameter of 10 mm. The design of the quencher is described in detail in Section 4.1.

A bottom support is provided to hold the quencher in place in the test tank. It connects the quencher rigidly to the bottom of the tank and is constructed in such a way as to make it possible to measure the loads exerted on the quencher due to vent clearing processes and steam condensation. The sliding joint provided between the quencher and the discharge line in the plant is simulated in the test stand hydraulically by a corresponding annular gap.

8.2.1.1.6 Test Tank

For SSES, the exhaust steam from the relief valves is conducted into the suppression pool and is condensed there. In the test facility, a section of that pool is simulated by a stiffened steel tank (see Figures 8.7, 8.8, 8.9). In the plant, the suppression pool can be subdivided conceptually into subspaces, each of which is associated with a steam supply line (see Figure 8.3). In order to adapt the conditions in the test tank to the dimensions of the smallest geometrical single sell, concrete shaped blocks were inserted into the test tank. The concrete shaped blocks are clearly illustrated in Figure 8.7. The exposed cross-sectional area of the water space is 7.2 m x 3.15 m = 22.7 m^2. It corresponds conservatively to the smallest individual cell in the plant.

Illuminating devices and viewing ports made possible the direct observation and also photographic recording of the underwater processes.

8.2.2 Instrumentation

Instrumentation is provided for controlling the test procedure, determining the prescribed measurement quantities, and recording them.

8.2.2.1 General Description

The instrumentation used in the Karlstein test facility consists of operating instrumentation and test instrumentation. Operating instrumentation assures the control of the test facility and its environment correlation. The test instrumentation records the load data which is used to verify the conservatism in the design loads as specified for the SSES in section 4.1 of this Design Assessment Report.

Details on the operating instrumentation are given in Section 8.2.2.3. A detailed description of the test instrumentation can be found in Section 8.2.2.4.

8.2.2.2 Instrumentation Identification

For identification, the measuring sensors are designated according to a system of letters and figures. The first one or two characters are letters which identify the type of instrument:

P	Pressure Transducer
T	Temperature Sensor (Thermocouple)
F	Flow Rate Measurements
L	Water Level Measurements
DG	Displacement Gage
SG	Strain Gage
I	Electrical Impulse Signal
LP	Level Probe

These letters are followed by a number which characterizes the location within the test facility where the instrument is situated. The facility was divided into sections as follows:

Section 1 contains the steam supply, including the accumulator (only transducers of the test stand instrumentation system are contained in this section).

Section 2 contains the steam line up to the safety relief valve and includes the buffer tank.

Section 3 contains the safety relief valve.

Section 4 contains the discharge line and quencher.

Section 5 contains the test tank.

The sensor designation is completed by adding a decimal point and a sequential number. For example, "P5.6" means: the number 6 pressure transducer in the test tank.

Additional abbreviations used are as follows:

DPS	Data Processing System
CTC	Coated Thermocouple
DCA	Direct Current Amplifier
CFA	Carrier Frequency Amplifier
HT-SG	High Temperature Strain Gage
SRV	Safety Relief Valve
PG	Pressure Gage
RTD	Resistor Temperature Detector

8.2.2.3 Operating Instrumentation

The operating instrumentation is provided for measurement of parameters in relation to the steam accumulator, the steam lines and the SRV's. A total of 30 sensors can be recorded by a process computer which is part of the operating instrumentation system. The data are stored on a magnetic disk and can be printed out.

The recording frequency of the process computer was adapted to align with the instrumentation channels, covering a range from 0.5 Hz, for those sensors where only small transients are to be expected, up to about 200 Hz for the sensors where higher frequency signals are expected (e.g. for pipe vibrations).

The operating instrumentation comprises the measuring devices used to monitor and control the system and also the data acquisition devices needed for that purpose. Typical measuring locations for the tests are illustrated in Figure 8.4 and listed in Table 8.1.

According to the type of acquisition and display, the measurement sensors can be classified into two groups: "Display on Control Console" and "Acquisition by Computer".

8.2.2.3.1 Display on Control Console

To enable the operating personnel to control the test equipment, a number of quantities which characterize the operating condition of the system are displayed continuously.

In particular, they are:

- Water level in : Steam accumulator, steam line, buffer tank, discharge line, test tank
- Pressure in : Steam accumulator, buffer tank, control line, discharge line
- Temperature in : Steam accumulator, buffer tank, discharge line, test tank

8.2.2.3.2 Acquisition by Computer

Most of the data sensors comprising the operating instrumentation are interrogated by a computer at prescribed time intervals before, during and after the test. The values are stored on a disk.

The data are printed out at programmed intervals. At an interrogation frequency of 200 Hz, the capacity of the storage device is sufficient for a recording time of 2 minutes.

The following measurement values are interrogated:

Water level	Steam accumulator, buffer tank discharge line, test tank
Pressure	Steam accumulator, buffer tank, steam line, control line, discharge line
Temperature	Before SRV, after SRV, surface of SRV, discharge line, test tank
Vibrations	Steam line before SRV, discharge line
Valve travel	SRV, vacuum breakers
Switching time	Electrical energization of SRV

8.2.2.4 Test Instrumentation

Mesurement values used to verify the test tasks are determined by the test instrumentation. It is necessary to include here a few typical measuring points that are already used for monitoring purposes in the operating instrumentation on the pipes and SRV. Since most of these processes are of a high-frequency nature, the data is acquired in analog form by means of carrier-frequency measuring amplifiers and dc amplifiers on analog magnetic tape, and to a large extent also on visicorders. The visicorder traces allow an initial review and a pre-evaluation of the test data.

8.2.2.4.1 Measuring Points

Measurements are made of the

- pressure on the steam line before the SRV;
- valve actuation and valve travel;
- pressure variation in the discharge line at four points between the SRV and quencher;
- temperature in the discharge line at three points between the SRV and quencher;
- water level in the discharge line before the quencher inlet at four positions for the long line and five positions for the short line;
- bending, axial and torsional strains on the bottom support;
- bending strains on the quencher;
- bending strain on a dummy vent pipe;
- temperature distribution in the test tank;
- temperature distribution at the quencher for the condensation test;
- wall pressures and bottom pressures in the test tank.

Typical measurement points for the vent clearing tests are illustrated in Figures 8.7, 8.8, 8.9 and listed in Table 8.2. Typical measurement points for the condensation tests are illustrated in Figures 8.10, 8.11, 8.12 and listed in Table 8.3.

8.2.2.4.2 Set-up of Measuring Instruments

All instrumentation is channelled to one central station situated in the control room of the laboratory.

Each instrumentation channel consists of the individual sensor, connecting cable, amplifier (carrier frequency amplifier or direct current amplifier), attenuator; and are recorded on magnetic tapes and visicorders, most channels being in parallel on both systems. Three magnetic tape recorders and three visicorders were used in the control room. Each unit allows the recording of 12 channels and, in addition, a time reference signal and a physical correlation trace.

The sensors are connected by shielded cable to the amplifiers which are located near the recorders in the control room. For the strain gages, displacement gages and pressure transducers, carrier frequency amplifiers were used which allow a frequency resolution of up to 1 KHz. For temperature measurements, direct current amplifiers (10 Hz) were used together with a 10 Hz. low pass filter.

8.2.2.5 Visual Recording

Three high-speed cameras were used to film the processes in the pool during the blowdown through the quencher. KWU uses a "HYCAM 120 m" for that purpose. Two LOCAM cameras (model 51-0003) were being made available by the Standford Research Institute (SRI).

The positioning of the cameras was as follows:

HYCAM camera in front of one bull's eye at quencher height;

LOCAM camera 1 in front of one bull's eye at a tank height of approximately 4m;

LOCAM camera 2 on the service platform above the tank at a height of approximately 9 m.

A correlation between the moving pictures and the data recordings on the Visicorder and magnetic tape was accomplished by means of a timing mark on the films.

8.3 TEST PARAMETERS AND MATRIX

8.3.1 Vent Clearing Tests

The test matrix for the vent clearing tests is presented in Figure 8.15. This figure shows the test number and parameter conditions used for each test.

The number of basic tests was 25. These 25 tests were split into 5 groups of tests where by each group covered a set of test parameters. Tests numbered 26 to 32 were additional tests which were not required to verify the quencher design but which could prove useful in evaluating the performance of the safety relief system. Tests number 27, 28, 30 and 31 were to investigate shorter than normal SRV opening times, but, as valve opening times were found to be quite fast, these tests were not added to the required tests. Tests number 26 and 32, with one locked vacuum breaker, were included into the test matrix. The results showed the effect of the locked vacuum breaker to be minimal so test number 29 was not added.

The allocation of each test group within the operation range of the safety relief system is shown in Figures 8.16 to 8.21 by test points.

Base parameters in Group 1 (Figure 8.16) are long discharge line length, normal discharge line air temperature, normal initial water level inside the discharge line and normal valve opening time. Each of the following groups vary one or more of these Group 1 base parameters; Group 2 (Figure 8.17) uses a low initial water level inside the SRV pipe; Group 3 (Figure 8.18) uses a high discharge line temperature; Group 4 (Figure 8.19) uses a short discharge line length and Group 5 (Figure 8.20) uses a short discharge line length and a high discharge line temperature.

Each of the basic 25 tests was comprised of two or more valve actuations where by only the first actuation is made at the specified conditions of the discharge line (so-called clean condition). Any other actuation was made at the prevailing discharge line temperature and water level (so-called Real Condition). In the case of only two actuations at a test point the time interval between the actuations was approximately 10 minutes. In the case of multiple actuations at a test point the time intervals between actuations were varied as follows:

For test points 4, 5, 14, 15 the time between successive actuations was 1.5/5/15/30/60/120 seconds, accounting for seven valve actuations.

For test points 19 and 20 the time between successive actuations was 1.5/5/15/30/60/120/5/15/600 seconds, accounting for ten valve actuations.

For vent clearing tests with only two SRV actuations, the hold-open time for the SRV was 2 seconds while for the multiple value actuation tests the hold-open time was 1.5 seconds.

Five test points were repeated, these were test points 4, 15, 19, 20 and 25. Repeat tests at a designated test point are indicated with a letter R in the test number i.e. Test number 20.R1.1 is the first value actuation of the repeat test at test point 20.1.1.

A compilation of actual parameters at the start of each test is tabulated in Table 8.4 for the long pipe test series and Table 8.5 for the short pipe test series.

8.3.2 Condensation Tests

In order to further verify the steam condensation capabilities of the quencher device and provide specific information regarding its steam condensation capabilities for the safety relief system operation range a series of eight extended blowdown tests were performed. These tests are designated as test numbers 33 to 40. Each test was performed with the short discharge line configuration as described in section 8.2.1.1.5 and with an initial discharge line temperature of approximately 90°C.

The location of the initial system conditions for each test point is plotted on the safety relief system operation range in Figure 8.22.

In order to initiate each test the SRV was actuated as was done in the vent clearing tests. The valve then remained open until the system pressure reached the predesignated value for that test. At this time the valve was closed and the test was completed. The total allowable pressure drop in the accumulator tank for each initial system pressure dictated the duration of each blowdown.

A compilation of actual parameters at the start of each test point in the condensation tests matrix is tabulated in Table 8.6.

8.4 TEST RESULTS

This section provides a compilation of the test results for the vent clearing and steam condensation tests conducted at the Kraftwerk Union laboratories in Karlstein, West Germany in order to verify the load specification and steam condensing characteristics of the quencher design for the Susquehanna Steam Electric Station. Included in this section is information about the boundary conditions at the beginning of each test, the results of the behavior of the SRV, primary system pressures, dynamic pressure loads on the pool boundaries and their primary frequency and the loads on the quencher and bottom support. This information is provided in the form of tables, figures and actual visicorder recordings.

8.4.1 Vent Clearing Test Results

Nineteen tests with a total of 67 vent clearing processes were performed with the long discharge line in the period from May 8, 1978 to June 7, 1978 and 13 tests with a total of 58 vent clearing processes were performed with the short discharge line in the period from June 27, 1978 to July 7, 1978.

8.4.1.1 Test Parameters

The most important of the parameters being investigated was described in Section 8.3. A detailed list of test parameters for each valve actuation is given for the long discharge line tests in Table 8.4 and for the short discharge line tests in Table 8.5.

This includes

- type of test
- length of discharge line
- accumulator pressure
- water temperature in the test tank
- water level in discharge line
- air temperature in discharge line

The accumulator pressure P1.1A and the buffer tank pressure P2.6A are the determinative values for the system pressure at the start of each test. The values were read by computer just prior to the start of the test. In addition these pressures were stored continuously on magnetic tape. If a long period passed between the last computer reading and the actual test start then the initial values for the accumulator pressure were taken from the corresponding computer plots. The initial accumulator pressures were also read from those plots for the multiple valve actuation tests.

For accumulator pressures below 30 bar (435 psi), measuring point P2.5 was used to determine the system pressure, since measuring points P1.1A and P2.6A were outside the measuring range.

The water temperature at the start of the test was taken either from the computer listings or, in the multiple valve actuation tests, from the computer plots.

Due to the inertia of the Barton cell, the measurement value for water level in the discharge line (measuring point L4.1) in the multiple actuation tests, especially for the 2nd, 3rd and if applicable, the 8th actuation, must be disregarded or considered only as an indicative value.

The temperature in the discharge line at the start of each test was taken from the computer listings or the computer plots for the multiple actuation tests.

8.4.1.2 Behavior of the SRV and System Pressures

To evaluate the valve behavior, the valve opening time, t_o, was determined from the recorded valve lift variation for all tests. This involves the time from the beginning of valve opening until attainment of the steadystate lift (see sketch below). These opening times are listed, for the long discharge line tests, in Table 8.7 and, for the short discharge line tests, in Table 8.8. The associated steady state lifts are also indicated. A plot of the measured valve opening times as a function of accumulator pressure at the start of each test is shown in Figure 8.23 for the long discharge line tests and Figure 8.24 for the short discharge line tests.

The so-called vent clearing times t_{Fr} are also given in Tables 8.7 and 8.8. This is the time from the beginning of valve opening until the instant of maximum pressure at measuring point P4.4 in the discharge line. (see sketch below)

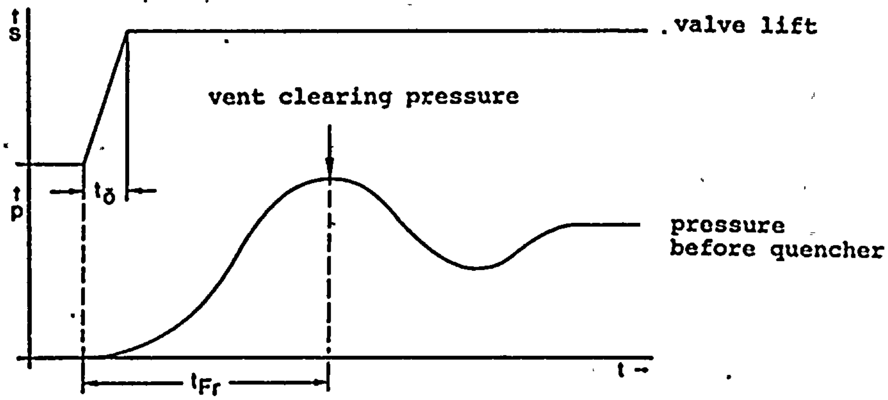

Two values are indicated in Tables 8.7 and 8.8 for system pressures measured in:

- buffer tank - P2.6
- before the SRV - P2.5
- in the discharge line - P4.1 to P4.4

These two values are the pressure at the vent clearing time (vent clearing pressure) and the pressure approximately 1.5 seconds after the start of test (steady pressure)

The initial parameters of relevance for the classification of tests are indicated in the row headings.

The vent clearing pressure in the discharge line before the quencher inlet (measuring point P4.4) is plotted versus system pressure (measuring point P2.6) under Clean Conditions in Figure 8.25 for the long discharge line tests and in Figure 8.26 for the short discharge line tests. See Section 8.5.2.1 for a discussion of the vent clearing pressures and their dependence on reactor pressure.

<u>8.4.1.3 Dynamic Pressure Loads on the Pool Boundaries</u>

As read off the Visicorder traces, the peak positive and peak negative pressure amplitudes during vent clearing for measuring points P5.1-P5.3 (bottom pressures) and P5.4-P5.10 (wall pressures) are compiled in Table 8.9 for the long discharge line tests and in Table 8.10 for the short discharge line tests. In addition, <u>approximate values</u> for the predominate frequency of the pressure oscillations are indicated. These frequencies were read from the visicorder traces.

Figures 8.27 and 8.28 show the measured peak positive pressure amplitudes at the tank bottom directly beneath the quencher (P5.2) and on the concrete wall at the quencher's mid-height

(P5.10) as a function of system pressure for the long discharge line and short discharge line tests. The test points plotted are all Clean Condition tests with cold water in the test tank (approximately 25° C) and discharge line cold (approximately 50° C). (Long discharge line tests 1.1, 2.1, 3.1, 4.1.1, 4.R1.1 and 32.1 and short discharge line tests 16.1, 17.1, 18.1, 19.1.1 and 19.R1.1)

As a comparison Figures 8.29 and 8.30 represent corresponding measuring points for tests performed under Real Condition (Long discharge line tests 1.2, 2.2, 3.2, 10.4 and 32.2 and short discharge line tets 16.2, 17.2 and 18.2). As can be seen the pressure amplitudes are slightly higher for the Clean Condition tests and no significant change with system pressure is observed.

Figures 8.31 and 8.32 show the measured peak positive pressure amplitudes at measuring points P5.2 and P5.10 for Clean Condition tests with heated water (45°C - 80°C0 in the test tank for the long discharge line tests and short discharge line tests respectively. (Long discharge line tests 5.1.1, 6.1, 7.1, 8.1, 9.1, 15.1.1 and 15.R1.1 and short discharge line tests 20.1.1, 20.R1.1, 22.1, 23.1, 24.1). Again, as a comparison, Figures 8.33 and 8.34 represent corresponding measuring points for tests performed under Real Conditions (Long discharge line tests 6.2, 7.2, 8.2, 9.2, 11.2 and 12.2 and short discharge line tests 20.R1.7, 22.2, 23.2 and 24.2) In contrast to the tests with cold water in the test tank, the pressure amplitudes are slightly higher for the Real Condition tests, but as with the cold water tests, no significant change with system pressure is observed.

Figures 8.35 to 8.40 show the measured peak positive pressure amplitudes at measuring points P5.2 and P5.10 for a number of multiple valve actuation tests plotted against the corresponding valve actuation.

Figures 8.41 to 8.65 show the first second of visicorder pressures traces (for the pool boundary pressures, P5.1-P5.10) from various tests.

<u>8.4.1.4 Loads On The Quencher and Bottom Support</u>

The bending strains on the two arms of the quencher and at the bottom support were each measured in two mutually perpendicular directions. The resultant bending strains and bending moments were calculated from these individual values. The strain-versus-time variations stored on magnetic tape were read for the maximum resultant during vent clearing. A high-pass filter having a cutoff frequency of 2 Hz was inserted in order to rule out any falsification of the evaluation due to slow drifting of the zero point. The upper frequency limit was at 400 Hz due to the mechanical conditions.

The maximum resultant bending strains determined in this manner and the bending moments calculated from them are compiled in Tables 8.11 and 8.12 for the long and short discharge line tests respectively. To clarify the direction distribution of the resulting bending moments on the quencher arms, the components of the maximum resultant bending moments are depicted in polar coordinates in Figures 8.66 and 8.67 for the long discharge line tests and Figures 8.68 and 8.69 for the short discharge line tests.

As shown the resultant bending moments on the quencher arms occur principally in the vertical direction.

Figures 8.70 and 8.71 for the long and short discharge line tests show a corresponding distribution of the maximum resultant bending moments at the bottom support.

Tables 8.11 and 8.12 also indicate the maximum torsional strains and torsional moments measured at the bottom support and the maximum vertical strains and vertical forces measured at the bottom support during vent clearing. This data is based on as evaluation of the visicorder traces.

8.4.2 Steam Condensation Test Results

Eight condensation tests with the short discharge line were performed in the period from July 18, 1978 to July 21, 1978.

8.4.2.1 Test Parameters

The most important of the parameters being investigated was described in Section 8.3. A detailed list of test parameters is given in Table 8.6. Compiled in that Table are the parameters at the beginning of the tests, such as:

- type of test
- length of discharge line
- accumulator pressure
- water temperature in test tank
- water level in discharge line
- water level in test tank
- air temperature in discharge line

The accumulator pressure P1.1A and buffer tank pressure P2.6A are the determinative values for the system pressure at the start of each test. The values were read by computer just prior to the start of the test. In addition, these pressures were stored continuously on tape but only up to 360 seconds after the start of tests 36.1 and 40.1. This was dictated by the limited storage capacity of the operating instrumentation computer's magnetic disk. This data was continuously stored on the visicorder traces and the test instrumentation magnetic tapes.

For accumulator pressures below 30 bar (435 psi), measuring point P2.5 was used to determine the system pressure, since measuring points P1.1A and P2.6A were outside the measuring range.

The water temperature at the start of a test was taken from the computer listings and at the end of a test from the computer plots.

The values for the water levels and air temperatures in the discharge line at the start of a test were taken from the computer listings.

Table 8.13 shows the relation between the test step, test number, and ranges of pressure and water temperature as they actually occurred.

8.4.2.2 Presentation of Test Results

First we will present a survey of the observed condensation phases. That is followed by a presentation of the dynamic pressure amplitudes in the water region of the test tank. Finally the temperature variations in the water region are described.

8.4.2.2.1 Survey of Observed Condensation Phases

In the operation field of the quencher as given by the test matrix, the observed condensation phases are indicated in Figure 8.71 for blowdowns along the upper and lower boundary lines of the operation field.

8.4.2.2.1.1 Blowdown at Low Water Temperature

For the blowdown along the lower boundary line, the following condensation phases were observed for the tested pressure range:

Absolute system Pressure in Bar	Condensation Phase	Tests
> 70 - 2.5	Stationary	33.2, 34.1, 35.1, and initial section of 36.1
2.5 - 2	Intermittent	Middle section of 36.1
2 - 1	In the pipe (1)	End section of 36.1

(1) It should be noted here that at the beginning of this phase a portion of the steam flow has emerged through the annular gap above the quencher inlet. As noted in Section 8.2.1.1.5,

this annular gap simulates hydraulically the sliding fit of the quencher installed at SSES.

Figure 8.73 shows a typical example of the measurement traces obtained with the bottom and wall pressure sensors for stationary operation of the quencher in the upper pressure range (test 33.2). Figure 8.74 shows a typical example of the lower pressure range (test 35.1). High-frequency pressure oscillations occur with very low amplitude, and without any fixed frequency.

To illustrate the intermittent operation, the variation of the bottom and wall pressures and two pipe pressures throughout the entire duration of test 36.1 is shown in an extremely time-compressed form in Figure 8.75. The intermittent condensation phase is clearly recognizable in the middle section of the test. Figure 8.76 shows a more time-expanded excerpt from that phase. Supplementarily, Figure 8.77 shows a typical powerful individual event in an extremely time-expanded form. The high-frequency pressure peaks superimposed on the low-frequency sinusoidal pressure pulsations are clearly discernible in both Figures 8.75 and 8.76.

For the phase of condensation in the pipe, the test traces exhibit negligibly low amplitudes, which are close to the resolution limit of the measuring chain. Therefore, no example of such a trace is shown.

8.4.2.2.1.2 Blowdown at High Water Temperature

For blowdown along the upper boundary line, the phases described in 8.4.2.2.1.1 were observed in practically the same pressure ranges. However, the appearance of the pressure oscillations differs to some extent from that of the pressure oscillations at low water temperature.

First, here is the observed relation between pressure range and condensation phase:

Absolute system Pressure in Bar	Condensation phase	Tests
>70 - 4	Stationary	37.2, 38.1, 39.1, and initial section of 40.1
4 - 2	Intermittent	Middle section of 40.1
2 - 1	In the pipe(1)	End section of 40.1

---

(1) It should be noted here that at the beginning of this phase a portion of the steam flow has emerged through the annular gap above the quencher inlet. As noted in Section 8.2.1.1.5, this annular gap simulates hydraulically the sliding fit of the quencher installed at SSES.

For stationary operation in the upper range of pressure, Figure 8.78 shows a typical example for test 37.2. The lower range of pressure for this phase is represented by an example from test 39.1 (Figure 8.79). There are also higher-frequency pressure oscillations with low and very low amplitude, respectively, and without any fixed frequency.

A typical example of intermittent operation is shown in Figure 8.80 by an excerpt from test 40.1. Compared to this phase at low water temperature (see especially Figure 8.76), a distinct attenuation of the strength of the pressure pulsations is observable at high water temperature. Superimposed high-frequency pressure peaks do not occur.

For the phase of condensation in the pipe, the test traces exhibit negligibly low amplitudes even at extremely high water temperature of more than 90°C.

8.4.2.2.2 Statistical Evaluation of the Dynamic Pressure Loads on the Pool Boundaries

As described in Section 8.4.2.2.1, the steam condensation does not have any uniform form throughout the entire range of system pressure and water temperature.

To now be able to quantify the distribution of dynamic pressure amplitudes during a blowdown from 70 bar to approximately 1 bar, the recordings from a representative bottom pressure sensor and wall pressure sensor for all the tests were statistically evaluated. This also allowed us to investigate the influence of system pressure and water temperature on the dynamic pressure amplitudes.

8.4.2.2.2.1 Dependence of Dynamic Bottom and Wall Pressures on System Pressure and Water Temperature

The pressure-time histories stored on magnetic tape for pressure sensors P5.2 (bottom pressure) and P5.10 (wall pressure) were each read for maximum value at uniform time intervals. A high-pass filter with a frequency cutoff of 2 Hz and a low-pass filter with a frequency cutoff of 500 Hz were inserted into the circuit. In this manner, a falsification of the evaluation due to slow drifting of the zero point or due to electrical interference was largely excluded.

For tests 33.2, 34.1, 35.1, 37.2, 38.1 and 39.1, a uniform interval of 1 second was chosen because of the relatively short test duration of a maximum of 64 seconds in test 39.1. In tests 36.1 and 40.1 with test durations of over 800 seconds, the uniform interval was 4 seconds. In these two tests, the phases of stationary and intermittent condensation and condensation in the pipe were covered separately at the same time. No error was introduced into the evaluation by the different choice of intervals, since the maximum values were covered in each case.

The extreme values determined for the positive and negative dynamic pressure amplitudes at the bottom and on the wall are plotted versus the transient variation of the system pressure in Figures 8.81 and 8.82. Due to the large number of extreme values, a selection was made with the aim of considering only the higher values.

The top half of the Figure shows the measured maximum pressure amplitudes for the blowdown at higher and high water temperature along the upper boundary line of the operation field. The bottom half shows them for the blowdown at low water temperature along the lower boundary line.

A similar illustration for the measured maximum wall pressure amplitudes is given in Figure 8.82.

The peak bottom-pressure and wall-pressure loads measured during the individual condensation phases are indicated as a function of water temperature in Table 8.14. From these peak values, we can ascertain a slight decrease of the pressure level with a hot pool for the stationary and intermittent condensation phases. For the phase of condensation in the pipe, of course, there are practically no differences in the pressure levels for cold and hot pool.

8.4.2.2.2.2 Occurrence Frequency Distributions of the Dynamic Bottom and Wall Pressures

In parallel with the determination of extreme values as described in Section 8.4.2.2.2.1, all positive and negative peak values between the zero passages of the pressure-vs.-time variations were determined in each time interval and classified according to magnitude.

This counting method, known as "peak count between zero passages" or "mean crossing peak count method", avoids the inclusion and consequential overassessment of small intermediate oscillations. Only the absolute maxima between two zero passages are included in the count.

The count result supplies the class occurrence frequency distribution at once. Positive and negative peak values were treated separately. Any error in the count results by the noise level on the magnetic tapes was largely eliminated by means of a prescribed amplitude suppression of 10 mV = 0.015 bar.

A uniform class interval of 0.025 bar was chosen for the histograms. In that way, the histograms of the individual tests were able to be combined into an overall distribution for blowdowns with cold and hot pool. The histograms of the positive and negative amplitudes of the dynamic bottom pressures at measuring point P5.2 are illustrated in Figures 8.83 and 8.84 for blowdowns with cold and hot water, respectively. Analogous historgrams for the wall pressures at measuring point P 5.10 are shown in Figures 8.85 and 8.86.

8.4.2.2.2.3 Statistical Characteristics of the Dynamic Bottom and Wall Pressures

Influences of test parameters can be read off from the statistically determined mean values, since those values are obviously much more typical than the magnitudes of individual and very rare maximum values. The mean values were determined by the group value method, using the following equation:

$$\overline{P}_G = \frac{\sum_{i=1}^{k} n_i \cdot \overline{P}_i}{\sum_{i=1}^{k} n_i}$$

where $\overline{P}_G$ = mean value; $\overline{P}_i$ = class mean value; n_i = class frequency.

The group value method was also used for the combining of the individual histograms of a blowdown to get the mutual freqeuncy distributions. Those mean values are indicated in Figures 8.83 to 8.86.

In general, the trends are supported by the maximum values. The unavoidable scatter of the maximum values is allowed for by forming the average value of the 10 highest amplitudes in each test. Due to the small number, they were determined by the single-value method:

$$\overline{P}_E = \frac{\sum_{i=1}^{N} P_i}{N}$$

where

$\overline{P}_E$ = mean value; P_i= single extreme value; N = number of extreme values

Tables 8.15 and 8.16 provide an overview of the abovementioned most important statistical characteristics of the pressure-time histories at the bottom and at the wall, respectively for tests 33.2 to 40.1. Indicated are:

- maximum value relative to the entire test,
- mean value relative to the entire test,
- lower limit value of the 10 highest values,
- mean value of the 10 highest values.

Beside the data concerning the system pressures and water temperatures, the condensation phases are also listed. In tests 36.1 and 40.1, the phases of stationary and intermittent condensation and condensation in the pipe were treated separately.

Figures 8.87 and 8.88 show plots of the mean values relative to the entire test or test section and the mean values of the 10 highest values, as functions of system pressure.

The mean values of the bottom and wall pressures are slightly higher for the blowdown with a cold pool. This trend, already alluded to in Section 8.4.2.2.2.1 on the basis of the absolute extreme values, is therefore verified statistically. The level of the mean values from the 10 highest values is higher by a factor of approximately 3-4 than the level of the mean values relative to the entire test or test section.

8.4.2.2.3 Temperature Variations in the Water Region of the Test Tank

Four tests were selected to illustrate the temperature variations in the water region of the test tank:

- test 33.2 for high system pressure and cold pool,
- test 35.1 for low system pressure and cold pool,
- test 37.2 for high system pressure and hot pool,
- test 39.1 for low system pressure and hot pool.

Figures 8.89 to 8.92 show the vertical temperature distribution obtained from the measuring points T 5.5, T 5.2, T 5.3 and T 5.4 arranged above one another on the concrete wall. In each case, the measured temperatures are scattered about a mean curve. The scatter is greatest for measuring point T 5.2 (approximate max. ±8° C). That measuring point is at the height of the quencher arm and is impinged upon directly by the sidewards directed flow impulse. The scatter is least for measuring point T 5.4 (approximate max. ±5° C). The scatter can be explained by the high degree of turbulence in the pool.

Figures 8.93 to 8.96 show the temperature variations at quencher arm 1 for the same tests. At measuring point T 5.8 located in the middle of the hole array (see figure 8.14) a distinct temperature increase of approximately 15-20°C, on the average, was recorded relative to the pool temperature. In contrast, the temperatures at the upper edge of the hole array (T5.9) and at the upper edge of the quencher arm (T5.10) are somewhat lower than the pool temperature at T5.1 due to a sufficient "cold water supply". This is an indication of the good circulation of water near the quencher. This confirmed the expected condensation behavior of the quencher as related to the layout of the hole array. (See Section 4.1.1.1).

8.4.2.2.4 Water Level in the Discharge Line When Opening and After Closing the SRV

In the tests with the long discharge line, the water level in the pipe was measured by the "Level Probes" LP 4.1 thru LP 4.4 at four positions, one above another.

In the tests with the short discharge line, this instrumentaiton was extended by the measuring point LP 4.5 above the measuring point LP 4.4; see Figure 8.8. The measurement signals from these Level Probes were recorded on visicorders and magnetic tape.

A Barton cell, measuring point L 4.1 in Figure 8.4, was used to set and measure the water level in the discharge line before test start. The reading of that measuring point was interrogated by the computer before and during the test and was stored.

The indications of the Level Probes and also the indications of the Barton cell were used to depict the time variation of the water level in the discharge line. It must be taken into consideration that the response speed of the Barton cell is too slow for the rapid changes of the water level during vent clearing and after the closing of the SRV. The measuring point was used essentially to determine the steady-state water levels in the discharge line.

Figures 8.101 and 8.102 show two typical examples of the variation of the water level in the pipe for the interval test 15.1 with the long discharge line and 20.1 with the short discharge line. It was found that in two instances in interval test 15.1 (Figure 8.101), the water column briefly exceeded the external water level, but fell back immediately. These two test points represent the maximum water column rise measured in the vent clearing tests.

In the interval test 20.1, the water column did <u>not</u> reach the level of the external water surface in any instance after closing of the SRV. The maximum water level rise was generally found, in all tests, to occur after the third valve actuation.

To evaluate the effect of vacuum breaker operation on the water column reflood following vent clearing; Test 32, with one locked vacuum breaker and a time interval of 3 seconds between the closing of the valve after the first actuation and the next actuation, was included. Figure 8-105 shows the variation of the movement of the water column in Test 32. As can be seen no adverse effects were recorded.

8.4.3 Checking and Calibration of the Measuring Instrumentation

The calibration and the electrical and physical checking of all sensors before, during and after the tests were performed in accordance with the Test and Calibration Specifications.

Fig. 8.97 shows diagrammatically the physical calibration of the sensors, the setting and calibration of the amplifiers and recording instruments, and the quality inspection of the sensors. Fig. 8.98 shows the time intervals stiplated for the checks and calibrations in the Test and Calibration Specifications. Fig. 8.99 clarifies the chain of the calibration system from the national standards of the Physikalisch-Technische Bundesanstalt (PTB) to the measuring instruments.

The pressure sensors P 5.1 thru P 5.10 used in the tests were fully operable until the end of the tests. The lowest insulation resistance of $1.2 \times 10^7\ \Omega$ measured at P 5.1 after the tests can be classified as "good". The pipe pressure sensor P 4.1 failed on 31 May 1978. It was replaced by a new sensor for the subsequent tests. With this new sensor P 4.1, the lowest insulation resistance for the group of pipe pressure sensors after the tests was $3 \times 10^8 \Omega$, which was very good.

There were no failures for the strain gauges SG 4.1 thru SG 4.8, SG 5.1 and SG 5.2. Here also, a very good insulation resistance level was recorded with a lowest value of $3 \times 10^8\ \Omega$ at SG 4.6 after the tests.

Likewise, none of the temperature measuring pionts T 5.1 thru T 5.10 failed. The lowest insulation resistance of $1.3 \times 10^6\ \Omega$ was sufficiently high.

8.4.4 Analysis of Measurement Errors

Based on information from the manufacturers of the measuring instruments, KWU's own investigations, and taking into consideration the experience accumulated in similar test projects, the maximum measurement errors for the individual sensors can be indicated as follows:

Pressure sensors P 5.1 thru P 5.10

	Error
Linearity error of the sensor	
2.5% of measured value in range of 0 to 2 bar	2.5%
Reproduction error of the sensor 0.2% of 5 bar	0.01 bar
Error of the measuring amplifier	0.5%
Error of the balancing unit and recorder	0.5%

Max. total error ± [0.01 bar + 3.5% of the measurement value]

Pressure sensors P 4.1 thru P 4.5	Error
Linearity error of the sensor 0.5% of measured value in range of 0 to 20 bar	0.5%
Reproduction error of the sensor 0.1% of 35 bar	0.035 bar
Error of the measuring amplifier	0.5%
Error of the balancing unit and recorder	0.5%

Max. total error ± [0.035 bar + 1.5% of the measurement value]

Pressure sensors P 2.3 and P 2.5	Error
Linearity error of the sensor 1% of measured value in range of 0 to 40 bar	1%
Reproduction error of the sensor 0.1% of 140 bar.	0.14 bar
Error of the measuring amplifier	0.5%
Error of the balancing unit and recorder	0.5%

Max. total error ± [0.14 bar + 2% of the measurement value]

Strain gauges SG 4.1 thru SG 4.8, SG 5.1, and SG 5.2	Error
Tolerance of the guage factor	3%
Influence of temperature on the guage factor	1%

Error of the measuring amplifier	0.5%
Error of the balancing unit an recorder	0.5%

Max. total error ± 5% of the measurement value

Temperature measuring points T 5.1 thru T 5.10

Error of the sensor	1°C
Error of the measuring amplifier	0.5%
Error of the balancing unit and recorder	0.5%

Max. total error ± [1°C + 1% of the measurement value]

After the first tests on May 10, 1978 and after conclusion of the tests on August 2, 1978, additional physical checks of the pressure sensors in the water region were performed by incremental lowering of the water level in the test tank. The max. deviations from the nominal value were approximately +0.01 and -0.02 bar. Fig. 8.100 illustrates a frequency distribution of these deviations combined from both checks and for all presure sensors. It shows a typical Gaussian distribution.

In order to record the high-frequency processes correctly in frequency and amplitude, the data was acquired in analog form on magnetic tape. For a sensor eigenfrequency of approximately 30 kHz, the dynamic range was limited not by the sensors but rather by the carrier-frequency measuring amplifiers located further on in the circuit. The frequency cutoff of the measuring amplifiers was at 1.5 kHz and that of the magnetic tape recorders was at 2.5 kHz. The frequency cutoffs of the visicorders were determined by the utilized galvanometers. These frequency cutoffs are approximately 1 kHz. The frequency response of each individual galvanometer was checked prior to the tests.

8.4.5 Repetition Tests and Reproducibility of the Results

To verify the reproducibility of the measurement results, a repetition of 5 tests was specified in the Test Matrix. Based on a preliminary assessment of the results after conclusion of the test series with the long and short discharge lines, the following tests were repeated (as mentioned previously):

Long line:

4.1 through 4.R1	Interval tests
15.1 through 15.R1	Interval tests

Short line:

19.1 through 19.R2	Interval tests
20.1 through 20.R1	Interval tests
25.1 through 25.R2	Single Actuation tests

In addition to the relevant initial conditions, Table 8.17 also gives the measured

- vent clearing pressure (measuring point P 4.4),
- max. dyn. bottom pressures (measuring point P 5.2),
- max. dyn. wall pressures (measuring point P 5.10) and
- frequencies of the pressure oscillations

for the first SRV actuation in each of the repetition tests ("Clean Conditions tests").

A comparison of the above-cited values for the repetition tests associated with each other demonstrates the good reproducibility under Clean Conditions. The <u>maximum</u> deviations from the mean value for each pair of repetition tests are (see Table 8.18):

- for the vent clearing pressure	±0.75 bar or ±6%
- for the bottom and wall pressures	±0.05 bar or ±7%
- for the frequency of the pressure oscillations	±0.5 Hz or ±7%

The <u>mean</u> deviations from the mean value of each pair of repetition tests, averaged for all 5 pairs of tests, are:

- for the vent clearing pressure	±0.37 bar or ±3%
- for the bottom and wall pressures	±0.02 bar or ±6%
- for the frequency of the press oscillations	±0.2 Hz Or ±5%

Figures 8.37 and 8.38 illustrates the max. dynamic pressures in the pool during the vent clearing for the multiple valve actuation repetition tests with the long line. Figures 8.39 and 8.40 shows the same thing for the multiple actuation repetition tests with the short line. In comparison with the first SRV actuations under Clean Conditions, some larger deviations are exhibited here in the tests under Real Conditions (2nd to 7th and 10th SRV actuations). The reason for these deviations is that the initial conditions differ significantly from each other.

The visicorder traces for each "clean condition" actuation at a repetition test point is provided:

Tests 4.1.1 and 4.R1.1 - Figures 8-41 and 8-42

Tests 15.1.1 and 15.R1.1 - Figures 8-46 and 8-47
Tests 19.1.1 and 19.R2.1 - Figures 8-48 and 8-49
Tests 20.1.1 and 20.R1.1 - Figures 8-59 and 8-60
Tests 25.1 and 25.R2 - Figures 8-64 and 8-65

A visual comparison of the traces from each repitition test also shows good reproducibility.

Accordingly, it can be said that:

- If the initial conditions of the tests are set in a controlled manner (Clean Conditions), then the test results are reproducible.

- If the initial conditions correspond to the randomly prevailing operating states (Real Conditions), then the measurement values lie in a larger scatter range.

8.5 DATA ANALYSIS AND VERIFICATION OF LOAD SPECIFICATION

8.5.1 Evaluation of Test Tank Effects on Boundary Pressure Measurements

In this Section, we present theoretical and experimental investigations which show that the Karlstein test tank represents a good simulation of the hydraulic conditions of the SSES suppression pool. We are concerned primarily with the effects exerted on the processes in the water by the existing boundary surfaces such as the water surface, tank bottom, movable or immovable tank walls. The results of the investigation facilitate the evaluation and transposition of the boundary loads measured in the tests to SSES.

8.5.1.1 Effects of Free Water Surface and Rigid Walls

The effects of the free water surface and the rigid walls of the tank on the fluid pressure will be explained first by means of the examples illustrated in Figure 8-104. The top half of the Figure shows the velocity potential and flow field of a spherical bubble subjected to overpressure or underpressure in an infinitely extended, incompressible fluid. The potential field is described by a simple 1/r law (Reference 35). If, for example, the same bubble is located in a cylindrical rigid tank which is partially filled with fluid, then the potential field and flow field have a visibly different appearance (Figure 8-104, bottom). The differences in the nonstationary fluid pressure, which is proportional to the velocity potential for sufficiently low flow velocity (pressure field = potential field; see Reference 4 for example), are clearly evident in the pressure profiles on the right side of the Figure 8-104. The free water surface constrains the pressure to zero, while the cylindrical wall causes an increaseingly more powerful pressure rise with increasing depth. The narrower the tank, the greater is the pressure rise. The calculations relating to Figure 8-104 were performed by the finite-elements method (Reference 34) for a tank diameter of 3 m and a water depth of 6 m. The bubble was 2.8 m deep and 0.8 m in diameter.

Besides the pressure field, there is also an effect on the water mass which is effectively entrained by the bubble during pulsation motions (pressure oscillations) and thus also the oscillation frequency. In the case shown in Figure 8-104, the bubble in the tank has a larger coupled mass than in the infinitely extended medium. This is manifested by the fact that the pulsation frequency of the bubble is correspondingly lower (see Section 8.5.3.2).

8.5.1.2 Method of Images

The method of images is an important aid which makes it possible to clearly understand the hydraulic actions of the water surface and rigid walls and to calculate them quantitatively in a simple way (Reference 35). It is based on the fact that the influence of a plane rigid wall on the flow field of a hydrodynamic point source can be represented by a superposition of the flow field without the wall (infinitely extended fluid) and the flow field of an image source of identical sign and identical strength located behind the wall (Fig. 8-105). The same holds for a plane free water surface, except that the image source has the opposite sign.

Using this method of images, the flow field of a point source in a rectangular vessel is obtained finally by repeated application of suitable imaging operations (Figure 8-105d and Figure 8-2).

The immediate significance of the method of images lies in the fact that a pulsating bubble can be conceived of as a hydrodynamic source, thus providing a simple method to calculate the pressure field. Of special importance for the performance of tests is the consequence derived by inversion of the method of images: A configuration of bubbles oscillating in parallel can be simplified in a test by surrounding one bubble with rigid walls. This will be clarified further in the following.

8.5.1.3 The Test Stand as a Single Cell

Based on the above discussion, an oscillating bubble in a rectangular vessel is equivalent to a plane field of simultaneously oscillating bubbles (Figure 8-2). From Figure 8-2 it follows further that vessels with several bubbles are also equivalent, since between each pair of bubbles the imaging wall section can also be omitted.

Application of the method of images to the transposition of a system of valves blowing down simultaneously in a plant to a test stand with a quencher leads to the cell division illustrated in Figure 8-3.

As discussed in section 8.1, the water space of the test stand was formed according to the interior single cells C, F, K and N (Figures 8-3 and 8-108), since they are the narrowest and will therefore exhibit the highest wall and bottom pressures. That can be seen by observing that, according to the imaging principle, they conservatively simulate more quenchers lying closer together than is actually the case in the SSES suppression pool.

8.5.1.4 Spatial Distributions of Pressure in the Test Tank

To get meaningful test results, pressure sensors have to be mounted at suitable points in the test tank. A series of theoretical investigations was performed in order to better assess their arrangement. They consisted of calculating the spatial distribution of pressure along the tank walls for various bubble configurations under water. The KWU computer code VELPOT was used for this investigation. A bubble was simulated by a point source normalized to unit source strength.

The results are illustrated in Figures 8-107 to 8-109. Figure 8-107 shows the calculated wall pressure distribution for a bubble in three different positions near the quencher:

Case 1 Source on the tank axis, 0.7 m above the quencher axis
Case 2 Source on the tank axis, at quencher elevation
Case 3 Source at center of the quencher (eccentric).

The results show that the eccentric arrangement of the quencher which became necessary because of space limitations in the tank, including the corresponding positioning of the pressure sensors (black squares in Figure 8-107), results, theoretically, in slightly higher measurement values for the pressures. The next calculation (case 4, Figure 8-108) serves to answer the question as to how the bubble's form influences the pressure distribution. To do that, the single source from case 3, figure 8-107, was replaced by four identical sources with the same total source strength. Figures 8-108 and 8-109 show that there are no major differences. Note also the good agreement seen between the measured pressures from shakedown test 08.1 and the calculated values in Figure 8.109.

The model cases 3 and 4 (single bubble at center of quencher and 4-bubble arrangement) are best adapted to the test stand geometry. Since the associated pressure distributions hardly differ at all (Figure 8-109), it is demonstrated that an exact knowledge of the air distribution under water is not necessary for a correct arrangement of the pressure sensors.

In order to demonstrate the conservative nature of the chosen single cell, as already explained in Section 8.5.1.3, the pressure distribution for model case 4 is compared to the distribution calculated for the Susquehanna plant in Figure 8-110. The pressure distribution in the test stand envelops the pressure distribution in the SSES. Furthermore, the pressure distribution in the test stand is enveloped by the specified distribution (Figure 8-111).

8.5.1.5 Investigation of the Influence of Movable Walls on the Measurement Results (Fluid-Structure Interaction)

8.5.1.5.1 General Remarks

In the preceding discussion, it was assumed that the single cell has rigid and immovable walls. The construction of the Karlstein test tank is such that the tank, despite a series of stiffening ribs (see Figures 8-10 to 8-12), still has a residual compliance. The time-varying loads acting during the blowdown of the quencher can therefore excite the tank into oscillation due to Fluid-Structure Interaction (FSI).

Using experimental and theoretical investigations, it will be shown that influences of tank oscillations on the measured boundary loads can be neglected. The experimental investigations consisted, firstly, of measuring the tank's response to a short pressure impulse which was produced by an explosive charge detonated near the quencher (Section 8.5.1.5.2). Measurements made during the start-up tests on the test stand then supplied the tank's response to the loads occurring during vent clearing (Section 8.5.1.5.3). Taking into consideration the inpulse response, it turns out that effects of tank oscillations at the eigenfrequencies are negligible. This statement is later confirmed by calculations and also is extended to forced oscillations.

8.5.1.5.2 Experimental Investigation of the Tank's Natural Oscillations

The experimental investigation of the tank's natural oscillations was performed with impulsive excitation by an explosive charge in the water and simultaneous measurement of the displacements of the wall and bottom sections and of the fluid pressure.

The arrangement of the charge and sensors in the tank is illustrated in Figure 8-112. The position of the charge was chosen such that the spatial load profile in the tank matches the profile of the blowdown loads as well as possible. The charge itself was a stoichiometric mixture of hydrogen and oxygen which was ignited in a plastically deformable flat container (Figure 8-113). Eight displacement transducers (WA 1 to WA 8) were available for the displacement measurements. They were positioned with the aim of obtaining the most useful information. The arrangement of the pressure measuring points in the water (P5.1 to P5.10, Figures 8-10 to 8-12) was the same as in the later blowdown tests. As for the evaluation of the pressure traces in Section 8.5.3, transducer P5.10 was chosen as reference pressure transducer.

The charge was located at different positions near the quencher as shown in figure 8-112, in order to obtain enveloping load profiles. A typical result is illustrated in Figure 8-114, which shows the recordings from displacement transducers WA1 to WA8 and pressure transducer P5.10 for test no. 2 (charge in position 2).

The lowest occurring frequencies are below 1 Hz, but have nothing to do with the tank's response, but rather represents a shift of the zero point. The lowest eigenfrequency of the tank is at approximately 13 Hz and is seen clearly in the response from transducers WA2 and WA3 oscillating in phase. Both gages are seated on the box-shaped stiffening rings as shown in figure 8-112. At the wall sections between the stiffeners (WA4 and WA6) and at the bottom (WA8), the frequencies that occur are mainly between 30 and 60 Hz. The oscillations of the flat lower stiffener rings (WA1 and WA5) are less pronounced. The smallest displacements are found at the concrete sections (WA7) , where some of the amplitudes are smaller by an order of magnitude. The pressure signal from P5.10 shows distinct excursions only during the first 100 ms.

To be able to better evaluate the tank's frequency response, the measured time variations were Fourier analyzed and power spectra were formed. The spectra associated with the displacement transducers on the steel wall (WA2), concrete wall (WA7) and bottom (WA8) and the pressure transducer P5.10 are shown in Figures 8-115 to 8-118. It turns out that the previously mentioned 13 Hz oscillation in the low-frequency range is of greatest importance. The associated tank deformation (eigenmode) can be derived from the point correlations shown in Figure 8-119. There, the displacements of the displacement transducers WA2, WA3 and WA7, filtered by a bandpass filter at 13 Hz, are plotted against each other at the same times.

The fit line through the set of points has a positive slope in the top graph and a negative slope in the bottom graph. Therefore, displacement transducer WA3 (steel wall above WA2; see Figure 8-106) oscillates in phase with WA2, while displacement transducer WA7 (concrete wall) oscillates out of phase. This means that the 13 Hz oscillation corresponds to an ovalizing motion of the wall (see Figure 8-120).

8.5.1.5.3 Experimental Investigation of the Tank's Response to Vent Clearing Loads

The investigations of the tank's response to vent clearing loads were performed during the test stand shakedown tests. To measure the tank's response, the choice was made to use one displacement transducer each on the steel wall (WA2), on the concrete wall (WA7) and on the bottom (WA8). The instrumentation is shown in Figure 8-121.

Test 08.1 represents a typical example of the shakedown tests that were run. The measured time histories of the wall and bottom displacements and of the reference pressure P5.10 are shown in Figure 8-122. The zero-point drift mentioned above was eliminated by using a 2 Hz high-pass filter. It can be seen that both the pressure and the displacements oscillate at the same principal frequency of 5.1 Hz. The steel wall (WA2) and bottom (WA8) move in phase. The very small movement of the concrete wall (WA7) is almost out of phase compared to the pressure P5.10.

In addition, the displacement transducer WA8 records a higher-frequency oscillation at 30 Hz. It has already begun weakly at test start, then develops strongly at about the time of the vent clearing, and then decays again about 300 ms later.

The physical interpretation of the 5 Hz oscillation is obvious. The pressure oscillation is caused by the pulsation of the air bubble which is created during vent clearing. At the same time, the tank carries out forced oscillations at the frequency of the forcing force (5 Hz pulsation of the air bubble). The sometimes phase-opposed nature of the displacements of the steel wall and bottom, on the one hand, and the concrete wall, on the other hand, makes it evident that the above-discussed ovalizing eigenmode plays a dominant role.

The origin of the rapidly decaying 30 Hz oscillation seen at WA-8 at the test start is attributed to local forces transmitted through the discharge line and the quencher support during vent clearing.

Figures 8-123 to 8-125 show the power spectral densities of the displacement time histories for gages WA2, WA7 and WA8 measured during shakedown test 08.1. Figure 8-126 shows the power spectral density of the pressure time history for P5.10 measured during shakedown test 08.1. A review of these figures shows very little influence from the 13 Hz tank eigenfrequency or from the 30 Hz local effect seen at WA8. Figure 8-126 showing the rsults from P5.10 shows practically no influence from either of these effects.

From this it can be concluded that for all practical purposes the Karlstein test tank is rigid and has no influence on the pool boundary pressure measurements made during the tests.

8.5.1.5.4 Theoretical Investigations and Model Calculations of the Influence of Fluid-Structure Interaction

8.5.1.5.4.1 Computation Models

The analysis described below to compute the FSI on the measured pressures in the Karlstein test tank was performed by using the KWU computer code KOVIB1A which was developed originally and used successfully for the analysis of fluid-structure interaction in the water pool of KWU's 69 Product Line BWR Plant.

The underlying theory follows from a uniform formulation of the mechanical processes based on potential theory and classical Lagrangean dynamics. It unifies the dynamics of the bubble and the FSI by using the results of modal analyses. In particular, the feedback effects between bubble and structure via the fluid are included.

8.5.1.5.4.2 Model Parameters and Input for Calculations Without FSI (rigid tank)

The model parameters and input quantities for calculations of the air bubble oscillations in the rigid tank are:

- air mass flow into the bubble,
- water temperature (= air temperature in stationary equilibrium),
- hydrostatic pressure at bubble position,
- hydrodynamic mass parameter of the bubble,
- spatial pressure distribution,
- initial values (bubble radius, etc.).

The total air mass (integrated air mass flow), water temperature and static pressure at the bubble position are obtained from the test data. The hydrodynamic mass constant of the bubble and the spatial pressure distribution are obtained from the corresponding potential calculations (Figure 8-107, case 1). The time variation of the air supply into the bubble was adjusted heuristically by means of systematic trial and error, in parallel with the initial values, in such a way that the calculated and measured time variations of the pressure at transducer P5.10 exhibited optimal agreement.

The start-up test 08.1 was used as reference test for these calculations. The air mass flow determined in this manner is illustrated in Figure 8-127.

8.5.1.5.4.3 Model Parameters and Input for Calculations with FSI

Just as for the determination of the air supply into the water pool, a semiempirical method is used for the structural dynamics data. They are determined on the basis of the eigenfrequency measurements described previously. Input data for the calculation are:

- eigenfrequency,
- modal mass,
- modal weight,
- dynamic pressure distribution.

Based on the impulse response of the tank (Figures 8-115 to 8-117), it is plausible to select the oscillation mode lying at 13 Hz. That fixes the frequency. The modal mass cannot be taken directly from the experiment, but rather can be determined indirectly via the measured unit displacements of the wall. The unit wall displacement is illustrated in Figure 8-128. It is obtained from displacements at the displacement transducers by bandpass filtering at 13 Hz and plotting simultaneous values of displacement which are normalized to 1 at the water surface. The displacement direction is defined as positive if the relevant wall section moves inward. The hydrodynamic component of the modal mass (coupled water mass) is then calculated by methods of potential theory.

The modal weight, which is equal to the integral load relative to the modal mass and averaged over the unit displacement, is based on the load distribution calculated for case 1 (Figure 8-107, centered bubble). The dynamic pressure distribution (see Figure 8-129) is obtained from the unit displacement by means of potential calculations.

8.5.1.5.4.4 Results of the FSI calculations

The results of the calculations concerning the influence of FSI are shown in Figures 8-130 and 8-131. Figure 8-130 shows the calculated time variation of the pressure at pressure transducer P5.10, first in the rigid tank (without FSI) and then in the elastic tank with the 13 Hz eigenfrequency. There is a very slight reduction in the pressure amplitudes, but it is certainly negligible in comparison to the scatter of the measurement values themselves.

As is evident from Figure 8-131, the frequency influence of FSI also can be neglected. In that Figure, the oscillation frequency of the bubble is plotted against the bubble volume. The bubble has a slightly lower frequency with FSI effects included than without.

A physically clear explanation of the very slight FSI effects found in the Karlstein Test Tank can be obtained by comparing the volumes of fluid which are moved by the oscillating wall and bottom and by the pulsating bubble . For a bubble volume (long line) of 2.2 m^3 and pressure fluctuations of ±0.4 bar (see Figure 8-126), the volume change of the bubble is approximately 1 m^3 isentropically.

In contrast to this, for displacements like those found in Figures 8-124 and 8-125 the walls and bottom use up only about 0.05 m^3, which is only 5% of the water volume coming from the bubble. Therefore, due to the compliance of the tank, 95% of the water flows upward instead of 100% (rigid tank).

Thus, the result of the experimental and theoretical FSI investigations is that effects of the compliance of the Karlstein test tank walls and bottom on the pressure loads measured on the boundaries of the tank during the tests can be neglected.

8.5.2 Verification of SRV System Load Specification Due to SRV Actuation

The pressures inside the SRV discharge line were measured at four measuring points: just behind the SRV at measuring point P 4.1, in the center of the blowdown pipe at measuring point P 4.2 (measuring point P 4.5 for the short discharge line), just above the normal water level at measuring point P 4.3, and just before the inlet of the quencher at measuring point P 4.4 (see Figure 8.4).

The long and short discharge lines are illustrated in Figures 8-5 and 8-6.

The measured pressures in the discharge line are documented in Section 8.4.1.

8.5.2.1 Pressures During the Vent Clearing Process

Typical measurement traces of the pressures in the discharge line are shown in Figures 8-132 and 8-133. The vent clearing pressure is read off at P4.4. As discussed in Section 8.4.1, the vent clearing pressure is defined as the pressure which is read off at the first pressure maximum at P4.4. A typical feature of this pressure variation is the dynamic overshoot of the pressure above the stationary value. This phenomenon does not occur in such a pronounced manner at the other pressure transducers along the discharge line. This dynamic effect indicates that the pressure required to expel the water column is greater than the pressure necessary to bring the steam mass flow through the quencher.

The expulsion of the water column is also clear from the different time variations at P 4.3 and P 4.4. The pressure at measuring point P 4.3 (above the water column) rises much more steeply than the pressure at measuring point P 4.4 (inside the water column). The difference between the two pressures is the pressure which is necessary for the acceleration of the water column.

At the time of the vent clearing, the two pressures have approximately equal values. But after the vent clearing they differ again, this time due to the different pressure losses caused by flow resistances in the pipe.

8.5.2.1.1 Vent Clearing Pressures for the Long Line

The steam mass flow through the SRV is a practically linear function of the stagnation pressure (reactor pressure). Since the steam mass flow is one of the main parameters for the pressure build-up in the air region of the discharge line and thus for the acceleration of the water column, we will plot the pressures in the discharge line as a function of reactor pressure. The pressure in the buffer tank (P2.6) and not the pressure in the steam line before the SRV is used as the reactor pressure for the tests since the pressure in the buffer tank more closely simulates the representative stagnation pressure in the reactor. (see Figure 8-134).

To describe the dependence of the vent clearing pressure on the reactor pressure, only those tests for which the initial conditions were set and thus known exactly were used. Those are the tests with so-called "clean conditions".

From Figures 8-135 and 8-136, it can be seen that the measurement results have good reproducibility for the tests with clean conditions. The pressures in the pipe increase practically linearly with reactor pressure.

The following trends can be observed:

1) A lowered water level in the discharge line results in lower pressures during the vent clearing.

2) A hot pipe results in higher pressures during the vent clearing. This is due to the smaller percentage of condensation on the pipe wall.

3) The pressure (at the time of vent clearing) behind the SRV is always higher than the vent clearing pressure close to the quencher.

   The difference is attributable to the flow loss along the line.

4) The pressure (at the time of vent clearing) behind the SRV increases with increasing reactor pressure (or increasing steam flow rate through the relief valve).

Besides the clean-condition tests, there is a large number of real-condition tests and interval tests. Since the initial conditions in them were random and were not varied in a controlled manner, the measurement values are scattered over a much wider band than in the clean-condition tests. Hence, these tests are not usable for trend analyses, but may be used for verification of maximum specification values.

The measured maximum values are:

Pressure behind the SRV (at vent clearing time): 19 bar at a reactor pressure of 72 bar

Vent clearing pressure before the quencher: 14.5 bar at a reactor pressure of 72 bar

8.5.2.1.2 Vent Clearing Pressures for the Short Line

Figures 8-137 and 8-138 show the measured pipe pressures plotted against reactor pressure for clean condition tests with the short discharge line. The same trends as seen with the long line are seen here.

Since the short line has a smaller air volume than the long line, while the water column to be cleared and other parameters remain the same, the pressures in the short line are higher than those in the long line.

The measured maximum values are:

Pressure behind the relief valve (at vent clearing time):

22 bar at a reactor pressure of 73 bar.

Vent clearing pressure before quencher:

18 bar at a reactor pressure of 73 bar.

8.5.2.1.3 Transposition of the Measurement Values to SSES and Comparison with the Design Specification

The verification tests in Karlstein were run with the actual geometry of the relief system, the actual SRV, and the highest water level in the discharge line (6.2 m above center of quencher) that occurs for SSES.

The measured vent clearing times for that water level and a high reactor pressure (69 - 81 bar) was between 250 and 400 ms.

For these vent clearing times, the opening time of the SRV (measured opening times: 29 - 60 ms) has no noticable effect on the vent clearing pressure (see Figure 8-139).

Hence, in regard to the vent clearing pressure, the only variable whose maximum value for SSES was not completely covered was the reactor pressure.

The following extrapolation applies for that:

a) Pressure behind the valve at vent clearing time
The Measured maximum value for the long line is
19 bar at a reactor pressure of 72 bar
A Slope of 25% is seen in figure 8-135.
Extrapolating to 88 bar, the result is:
P_{max} = 23 bar for the long line
The Measured maximum value for the short line is
22 bar at a reactor presssure of 73 bar
A Slope of 25% is seen in figure 8-137.
Extrapolating to 88 bar, the result is:
P_{max} = 26 bar for the short line
The design value given in Section 4.1.2.1 is
550 psi = 37.93 bar.

The Karlstein tests demonstrate that the design value is very conservative for the vent clearing case.

b) Vent clearing pressure
The measured maximum value for the long line is
14.5 bar for reactor pressure of 72 bar.
A Slope of 12.5% is seen in figure 8-136.
Extrapolating to a reactor pressure of 88 bar results in
P_{max} = 16.5 bar for the long line.
The measured maximum value for the short line is
18 bar at a reactor pressure of 73 bar.
A Slope of 12.5% is seen in figure 8-138.
Extrapolating to a reactor pressure of 88 bar results in
P_{max} = 20 bar for the short line.
The specification value given in Section 4.1.1.2 is
P_{max}= 27 bar

The Karlstein tests demonstrate that the specification value for the vent clearing pressure is very conservative.

8.5.2.2 Pressures During the Stationary Condensation of Steam

About one second after the opening of the SRV, the vent clearing process is completed and the phase of sationary steam condensation begins.

In this phase, the pressures in the discharge line are determined by the steam mass flow and the flow resistance. Since the steam mass flow is proportional to the reactor pressure, here again we will investigate the dependence of the pipe pressures to the reactor pressure.

8.5.2.2.1 Long Line

Figures 8-140 and 8-141 show the dependence of the steady state pressure on the reactor pressure.

We see that the relation can be represented very well by a straight line.

As a result of pipe friction, the stationary pressure behind the SRV has higher values than the pressures just before the quencher. It also exhibits a faster increase with reactor pressure.

The measured maximum values are:
17.5 bar at reactor pressure of 72 bar
for the pressure behind the SRV (P4.1),
10 bar at reactor pressure of 70 bar
for the pressure before the inlet to the quencher (P4.4)

8.5.2.2.2 Short Line

Figures 8-142 and 8-143 show the dependence of the steady state pressure on the reactor pressure.

The behavior of the pressure before the quencher (P 4.4) is practically identical for the short line and long line. This is not surprising, since this pressure depends only on the flow resistance of the quencher.

The pressures behind the SRV are lower than those for the long line, but display the same increase with reactor pressure.

The different flow resistances of the two discharge lines are manifested here.

To clarify this effect, the variation of the stationary pressure at the measuring points along the discharge line are plotted in Figure 8-144 for the short and long lines. The average pressures were used, i.e., the pressures were read off from the interpolation lines at 88 bar (see Figures 8-140 to 8-143).

The measured maximum values for the short line are:
Pressure behind the SRV (P4.1)
16 bar at a reactor pressure of 72 bar, and
15 bar at a reactor pressure of 63 bar

Pressure before inlet to the quencher (P4.4)
9.5 bar at a reactor pressure of 71 bar, and
9.0 bar at a reactor pressure of 65 bar.

8.5.2.2.3 Transposition of the Measurement Values to SSES and comparison with the Design Specification

As was the case with the vent clearing pressure, the only variable whose maximum value in the SSES was not completely covered by the test stand was the reactor pressure.

An extrapolation of the measured maximum values to a reactor pressure of 88 bar yields the following results:

a) Long Line

The measured maximum value behind the SRV
is 17.5 bar at a reactor pressure of 72 bar.
A Slope of 22% is seen in figure 8-140.
Extrapolating to 88 bar, the result is:
P_{max} = 21 bar
The measured maximum value before quencher inlet is
10 bar at a reactor pressure of 70 bar.
A Slope of 16% is seen in figure 8-141.
Extrapolating to 88 bar, the result is:
P_{max} = 13 bar.

b) Short Line

The measured maximum value behind the SRV is 16 bar at a reactor pressure of 72 bar and 15 bar at a reactor pressure of 63 bar. A Slope of 22% is seen in figure 8-142.

Extrapolated to 88 bar the result is: P_{max} = 19.6 bar and 20.5 bar, respectively.

The measured maximum value before quencher inlet is
9.5 bar at a reactor pressure of 71 bar and 9 bar
at a reactor pressure of 65 bar.
A Slope of 16% is seen in figure 8-143.
Extrapolated to 88 bar, the result is:
P_{max} = 12.5 bar and 13.0 bar, respectively.

It can be stated that the design value of 550 psi = 37.93 bar for the stationary pressure behind the valve is very conservative.

8.5.2.3 External Loads on the Quencher and Bottom Support

In this Section we shall discuss the measurement results which provide information about the external loads on the quencher and bottom support. The measuring points provided for that purpose are shown in Figure 8-13, and are as follows:

SG 4.1/4.2	Bending at quencher arm 1
SG 4.3/4.4	Bending at quencher arm 2
SG 4.5/4.6	Bending at the bottom support
SG 4.7	Longitudinal strain at the bottom support
SG 4.8	Torsion at the bottom support

Strains were measured at all measuring points. The measured strains were used to calculate the loads which produced the strains. The loads thus calculated are static equivalent loads which contain hydraulic and also structural-dynamical effects.

8.5.2.3.1 Vertical Force

8.5.2.3.1.1 Measurement of the Vertical Force

To measure the vertical force, two strain gauges, SG 4.7, were connected in such a way that they measure strains resulting from vertical forces.

The following relation exists between the load and strain:

$$F_B = A_B \cdot E \cdot \varepsilon \qquad \text{where} \quad A_B = .016\ m^2$$

$$F_B = 3.3 \cdot \varepsilon \quad kN \qquad E = 2.06 \times 10^5\ N/mm^2$$

If we insert ε in $\mu m/m$, we then get the vertical force in kN.

This equation was used to convert the measured strains into vertical forces.

8.5.2.3.1.2 Measured Vertical Forces

Figure 8-145 shows a typical measurement trace for the vertical force. It increases rapidly during the expulsion of the water column and, after reaching the maximum value, returns quickly to zero.

8.5.2.3.1.2.1 Long Line

The vertical force exhibits a strong relationship with vent clearing pressure as shown in Figure 8-146. This holds true for all tests, even those with random initial conditions such as the real conditions and multiple actuation test.

As discussed in Section 8.5.2.1.3, the vent clearing pressure is inturn influenced by the reactor pressure, initial water column in the discharge line, discharge line temperature, etc. and was extrapolated out to a maximum reactor pressure of 88 bar. Therefore, the maximum vertical load will be extrapolated to the maximum vent clearing pressure from Section 8.5.2.1.3.

The measured maximum value for the vertical force is:

149 kN at a 12.8 bar vent clearing pressure.

8.5.2.3.1.2.2 Short Line

Figure 8-147 illustrates the dependence of the vertical force on the vent clearing pressure. In principle, the same discussion as in Section 8.5.2.3.1.2.1 for the long line applies here also.

The measured maximum value for the vertical force is:
192 kN at a 16.8 bar vent-clearing pressure.

The vertical forces relative to the vent clearing pressure are practically the same.

8.5.2.3.1.3 Transposition of the Measurement Values to SSES

As was discussed previously for the extrapolation of the vent clearing pressures, the measurement values for the vertical force can also be transposed directly to the plant. For verification of extreme conditions in the plant, the measurement values are extrapolated to a reactor pressure of 88 bar. The extrapolation can be performed directly via the vent clearing pressure.

8.5.2.3.1.3.1 Long Line

The measured maximum value was:
149 kN at a 12.8 bar vent-clearing pressure
Slope = 13 kN/bar (Figure 8-146)

According to Section 8.5.2.1.3, the extrapolated vent-clearing pressure for the long line was 16 bar.

Extrapolation of the vertical force to 16 bar yields:

$F_{V\,max}$ = 190 kN.

8.5.2.3.1.3.2 Short line

The measured maximum value was:
192 kN at 16.8 bar vent-clearing pressure
Slope = 13 kN/bar (Figure 8-147)

According to Section 8.5.2.1.3 the extrapolated vent clearing pressure for the short line was 20 bar.

Extrapolation of the vertical force to 20 bar yields:

$F_{Ymax} = 234$ kN

In addition Figure 8-147, shows a measured value of 149 kN at a 12 bar vent-clearing pressure. This leads to a maximum extrapolated vertical force of:

$F_{Y max} = 252$ kN.

8.5.2.3.1.3.3 Summary

The extrapolation of the measurement results for the vertical force yields a maximum value of:

$F_{Y max} = 252$ kN.

In Figure 4-11, the specified vertical force is given as 860 kN.

On the basis of the measurement results, the specification value can be viewed as extremely conservative, both in the maximum value and also in the load-versus-time function.

8.5.2.3.2 Torsional Moment

8.5.2.3.2.1 Measurement of the Torsional Moment

To measure the torsional moment, two strain gauges (SG 4.8 - Figure 8-13) were connected in such a way that they measure strain resulting from torsional moment only.

According to Reference 41, there is a very simple relation between the torsion or shear strain and the measured strain, when the strain gauges are mounted at a 45° angle relative to the principal shear stress direction.

We have:

$$\varepsilon = (1/2)\gamma$$

ε = strain

γ = shear strain

Therefore, since the strain gauges SG 4.8 were mounted at a 45° inclination to the vertical axis, we have:

$$\gamma = \frac{\tau}{G}$$

τ = shear stress

G = shear modulus

$$\gamma = 2 \cdot \varepsilon \text{ and } r = \frac{D_a}{2}$$

$$\tau = \frac{M_T}{I_p} \cdot r$$

M_T = torsional moment

I_p = polar moment of inertia

r = outside radius of the twisted cylindrical bar

$$\gamma = \frac{M_T}{G \cdot I_p} \cdot r$$

We thus obtain the relation between torsional moment and measured strain:

$$M_T = \frac{4 \cdot \varepsilon \cdot G \cdot I_p}{D_a}$$

The shear modulus is defined as

$$G = \frac{E}{2(1 + \mu)} \qquad \mu = \text{Poisson's ratio}$$

With $E = 2.06 \times 10^5$ N/mm² and

$$\mu = 0.3$$

We get:

$G = 7.9 \times 10^4$ N/mm²

The polar moment of inertia is defined as

$$I_p = \frac{\pi}{32} \cdot D_a^4 \; (1 - D_i^4 / D_a^4)$$

Therefore:

$I_p = 4.64 \times 10^{-4}$ m^4 .

Inserting the various numerical values, we get:

$$M_T = 0.413 \; \varepsilon$$

Inserting ε in μm/m, this equation gives us the torsional moment in kN-m.

This equation was used to convert the measured strains at SG 4.8 into torsional moments.

The torsional moments obtained in this manner represent static equivalent loads.

8.5.2.3.2.2 Measured Torsional Moments

Figure 8-148 shows a typical measurement trace for the torsional moments. After the end of the vent clearing process, (approximately 1 second after test start) the amplitudes of the measured torsional moments are very small compared to the maximum amplitude during the vent clearing process. There is a factor of 6-7 difference between the two of them. The maximum amplitude of the torsional moment occurs much later than the expulsion of the water column.

8.5.2.3.2.2.1 Long Line

The torsional moment at the bottom support has its origin only in unsymmetrical processes at the quencher during the vent clearing and during the transition to stationary condensation.

Figure 8-149 shows the dependence of the torsional moment on the vent clearing pressure. Since the vent clearing pressure is a direct influencing parameter (see Section 8.5.2.3.1.2.1) we will correlate the torsional moment with that value.

The sharply pronounced scatter band is an indication that a random process is superimposed on that dependence. That is expressed by the fact that the torsional moment is brought about by random unsymmetry.

The measured maximum value of the torsional moment is:

$M_{T\,max}$ = 55.8 kN-m at a 14 bar vent-clearing pressure.

8.5.2.3.2.2.2 Short Line

Figure 8-150 again shows the dependences of the torsional moment on the vent clearing pressure. In principle, the situation is the same as in the preceding Section for the long line.

The measured maximum value of the torsional moment is:

39.2 kN-m at a 18 bar vent-clearing pressure.

8.5.2.3.2.3 Transposition of the Measurement Values to SSES

When transposing the measurement results to SSES, we shall consider in a conservative manner the load carried by the discharge line, which in the test stand is connected rigidly (but not in a leaktight manner) to the quencher and bottom support by means of weld brackets(see Figure 8-13 and 8-14) in contrast to the free moving sliding joint at SSES. To do that, we make the assumption that the discharge line is fixed in a torsion resisting manner at the first bend above the quencher.

That results in the following picture:

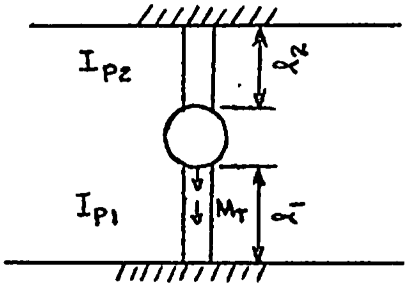

Discharge Line

Quencher

Bottom support

The torsional moment M_T acts at the quencher. The torsional moment M_{T1} was measured at the bottom support. The discharge line carries the torsional moment M_{T2}.

Therefore:

$$M_T = M_{T1} + M_{T2}$$

From the equality of the rotation, we get:

$$\gamma_1 \cdot \ell_1 = \gamma_2 \cdot \ell_2$$

$$\gamma = \frac{\tau}{G} = \frac{M_T\, r}{I_p\, G}$$

Therefore:

$$\frac{M_{T1} \cdot r_1 \cdot \ell_1}{G \cdot I_{p1}} = \frac{M_{T2} \cdot r_2 \cdot \ell_2}{G \cdot I_{p2}}$$

$$\frac{M_{T1}}{M_{T2}} = \frac{I_{p1}}{I_{p2}} \cdot \frac{r_2 \cdot \ell_2}{r_1 \cdot \ell_1}$$

We have the following dimensions:

$r_{1a} = 0.1775$ m $\qquad r_{2a} = 0.162$ m

$r_{1i} = 0.125$ m $\qquad r_{2i} = 0.1445$ m

$\ell_1 = 0.45$ m $\qquad \ell_2 = 11.313$ m

Therefore:

$$I_{p1} = 4.64 \cdot 10^{-4}\ m^4$$

$$I_{p2} = 4.0 \cdot 10^{-4}\ m^4$$

Therefore:

$$\frac{M_{T1}}{M_{T2}} = \frac{4.64}{4} \cdot \frac{0.162}{0.1775} \cdot \frac{11.313}{0.45} = 26.6$$

$$M_{T2} = \frac{1}{26.6}\ M_{T1}$$

$$M_T = M_{T1} + M_{T2} = M_{T1}\ (1 + \frac{1}{26.6})$$

$$M_T = 1.0376 \cdot M_{T1}$$

Thus, the load transmitted to the discharge line is less than 4% of that transmitted to the bottom support.

If, without taking into consideration the discharge line, we first use Figures 8-149 and 8-150 as the basis for an extrapolation of the measured maximum values to maximum vent-clearing pressure for the corresponding discharge line, then we get the following maximum values:

a) long line

$M_{T1\ Max} = 59.8$ kN-m

b) short line

$M_{T1\ Max} = 43.2$ kN-m

If we now consider the torsion carried by the discharge line, then this value is increased to a maximum of:

$M_{T1\ Max} = 62$ kN-m

The torsional moment specified in 4.1.2.6 for the quencher support was 40 kN-m to be applied as a step function. A torsional moment step function applied to an undamped one mass oscillator (quencher acting as inertial mass and bottom support as a torsional spring) corresponds to a maximum response of:

M_{TA} = 2(40) kN-m = 80 kN-m

Since the maximum torsional moment derived from the Karlstein tests is $M_{T,Max}$ = 62 kN-m, the specification is conservative.

8.5.2.3.3 Bending Moments at the Quencher Arms

8.5.2.3.3.1 Measurement of the Bending Moments

In the Karlstein tests, the bending moments were measured in the horizontal plane (parallel to the tank's bottom) and also in the vertical plane, at both of the quencher arms.

To accomplish that, two strain gauges each were connected in such a way that they measured unsymmetrical strains resulting from normal stresses (unsymmetrical component). The following strain gauges were mounted for that purpose (see Figure 8-13:

SG 4.1) Moments in vertical direction
SG 4.3)

SG 4.2) Moments in horizontal directon
SG 4.4)

The strain gauges were mounted approximately 150 mm from the weld between the quencher arm and the central ball.

The section modulus of one quencher arm is:

$$W = \frac{\pi}{32} D_a^3 \left(1 - \frac{D_i^4}{D_a^4}\right)$$

$$D_a = 0.4064 \text{ m}$$

$$D_i = 0.3744 \text{ m}$$

We have:

$$\sigma = \varepsilon \cdot E = M_B/W$$

$$M_B = \varepsilon \cdot E \cdot W$$

This leads to the equation between quantities: $M_B = 0.38 \cdot \varepsilon$

This gives the bending moment in kN-m, if ε is inserted in μ m/m.

With this equation, all the measured bending strains were converted into bending moments. The bending moments thus calculated are static equivalent loads.

8.5.2.3.3.2 Measured Bending Moments

Figure 8-151 shows a typical measurement trace of the measured bending moments at the quencher arms. We see clearly that the maximum values occur much later than the clearing of the quencher.

The evaluation of the individual bending moments relates to the total resultant bending moment, i.e., the bending moment which actually loads the quencher arm. The resultant bending moment is obtained by using the relationship:

$$M_{res} = \sqrt{M_y^2 + M_z^2}$$

The bending moments M_y are read off at SG 4.2 and 4.4. The bending moments M_z are read off at SG 4.1 and 4.3. The resultant bending moments exhibit no deterministic dependence on the vent clearing pressure, as shown in Figure 8-152. Therefore, the resultant bending moments on the quencher arms must be considered as statistical values.

The measured maximum value of the resultant bending moment is 63 kN-m.

8.5.2.3.3.3 Transposition of the Measurement Results into the Weld

In Section 4.1.2.5, the bending moments in the weld were specified. In the Karlstein test stand, the strain gauges were mounted about 150 mm from the weld in order not to measure localized stresses due to the weld and the intersection between the ball central body and the quencher arm. Available experience indicates that this distance is sufficient to measure a stress profile which is independent of shape factors.

From the specified force and moment (Table 4-10), we obtain for the distance between the weld and the force producing the bending moment:

$$l_F = \frac{19}{29} = 0.655$$

By treating the quencher arm as a cantilever beam, we obtain for the maximum stress and thus for the maximum bending moment:

$$M_{B\,max}/0.655 = M_{B\,meas}/(0.655-0.15)$$

$M_{B\,max}$ = bending moment in the weld

$M_{B\,max}$ = measured bending moment

Therefore:

$$M_{B\,max} = 1.297\ M_{B\,meas}$$

Thus, based on the measured maximum resultant bending moment of 62 KN-m (see Section 8.5.2.3.3.2), we obtain the following maximum bending moment in the weld:

- Maximum resultant bending moment: 81 kN-m

8.5.2.3.3.4 Specified Static Equivalent Loads

As already noted above, the measured bending moments are to be considered as static equivalent loads.

In Section 4.1.2.5 Table 4-10, two contributions were specified with respect to the bending moment in the weld:

a) a step function having a step height of 19 kN-m

b) a maximum differential pressure which, according to Section 4.1.3.7, is 0.8 bar from KKB trace No. 35 with a 0.5 multiplier. This results in a maximum differential pressure of 0.4 bar.

The contribution of the differential pressure is to be viewed statically, since, according to Section 4.1.3.5, the frequency of the differential pressure is approximately 6 Hz. The bending eigenfrequency of the quencher arm is on the order of 100 Hz. The contribution of the differential pressure to the bending moment in the weld is thus:

11.4 kN-m

The contribution of the step funcion is to be viewed dynamically. Therefore, the same considerations are applicable as those made for the torsional moments in Section 8.5.2.3.2.3. Accordingly, we have the following static equivalent loads:

Component in one Direction

Contribution from step function = 2 X 19 = 38 KN-m

Contribution from differential pressure = 11.4 KN-m

Total = 49.4 KN-m

Resultant Moment

Contribution from step function = 38 x $\sqrt{2}$ = 53.7 KN-m

Contribution from differential pressure = 11.4 KN-m

Total = 65.1 KN-m

8.5.2.3.3.5 Evaluation of the Measurement Results

As already mentioned in Section 8.5.2.3.3.2, the bending moments on the quencher arm are to be treated as statistical values. Figure 8-153 shows the frequency distribution of the measured maximum bending moments in each tests and the resulting frequency disribution of the values transposed in to the weld.

The frequency distributions are based on the peak maximum value of each individual test, which were measured either at SG 4.1/4.2 or at SG 4.3/4.4.

The specified static equivalent loads (see Section 8.5.2.3.3.4 are introduced for 7000 responses of the relief valve. Therefore, the loads are to be evaluated in a fatigue analysis.

It follows from Figure 8-153 that the mean value of the measured maximum values transposed into the weld is 35 kN-m.

Except for three cases, the specified resultant bending moments also cover the maximum measured values. The quencher is being evaluated for these measured maximum values.

It should be noted that both the specified stationary internal quencher pressure of 22.0 bar and the resulting thermal load of 219°C were found to be very conservative when compared to the maximum extrapolated values of 13.0 bar and the resulting saturated steam temperature of 195°C measured during the tests. (Section 8.5.2.2.3).

8.5.2.3.4 Bending Moments at the Bottom Support

8.5.2.3.4.1 Measurement of the Bending Moments

To measure the bending moments a the bottom support, two strain gauges capable of measuring the bending strains were mounted. In the measurement arrangement, the bending strains could be measured in two mutually perpendicular directions (see Figure 8-13). The strains for moments about the x-axis were measured with the strain gauges SG 4.5. The strains for moments about the y-axis were measured with the strain gauge SG 4.6.

The section modulus of the bottom support is:

$$W = \frac{\pi}{32} D_a^3 \left(1 - \frac{D_i^4}{D_a^4}\right)$$

$$W = 1.307 \times 10^{-3} \text{ m}^3$$

We have

$$\sigma = E \cdot \varepsilon = M_B/W$$

This leads to the equation:

$$M_B = 0.27 \cdot \varepsilon$$

This equation gives the bending moment in kN-m, if ε is inserted in µm/m.

This equation was used to convert all measured bending strains of the bottom support into bending moments. The bending moments thus calculated are static equivalent loads.

<u>8.5.2.3.4.2 Measured Bending Moments</u>

In Figure 8-151, the bending moments at the bottom support can be seen under the traces of the bending moments at the quencher arms.

The maximum values occur at a later time than the vent clearing. But they occur at the same time as the maximum values of the bending strains at the quencher arms. The maximum strain resulting from torsion does not occur at the time of the maximum bending strain (see Figure 8-151, SG 4.8).

The evaluation of the bending moments relates to the resultant bending moment, i.e., the bending moment which actually loads the bottom support. The resultant bending moment is obtained by interconnecting the actual load-versus-time functions of the individual components through the relation:

$$M_{res} = \sqrt{M_x^2 + M_y^2}$$

The bending moments M_x are read off at SG 4.5 and the bending moments M_y at SG 4.6.

The maximum resultant bending moment was 54.5 kN-m.

The resultant bending moments display no dependence on the vent clearing presure, as shown in Figure 8-154. Hence, the same conclusions that were drawn for the bending moments at the quencher arms are applicable here, also.

8.5.2.3.4.3 Specified Static Equivalent Load

As already mentioned, the measured bending moments are to be viewed as static equivalent loads.

The bending moments at the bottom support are introduced through the quencher.

Section 4.1.2.4 and Table 4-7 specify a transverse force of 44 kN on the quencher was used as step function.

In addition, a maximum differential pressure of 0.4 bar on the quencher was specified. The contribution resulting from the differential pressure is to be viewed as a statically acting load. It amounts to 48 kN.

Note: The discharge line and the bottom support were not considered here. The presssure difference was formulated only over the projected area of the quencher.

The specification then yields the following transverse forces on the quencher:

Contribution from step function = 2 x 44	= 88 kN
Contribution from differential pressure	= 48 kN
Total	= 136 kN

Strain gauges SG 4.5 and SG 4.6 were mounted approximately 0.5 m below the center of the quencher. Transposed to this location, the specification yields:

68 kN-m

8.5.2.3.4.4 Evaluation of the Measurement Results

Figure 8-155 shows the frequency distribution of the measured maximum bending moments at the bottom support. The measured maximum values are also covered by the specification.

Thus, the Karlstein tests have demonstrated that the specified transverse forces on the quencher can be viewed as very conservative.

8.5.2.3.5 Forces on the Quencher

In the Karlstein Quencher Tests, only bending moments were able to be determined for the quencher itself. In Section 4.1.2, forces and moments on the quencher were specified. The specified moments were calculated from the forces. The measured moments are within the specification. Therefore, we can conclude that the forces are also verified.

8.5.2.3.6 Influence of an Adjacent Quencher

During the clearing of the quencher, strong turbulences and eddies of the expelled and ambient water develop around the discharging quencher. In particular, after the vent clearing the quencher is surrounded by a large number of air bubbles which represent a locally compressible volume in the water. This state, which forms around the discharging quencher, prevents effects from the blowdown of an adjacent quencher from penetrating to the quencher under consideration.

It is therefore understandable that, in the KWU in plant tests within the Brunsbuttel and Philippsburg nuclear power plants, no increase of the load on the quencher and bottom support was found for the response of several quenchers in comparison to the response of one quencher (Reference 6).

An effect of a load on one quencher due to the firing of an adjacent quencher is to be observed only when the adjacent quencher blows down alone.

In that case, a detailed evaluation was made for the Brunsbuttel blowdown tests (Reference 38).

The result of the investigation was that the measured loads are enveloped by a pressure difference of 0.2 bar applied over the adjacent internal structures in the pool at the quencher level, i.e., also over the quencher.

A maximum pressure difference of 0.4 bar over the quencher arms was specified for SSES. The vent clearing pressures and dynamic pressures in the water pool obtained for SSES from the Karlstein tests are of the same order of magnitude as the corresponding measurement results in Brunsbuttel.

Therefore, the specified differential pressure of 0.4 bar over the quencher arms can be viewed as conservatively enveloping.

8.5.2.3.7 Loads on the Quencher During Steam Condensation

The maximum mechanical and thermal loads on the quencher during the condensation phase occur during the phase of intermittent condensation. In Section 4.1.2.7, the loads resulting from intermittent condensation were taken as the basis for the fatigue design of the quencher.

The evaluation of the loads on the quencher during steam condensation in the Karlstein tests therefore relates primarily to the phase of intermittent condensation.

8.5.2.3.7.1 Manifestation Forms of Intermittent Condensation in the Karlstein Tests

As discussed in Section 8.1.3, the condensation tests were performed along the lower and upper boundary lines of the operation field for water temperatures ≤30°C and also for water temperatures ≥59°C. In both regions, the intermittent condensation phase occurs for very low reactor pressures (approximately between 2 and 4 bar). In Section 8.4.2 it is shown that the maximum values for the dynamic pressures in the water region occur during intermittent condensation in cold water. The same is true also for the loads on the quencher.

For the evaluation and comparison with the specification, we use the measurement values of the bending moments at the quencher during the intermittent condensation in the cold pool. The measurement values are documented in Section 8.4.2.

8.5.2.3.7.2 Illustration of the Measurement Values

The time duration of the intermittent condensation in the cold pool was about 100 seconds. The total number of condensation events at the quencher was 52. The maximum measurement values occurred in the vertical direction at SG 4.3.

The frequency distribution of the resultant bending moments (SG 4.3/4.4) at the quencher arm is show in Figure 8-156. The mean value of the maximum measurement values of each event is 11.8 kN-m. The maximum measured value was 66.5 kN-m.

The frequency distribution of the resultant bending moments (SG 4.5/4.6) at the bottom support is shown in figure 8-158.

The mean value of the measurement values is 8.9 kN-m. The maximum value was approximately 30 kN-m.

The measured maximum value of the torsional moment during the intermittent condensation is 6.2 kN-m.

8.5.2.3.7.3 Evaluation of the Measurement Results for the Quencher Arm

Figure 8-157 shows the frequency distribution of the resultant bending moments, which were transformed from the measuring point into the weld (see Section 8.5.2.3.3.3. The mean value of these bending moments is 15.2 kN-m. The maximum value is 86 kN-m.

The measured bending moments represent static equivalent loads. In Section 4.1.2.7 and Table 4-12, a value of 25.4 kN-m was specified for the equivalent load for the resultant bending moment in the weld during intermittent condensation. The loads specified are formulated for an occurrence frequency of 10^6.

In the fatigue analysis, the mechanical loads represent only one load component. Another part of the fatigue loading is produced by the alternating thermal loading. The assumption made in the specification was 10^6 temperature steps from 35°C to 133°C and from 133°C to 35°C.

The low-frequency oscillations of the pipe's internal pressure measured at P4.4 are used as a basis for the measured temperature alternation. The saturated-steam temperatures are then correlated with those pressures.

The pressure oscillations have an oscillation frequency of about 0.5 Hz and a maximum amplitude of 0.5 bar overpressure = approx. 2 bar absolute pressure. This pressure lies below the specified value of 3 bar.

The measured maximum pressure of 2 bar corresponds to a saturated-steam temperature of 120°C. Assuming that the inflowing water in SSES is at a temperature cf at least 35°C, then the temperature step is 85°C.

A temperature step of 98°C is assumed in the specification, so that there is a reserve of 13°C.

The measurement values forming the basis for the evaluation and comparison with the specification were observed only during the phase of intermittent condensation with cold water in the test tank.

As with the boundary pressures in the test tank (Section 8.4.2), the loads on the quencher were considerably lower during the intermittent condensation phase with warm water than during intermittent condensation with cold water. The measured maximum bending moment during this condensation phase was <1 kN-m relative to the weld seam.

In addition, KWU in plant tests in the Brunsbuttel nuclear power plant showed that for a pool water temperature of approximately 35° and above, intermittent condensation loads on a quencher were smaller. This indicates that the region where intermittent condensation loads of any consequence can be expected is limited to that of very low pool temperatures (approximately 25°C) and very low steam mass flows and that heating of the pool a small amount results in a reduction in loading.

8.5.2.3.7.4 Evaluation of the Measurement Results for the Bottom Support

An impulsively acting transverse force of 17.5 kN was specified on the quencher for intermittent condensation.

The distance from the middle of the quencher to the measuring point for the bending moments at the bottom support is 0.5 m, so that the specified bending moment with respect to the bottom support is:

(17.5 kN x 2) x 0.5 m = 17.5 KNm (static equivalent load)

The maximum resultant bending moment from the tests is approximately 30 KN-m.

8.5.2.3.7.5 Evaluation of the Measured Torsional Moments

An impulsively acting torsional moment of 19 kN-m was specified for the intermittent condensation.

This step function yields a torsional moment of:

38 kN-m as the static equivalent load

The specified torsional moments conservatively envelop the measured maximum value of 6.2 kN-m.

8.5.2.3.7.6 Evaluation of the Measured Maximum Moments at the Quencher Arm during Intermittent Condensation

A maximum resultant bending moment of 66.5 kN-m at the quencher arm was measured in the intermittent condensation phase, which results in a moment of 86 kN-m in the weld. The measured maximum values of the resultant bending moments at the quencher arm during intermittent condensation are on the order of magnitude of the measured maximum vlaues during the vent clearing phase (Section 8.5.2.3.3.2).

For the vent clearing, a temperature difference of 184°C was specified. For the intermittent condensation, a temperature difference of 98°C was specified.

The total stresses loading the quencher arm are composed of mechanical and thermal stresses. The thermal stresses are distinctly larger than the mechanical stresses.

The maximum resultant bending moment at the quencher arm for intermittent condensation exceed the value specified for the vent clearing by about 40%. However, the associated temperature jump is only about half as large as for the vent clearing.

8.5.3 Verification of Suppression Pool Boundary Load Specification Due to SRV Actuation

In Section 4.1.3, three pressure time histories are specified as the basis for the containment analysis due to SRV actuation. The three traces were taken from a large number of bottom pressure time histories from various KKB in plant tests.

The evaluation of the pressure oscillation measurements in the Karlstein vent clearing tests will therefore concentrate on demonstrating that the pressure time histories specified are enveloping.

Accordingly, analysis and assessment of the individual measured pressure time histories is restricted to a minimum.

8.5.3.1 Evaluation of the Local Effects Seen at Pressure Transducer P5.5

As shown in Figures 8-10 to 8-12, the pressure transducer P5.5 is mounted on the concrete wall opposite the middle of the hole array on the quencher arm.

About 0.25 seconds after expulsion of the water column, P5.5, in comparison with the other pressure transducers, exhibits high-frequency positive pressure peaks which are not observed at the neighboring pressure transducers. This effect is from the local turbulences.

These high frequency pressure peaks have a small energy content so that their range of action is limited to the immediate vicinity of the pressure transducer.

The following Table should make this clear. In this Table, the ratio of the measured pressure amplitudes of the neighboring pressure transducers (P5.10 and P5.4) to the pressure maximum at P5.5 is indicated for all tests which exhibited a maximum pressure amplitude ≥ 1 bar at pressure transducer P5.5.

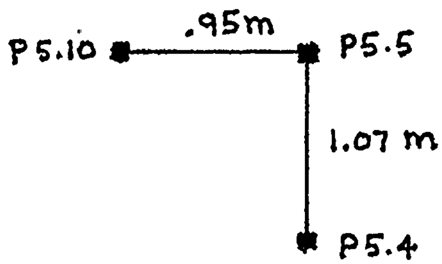

Test	P5.4 (bar)	P5.10 (bar)	P5.5 (bar)	P5.4/5.5	P5.10/P5.5
4.1.6	0,6	0,55	1,0	0,6	0,55
5.1.7	0,45	0,4	1,0	0,45	0,4
10.R1.7	0,73	0,55	1,7	0,43	0,32
20.R1.9	0,45	0,4	1,0	0,45	0,4
20.R1.10	1,0	0,65	1,73	0,58	0,38
25.1	0,55	0,6	1,0	0,55	0,6
25.R2	0,85	0,8	1,55	0,55	0,52

From this Table we can see that the measurement value has decayed by half at about 1 m from the measuring point P5.5.

The comparison measurement points P5.4 and P5.10 are in the region of origination of the air bubble oscillation, so that no attenuation effect due to distance effects could occur at that measuring point. Therefore, the sharp decrease of the pressure amplitude which is measured nevertheless shows clearly that the pressure measured at pressure transducer P5.5 is limited to its local vicinity.

As further verification that this effect is limited to the area around pressure transducer P5.5, a comparison is mâde between the power spectral densities from P 5.5 and the bottom pressure transducer P 5.2.

The following tests were selected:

Test 11.1 This test exhibited the highest power spectrum at the dominant frequency

Test 4.1.6 This test exhibited the highest pressure amplitude at P5.5 for the long discharge line

Test 20.R1.10 This test exhibited the highest pressure amplitude at P5.5 for the short discharge line.

The comparison can be summarized as follows:

At the dominant frequency, the power densities are the same magnitude for the pressure oscillations at the bottom pressure transducer P5.2 and at pressure transducer P5.5.

The differences at the higher frequencies is significant. For tests 4.1.6 and 20.R1.10 the frequency spectrum of P5.5 exhibits significantly higher power densities at higher frequencies than the corresponding frequency spectrum at pressure transducer P5.2.

This significant factor is not noted for the frequency spectrum of test 11.1 (see Figures 8-159 and 8-160). In that test, the difference between the maximum pressure amplitudes for pressure transducers P5.5 and P5.2 was 0.13 bar. The pressure ratio is P5.5/P5.2 = 0.78/0.65 = 1.2.

In test 4.1.6, the difference in the power densities at the higher frequencies is already more strongly evident (see Figures 8-161 and 8-162). In that test, the difference between the maximum pressure amplitudes for P5.5 and P5.2 was 0.5 bar. The pressure ratio is P5.5/P5.2 = 1/0.5 = 2.

The difference in the power densities at the higher frequencies is quite strongly pronounced in tests 20.R1.10 (see Figures 8-163 and 8-164). The difference in the maximum pressure amplitudes for P5.5 and P5.2 was 1.1 bar in that test. The pressure ratio is P5.5/P5.2 = 1.73/0.63 = 2.75.

The pressure differences or pressure ratios are not discernible in the power spectra for the dominant frequencies, but are at the higher frequencies. From that we can conclude that the pressure oscillation which was measured at pressure transducer P5.5 has approximately the same amplitude at the dominant frequency as the pressure oscillations which were measured elsewhere in the vicinity of the quencher, e.g., at P5.2.

In addition, higher frequency pressure oscillation components having a high amplitude are occasionally superimposed on the fundamental oscillation in the pressure oscillations at P5.5. The higher frequency components, which occur at pressure transducer P5.5, decay rapidly in time and space, so that the effect of the high frequency pressure oscillations remains limited to the immediate vicinity of measuring location P5.5. Therefore, as stated before, the measurement results for the dynamic pressures at P5.5 represent local events having no global effect on the containment.

We will therefore not consider the positive pressure measurements at P5.5 when verifying the design specification for the overall containment analysis the results from this gage are included for the verification of the loadings on the columns.

8.5.3.2 Verification of the Specified Pressure Amplitudes and Vertical Pressure Profiles after Vent Clearing

The measured peak pressure amplitudes for the 125 vent clearing tests are tabulated in Tables 8.9 and 8.10. Section 8.4.1 also presents a number of Figures (8.27 to 8.34) which show that the pressure amplitudes measured in the tests had no significant dependence on the initial reactor pressure. Therefore, no modification to the measured pressures will be made to account for differences in the reactor pressure between SSES and the Karlstein test stand. In addition, as explained in the previous section, the positive pressure measurements a P5.5 will not be considered when verifying the design specification for the overall containment analysis.

8.5.3.2.1 Overpressures

The maximum over pressure amplitude measured on the boundary of the Karlstein test tank was 1.0 bar. That pressure was measured at the concrete wall (p5.4) in test 20.R1.10. A maximum pressure amplitude of 1.2 bar is specified in section 4.1.3 (KKB Pressure Trace No. 35 with the 1.5 multiplier). The maximum specified overpressure amplitude of 1.2 bar evelops the measured maximum overpresure amplitude of 1.0 bar.

8.5.3.2.1.1 Vertical Pressure Profile

It can be assumed that the maximum dynamic pressure will occur in a sphere which surrounds the quencher and has approximately the radius of a quencher arm, (5'-0").

At some distance from it, the maximum value will be attenuated in accordance with a distance law. For an infinite water space, the 1/R law is applicable for the decrease of the pressure with distance from the source. That law applies in all directions, i.e., in the vertical direction also. The validity of the 1/R law is based on the assumption of a stationary (i.e., fixed position) oscillating bubble in the infinite water space. That ideal case does not hold for the clearing of the relief system. Already shortly after the expulsion of the air-steam mixture, small air particles move to the surface of the pool because of buoyancy. Even more important, however, is the fact that the water surface and the tank boundary surfaces influence the distance law and that the pressure amplitude must vanish at the water surface itself.

Accordingly, a pressure profile in the vertical direction is specified in Section 4.1.3.4 providing for a constant pressure at 6'0 (1.83 m) above the suppression pools bottom and, starting at that height, a linear decrease of pressure up to the water surface.

Figure 8-165 shows that the maximum specified pressure distribution very conservatively envelops the measured maximum pressure amplitudes. The conservativeness becomes clearly evident if, based on the measured maximum value of wall pressure amplitude of 1 bar at pressure transducer P5.4, we assume a linear decrease of pressure from that measuring point to the water surface. That assumed linear pressure decrease (depicted in Figure 8-165 by a dashed line) also envelops the maximum pressure amplitudes measured in the vertical direction. In comparison with the assumed linear pressure decrease and the specified pressure distribution, the conservativeness of the specification becomes obvious.

8.5.3.2.1.2 Vertical Pressure Profile Including Local Effects at P5.5

For the evaluation of the unpertubed pressure distribution in the vertical direciton, the measuring point P5.5 was omitted, even though it lies in a direct line with the pressure transducers P5.4, P5.6 and P5.7. Because of the local effect for P5.5, a separate analysis shall be performed here.

That analysis starts with an estimation of the vertical zone of influence associated with the pressure peak measured at P5.5.

The lateral holes in the quencher arms extend over an angle range of 72° on each side. The holes are drilled radially, so that in first approximation we can assume a source flow of the emerging fluid. The high-frequency pressure peak at P5.5 occurs at a much later time than the vent clearing. It can be supposed that at that time there is a steam-air mixture flowing out of the quencher. The steam-air jets emerging from the holes have a high degree of turbulence. Thus, the edges are very soon mixed with the surrounding water. Furthermore, the emerging steam is condensed immediately and the expelled air is cooled down quickly, so that the expelled compact volume is reduced rapidly. Therefore to estimate the range of action, it is assumed that the source flow acts over a mean angle range of $\theta_m = \theta/2 = 72°/2 = 36°$. The total range of action is then

b = x tan 36° x = 1.575 m (distance from centerline of
b = 1.14 m quencher arm to concrete wall)

This range of action of 1.14 m is divided into equal parts above and below the measuring point P5.5, so that we obtain a range of action of ±0.57 m relative to the measurement location.

Based on this range of actin the measured vertical pressure distribution considering the local effect is compared with the specified pressure distribution in Figure 8-166. The base points of the pressure elevation at P5.5 were placed on the straight line of the linear pressure drop symmetrically with respect to the quencher's center plane.

From Figure 8-166 it can be seen that the maximum specified pressure distribution results in a larger resultant force on the containment boundary and columns than does the measured pressure distribution including consideration of the local effect. This means that the overall specified pressure distributrion in the vertical direction also envelopes the local pressure elevation at P5.5.

8.5.3.2.2 Underpressures

The maximum underpressure amplitude measured on the boundary of Karlstein test tank was -0.68 bar. That pressure was measured a the concrete wall (P5.10) in test 25.R2. A maximum underpressure amplitude of -0.56 bar is specified in Section 4.1.3 (KKB Pressure Trace No. 76 with the 1.5 multiplier).

The next largest underpressure recorded during test 25.R2 was -0.50 bar.

The next largest underpressure recorded anywhere during the vent clearing tests was -0.58 bar at P5.2 in test 25.1.

Except for the two measurement values called out above all other measured underpressures were bounded by the maximum specified value of -0.56 bar.

8.5.3.2.2.1 Vertical Pressure Profile

Figure 8.167 shows a plot of the maximum specified underpressure distribution and the maximum measured underpressure values for the Karlstein tests.

It can be seen that, except for the one value at P5.10 for test 25.R2, the maximum specified pressure distribution envelops the maximum measured pressure amplitudes.

In addition, for SSES, the most unfavorable boundary condition in this comparison is the low liquid level of 22 ft = 6.70 m in the suppression pool.

The hydrostatic pressure distribution with respect to that liquid level is indicated by a dashed line in Figure 8-167.

The comparison of the measured worst underpressure distribution with the hydrostatic water load resulting from the worst boundary condition for this comparison (lowest water level in the suppression pool) shows that the compressive forces from the water load and the tensile forces from the underpressure distribution maintain the equilibrium. Thus, the Karlstein tests have, in addition, demonstrated that the blowdown of the SSES relief system with the quencher does not result in any resultant tensile forces on the steel liner, even for the worst possible superposition.

8.5.3.3 Verification of the Pressure Time Histories Used for the SSES Containment Analysis

In order to verify that the pressure time histories used for the SSES dynamic analysis due to SRV actuation are bounding, the Power Spectral Densities (PSDs) of the specified time histories (with the appropriate amplitude increase and frequency range from Section 4.1.3) are compared with the PSD's of the appropriate time histories recorded in the Karlstein test tank and transposed to the SSES suppression pool.

Statements concerning the clearing of parallel quenchers are based on the unrealistic and extremely conservative assumption that the expelled air bubbles are equally large and oscillate in phase. A quantification of that conservativeness is not given.

We will first discuss and verify the theory to be used to transpose the oscillation frequencies measured in the test tank to the suppression pool. Then, the appropriate multipliers for this frequency transposition will be established. A discussion is also provided for transposing the measured pressure amplitudes to the suppression pool. Finally, the actual verification is presented.

8.5.3.3.1 Transposition Method for the Oscillation Frequency

The theoretical basis for the transposition of the pressure time histories measured in the Karlstein tests to the SSES suppression pool is provided by the KWU computer codes VELPOT and KOVIB1A.

By using the test results from the PP&L quencher tests in Karlstein, the GKM quencher tests, and the non-nuclear hot tests in the Brunsbuttel nuclear power plant (KKB hot tests), we shall first confirm experimentally the correctness of the transposition theory. That is followed by a calculation of the frequencies for the following three blowdown cases:

(1) Simultaneous blowdown of all 16 quenchers
(2) Simultaneous blowdown of the 6 quenchers related to the automatic depressurization system (ADS)
(3) Blowdown of one outer quencher

For each case, a comparison of the theoretically calculated frequencies with the frequencies measured in the test stand) provides a number (frequency multiplier) by which a frequency measured in the test stand must be multiplied in order to get the corresponding frequency in the SSES suppression pool.

A factor for the influence of the suppression pool overpressure is also determined in the same way. The corresponding measured pressure time history is transposed to the plant by dividing by this factor .

8.5.3.3.1.1 Calculation of Measured Oscillation Frequencies

8.5.3.3.1.1.1 PP&L Tests at Karlstein

Since it was found that Fluid-Structure Interaction in the Karlstein test tank has no significant influence on the measured pressure time histories, it is sufficient to carry out the analysis for a rigid tank. The comparison of calculated and measured oscillation frequencies will be based on the assumption of equal bubble volumes. The measured oscillation frequencies are taken from Tables 8.9 and 8.10 . The associated bubble volumes were calculated from the test data, using the formula:

$$V_B = V_{pipe} \frac{[P_{pipe} - \varepsilon P_{sat} (T_{pipe})]}{[P_h - P_{sat} (T_{pool})]} \frac{T_{pool}}{T_{pipe}}$$

V_{pipe}	free pipe volume (m^3)
P_{pipe}	pressure in pipe (bar)
P_h	hydrostatic pressure at the quencher location (bar)
P_{sat}	saturation steam pressure (bar)
ε	relative humidity ($\varepsilon = 1$ at 100%)
T_{pool}	water temperature (°C)
T_{pipe}	mean temperature in pipe (°C)

The averaging of the temperature in the pipe is performed by using the formula

$$\frac{1}{T_{pipe}} = \frac{1}{N} \sum_{i=1}^{N} \frac{1}{T_i}$$

where the pipe was divided into N equal sections. The temperature T_i in the i th section was obtained by interpolation between the measured temperatures.

The comparison between the measured and calculated bubble frequency is shown in Figures 8-168 and 8-169 in which the bubble pulsation frequency is plotted versus the equilibrium volume at static pressure. For the measurement points in Figure 8-168 it was assumed that dry air was in the pipe prior to the test start, while wet air (100% humidity) was assumed in Figure 8-169. In general, good agreement is found between the theory and measured frequency. However, we cannot overlook the fact that the measured frequencies in figure 8-168) are higher than the calculated ones, especially for small bubble volumes. This may be related to the fact that the active volume of air under water is actually smaller than the volume found for dry air from the test data. This is hinted at by the calculation of the bubble volume under the assumption of 100% humidity in the pipe. There the measurement points are closer to the calculated curve (Figure 8.169). In order to keep the uncertainties associated with such effects as small as possible, only tests for which the initial pipe temperature was below 70°C were chosen for the comparison with the theoretical case.

8.5.3.3.1.1.2 GKM Model Quencher Tests

Another sorce used to verify the theory is offered by the GKM quencher tests (Ref. 1). Since the pipe temperatures there were in the vicinity of 30°C or below, uncertainties in the bubble volume under water are distinctly smaller than in the Karlstein tests. In addition, the GKM tests were also run with backpressure in the suppression chamber, so that information derived from the computer codes for blowdown of the quencher during a loss-of-coolant accident can also be verified. The results can be found in Figures 8-170 and 8-171. Figure 8-170 shows the calculated and measured dependence of the pulsation frequency on the bubble volume for various submergences (2 m, 4 m and 6 m) with atmospheric pressure in the suppression chamber. The theory and measured frequency agree even better here than in the Karlstein quencher tests. This is probably due to the fact that the bubble volumes determined from the measurement values have a much smaller scatter due to the low temperatures in the pipe. The influence of backpressure on the pulsation frequency is shown in Figure 8-171. Here again, the theory is verified by the test data.

8.5.3.3.1.1.3 KKB Hot Tests

In order to demonstrate the correctness of the theory for in-plant conditions also, calculations were performed for the blowdown tests with one valve in the non-nuclear hot tests in the Brunsbuttel BWR plant (Ref. 3). Figure 8-172 shows the results. The agreement between the calculated and measured frequency is similar to that in the Karlstein tests. The same is true for the scatter range of the measurement values. Since the pipe temperature here was at about 90°C, a larger scatter actually would have been expected, but did not occur because the pipe was carefully flushed with air prior to the beginning of these tests.

8.5.3.3.1.1.4 Conclusion from the Frequency Calculations

The test calculations described above show that the theory (VELPOT and KOVIB1A computer programs) describes the measured frequencies not only in one special case, but also for a broad range of geometries and backpressure:

(1) The size of the water space varies from approximately 7 m^2 (GKM) to approximately 23 m^2 (test tank at Karlstein) to approximately 400 m^2 (suppression chamber in Brunsbuttel nuclear power plant).

(2) The quencher submergence ranged from approximately 2 m to 6 m.

(3) The bubble equilibrium volume varied between approximately 0.15 m^3 to 3.7 m^3.

(4) The suppression chamber pressure varied from 1 bar to 3 bar.

(5) The water temperature in the suppression pool varied between approximatley 16°C to 80°C.

Thus, the theory can be considered verified and can be used to transpose the pulsation frequencies measured in the Karlstein test stand to the SSES suppression pool.

8.5.3.3.2 Multipliers for Conversion of the Bubble Frequencies from the Test Stand to SSES

Using the VELPOT and KOVIB1A computer codes, the following three blowdown cases are analyzed:

(1) Simultaneous blowdown of all 16 quenchers

(2) Simultaneous blowdown of the quenchers A, B, G, K, M, P which are included in the ADS

(3) Blowdown of one quencher (quencher B)

The results are illustrated in Figure 8-173 which shows the pulsation frequency as a function of bubble volume (bubble in hydrostatic equilibrium). The behavior of the frequency curve for the 16-quencher case in the plant is practically the same as for the test stand (Figure 168), thereby confirming once again the suitability of the test stand geometry that was chosen. In the case of the 6 quenchers in the ADS case, the frequencies are higher due to the larger single cell corresponding to the smaller hydrodynamic bubble mass. They are even higher in the case of one quencher.

Based on the results shown in Figures 8-168 and 8-173, a simple formula can be given for converting from the measured bubble frequencies to these frequencies found in the plant by asking: By what factor ("multiplier") must a bubble frequency measured in the test stand be multiplied to get a corresponding frequency in the plant? This multiplier is plotted in Figure 8-174 versus the (measured) starting frequency. Thus, we have:

$$V_{plant} = f_v (V_{test}) \cdot V_{test}$$

in which the multiplier f_V for a given initial frequency can be read off from Figure 8-173.

The graph in Figure 8-173 is applicable only for cases with a pressure of 1 bar in the suppression pool air space. However, the blowdown for the ADS case during a loss-of-coolant accident is associated with a suppresson pool overpressure.

$$p_{KK} > 1 \text{ bar}$$

An additional multiplier $f_{P_{KK}} (p_{KK})$ is necessary for such cases, so that the frequency conversion must be written in a more general manner:

$$V_{plant} = f_{P_{kk}} (P_{kk}) \cdot f_v (V_{test}) \cdot V_{test}$$

The multiplier $f_{P_{KK}} (p_{KK})$ can be taken from Figure 8-175. For a suppression chamber pressure of) bar, it has the a value of 1, as it must be.

The multipliers for the frequency also fix the multipliers for the oscillation period when transposing the pressure time histories measured in the test stand to the plant:

$$t_{plant} = \frac{t_{test}}{f_{P_{kk}} (P_{kk}) \quad f_v (V_{test})}$$

8.5.3.3.3 Transposition Method for the Pressure Amplitudes

As already described in detail in Section 8.5.1, the test stand was so designed and the pressure transducers were so arranged that the measured pressure amplitudes can be transposed to the plant without change. Correspondingly, a 1:1 transposition is made. Because of its obvious conservativeness, such a 1:1

amplitude transposition offers the advantage that more exact quantitative proofs do not have to be provided. The most significant conservative features are the following:

(1) In blowdown cases with several quenchers, it is assumed that all bubbles are equally large and oscillate in phase. Deviations from this assumption (such as actually occur in the plant) result only in lower pressure amplitudes.

(2) Blowdown cases with less than 16 quenchers are assigned the same pessure amplitude as the 16-quencher case. In reality, such cases have a lower amplitude due to the geometry (larger single cell).

The conservativeness described in (1) has not yet been proven experimentally in any quencher tests, but it is already obvious from a theoretical viewpoint, since a time-shifted superposition of two temporal maxima always yields smaller values than an addition of the maximum values.

Concerning the conservativeness of (2), there are a number qualitative indications from the Karlstein tests themselves, from corresponding model studies at the Karlstein model test stand (Ref. 1), and from calculations with the VELPOT and KOVIB1A programs. The information obtained from all three of these investigations shall be described in the following sections.

In addition, we will also examine whether the conservative features are affected by a possible backpressure in the suppression pool air space.

8.5.3.3.3.1 PP&L Quencher Tests at Karlstein

Indications of the conservativeness discussed in (2) above are obtained from the Karlstein tests on the basis of Figure 8-176 which illustrates the measured relationship between excitation (relative amplitude) and pressure oscillation frequency for the Karlstein tests.

The frequency analysis for each pressure time history has at least two maxima of the power density. One power density maximum lies at low frequencies and the other at somewhat higher frequencies. There is a factor of approximately two between the two freqeuncies. The first peak of the power density (low frequency) is always larger than the second peak of the power density (higher frequency). Accordingly, the low frequency is always designated as the dominant frequency

For pressure transducer P5.10, the power densities of all analyzed tests are evaluated in Figure 8-176. Different analysis times were selected for tests having different pressure oscillation frequencies. The time was so chosen that approximately the same oscillation periods could always be evaluated.

The following analysis times were selected for the evaluation:

3 Hz Time: 0 - 1.8 seconds
5 Hz Time: 0 - 1.3 seconds
9 Hz Time: 0 - 0.6 seconds

The area beneath the frequency spectrum was determined and then the square root of that numerical value was taken. That results in values having the dimension "bar".

Those numerical values were normalized to the maximum value.

The results are then "relative pressures" with respect to the calculated maximum pressure from the frequency spectra.

Since no dominant frequencies higher than 6.5 Hz were measured in the Karlstein tests, the second peaks were also used to evaluate the higher frequencies. Hence, the power densities of both the dominant frequency and the next higher frequency are evaluated in Figure 8-176.

Based on an empirical evaluation, it follows from Figure 8-176 that the pressure oscillations with higher frequencies have smaller energy content than the pressure oscillations with lower frequencies.

In addition, as shown in Figure 8-169, the bubble frequency increases with decreasing bubble volume. But decreasing bubble volume with constant single-cell size means, according to the laws of similarity, the same thing as increasing the cell size with constant bubble volume. Therefore, from the Karlstein test data, it can be said that the pressure amplitudes decrease with increasing cell size.

8.5.3.3.3.2 KWU Quencher Tests in the Model Test Stand in Karlstein

During the development of the KWU quencher, tests were performed to examine the influence of the size of the water space (specifically: free water surface) in the model test stand in Karlstein (Ref. 1). The results are illustrated in Figure 8-177, which was taken from Refence 1. It shows directly how the bottom pressure amplitudes decrease with increasing size of the water space (single cell).

8.5.3.3.3.3 Analytical Calculations

The conservativeness described in (2) above is also confirmed from results of calculations with the VELPOT and KOVIB1A programs. As for the frequency conversion, appropriate multipliers can be determined also for the conversion of the pressure amplitudes from the test stand to the plant. They depend on the influence of the water space on the stationary velocity potential (spatial pressure distribution normalized to unit source strength) and on the hydrodynamic source strength associated with the bubble dynamics. The source strength itself is dependent in turn on the pressure in the bubble, which is determined by the interplay of bubble volume and air supply into the bubble. Since the air supply varies according to the different operating conditions during the blowdown, only a conservative estimate can be given within the framework of the present investigations.

The conversion from test stand to the plant for one quencher may serve as an example here. We obtain for the bottom pressure beneath the quencher:

$$P_{plant} \text{ (1 quencher) } < 0.7 \, P_{test}$$

as upper value.

8.5.3.3.3.4 Influence of Backpressure on the Pressure Amplitudes

As for the bubble oscillation frequency, the question of the effect of backpressure in the suppression pool air space must be investigated.

Figure 8-178 shows the bottom pressure amplitudes measured in the GKM model quencher tests for a suppression pool air space pressures of 1 and 3 bar. As can be seen, the pressure amplitudes do not depend on the suppression pool air space pressure.

8.5.3.3.4 Verification of Design Specification

In the transposition of the pressure oscillations measured in Karlstein to the SSES, the extremely conservative assumption that the same pressure time histories are acting at all quenchers simultaneously is used. Differences in the pressure time histories originating from the different discharge lines are neglected. Therefore, each measured pressure oscillation in the Karlstein vent clearing tests is a representative containment load for all load cases:

symmetrical load case (simultaneous response of all 16 SRV's

unsymmetrical load case (response of one or three adjacent SRV's

automatic depressurization in loss-of-coolant accident

A transposition of the measurement results to the plant is performed for these load cases.

The Karlstein test tank forms a conservative single cell. Therefore, conservative enveloping pressure amplitudes were measured in that test stand. When transposing the pressure oscillations from the single cell to the plant, there is an increase of the pressure oscillation frequencies as discussed in Section 8.5.3.3.2. As stated previously, the increase of the pressure oscillation frequencies is accompanied by a decrease of the amplitudes. The decrease of the amplitudes is neglected for this evaluation. The amplitudes of the measured pressure oscillations remain constant for all frequencies. That is an additional conservative feature, as already discussed in Section 8.5.3.3.3.

8.5.3.3.4.1 Frequency Analyses of Selected Tests

The pressure time histories for selected Karlstein tests are illustrated in Figures 8-41 to 8-65.

The freqeuncy analyses were carried out with the Fourier Analyzer 5451 made by Hewlett Packard.

The frequency analyses were generated as power spectral densities. The frequencies at which a structure is excited into oscillation can be read off from the power spectral densities.

Freqeuncy analyses were performed for pressure transducers P5.2, P5.4, P5.5, and P5.10 and for the following tests:

4.1.1, 4.1.6, 12.1, 11.1, 19.R2.7, 20.R1.1, 20.R1.10, 21.1, 21.2, 25.R2.

Pressure oscillations at both the wall and the bottom are considered in the freqeuncy analyses. Also considered was the frequency analysis for pressure transducer P5.5, which shows the "local effect".

The limitation of the measured frequencies of the pressure oscillations was determinative in selecting the tests to be analyzed. The tests selected were those which exhibited pressure amplitudes ≥0.3 bar both at low frequency and also at higher frequencies.

The frequency spectra for several Karlstein tests are illustrated in Figures 8-179 to 8-182 for pressure transducers P5.10 and P5.4.

The frequency spectra for two tests with the long discharge line and lowered water level are shown in Figure 8-179. The principal frequency of the pressure oscillations is at 2-3 Hz for these tests.

They are the lowest pressure oscillation frequencies that were measured in the Karlstein tests.

Figure 8-180 shows the difference in the pressure oscillation frequencies from clean-condition tests to real-condition and/or multiple-actuation tests for the long line.

The pressure oscillations have a principal freqeuncy of 3.5 Hz in test 4.1.1 (clean condition) and 5 Hz in test 4.1.6 (real condition). For the short discharge line, the frequency shifts from clean to real condition are illustrated in Figure 8-181 for tests 21.1 and 21.2. The result for the short line is:

clean condition: pressure oscillation frequency 5 Hz
real condition: pressure oscillation frequency 6.5 Hz

The following can be said about the measured <u>principal frequencies</u> for the Karlstein tests:

1) The lowest pressure oscillation frequency was measured in the tests with the long line and a discharge line water level lowered to 2.5 m above the middle of the quencher. It was 2.0 - 3 Hz.

2) For the clean-condition tests, pressure oscillation frequencies of 3.5 - 4 Hz were measured with the long discharge line.

3) For the clean-condition tests, pressure oscillation frequencies of 4.5 - 5 Hz were measured with the short discharge line.

4) The highest frequency for the Karlstein tests was measured for the real-condition and/or multiple-actuation tests. The measured frequencies were 6 - 6.5 Hz.

Figure 8-183 shows frequency analyses for different pressure transducers for one test.

P 5.2 - sits on the bottom beneath the middle of a quencher arm.

P 5.4 - is mounted on the concrete wall at the intersection of wall and bottom.

P 5.10 - sits on the concrete wall opposite the center point of the ball of the quencher.

The frequency spectra of the pressure transducers all display a power maximum at the same frequency (3 Hz). Therefore, the location of the measurement and the structure of the mounting position in the water region of the Karlstein test stand have no influence on the measured frequency of the pressure oscillations.

8.5.3.3.4.2 Shifting of the PSD's in the Transposition from the Test Stand to SSES

The comparison of the pressure time histories measured in the Karlstein quencher tests with the pressure time histories specified in Section 4.1.3 is accomplished by using the frequency power spectra.

The frequency spectra of the KKB traces forming the basis of the specification in Section 4.1.3 and are illustrated in Figures 4-31 to 4-33.

The specified pressure oscillations have their dominant frequency in the range of 6.5 - 8 Hz.

To cover the pressure oscillation frequencies for SSES, the following rule for treatment of the traces was given:

> The three traces should be time-expanded by a factor in the range from 0.9 to 1.8.
>
> The pressure amplitudes should be multiplied by a factor of 1.5.

To be able to make a comparison with the measured pressure oscillations, it is necessary that the frequency spectra of the three traces be shifted in frequency and stretched in amplitude. In this Section, we illustrate a method by which those operations on the frequency spectra can be performed.

8.5.3.3.4.2.1 Frequency shift

The amplitudes are preserved in the frequency shift. To ensure that, the area under the power spectrum must be held constant. Since the analysis time range for the frequency analysis is finite, it must be made certain that the comparison involves only spectra in which approximately the same number of oscillation periods were analyzed. The traces are expanded or compressed by the factor f_V, while keeping the zero point fixed.

Let us designate the expanded or compressed frequency by f' and the original frequency by f.

A power spectrum can always be subdivided approximately into triangles whose base is the frequency and whose altitude is the power density. In the original spectrum, the area beneath a triangle is:

$$A = \frac{f_2 - f_1}{2} \cdot h$$

For the new frequency:

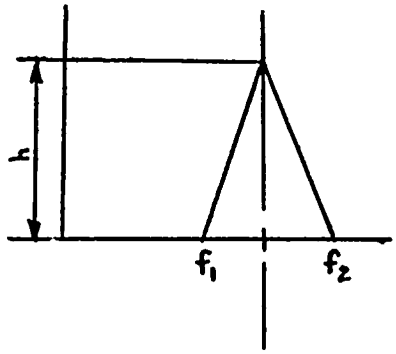

$$f_1' = f_V \times f_1$$

$$f_2' = f_V \times f_2$$

Therefore, we have for the new area:

$$A' = \frac{f_2' - f_1'}{2} \cdot h'$$

But since A' = A,

$$h = f_V\ h' \qquad h' = \frac{h}{f_V}$$

The power density of the shifted spectrum is inversely proportional to the frequency multiplier.

In this definition, the frequency multipliers are to be taken from Section 4.1.3. From the factor 1.8 we get $f_V = 1/1.8$ and from the factor 0.9 we get $f_V = 1/0.9$. If the frequency is reduced to half, the power density is doubled.

8.5.3.3.4.2.2 Amplitude Stretching

The following relation prevails between the amplitude of a load-vs.-time function and the power density:

$$a = k\sqrt{\frac{h}{2}\ \Delta f'} \qquad k = \text{correction factor}$$

For the stretched amplitude, we have a' = f a. The relation between power density and amplitude is preserved by the stretching, so that the same correction factor is also valid after the stretching. Therefore:

$$a' = k\sqrt{\frac{h'}{2}\ \Delta f'}$$

and thus:

$$\frac{a}{a'} = \sqrt{\frac{h}{h'}} \quad , \quad \frac{1}{f_a} = \sqrt{\frac{h}{h'}} \quad > h' = f_a^{\,2} \cdot h$$

The power density ratio in the amplitude stretching is proportional to the square of the amplitude multiplier.

8.5.3.3.4.3 Symmetrical Load Case (Simultaneous Blowdown of all 16 SRV's)

All the Karlstein clean-condition and real-condition tests are used to evaluate this load case. The multiple actuation tests are considered as irrelevant to the plant for this load case. The one exception is the 10th blowdown test of an entire multiple actuation test with the short discharge line. Those tests are started 10 minutes after completion of the 9th blowdown test. They are thus subject to the same conditions as the real-condition tests. Accordingly, the 10th blowdown tests of a multiple actuation test with the short discharge line are treated as real-condition tests.

The test tank in Karlstein represents the smallest single cell with respect to the water space. That means that the maximum possible pressure amplitudes for SSES were measured.

According to Section 8.5.3.2, the measured pressure amplitudes are covered by the specification.

For this load case, the measured frequencies of the pressure oscillations can also be transposed directly from the Karlstein test stand to SSES (see Section 8.5.3.2).

Thus, all the pressure time history can be transposed directly from the test stand to SSES. In order to show that the measured time histories are also enveloped by the specification, the frequency spectra of the measured pressure oscillations are compared with the frequency spectra of the specified traces. Since the measured frequencies differ from the frequencies of the specified traces, the spectra must be treated by the method illustrated in Section 8.5.3.3.4.2 and brought into coincidence at the dominant frequency.

The pressure oscillations measured at pressure transducer P 5.2 are used for this comparison, since, the pressure transducer P5.2 exhibits the highest power spectrum of all the pressure transducers that are useable for the overall loading of the containment (P5.5 is not considered - see Section 8.5.3.1). Pressure transducer P 5.2 is mounted on the bottom of the test tank, directly beneath a quencher arm. That position is also present in SSES. Therefore, this pressure transducer measures pressure oscillations having the greatest relevance to SSES. Furthermore, the specified traces are also results of a measurement made with a bottom pressure transducer whose location was similar to that of P5.2.

The comparison of the frequency power spectra is shown in Figures 8-184 to 8-188.

We see that the frequency spectra of the KKB traces, which were frequency-shifted and amplitude-stretched as described in Section 8.5.3.3.4.2 envelop the frequency spectra of the measured pressure oscillations.

Therefore, it can be stated that:

a) the Karlstein measurement results are conservative for the load case of simultaneous clearing of all 16 quenchers (single-cell effect);

b) for this load case, the pressure oscillations are enveloped by the specification with respect to their amplitude, their frequency power spectra, and their spatial distribution.

8.5.3.3.4.4 Unsymmetrical Load Case (Blowdown Via One SRV)

For this load case, all determinative parameters, except for the water surface area, were simulated in the Karlstein test stand according to their actual values for SSES.

For the load case of vent clearing with one quencher, a larger water surface area is available to the quencher in SSES than in the test in the Karlstein test stand.

Accordingly, the pressure oscillation frequencies are raised and the pressure amplitudes are lowered. In this verification, we conservatively make no allowance for the amplitude decrease with increasing water surface area.

The frequencies calculated according to Section 8.5.3.3.2 for the load case of blowdown via one SRV are compiled in the following table:

		Frequency of the pressure oscillations (Hz)			
		Measured	Frequency multiplier	Plant	Specified frequency band
long line	CLEAN CONDITIONS	3.5-4	1.54-1.48	5.4-5.9	3.75-8.9
long line	REAL CONDITIONS	5	1.42	7.1	
short line	CLEAN CONDITIONS	5	1.42	7.1	
short line	REAL CONDITIONS	6.5	1.37	8.9	

The frequencies transposed to the plant are all enveloped by the specified frequency band.

For the load case of vent clearing of one quencher, the multiple actuation tests must also be considered (they were included under "real conditions" in the Table above).

For the load case of simultaneous blowdown of 16 quenchers, it was shown that the measured power spectra are enveloped by the specified power spectra. That statement applies for all frequency ranges. If two power spectra are brought into coincidence at one frequency and if both spectra are subjected to the same frequency shift, then there is no change in the relation of the two spectra to each other.

Therefore, the power spectra of the clean-condition and real-condition tests are also covered by the specification in the load case of vent clearing of one quencher, since, as stated above, the transposed frequencies from the test are all enveloped by the specification frequency range.

For the multiple actuation tests, test 4.1.6 is considered to be enveloping for the long discharge line, since it provided the highest pressure amplitudes.

For the short discharge line, test 20.R1.10 (which formally can be classified as a multiple actuation test) is considered to be enveloping for the same reason. Classified as a real-condition test, it was shown in the preceding Section that the specified traces envelop the pressure time histories for that test.

In Figure 8-189 it is shown that the power spectrum of test 4.1.6 is also enveloped by the specified KKB traces.

Even under the very conservative assumption that the pressure amplitudes measured in Karlstein can be transferred without change for the load case of vent clearing of one quencher, the pressure time histories are enveloped by the specified traces.

8.5.3.3.4.5 Unsymmetrical Load Case (Blowdown via Three Adjacent SRV's)

This load case is bounded by the load cases of simultaneous vent clearing of 16 quenchers and vent clearing of one quencher.

8.5.3.3.4.6 Automatic Depressurization System (ADS) Load Case

In this section we discuss the load case that considers the firing of the six quenchers associated with the ADS under LOCA conditions.

As shown in Figure 8-190, the following conditions prevail in the suppression chamber when the automatic depressurization system is actuated during IBA:

Absolute pressure in the wetwell air space, approximately	2.55 bar
Pressure difference between drywell and suppression chamber	0.42 bar

The Karlstein tests with lowered water level in the discharge line are used to verify the ADS case. These tests are used as they correctly simulate the discharge line as it would be with a positive pressure differential of approximately 0.42 bar in the drywell. This positive pressure differential would result in the lowering of the water level in the discharge line to the elevation of the bottom of the downcomers as was simulated for tests 10.3, 11.1, 12.1 and 13.1. Of those tests, the test 11.1 (enveloping in amplitude and power density) is used as the basis for the verification.

The amplitude-reducing influence of the larger water surface area assigned to the individual quencher in the ADS case is conservatively neglected.

Also, since earlier KWU tests proved that the backpressure in the suppression chamber has no influence on the pressure amplitudes, the measured pressure amplitudes are taken unaltered from the corresponding Karlstein tests, in which the measurements were made at atmospheric pressure.

The predominant frequency in test 11.1 is at 3 Hz. According to Section 8.5.3.3.2, Figures 8-174 and 8-175, the following frequency multipliers are obtained for the ADS case for transposition of the pressure oscillations from test 11.1 to the plant:

Influence of the larger water surface area	1.35
Influence of the 2.55 bar backpressure	1.4
Total frequency factor	1.9
Dominant frequency	5.7 Hz

Note:

The measured lowest dominant pressure oscillation frequency was measured in tests 12.1 and 13.1, which fall into the same category as test 11.1. With the total multiplier 1.9, the frequencies are raised to 3.8 Hz and thus lie within the specified frequency band (see Section 8.5.3.3.5).

The dominant frequency is within the specified frequency band.

The comparison between the prepared trace from pressure transducer P5.2 for test 11.1 and the specification is shown in Figure 8-191. As for the other load cases, the comparison is made in the power spectra of the pressure time histories. The spectrum of test 11.1 was shifted from the dominant frequency of 3 Hz to the dominant freqeuncy of 5.7 Hz while preserving the area (amplitude).

The KKB trace of test 76 was shifted from 8 Hz to 5.7 Hz while preserving the area, and then stretched by a factor of 1.5 in amplitude. Figure 8-191 shows that the trace from the specification, treated in this manner, envelops the trace of Karlstein test 11.1 transformerd to the ADS case since the total energy represented by the area under the power spectrum curve from the specification is greater than that from the Karlstein test 11.1.

8.5.3.3.4.7 Summary

It has been demonstrated that the frequency power spectrum of the pressure oscillations in the suppression chamber are enveloped by the frequency power spectrum specified in Section 4.1.3 for all load cases. Thus, the design specification provides enveloping loads also for the dynamic excitation of the SSES containment by vent clearing of the relief system with the quencher.

8.5.3.3.5 Evaluation of the Measured Pressure Oscillations During Condensation

As discussed in Section 8.4.2, three regimes can be distinguised in the condensation process:

a) The quencher is cleared continually.

b) The quencher is not cleared continually.

c) Only the sliding joint is cleared, and the steam condenses in the discharge line.

8.5.3.3.5.1 The Quencher is Cleared Continually

The steam is condensed continually in the water pool outside the quencher. Calm condensation prevails for cold water and also for hot water in the blowdown tank (see Figures 8-78 and 8-79).

The measured maximum pressure amplitude is ±0.13 bar. This condensation phase was measured for reactor pressures up to about 4 bar. The frequencies of the pressure oscillations are 70-120 Hz for a cold pool and 20-45 Hz for a hot pool.

8.5.3.3.5.2 The Quencher is not Cleared Continually

This condensaton phase begins when the condensation rate outside the quencher is greater than the steam mass flow through the line. The pressure in the quencher drops below the hydrostatic pressure of the surrounding water. The water penetrates into the quencher. The condensation surface area is thereby decreased and so is the condensation rate. The result is a pressure rise in the discharge line, so that the water that has flowed in is expelled again.

The inflow of water from the suppression chamber into the quencher and the subsequent braking and re-expulsion of the water is a nonstationary process which occurs periodically.

For that reason, this condensation phase is also called intermittent condensation.

The phenomenon of intermittent condensaton is dependent on the water temperature. For cold water there is a higher rate of condensation outside the quencher, resulting in a larger generation of negative pressure inside the quencher and therefore a more vigorous flow of water into the quencher.

For a cold water pool, the profile of the dynamic pressures is similar to the profile which is familiar from the chugging phase of the condensation at the vent pipes; see Figure 8-76.

For heated water in the suppression chamber, the condensation rate outside the quencher is smaller, so that the entire process takes on the form of a low-frequency pressure oscillation (See Figure 8-80).

The tests in Karlstein yielded as maximum measurement result for the dynamic pressure: + 0.28, - 0.18 bar, for a cold pool. The time between two events is about 1.0 second. For a heated pool, the measured maximum amplitude is +0.12, - 0.07, bar.

8.5.3.3.5.3 Condensation in the Discharge Line and Thru the Sliding Joint

If the steam flow decreases further, a condition is finally reached in which the quencher is no longer cleared, but rather remains continually filled with water. Then there is steady-state condensation of steam inside the discharge line. This condensation phase proceeds very calmly and begins at reactor pressures below 2 bar.

In this condensation phase, maximum dynamic pressures of +0.08, -0.04 bar were measured in the water pool during the Karlstein tests.

8.5.3.3.5.4 Transposition of the Measurement Results to SSES

In regard to steam condensation, the conditions of the Karlstein test stand are direclty transposable to the conditions of SSES. On the whole, the pressure amplitudes during condensation are small compared to those during vent clearing and therefore are covered by the latter.

8.5.4 Pool Mixing During SRV Actuation and Thermal Performance of the Quencher

8.5.4.1 Introduction

When an SRV responds, steam is condensed in the water of the suppression pool via a quencher. As this happens, the water must absorb the heat of vaporization of the steam, and so it is heated. When there is a long-lasting discharge of steam via a quencher, all the water in the suppression chamber should particpate in the heating, so as to limit the local heating in the vicinity of the discharging quencher.

In order to obtain good mixing of the hotter and colder water in the pool, all quenchers are positioned at a small distance from the bottom (3'6" = 1.07 m)(see Figure 8-192)). The water heated near a quencher is specifically lighter than the colder water lying above it. Therefore, the warmer water will rise and mix with the colder water.

To obtain an additional mixing effect, the hole occupancy of the quenchers were made slightly unsymmetrical (approximately 8%). Whereas the quencher arms have the same hole occupancies on the sides, only one arm of each quencher has holes on the end cap. In that way, a unilateral thrust can be exerted on the water in the suppression pool.

In the top view of the quencher arrangement (Figure 8-193), we see that the quenchers are arranged in two graduated circles. Along the inner graduated circle, the quencher arms all point in the circumferential direction, and the end cap with holes all point in the same circumferential direction. On the outer graduated circle, the columns would practically prevent a thrust effect if the quenchers were arranged in the same manner. Therefore, the quenchers were directed more radially, but turned by an angle of $\phi = 30°$ in the circumferential direction from the radii. In this way, 50% of the thrust still acts in the circumferential direction (equidirectionally with the thrust of the quenchers on the inner graduated circle). It should be noted that this new arrangement supersedes the original arrangement shown in Figure 1-4.

In the following, we shall estimate the acceleration of the water pool for the case in which one quencher on the outer graduated circle is operated for a long period of time at a reactor pressure of 70 bar (valve failure in open position). Then we shall present some measurement results from a test with a 4-arm quencher in the Brunsbuttel nuclear power plant and some information from the GKM Model quencher tests related to steam condensation with a quencher.

8.5.4.2 Equation of Motion of the Rotating Pool

It is assumed that the water flow in the rotating pool can be considered as a straight-line channel flow due to the small curvature of the graduated circle and the low circumferential velocity.

If we place the origin of the coordinate system at the center of the discharging quencher, then the equation of motion of the rotating pool reads:

$$m_w \ddot{x} + \tilde{c}_w \frac{\S}{2} \dot{x}^2 = F_{eff}$$

m_w = mass of water to be accelerated in the suppression chamber

c_w = sum of all flow resistances

F_{eff} = effective driving force

This differential equation has the general form:

$$\ddot{x} + a\dot{x}^2 = b$$

Substituting $\dot{x} = u$, the differential equation takes the form:

$$\dot{u} + au^2 = b$$

This differential equation is a special form of the Riccati differential equation.

The general solution of the differential equations reads Ref. 53:

$$u(t, \xi, \eta) = \frac{\eta\sqrt{a \cdot b} + b \operatorname{Tanh} \sqrt{a \cdot b}\ (t - \xi)}{\sqrt{a \cdot b} + a \cdot \eta \cdot \operatorname{Tanh} \sqrt{a \cdot b}\ (t - \varepsilon)}$$

The initial condition for t = 0 reads:

$$\mu(0,\xi,\eta) = 0 \qquad 0 = \frac{\eta \sqrt{a \cdot b} + b \cdot \operatorname{Tanh} \sqrt{a \cdot b}\ (-\xi)}{\sqrt{a \cdot b} = a \cdot \eta \cdot \operatorname{Tanh} \sqrt{a \cdot b}\ (-\xi)}$$

This conditional equation is satisfied only if ξ and η = 0.

The initial condition then leads to the solution:

$$\mu\ (t) = \frac{b\ .\ \mathrm{Tanh}\sqrt{a\ .\ b}\ \ .\ t}{\sqrt{a\ .\ b}}$$

Since u(t) = X(t), the equation for the velocity of the rotating pool reads:

$$x\ (t) = \frac{b}{\sqrt{a\ .\ b}}\ \mathrm{Tanh}\sqrt{a\ .\ b}\ \ t$$

For the distance covered, we have:

$$x\ (t) = {}_0\!\int^t \dot{x}\ (\tau)\ d\ \tau$$

The solution reads:

$$X\ (t) = \frac{1}{\alpha}\ \ln\ |\ \cosh\ |\overline{a\ .\ b}\ \ .\ t\ |$$

8.5.4.3 Determination of the Flow Resistances

The following resistances are considered:

a) Wall resistance of the channel

b) Resistance for flow around the discharge lines with quenchers and bottom support

c) Resistance for flow around the vent pipes

d) Resistance for flow around the columns

The channel has the following dimensions:

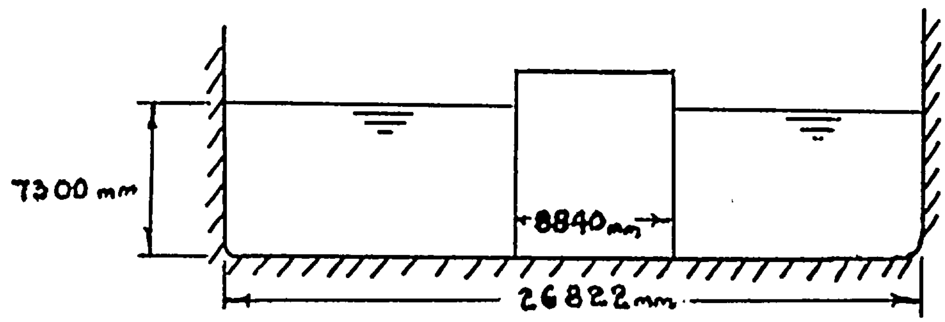

The hydraulic diameter of the channel is:

$$d_h = \frac{A}{U} = \frac{7.3 \left(\frac{26.822 - 8.84}{2} \right)}{(2 \times 7.3) + \left(\frac{26.822 - 8.84}{2} \right)} \doteq 2.8 \text{ m}$$

For the Reynolds number, we have:

$$Re \doteq \frac{W.d_h}{\nu}$$

According to Reference 36, the kinematic viscosity for water at 40°C is $\nu = 0.651 \times 10^{-6}$ m²/s.

If we assume a velocity of 10^{-2} m/s so as to cover the start-up phase also, we get:

$$Re + \frac{10^{-2} \times 2.8}{.651 \times 10^{-6}} = 4.3 \times 10^{4}$$

The SSES suppession pool is lined with a steel liner which cannot be considered hydraulically smooth. For such large steel structures it must be assumed that the individual plates are not joined together with their edges parallel, so that the flow resistance is increased by projecting edges. We therefore conservatively assume an absolute roughness of k = 2 mm. Then we have:

$$\frac{K}{d_h} = \frac{2}{2.8 \times 10^{3}} = 7.1 \times 10^{-4}$$

This corresponds to a friction coefficient of $\lambda = 0.022$.

The resistance coefficient is then:

$$\Gamma_w = \lambda \cdot \frac{1m}{d_h}$$

$$1m = D_m \cdot \pi = \frac{26.844 + 8.84}{2} \cdot \pi \doteq 56 \text{ m}$$

$$\Gamma_w = .022 \frac{(56)}{(2.8)} = .44$$

Cylindrical bodies are immersed into the water of the suppression chamber. They are the discharge lines with quenchers, the vent pipes, and the steel columns.

	Outside diameter m	Submergence m	Quantity
Discharge lines	0.324	7.3	16
Vent pipes	0.61	3.35	87
Steel columns	1.06	7.3	12

For the individual structural components, we then have the following Reynolds number:

$w = 0.01$ m/s (see above) $\qquad R_e = \frac{w}{\nu} d_a$

For the roughness, we assume k = 0.2 mm. Then, according to Reference 39:

	Reynolds number	k/d	Submergence d	C
Discharge line with quencher with bottom support	5×10^3	6.17×10^{-4}	22.5	0.73
Vent pipe	9.4×10^3	6.28×10^{-4}	5.5	0.73
Column	1.63×10^4	1.9×10^{-4}	6.9	0.73

The resistance force is then:

$$F_W = (\Gamma_W \cdot A_W + c_{WA} \cdot A_A + c_{WK} \cdot A_K + c_{WS} \cdot A_S) \frac{\rho}{2} w^2$$

The surface area on which the wall resistance acts is:

$$A_W = \frac{\pi \times (2.8)^2}{4} = 6.16 \text{ m}^2$$

Furthermore:

$$\tilde{c}_w = 6.16 \times .44 + .73 \times 50 + .73 \times 177.8 + .73 \times 93$$

$$A_A = 16 \times 0.324 \times 9.6 = 50 \text{ m}^2 \qquad \tilde{c}_w = 238\text{m}^2$$

$$A_K = 87 \times .61 \times 3.35 = 177.8 \text{ m}^2$$

$$A_S = 12 \times 1.06 \times 7.3 = 93 \text{ m}^2$$

Since the water region of the suppression chamber also contains a few structural components which were not considered here, an additional allowance shall be made. We choose: $\tilde{c}_w = 300\text{m}^2$

8.5.4.4 Determination of the Force Moving the Pool

Forces on the water mass in the suppression pool are produced by thrust from the boreholes on one of the end caps which are present on each of the quenchers. The smallest thrust force is produced by the quenchers along the outer graduated circle, since they do not have their thrust boreholes arranged in the circumferential direction.

The quenchers along the outer graduated circle are turned by an angle ϕ = 30° relative to the radial direction.

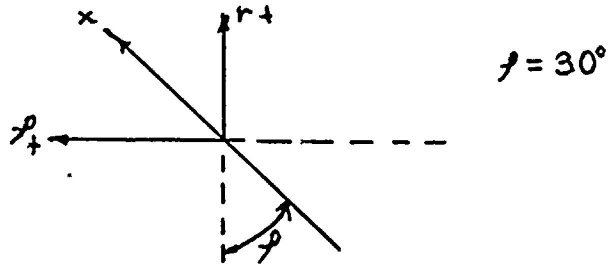

The thrust force results from the impulse of the outflowing steam.

$$F = \Delta P \times A_{D\ddot{U}} + \rho_D \times W_D^2 \times A_{D\ddot{U}}$$

$A_{D\ddot{U}}$ = effective outlet area of quencher

ΔP = difference between pressure in the quencher and ambient pressure

ρ_D = density of the outflowing steam

W_D = velocity of the outflowing steam

As an effective outlet area of a quencher end cap, there is available:

$$A_{D\ddot{U}} = \alpha_C \times A_{DU\ geom}$$

$$\alpha_C = 0.8 \text{ (Section 8.5.2.3)}$$

$$A_{D\ddot{U}\ geom} = 88 \times \left(\frac{(.01)^2 \times \pi}{4}\right) = 6.9 \times 10^{-3}\ m^2$$

$$A_{D\ddot{U}\ geom} = 5.52 \times 10^{-3}\ m^2$$

A constant reactor pressure of 70 bar is chosen for the estimate of the effectiveness of the rotating pool.

According to Reference 37, the mass flow through the relief valve at a reactor pressure of 70 bar is:

$m = 111$ kg/s

The resulting stagnation pressure in the quencher is:

$p_o = 11$ bar

and the steam pressure in the quencher holes is:

$p_D = 6.4$ bar

Therefore, $\rho_D = 3.4$ kg/m³ $W_D = 462$ m/s

The force acting in the circumferential direction is then:

$$F_{eff} = F_X \sin \psi$$

$$F_{eff} = (\Delta P + \rho_o + W_D^2)\ A_{D\ddot{U}} \times \sin \psi \quad \text{with} \quad \psi = 30^\circ$$

Therefore:

$$F_{eff} = 2.0\ KN + 1.5\ KN = 3.5\ KN$$

8.5.4.5 Working Equations for the Rotating Pool of SSES

The equation of motion for the rotating pool reads:

$$m_w \ddot{x} + \tilde{c}_w \frac{\S}{2} \dot{x}^2 = F_{eff}$$

This differential equation was solved in general form in Section 8.5.4.2.

To determine the mass of water which is to be moved, we must consider the internal structures which reduce the water mass. We have:

$$m_W = {}_W [\frac{\pi}{4} (26.822)^2 - (8.84)^2) \times .73 - \frac{\pi}{4} \times (.324)^2 \times 7.3 \times 16$$

$$- \frac{\pi}{4} \times (.61)^2 \times 3.35 \times 87 - \frac{\pi}{4} \times (1.06)^2 \times 12 \times 7.3]$$

$$m_W = 3.5 \times 10^6\ Kg$$

For the total resistance coefficient we have according to Section 8.5.4.3:

$$\tilde{C}_W = 300 m^2$$

and for the effectively acting force we have according to Section 8.5.4.4:

$$F_{eff} = 3.5\ KN$$

Therefore, the equation of motion reads:

$$3.5 \times 10^{6} \times \ddot{X} + 1.5 \times 10^{5} \times \dot{X}^{2} = 3.5 \times 10^{-3}$$

or

$$\ddot{X} + \alpha X^{2} = b$$

Therefore, for:

$$\alpha = 4.3 \times 10^{-2} \qquad b = 9.9 \times 10^{-4} \qquad \sqrt{\alpha\ b} = 6.55 \times 10^{-3}\ t$$

The equation for the velocity of the rotating pool reads:

$$\dot{X}\ (t) = 1.52 \times 10^{-1}\ \mathrm{Tanh}\ 6.55 \times 10^{-3} t$$

The equation for the displacement reads:

$$X(t) = 23.2\ \ln\ |\cosh 6.55 \times 10^{-3} t|$$

The results are illustrated in Figures 8-194 and 8-195.

8.5.4.6 Estimate of the Heating of the Suppression Chamber Water

The local heating of the suppression chamber water results from the balance of the heat brought in by the condensing steam and the heat dissipated by the flowing water.

As time passes, however, the pool is set into motion by the impulse of the inflowing steam and reaches a velocity such that most of the heat brought in is distributed over a larger volume of water than the assumed local volume. The difference between the local and mean water temperature decreases.

8.5.4.7 Experimental Proofs

8.5.4.7.1 Model Tank Tests

Thrust measurements on a steam jet were made in the Karlstein model tank in the Spring of 1973 (Ref. 40).

The test set-up is illustrated in Figure 8-196.

The steam pipe is connected by a spring to the side wall of the model tank. The excursion of the spring with the steam pipe is measured by a displacement transducer.

The measurement system was calibrated by determining the excursion of the steam pipe for a defined force.

The steam outlet opening had a diameter of 10 mm.

The mass flow density was 600 to 630 kg/m²s.

The measured reaction forces were 20 - 28 N.

A short calculation yields:

Outlet area	$= 7.854 \times 10^{-5} m^2$
Rest pressure before the outlet opening	= 4.5 bar
Pressure after the outlet opening	= 2.6 bar
Steam density (at 2.6 bar)	$= 1.44 \ kg/m^3$

The resulting outlet velocity is:

$$W = \sqrt{K\frac{P}{\rho}} = \sqrt{1.135 \ \frac{2.6 \times 10^5}{1.44}}$$

W - 452.7 m/s
and the thrust force is:

$$F = (\rho W^2 + \Delta P) \ A_{eff}$$

$$A_{eff} = 0.8 \times A_{geom}$$

$$\therefore F = (1.44 \times (452.72)^2 + 1.6 \times 10^5) \times 0.8 \times 7.854 \times 10^{-5}$$

$$F = 28.4 \ N$$

The measured values are lower than the calculated values.

The measurements have proved clearly that the impulse of the emerging steam jet becomes active as a thrust and that, with respect to the velocity buildup of the rotating pool (and thus for the maximum local heating), it is conservatively bounded by the calculated values.

8.5.4.7.2 KKB Test During the Nuclear Commissioning

The pressure relief system was tested during the commissioning phase of the Brunsbuttel nuclear power plant. In one such test, a relief valve was held open for a time of about 270 seconds. The suppression chamber cooling system was switched on during the test. Water was drawn off in the lower part of the pool, cooled, and sprayed from pipes provided with holes and located under the top of the suppression chamber.

12 measuring points are mounted in the water region of the suppression chamber. They are arranged at three different elevations (14 m, 16.5 m, 18.2 m) and at four different circumferential positions (5°, 75°, 195°, 245°). The water level is at a height of 18.89 m.

Figure 8-197 shows a three dimensional spatial representation of the measured temperature field in the water just before test start (curve 1) and at 228 seconds after test start (curve 2). In Figure 8-197, the vertical position of the transducer is represented on the ordinate and the circumferential position on the abscissa. The temperature axis points to the rear. The heating of the pool is indicated as the difference of curves 2 and 1 at three elevation positions. The mean water temperature was approximately 32.3°C before the test and approximately 42.8°C at 228 s later. The maximum measured temperature was 50°C, so that the maximum deviation from the mean was 7.2°C.

The discharging quencher was located at 285° at an elevation of 14.915 m and accelerated the water toward the left in the Figure.

Correspondingly, the water temperature is higher above and to the left of the quencher. From that we can see the effectiveness of the quencher's arrangement near the bottom and of the unsymmetrical hole arrangement with respect to uniform utilization of the heat sink of the water pool.

8.5.4.7.3 GKM Half Scale Quencher Condensation Test

A series of intermediate scale (1:2) condensation tests were performed in the GKM test stand to demonstrate the high temperature performance of the quenchers (Ref. 27). Condensation tests were run on seven different versions of the quencher device. The last three versions had 10-mm diameter holes on the quencher arms. The spacing of the hole centerlines was 1.5 diameters circumferentially and 5.0 diameters axially. This hole pattern is also adopted in the actual SSES quencher design. These tests were run at a water temperature ranging from 13°C to 100°C (56°F-212°F) and a steam mass flux (with respect to the hole area) range of 8 to 495 kg/m² (1.6 to 101 lbm/ft²s). Water temperatures as high as 107°C (225°F) were measured at certain locations in these tests.

8.5.4.8 Summary

The Karlstein quencher tests and previous GKM half scale quencher tests show clearly that smooth steam condensation can be achieved at elevated temperatures which approach the local saturation limit.

In addition the calculations and KKB in plant tests provide information which suggest that pool mixing is enhanced by steam discharge through the holes in the end caps of the quencher.

8.5.5 Verification of Submerged Structures Load Specification Due To SRV Actuation

Section 4.1.3.7 gives the design specification for the loads on submerged structures due to SRV actuation. The basis for the specification is the three pressure time histories used for the containment analysis but instead of a constant amplitude multiplier of 1.5 various multipliers, related to the crossectional area of the object, are used. (see Table 4-15).

The loading on the columns including the localized effect at P5.5 has been discussed in Section 8.5.3.2.1.2.

In addition the effects of air bubble oscillation loads on the quenchers have been discussed in Section 8.5.2.3.6.

The following section will discuss the loadings on the vent pipes as measured in the Karlstein test tank and provide a description of the influence for the expelled water during vent clearing.

8.5.5.1 Loads on the Vent Pipe

8.5.5.1.1 Measurement of the Loads

In order to determine the loading of the vent pipe near a quencher, a vent pipe having the same outside diameter and wall thickness as that in SSES was installed in the Karlstein test stand and supported by typical bracing. (see Figure 8-10).

Underneath the bracing, bending strains were measured in two mutually perpendicular planes by means of strain gauges (SG 5.1 and SG 5.2) (see Figures 8-11 and 8-12). The strain gauges were mounted about 100 mm below the bracing.

The outside diameter of the vent pipe is:

$$D_a = 0.609 \text{ m}$$

and the inside diameter is:

$$D_i = 0.589 \text{ m}$$

Thus, the cross-sectional area is:

$$A = 0.0188 \text{ m}^2$$

and the moment of resistance is:

$$W = \frac{\pi}{32} D_a \left(1 - \frac{D_1^4}{D_o^4}\right) = 2.77 \times 10^{-3} \text{ m}^3$$

We have:

$$\sigma \times W = M_B = \varepsilon \times E \times W$$

Therefore:

$$M_B = 2.77 \times 10^{-3} \cdot 10^{11} \cdot \varepsilon$$

and hence;

$$M_B = 0.57\varepsilon$$

If we insert ε in micrometers per meter into this equation, we obtain the bending moment in kN-m.

The bending moments calculated in this manner are static equivalent loads.

8.5.5.1.2 Measured Bending Moments

Figures 8-198 to 8-200 show the dependence of the measured resultant bending moments on the reactor pressure, vent clearing pressure, and pressure oscillation amplitude that were measured near the vent pipe on the concrete wall.

Only the tests with clean conditions were used for the plot of the measured bending moments versus reactor pressure, whereas all tests in the reactor pressure range of 60-81 bar were used for the plots of the bending moment versus vent clearing pressure and pressure oscillation amplitude.

The measurements of the bending strains at the vent pipe were performed only for the tests with the long discharge line.

The measured maximum bending moment was

14.6 kN-m at a 74 bar reactor pressure and a

13.8 bar vent clearing pressure.

8.5.5.1.3 Extrapolation of the Measurement Results and Comparison with the Specified Value

If the measurement values are extrapolated to the extreme conditions in the plant on the basis of Figures 8-198 and 8-199, we get the following extrapolated maximum values:

16.5 kN-m with respect to an 88 bar reactor pressure,

19.0 kN-m with respect to the vent clearing pressure of 16.5 bar for the long discharge pipe, as extrapolated in Section 8.4 for the extreme boundary conditions in the plant.

In the specification, a maximum pressure difference of 0.75 x 0.8 = 0.6 bar was specified for the vent pipe with the distribution illustrated in Figure 4-24. The pressure distribution for the vent pipe installed in the Karlstein test stand is shown in Figure 8-201. The following relation applies for the pressure at the end of a vent pipe:

$$\frac{\Delta P_0}{7.3-1.83} = \frac{\Delta P}{7.3-3.65} \qquad \Delta P = 0.4 \text{ bar}$$

At the clamping point of the vent strut, we have:

$$\frac{\Delta PO}{7.3-1.83} = \frac{\Delta P}{7.3-6.3} \qquad \Delta P = 0.1 \text{ bar}$$

The pressure distribution from the end of the vent pipe to the clamping point of the vent-pipe strut is trapezoidal.

The lever arm of the acting force with respect to the clamping point is:

$$\frac{0.1+0.4}{2} L_S = 0.1 \times \frac{2.65}{2} + \frac{(0.4-0.1)}{(2)} \times \frac{2}{3} \times 2.65$$

$$L_S = 1.59 \text{ m}$$

For the bending moment at the clamping point we get:

$$M_{B_{SP}} = \left(\frac{(0.1 + 0.4)}{2} \times 2.65 \times 0.6 \times 1.59\right) 10^{-2}$$

$$M_{B_{SP}} = 63 \text{ kNm}$$

Relative to the strain gauges, we have:

$$M_{B_{SP}} = 57 \text{ kNm}$$

The extrapolated maximum moment was 19 kN-m.

It is thus demonstrated that the specification envelops the measurement values and their extrapolation.

The proof that the specification envelops the measurement values and their extrapolation is based on a purely static analysis. Such an analysis is permissible because the exciting pressure oscillations have a frequency of 4-6 Hz. However, the strain gauges indicate a natural oscillation frequency of 17-20 Hz for the vent pipe which is very close to the natural frequency of the vent in SSES (19 Hz) (see Figure 8-202). Hence, it can be assumed that the dynamic load factor is close to one.

8.5.5.2 Influence of Expelled Water During Vent Clearing

A review of the high speed films and pressure traces at P5.5 from the Karlstein tests shows negligable influence of the expelled water at this gage. In addition the total penetration of the expelled water appears to be approximately 3 feet for a 70 bar initial system pressure. Therefore, no additional loading, other than that already included in the pressure traces will be considered.

(A time correlation of a high speed film to pressure trace at P5.5 will be supplied later.)

8.5.5.3 Summary

The loads measured on the dummy vent pipe are static equivalent loads, but loads which are a sum of individual components. In the specification, the transverse loads on internal structures originating from the blowdown of the relief system are formulated as differential pressures across the internal structures. The differential pressures have the same pressure time history as the dynamic pressures in the water region of the suppression chamber.

This formulation of the transverse loads on the vent pipe (more generally on the internal structures in the water region of the suppression pool) yields the enveloping static equivalent load. This was also verified by the KKB tests with the actual relief system (Ref. 38). The maximum differential pressures calculated from the measurement results are p = 0.16 bar at the quencher arm, and p=0.11 bar at the protective pipe on the discharge line. They are both conservatively bounded by the KKB specified value of p=0.2 bar. The KKB test results shows that there is a clear separation between the specified loads and the maximum measured loads for both the lateral and vertical loads on internals in the pool of the suppression pool.

Based on the verification of the transverse loads by the KKB tests and based on the comparison between specification and measurement for the Karlstein tests (see Section 8.5.5.1), it can be stated that the values formulated in the specification for the transverse loads on internal structures in the water region yield enveloping static equivalent loads.

KEY:
1. Relief valve
2. Compressed air
3. HP steam line
4. Heating
5. SRV
6. Condensate

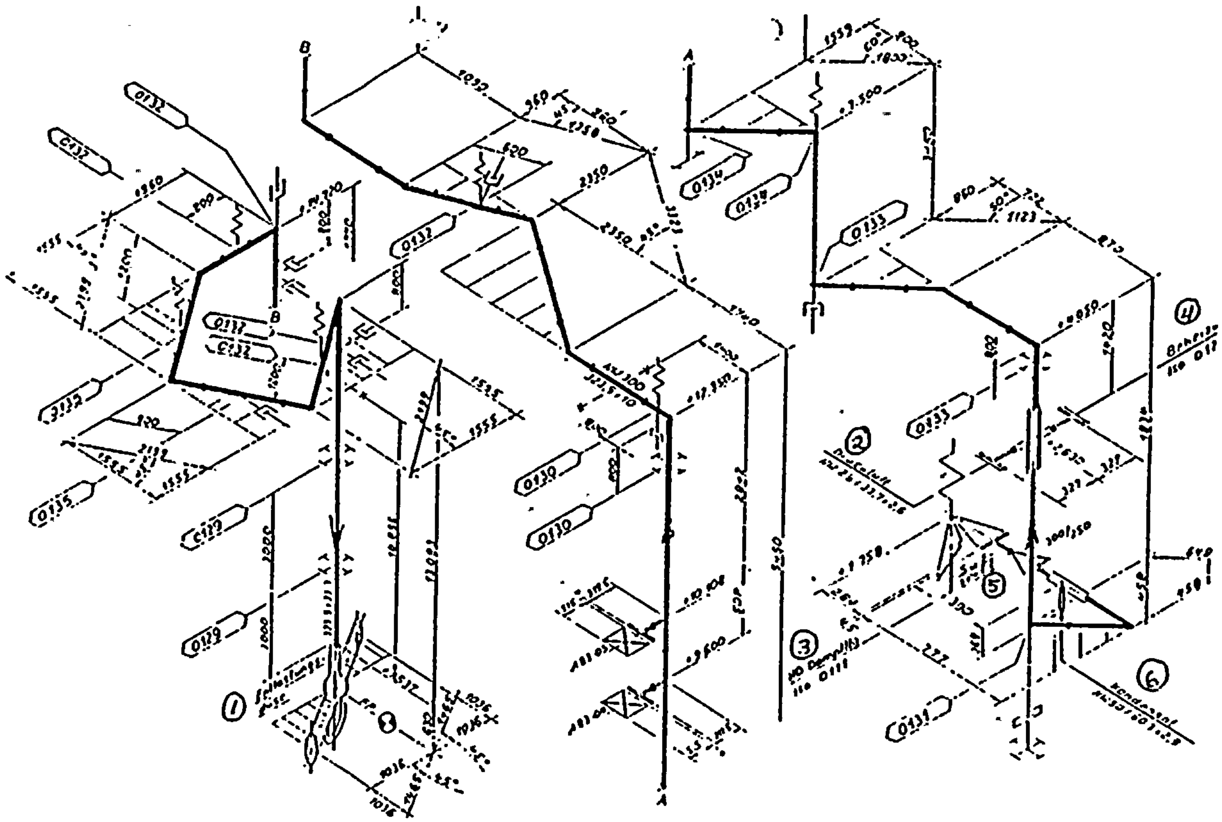

REV 1 3/79

SUSQUEHANNA STEAM ELECTRIC STATION
UNITS 1 AND 2
DESIGN ASSESSMENT REPORT

LONG DISCHARGE LINE CONFIGURATION

FIGURE 8.5

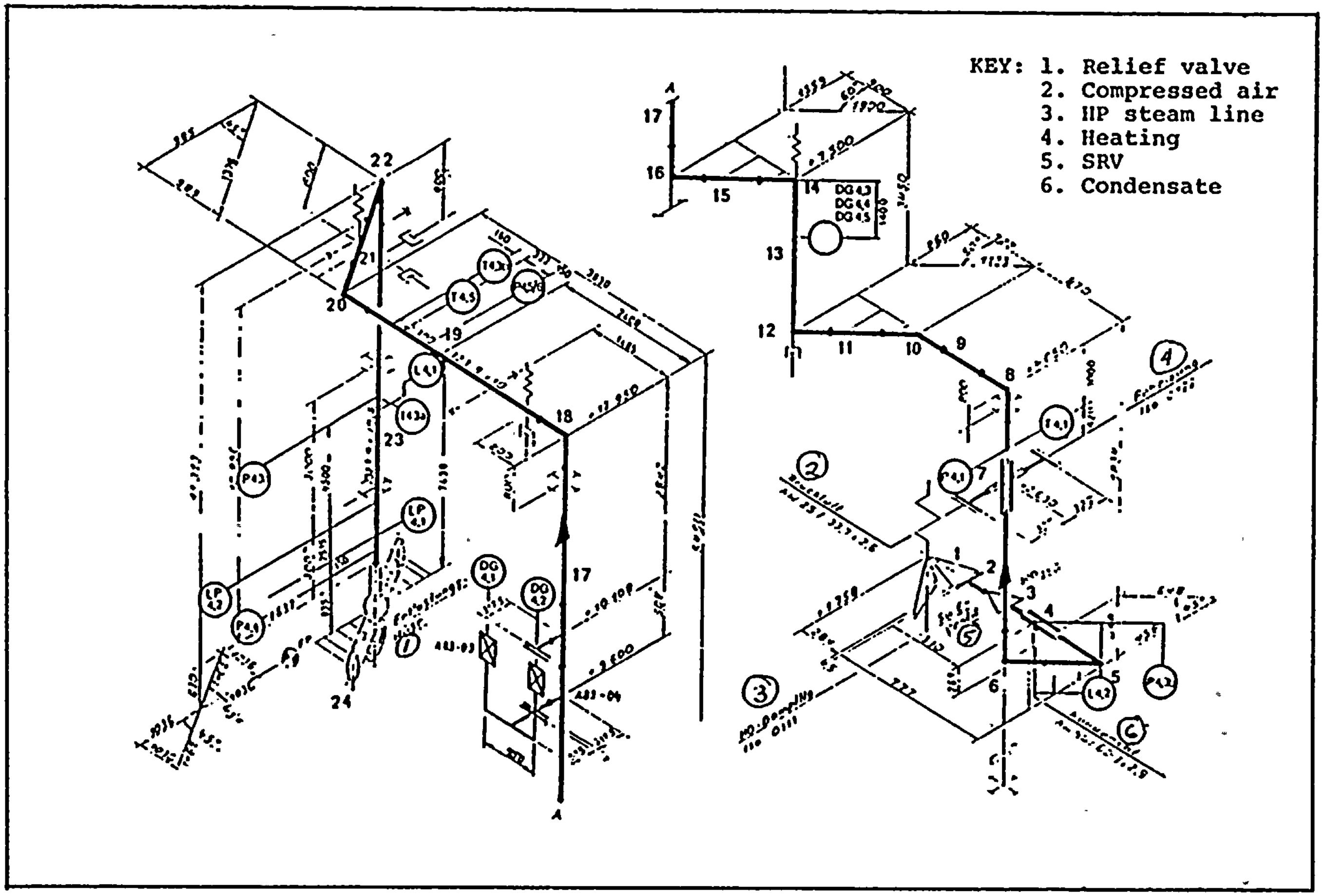

REV 1 3/79

SUSQUEHANNA STEAM ELECTRIC STATION
UNITS 1 AND 2
DESIGN ASSESSMENT REPORT

SHORT DISCHARGE LINE CONFIGURATION

FIGURE 8.6

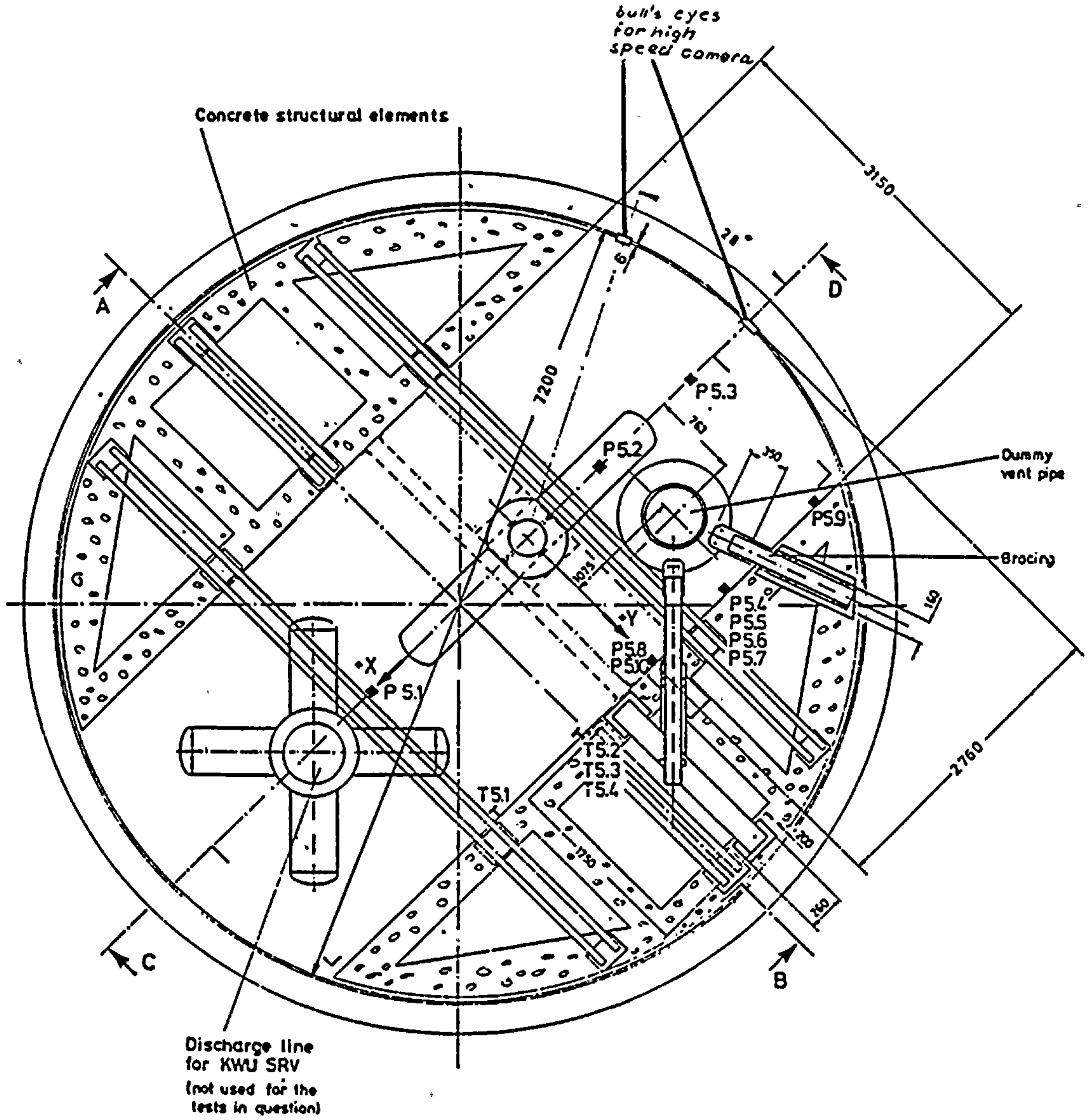

REV 1 3/79

SUSQUEHANNA STEAM ELECTRIC STATION
UNITS 1 AND 2
DESIGN ASSESSMENT REPORT

KARLSTEIN TEST TANK PLAN VIEW TYPICAL VENT CLEARING INSTRUMENTATION

FIGURE 8.7

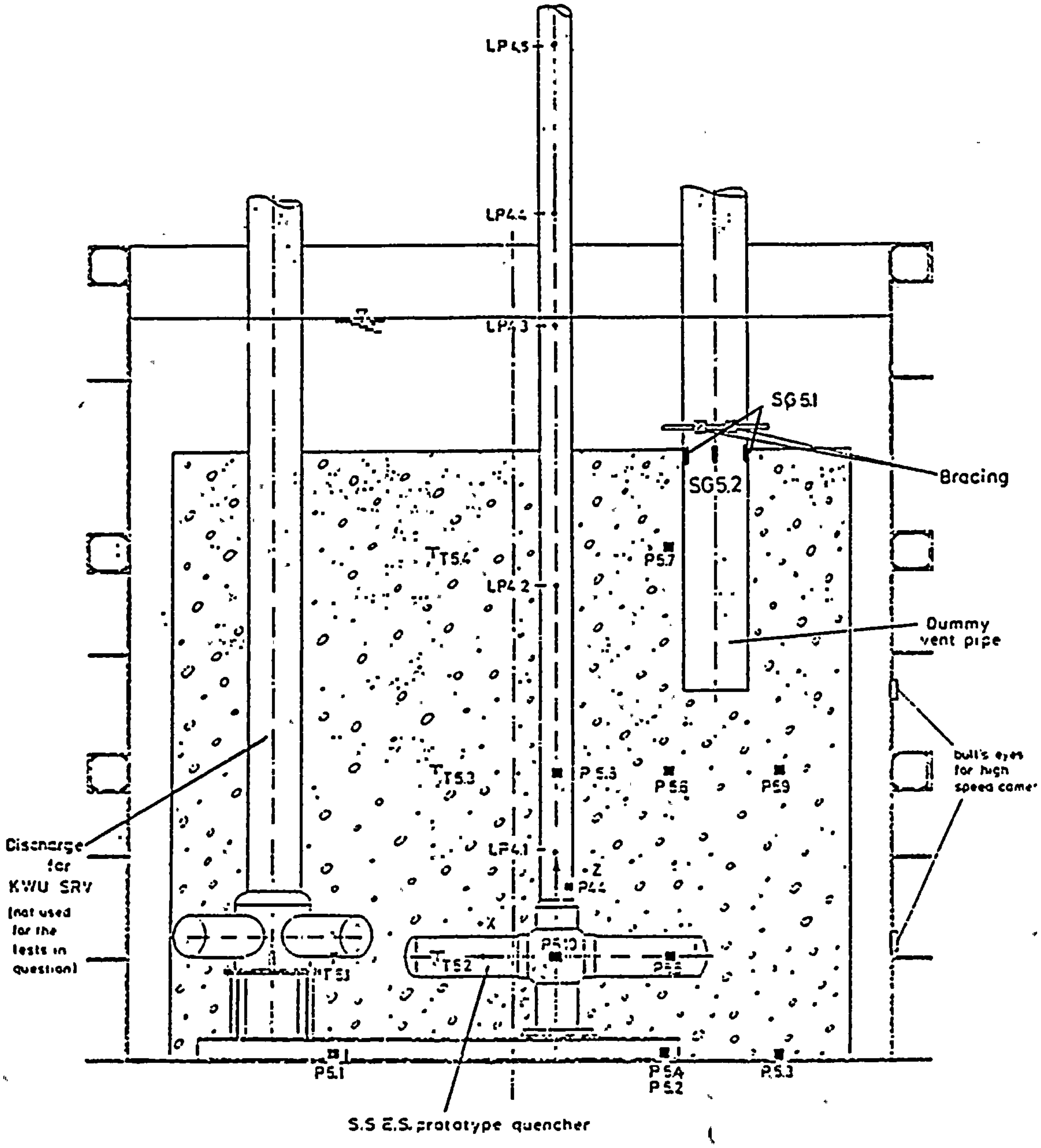

REV 1 3/79

SUSQUEHANNA STEAM ELECTRIC STATION
UNITS 1 AND 2
DESIGN ASSESSMENT REPORT

KARLSTEIN TEST TANK C-D VIEW TYPICAL VENT CLEARING INSTRUMENTATION

FIGURE 8.8

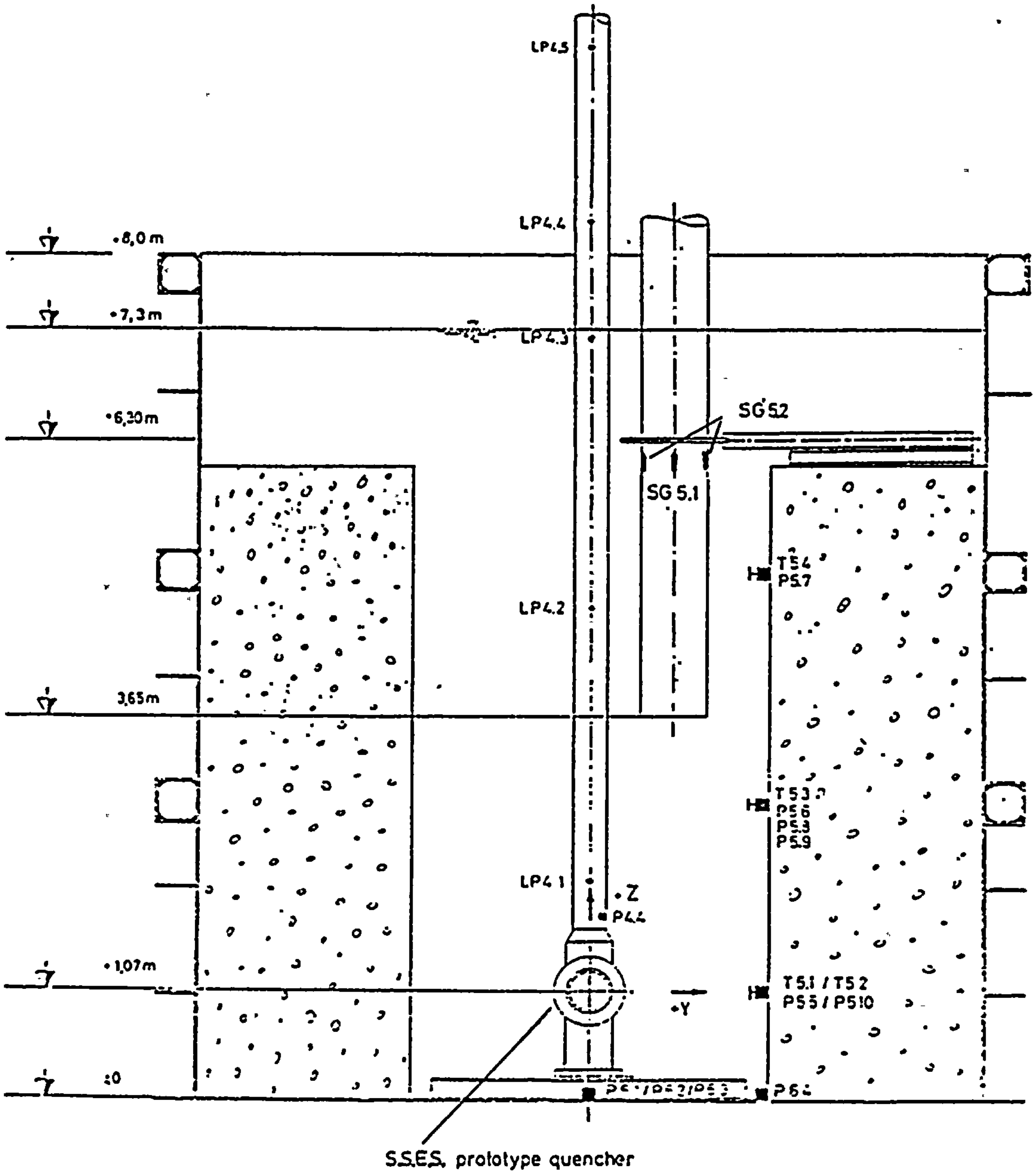

REV 1 3/79

SUSQUEHANNA STEAM ELECTRIC STATION
UNITS 1 AND 2
DESIGN ASSESSMENT REPORT

KARLSTEIN TEST TANK A-B VIEW TYPICAL VENT CLEARING INSTRUMENTATION

FIGURE 8.9

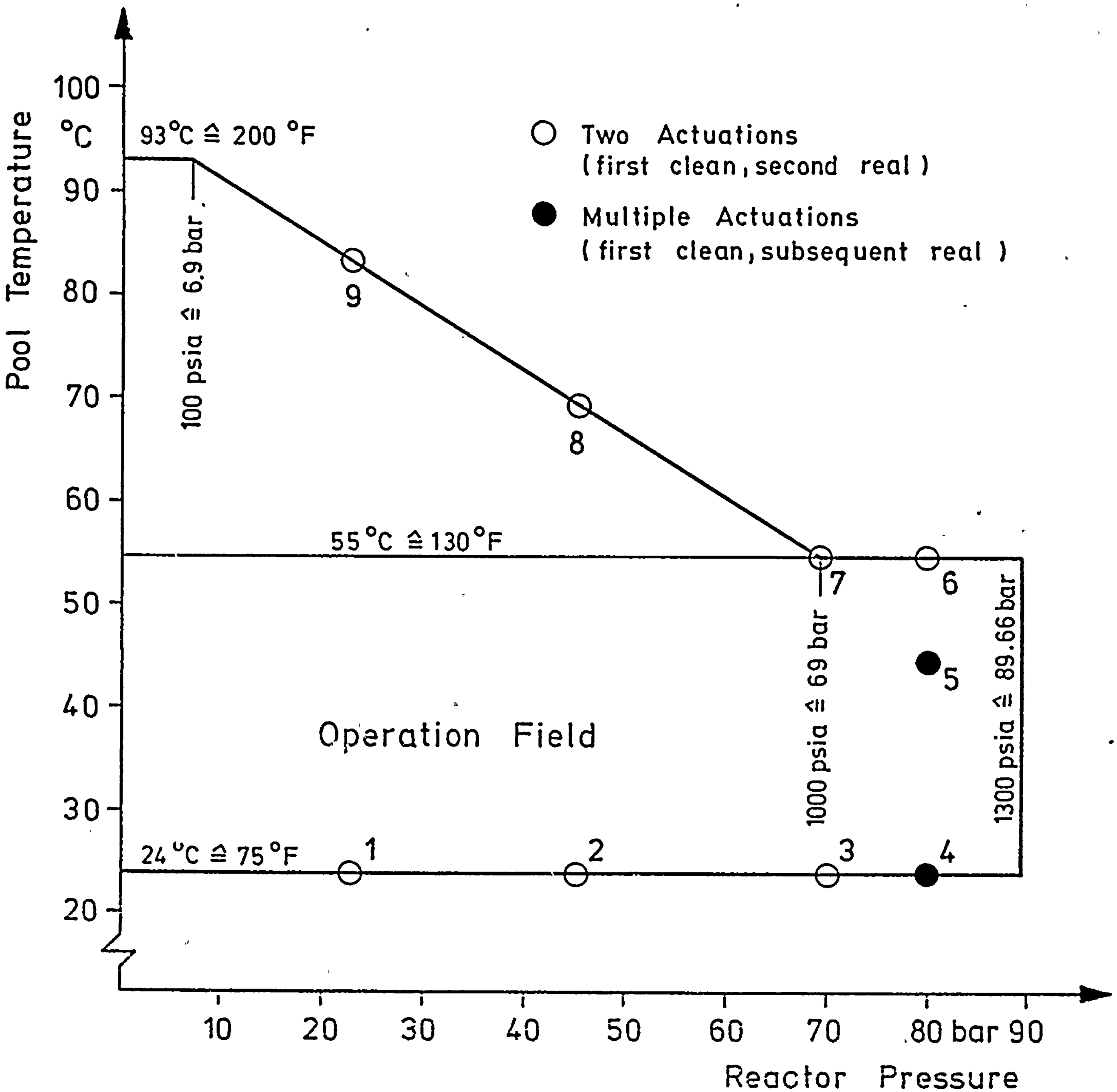

REV 1 3/79

SUSQUEHANNA STEAM ELECTRIC STATION
UNITS 1 AND 2
DESIGN ASSESSMENT REPORT

LOCATION OF TEST GROUP NO. 1
IN THE OPERATION FIELD

FIGURE 8.16

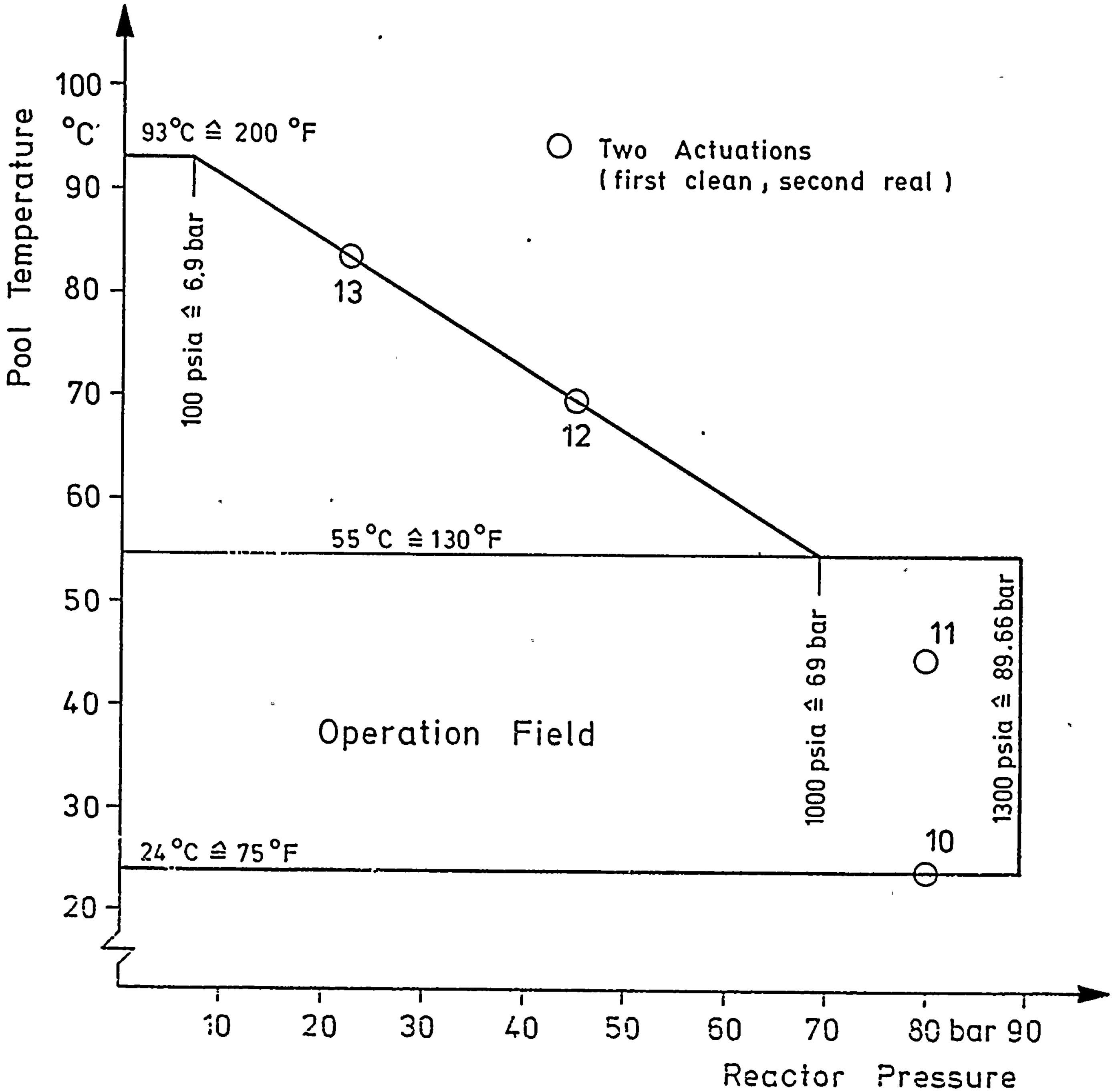

REV 1 3/79

SUSQUEHANNA STEAM ELECTRIC STATION
UNITS 1 AND 2
DESIGN ASSESSMENT REPORT

LOCATION OF TEST GROUP NO. 2
IN THE OPERATION FIELD

FIGURE 8.17

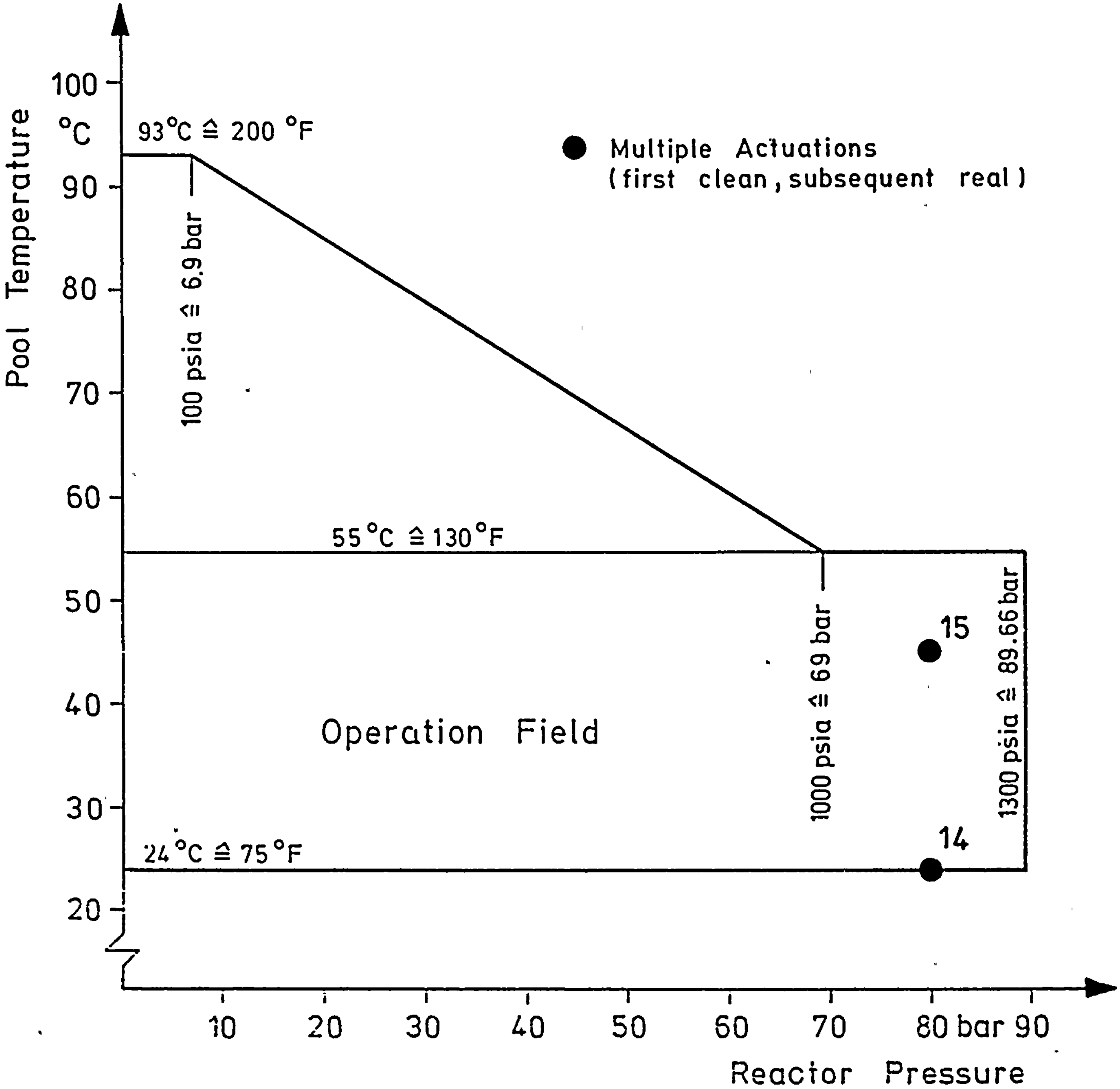

REV 1 3/79

SUSQUEHANNA STEAM ELECTRIC STATION
UNITS 1 AND 2
DESIGN ASSESSMENT REPORT

LOCATION OF TEST GROUP NO. 3
IN THE OPERATION FIELD

FIGURE 8.18

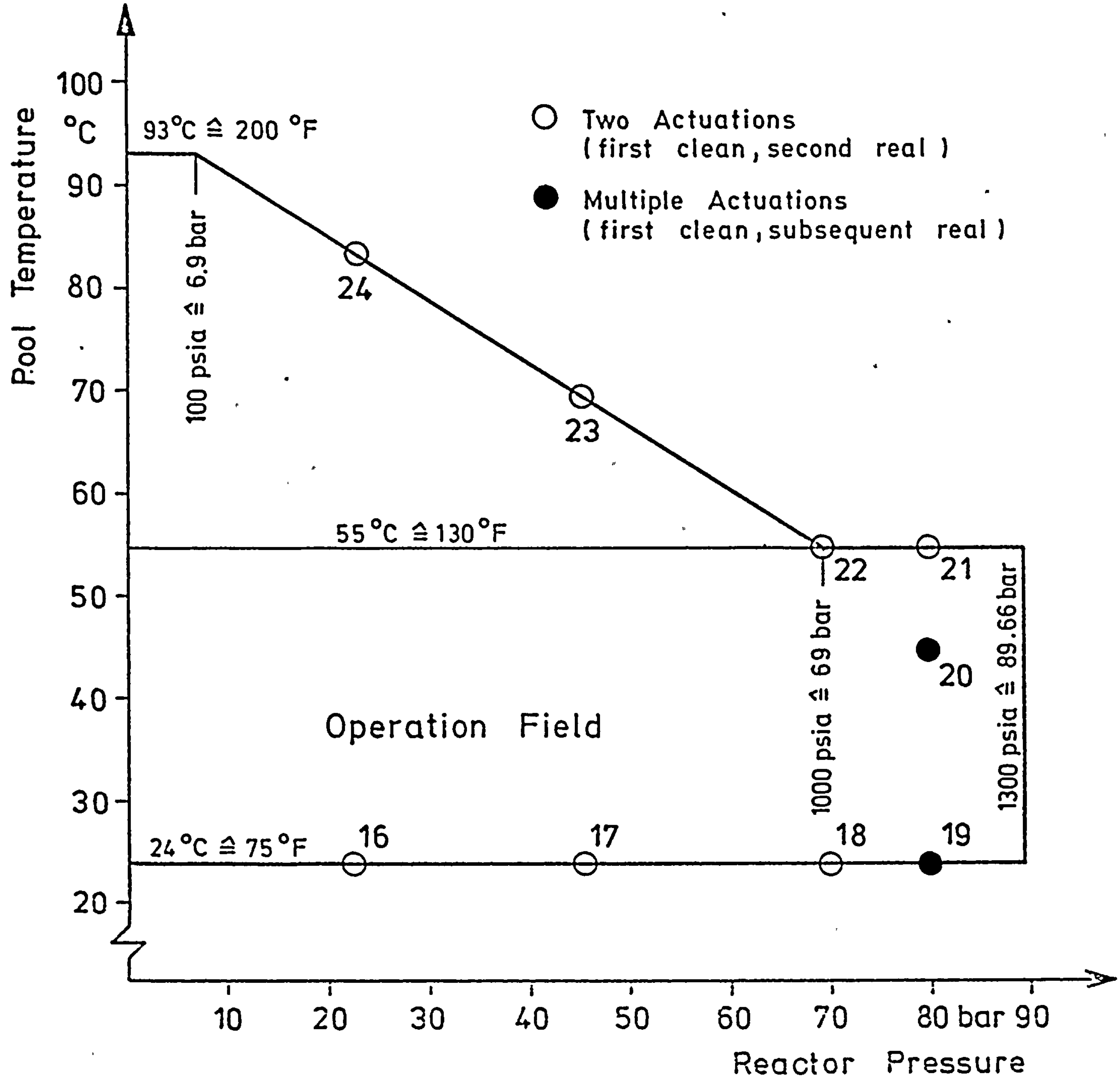

REV 1 3/79

SUSQUEHANNA STEAM ELECTRIC STATION
UNITS 1 AND 2
DESIGN ASSESSMENT REPORT

LOCATION OF TEST GROUP NO. 4
IN THE OPERATION FIELD

FIGURE 8.19

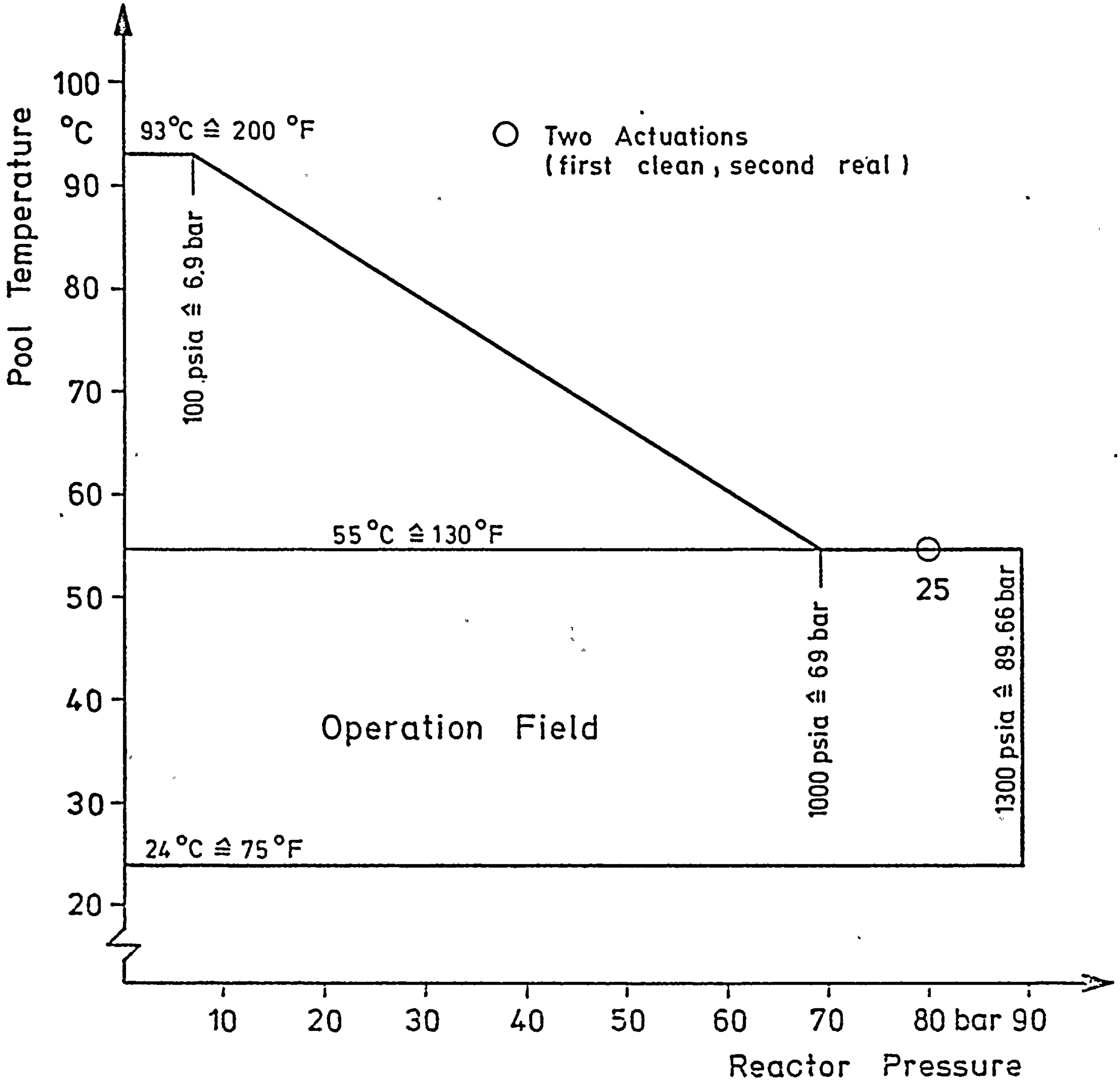

REV 1 3/79

SUSQUEHANNA STEAM ELECTRIC STATION
UNITS 1 AND 2
DESIGN ASSESSMENT REPORT

LOCATION OF TEST GROUP NO. 5
IN THE OPERATION FIELD

FIGURE 8.20

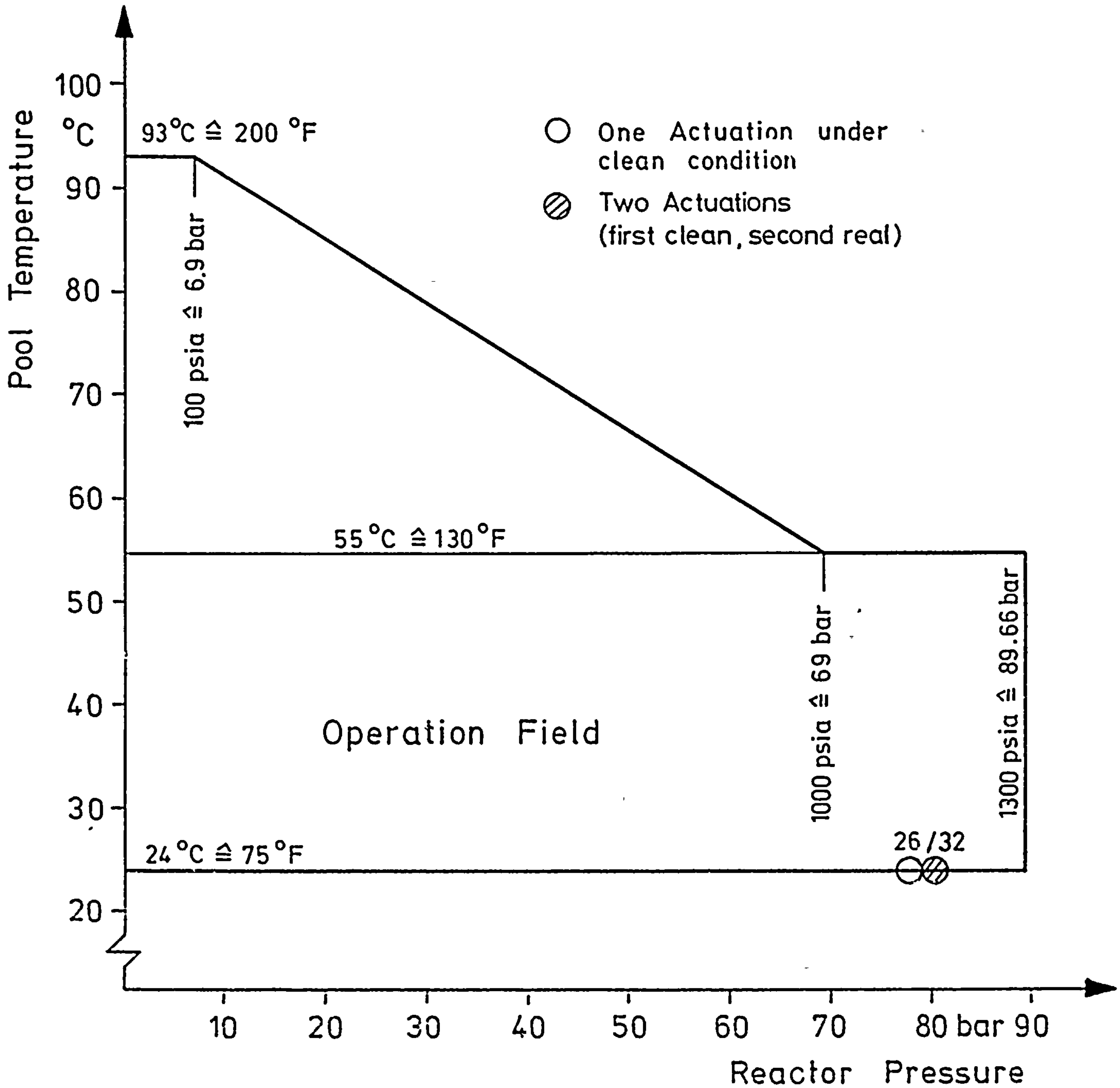

REV 1 3/79

SUSQUEHANNA STEAM ELECTRIC STATION
UNITS 1 AND 2
DESIGN ASSESSMENT REPORT

LOCATION OF TEST GROUP NO. 6
IN THE OPERATION FIELD

FIGURE 8.21

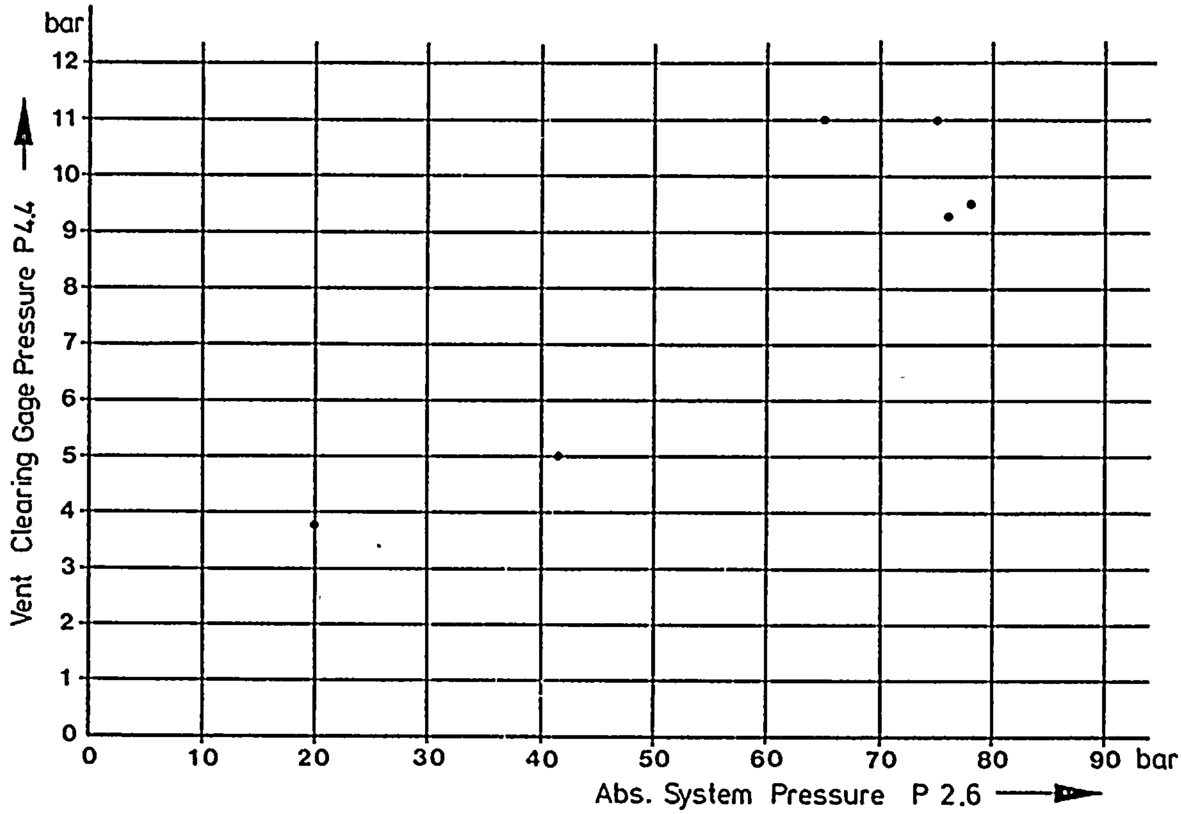

REV 1 3/79

SUSQUEHANNA STEAM ELECTRIC STATION
UNITS 1 AND 2
DESIGN ASSESSMENT REPORT

VENT CLEARING PRESSURE
VERSUS SYSTEM PRESSURE
LONG LINE VENT CLEARING
TESTS

FIGURE 8.25

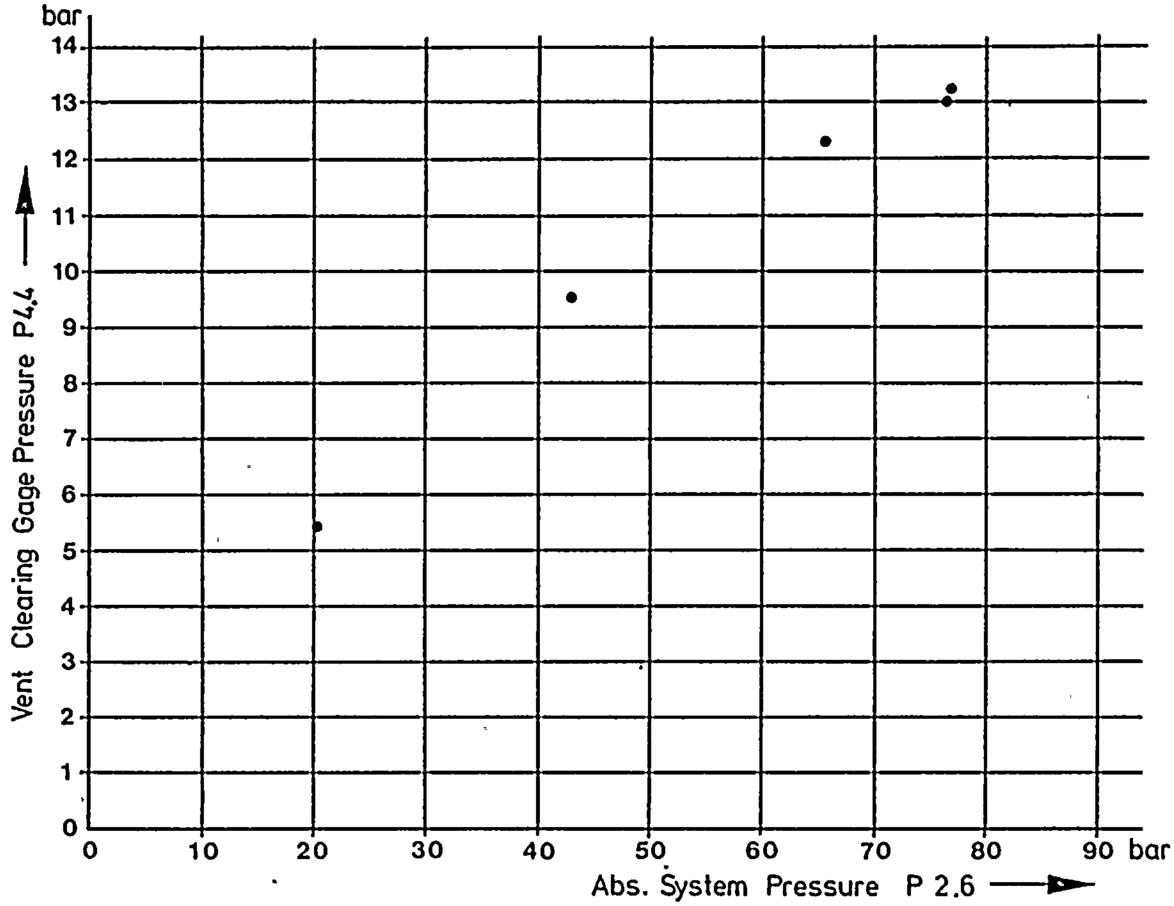

REV 1 3/79

SUSQUEHANNA STEAM ELECTRIC STATION
UNITS 1 AND 2
DESIGN ASSESSMENT REPORT

VENT CLEANING PRESSURE VERSUS SYSTEM PRESSURE SHORT LINE VENT CLEANING TESTS

FIGURE 8.26

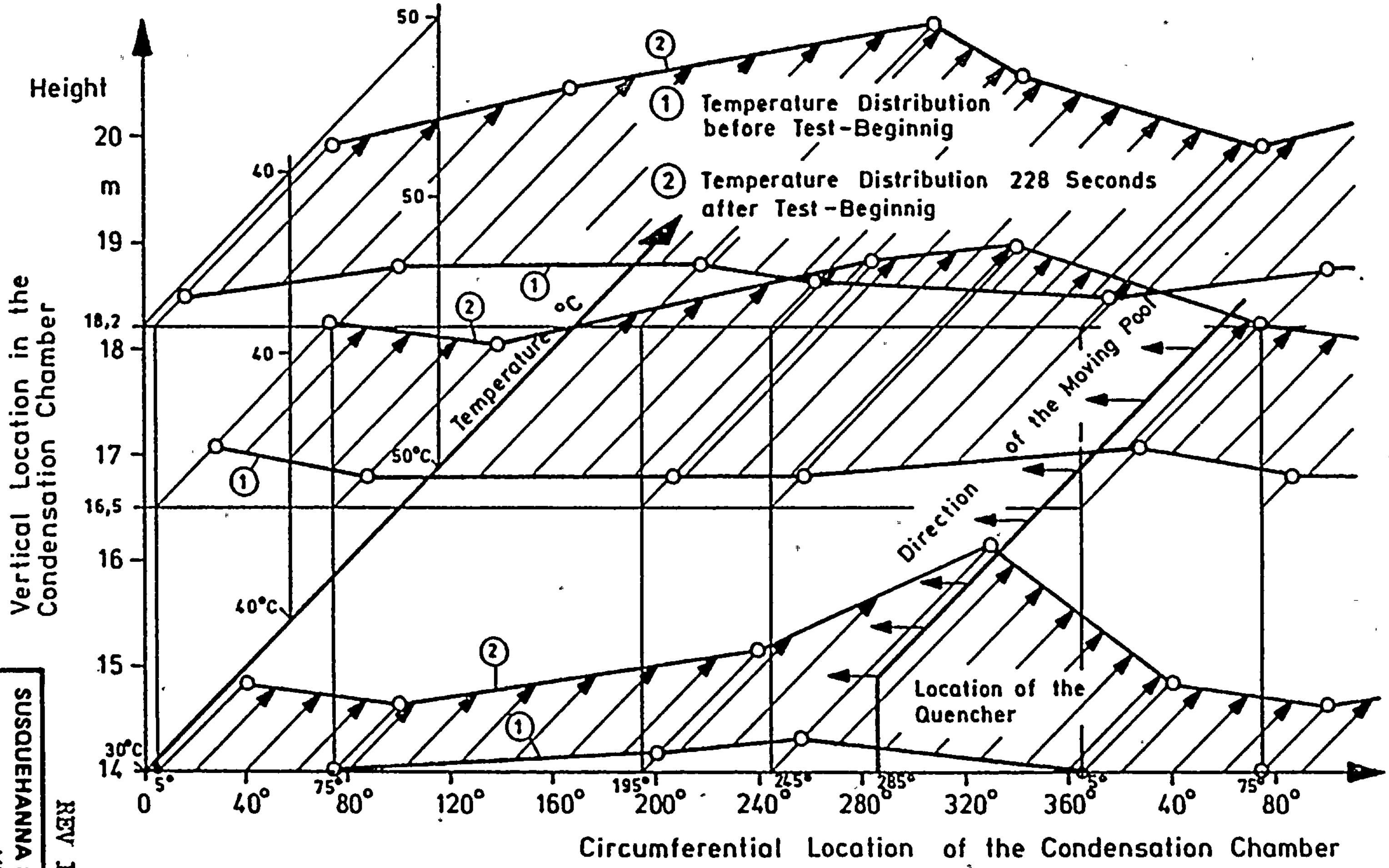

SUSQUEHANNA STEAM ELECTRIC STATION
UNITS 1 AND 2
DESIGN ASSESSMENT REPORT

REV 1 3/79

MEASURED TEMPERATURE DISTRIBUTION IN THE KKB SUPPRESSION POOL

FIGURE 8.197

50-387 SUPERSEDED Pgs Per Rev 2.
Ltr dtd 6/9 JUNE 80 2 JULY 80

PREFACE

~~This Report contains data, descriptions and anaylsis relative to the adequacy of the Susquehanna Steam Electric Station design to accommodate loads resulting from a safety relief valve (SRV) discharge and/or a loss-of-coolant accident (LOCA).~~

DAR TABLE OF CONTENTS

TABLE OF CONTENTS (Continued)

TABLE OF CONTENTS (Continued)

CHAPTER 1

GENERAL INFORMATION

TABLE OF CONTENTS

CHAPTER 1

FIGURES

CHAPTER 1

TABLES

1.0 GENERAL INFORMATION

1.1 PURPOSE AND ORGANIZATION OF REPORT

The purpose of this report is to present evidence that the Susquehanna Steam Electric Station (SSES) design margins are adequate should the plant be subjected to the recently defined thermohydrodynamic loads which result from safety relief valve (SRV) operations and/or discharges during a loss-of-coolant accident (LOCA) in a GE boiling water reactor (BWR).

1.3 QUENCHER DISCHARGE DEVICE

The criteria used for selection of the SRV discharge device for SSES were minimization of pressure oscillation loads in the suppression pool and stable condensation of steam for the range of suppression pool temperatures over which safety relief valves can be expected to operate. The options considered for satisfying these criteria were the rams-head tee, the quencher discharge device, and variations on these designs. Evaluation of the two principal devices indicated that the quencher offered significant advantages over the rams-head, including improved thermal performance at higher pool operating temperatures, as well as reduced loads.

A thermohydraulic quencher design for the safety relief system of the SSES is being engineered by Kraftwerk Union (KWU) to satisfy the above criteria. The SSES quencher design is different from that presented in the Mark II DFFR in that it has been optimized based on parametric test studies which were conducted by KWU in order to minimize SRV discharge loads.

Kraftwerk Union has supplied to PP&L a package of significant design and test reports pertaining to the quencher development to demonstrate design adequacy and quality of their device (refer to Table 1-1). With regard to the "second pop" phenomenon, KWU tests have indicated that, due to the quencher flow resistance, the water level in the SRV discharge pipe following initial discharge does not rise above the water level of the suppression pool. Refer to Subsection 4.1.3.6 for a further discussion.

To verify KWU's design approach, a full-scale SSES unique unit cell test, as described in Chapter 8, is being performed by KWU for PP&L. Section 4.1 presents the analysis methods of the SRV discharge loading.

1.4 MARK II SUPPORTING PROGRAM

PP&L is a member of the Mark II owners group that was formed in June, 1975 to define and investigate the dynamic loads due to SRV discharge and LOCA. The Mark II owners group containment program concentrated initially on the tasks required for the licensing of the lead plants (Zimmer, LaSalle, and Shoreham). This phase of work, called the short term program, is essentially complete (as of January, 1978) and a longer term program is underway. The final goal of the Mark II program is to evolve a complete DFFR which will support the plant-unique DARs submitted by each plant for its license to operate.

After gaining some understanding of the containment loads through the initial Mark II work, PP&L decided to find a qualified consultant to supplement in-house technical resources and assist in the determination of a realistic course of action for Susquehanna. In November, 1976, Stanford Research Institute, now called Stanford Research Institute International (SRI), was selected, and an information exchange between SRI and PP&L ensued to determine what caused the greatest loads on the containment structure. After conducting a complete review of known data from the Mark II program and other knowledgeable persons and organizations, PP&L and SRI decided that the loads from main steam safety relief valve (SRV) discharge were the key loads to be controlled. A study of possible methods of controlling the load and a review of what activities were occurring in Europe led PP&L and SRI to the conclusion that an SRV discharge mitigating device (quencher) should be employed to reduce this loading on the Susquehanna containment. Although the Mark II owners group had quencher-related tasks in their program, these tasks were not sufficiently timely to satisfy SSES-construction schedule needs.

From reviewing the work done in Europe by such firms as ASEATOM, MARVIKEN, and Kraftwerk Union, PP&L discovered that all known quencher designs were based on data from Kraftwerk Union (KWU). Thus, in March, 1977, SRI, Bechtel (the SSES Architect/Engineer) and PP&L visited KWU for discussion and tour of quencher-related facilities. In late July, 1977, PP&L employed the services of KWU to design a SSES-unique quencher device (see Section 1.3).

The definition of LOCA loads (Section 4.2) is in accordance with the Mark II program. Due to the schedule restrictions for Susquehanna. PP&L will define the thermo-hydrodynamic loads resulting from SRV discharge using an approach developed by KWU. This approach (presented in Section 4.1) differs from that of the Mark II program.See Table 1-1 for a summary of the documentation supporting SSES licensing.

1.5 PLANT DESCRIPTION

The SSES, Units 1 and 2, is being built in Salem Township, Luzerne County, about 5 miles northeast of the Borough of Berwick. Two generating units of approximately 1,100 megawatts each are scheduled for operation: Unit 1 for November 1, 1980, and Unit 2 for May 1, 1982. General Electric is supplying the nuclear steam supply systems; Bechtel Power Corporation is the architect-engineer and constructor.

The reactor building contains the major nuclear systems and equipment. The nuclear reactors for Units 1 and 2 are boiling water, direct cycle types with a rated heat output of 11.2×10^9 Btu/hr. Each reactor supplies 13.4×10^6 lb/hr of steam to the tandem compound, double flow turbines.

1.5.1 Primary Containment

The containment is a reinforced concrete structure consisting of a cylindrical suppression chamber beneath a truncated conical drywell. Figure 1-1 shows the geometry of the containment and internal structures. The conical portion of the primary containment (drywell) encloses the reactor vessel, reactor coolant recirculation loops, and associated components of the reactor coolant system. The drywell is separated from the wetwell, ie, the pressure suppression chamber and pool, by the drywell floor, also named the diaphragm slab. Major systems and components in the containment include the vent pipe system (downcomers) connecting the drywell and wetwell, isolation valves, vacuum relief system, containment cooling systems, and other service equipment. The cone and cylinder form a structurally integrated reinforced concrete vessel, lined with steel plate and closed at the top of the drywell with a steel domed head. The carbon steel liner plate is anchored to the concrete by structural steel members embedded in the concrete and welded to the plate.

The entire containment is structurally separated from the surrounding reactor building except at the base foundation slab (a reinforced concrete mat, top lined with a carbon steel liner plate) where a cold joint between the two adjoining foundation slabs is provided. The containment structure dimensions and parameters are listed in Tables 1-2 and 1-3. A detailed plant description can be found in the SSES FSAR, Section 3.8.

1.5.1.1 Penetrations

Services and communication between the inside and outside of the containment are made possible by penetrations through the containment wall. The basic types of penetrations are the drywell head, access hatches (equipment hatches, personnel lock, suppression chamber access hatches, CRD removal hatch), electrical penetrations, and pipe penetrations. The piping penetrations consist basically of a pipe with plate flange welded to it. The plate flange is embedded in the concrete wall and provides an anchorage for the penetration to resist normal operating and accident pipe reaction loads.

1.5.1.2 Internal Structures

The internal structures consist of reinforced concrete and structural steel and have the major functions of supporting and shielding the reactor vessel, supporting the piping and equipment, and forming the pressure suppression boundary. These structures include the drywell floor (diaphragm slab), the reactor pedestal (a concentric cylindrical reinforced concrete shell resting on the containment base foundation slab and supporting the reactor vessel), the reactor shield wall, the suppression chamber columns (hollow steel pipe columns supporting the diaphragm slab), the drywell platforms, the seismic trusses, the quencher supports, and the reactor steam supply system supports. See Figures 1-1 through 1-4 and Tables 1-2 and 1-3.

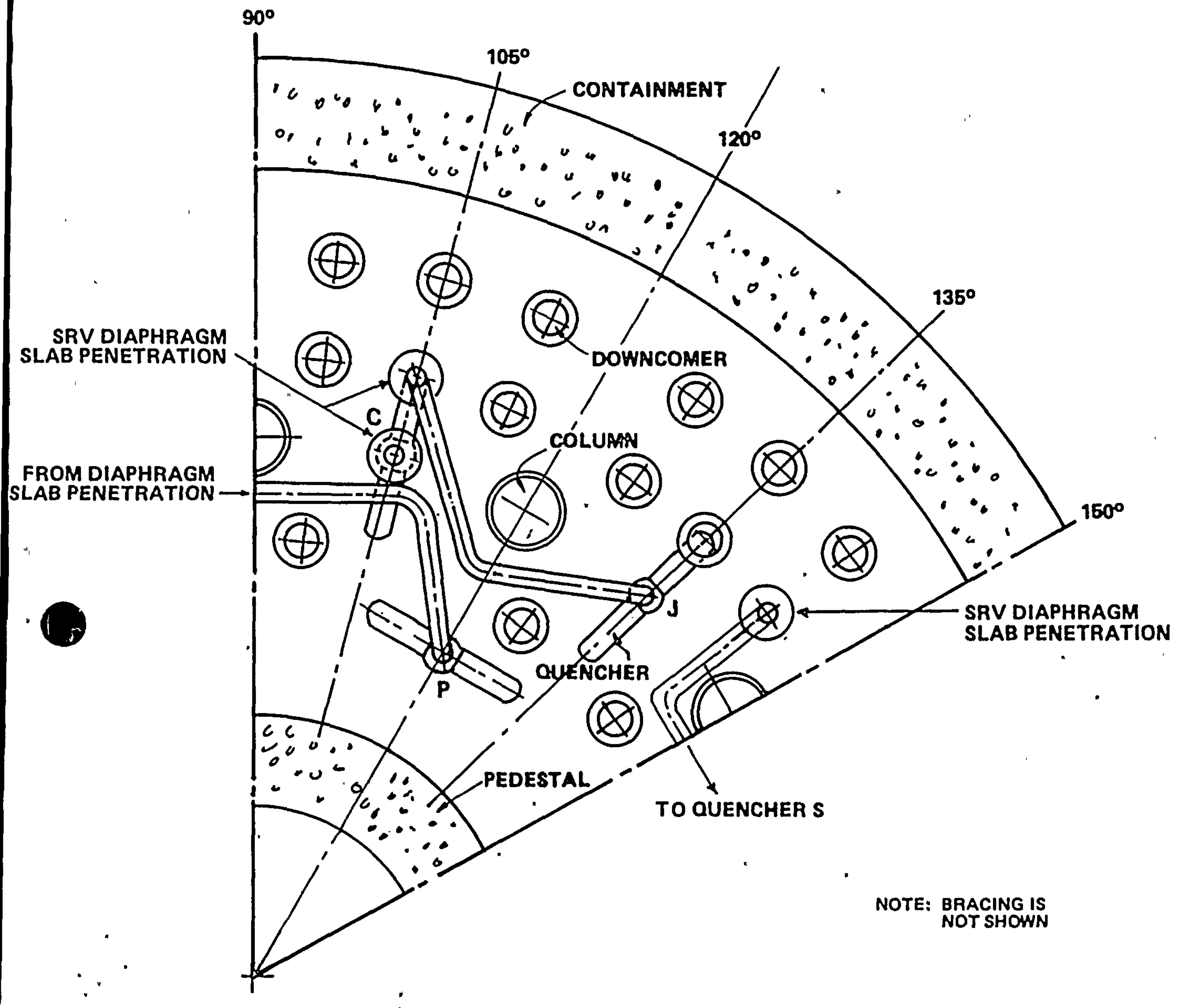

NOTE: BRACING IS NOT SHOWN

SUSQUEHANNA STEAM ELECTRIC STATION UNITS 1 AND 2 DESIGN ASSESSMENT REPORT
SUPPRESSION CHAMBER PARTIAL PLAN
FIGURE 1-2

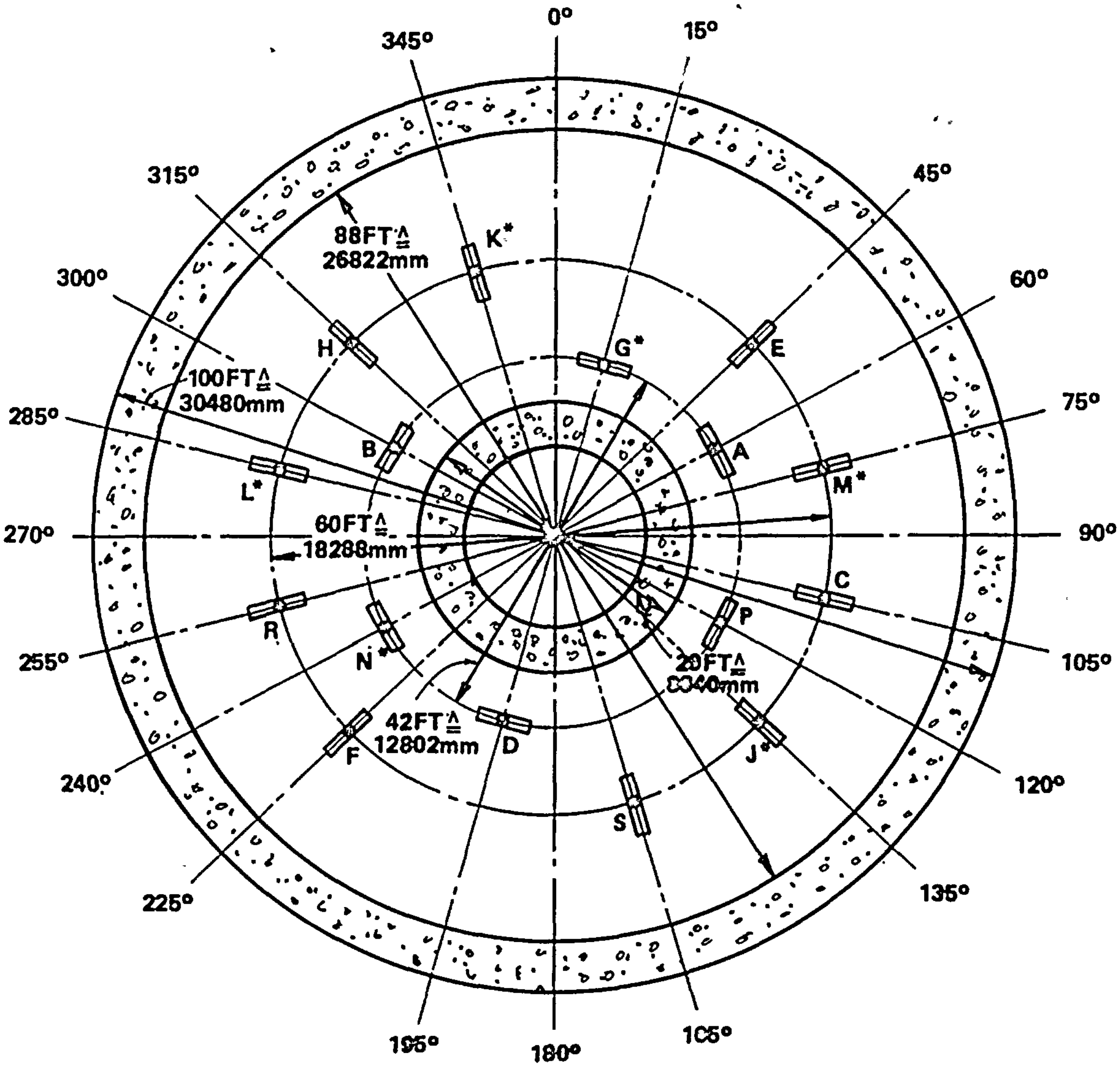

NOTE: * INDICATES ADS-ASSOCIATED QUENCHER

SUSQUEHANNA STEAM ELECTRIC STATION UNITS 1 AND 2 DESIGN ASSESSMENT REPORT
QUENCHER DISTRIBUTION
FIGURE 1-4

TABLE 1-1

SSES LICENSING BASIS

I. Mark II Containment - Supporting Program

A. LOCA - Related Tasks

Task Number	Activity	Activity Type	Target Completion	Documentation	Used for SSES Licensing
A.1.	"4T" Phases I, II, III	Phase I Test Report	Completed	NEDO/NEDE 13442-P-01 - 5/76	Yes
		Phase I Application Memorandum	Completed	Application Memo - 6/76	Yes
		Phase II & III Test Report	Completed	NEDO/NEDE 13468-P - 12/76	Yes
		Phase II & III Application Memorandum	Completed	Application Memo - 1/77	Yes
A.2.	Pool Swell Model Report	Model Report	Completed	NEDO/NEDE 21544-P - 12/76	Yes
A.3.	Impact Tests	PSTF 1/3 Scale Tests	Completed	NEDE 13426-P - 8/75	Yes
		Mark I 1/2 Scale Tests	Completed	NEDC 20989-2P - 9/75	Yes
A.4.	Impact Model	PSTF 1/3 Scale Tests	Completed	NEDE 13426-P - 8/75	Yes
		Mark I 1/2 Scale Tests	Completed	NEDC 20989-2P - 9/75	No
-	EPRI 1/13 Scale Tests	EPRI Report	Completed	EPRI NP-441 - 4/77	Yes
A.5.	Loads on Submerged Structures	LOCA/RH Air Bubble Model	12/77	NEDE 21471	Undecided
		LOCA/RH Water Jet Model	12/77	NEDE 21472	Undecided
		Applications Methods	12/77	NEDE 21730	Undecided
		Test Reports	1Q/78	Report	Undecided
A.6.	Chugging Analysis and Testing	Single Cell Report	Completed	NEDE 23703-P-11/77	Yes
		4T FSI Report	1/78	NEDE 23710-P	No
		Multivent Model	12/77	NEDE 21669-P	No
A.7.	Chugging Single Vent	CREARE Report	4Q/77	Report	No
A.8.	EPRI Test Evaluation	EPRI - 4T Comparison	Completed	NEDO 21667-8/77	Yes
A.9.	Multivent Subscale Testing and Analysis	Facility Description and Test Plan	4Q/77	Report	Undecided
		Test Report	1979	Final Report	Undecided

Task Number	Activity	Activity Type	Target Completion	Documentation	Used for SSES Licensing
A.10.	Single Vent Lateral Loads	Analysis Report	4Q/77	Report	Undecided
B.	SRV Related Tasks				
B.1.	Quencher Model	DFFR Model	Completed	NEDO/NEDE 21061-P - 9/76	No
		Confirmatory Tests	3Q/78	Report	No
B.2.	Ramshead Model	Analysis	Completed	NEDO/NEDE 21061-P - 9/76	No
B.3.	Monticello In-Plant SRV Tests	Preliminary Test Report	Completed	NEDC 21465-P - 12/76	No
		Hydrodynamic Report	Completed	NEDC 21581-P - 8/77	No
B.4.	Consecutive Actuation Transient Analysis	Analytical Models	4Q/77	Report	No
B.5.	SRV Quencher In-Plant Caorso Tests	Test Plan	Completed	NEDM 20988 - 12/76	No
		Advance Test Report	1Q/78	Report	No
		Final Report	4Q/78	Report	No
B.6.	Thermal Mixing Model	Analytical Model	4Q/78	NEDC 23689	No
B.7.	SRV Water Clearing	Analysis	3Q/78	Report	No
B.8.	Quencher Air Bubble Frequency	Analytical Model	4Q/77	Report	No
B.9.	Monticello Fluid Structure Interaction (FSI)	Analysis	1Q/78	Report	No
B.10.	DFFR Ramshead Model Comparison to Monticello Data	Data/Model Comparison	Completed	NSC-GEN 0394-10/77	No
B.11.	Ramshead SRV Methodology Summary	Analytical Methods	Completed	NEDO 24070-11/77	No
B.12.	Structural Response to SRV Discharge	Analytical Report	4Q/77	Report	No
B.13.	Quencher Empirical Model Update	Analytical Model and Correlation	1Q/79	Report	No

Task Number	Activity	Activity Type	Target Completion	Documentation	Used for SSES Licensing
C.	Miscellaneous Tasks				
C.1.	DFFR, Rev. 3	Revision	1Q/78	NEDO/NEDE 21061 Revision 3	Not yet available
C.2.	Mass and Energy Release Report	Analytical Report	3/77	GB-77-65	Yes
C.3.	NRC Round 1 Questions	DFFR Amendment 1	Completed	NEDO/NEDE 21061 Amendment 1 - 12/76	Yes
		DFFR Amendment 1, Supplement 1	12/77	NEDO/NEDE 21061 Amendment 1, Supplement 1	Yes
C.4.	Decoupling Chugging and SRV Loads		On hold		-
C.5.	SRSS Justification	SRSS Report	Completed	NEDO/NEDE 24010 - 7/77	Yes
C.6.	NRC Round 2 Questions	DFFR Amendment 2	Completed	NEDO/NEDE 21061 Amendment 2 - 6/77	Yes
		DFFR Amendment 2, Supplement 1	Completed	NEDO/NEDE 21061 Amendment 2, Supplement 1 - 8/77	Yes
		DFFR Amendment 2,		NEDO/NEDE 21061 Amendment 2,	
		Supplement 2	Completed	Supplement 2	Yes
		Supplement 3	4Q/77	Supplement 3	Yes
C.7.	Justification of "4T" Bounding Loads	Chugging Loads Justification	Completed	NEDO/NEDE 23617-P-8/77	Undecided
				NEDO/NEDE 24013-P-8/77	Undecided
				NEDO/NEDE 24104-P-8/77	Undecided
				NEDO/NEDE 24015-P-8/77	Undecided
				NEDO/NEDE 24016-P-8/77	Undecided
				NEDO/NEDE 24017-P-8/77	Undecided
				NEDO/NEDE 23627-P-8/77	Undecided
C.8.	FSI Effects in Mark II Containments	Evaluation of FSI Effects	1Q/78	Report	Undecided
C.9.	Monitor World Tests	Monitoring World Pressure Suppression Tests		Reports (Quarterly)	No

II. KWU Tests and Reports (supplied to PP&L)

Document Number	Title	Status	Documentation	Used for SSES Licensing
1.	Formation and oscillation of a spherical gas bubble	Completed	AEG - Report 2241	Yes
2.	Analytical model for clarification of pressure pulsation in the wetwell after vent cleaning	Completed	AEG - Report 2208	Yes

Document Number	Title	Status	Documentation	Used for SSES Licensing
3.	Tests on mixed condensation with model quenchers	Completed	KWV - Report 2593	Yes
4.	Condensation and vent clearing tests at GKM with quenchers	Completed	KWV - Report 2594	Yes
5.	Concept and design of the pressure relief system with quenchers	Completed	KWV - Report 2703	Yes
6.	KKB vent clearing with quencher	Completed	KWV - Report 2796	Yes
7.	Tests on condensation with quenchers when submergence of quencher arms is shallow	Completed	KWV - Report 2840	Yes
8.	KKB - Concept and task of pressure relief system	Completed	KWV - Report 2871	Yes
9.	Experimental approach to vent clearing in a model tank	Completed	KWV - Report 3129	Yes
10.	KKB - Specification of blowdown tests during non-nuclear hot functional test - Rev. I dated October 4, 1974	Completed	KWU/V 822 Report	Yes
11.	Anticipated data for blowdown tests with pressure relief system during the non-nuclear hot functional test at nuclear power station Brunsbuttel (KKB)	Completed	KWU - Report 3141	Yes
12.	Results of the non-nuclear hot functional tests with the pressure relief system in the nuclear power station Brunsbuttel	Completed	KWU - Report 3267	Yes
13.	Analysis of the loads measured on the pressure relief system during the non-nuclear hot functional test at KKB	Completed	KWU - Report 3346	Yes
14.	KKB - Listing of test parameters and important test data of the non-nuclear hot functional tests with the pressure relief system	Completed	KWU - Working Report R 521/40/77	Yes
15.	KKB - Specification of additional tests for testing of the pressure relief valves during the nuclear start-up, Rev. 1	Completed	KWU/V 822 TA	Yes
16.	KKB - Results from nuclear start-up testing of pressure relief system	Completed	KWU - Working Report R 142-136/76	Yes
17.	Nuclear Power Station Phillipsburg - Unit 1 Hot Functional Test: Specification of pressure relief valve tests as well as emergency cooling and wetwell cooling systems	Completed	KWU/V 822/RF 13	Yes

Document Number	Title	Status	Documentation	Used for SSES Licensing
18.	Results of the non-nuclear hot functional tests with the pressure relief system in the nuclear power station Phillipsburg	Completed	KWU - Working Report R 142-38/77	Yes
19.	KKPI - Listing of test parameters and important test data of the non-nuclear hot functional tests with the pressure relief system	Completed	KWU - Working Report R 521/41/77	Yes
20.	Air oscillations during vent clearing with single and double pipes	Completed	AEG - Report 2327	Yes

616715/cak

TABLE 1-3

SSES CONTAINMENT DESIGN PARAMETERS

A. Drywell and Suppression Chamber		Drywell	Suppression Chamber
1. Internal Design Pressure		53 psig	45 psig
2. External Design Pressure		5 psid	5 psid
3. Drywell Floor Design Differential Pressure			
Upward		28 psid	
Downward		28 psid	
4. Design Temperature		340°F	220°F
5. Drywell Free Volume (including vents)	(Minimum)	239,337 ft^3	
	(Normal)	239,593 ft^3	
	(Maximum)	239,850 ft^3	
6. Suppression Chamber Free Volume	(Minimum)		148,590 ft^3
	(Normal)		153,860 ft^3
	(Maximum)		159,130 ft^3
7. Suppression Chamber Water Volume	(Minimum)		122,410 ft^3
	(Normal)		126,980 ft^3
	(Maximum)		131,550 ft^3
8. Pool Cross-Section Area			
Gross (Outside Pedestal)			5379 ft^2
Total Gross (Including Pedestal Water Area)			5679 ft^2
Free (Outside Pedestal)			5065 ft^2
Total Free			5365 ft^2

CHAPTER 2

SUMMARY

TABLE OF CONTENTS

2.0 SUMMARY

This Design Assessment Report contains the SSES adequacy evaluation for dynamic loads due to LOCA and SRV discharge.

2.1 LOAD DEFINITION SUMMARY

2.1.1 SRV Load Definition Summary

Hydrodynamic loads resulting from SRV actuation fall into two distinct categories: loads on the SRV system itself (the discharge line and the discharge quencher device), and the air clearing loads on the suppression pool walls and submerged structures.

Loads on the SRV system during SRV actuation include loads on the SRV piping due to effects of steady backpressure, transient water slug clearing, and SRV line temperature. Determination of loading on the quencher body, arms, and support is based on transients resulting from valve opening (water clearing and air clearing), valve closing, and operation of an adjacent quencher.

Air clearing loads are examined for four loading cases: symmetric (all valve) SRV actuation, asymmetric SRV actuation, single SRV actuation, and Automatic Depressurization System (ADS) actuation. Dynamic forcing functions for loading of the containment walls, pedestal, basemat, and submerged structures are developed using techniques developed in Section 4.1. Loads on the SRV system due to SRV actuation are discussed in Subsection 4.1.2, and loads on suppression pool structures due to SRV actuation are discussed in Subsection 4.1.3. A full scale, unit cell test program is being employed to verify SSES unique SRV loading as described in Chapter 8.

2.1.2 LOCA Load Definition Summary

The spectrum of LOCA-induced loads on the SSES containment structure is characterized by LOCA loads associated with poolswell, condensation oscillation and chugging loads, as well as long term LOCA loads.

The LOCA loads associated with poolswell result from short duration transients and include downcomer clearing loads, water jet loads, poolswell impact and drag loads, pool fallback drag loads, poolswell air bubble loads, and loads due to drywell and wetwell temperature and pressure transients. Techniques used to evaluate these loads are described in Subsection 4.2.1.

Condensation oscillations result from mixed flow (air/steam) and pure steam flow effects in the suppression pool. Chugging loads result from low mass flux pure steam condensation. The load definitions for these phenomena are contained in Subsection 4.2.2.

Long term LOCA loads result from those wetwell and drywell pressure and temperature transients which are associated with design basis accidents (DBA), intermediate accidents (IBA), and small break accidents (SBA). Their load definitions are contained in Subsection 4.2.3.

Structures directly affected by LOCA loads include the drywell walls and floor, wetwell walls, RPV pedestal, basemat, liner plate, columns, downcomers, downcomer bracing system, quenchers, and wetwell piping. Their loading conditions are described in Subsection 4.2.4.

2.2 DESIGN ASSESSMENT SUMMARY

Design assessment of the SSES structures and components is achieved by analyzing the response of the structures and components to the load combinations explained in Chapter 5. In Chapter 7, predicted stresses and responses (from the loads defined in Chapter 4 and combined as described in Chapter 5) are compared with the applicable code allowable values identified in Chapter 6; the SSES design will be assessed as adequate by virtue of design capabilities exceeding the stresses or responses resulting from SRV discharge or LOCA loads.

2.2.1 Containment Structure and Reactor Building Assessment Summary

2.2.1.1 Containment Structure Assessment Summary

The primary containment walls, base slab, diaphragm slab, reactor pedestal, and reactor shield are analyzed for the effects of SRV and LOCA in accordance with Table 5-1. The ANSYS finite element program is used for the dynamic analysis of structures.

Response spectra curves are developed at various locations within the containment structure to assess the adequacy of components. Stress resultants due to dynamic loads are combined with other loads in accordance with Table 5-1 to evaluate rebar and concrete stresses. Design safety margins will are defined by comparing the actual concrete and rebar stresses at critical sections with the code allowable values.

2.2.1.2 Reactor Building Assessment Summary

The reactor building is assessed for the effects of SRV and LOCA loads in accordance with Table 5-1.

Containment basemat acceleration time histories are used to investigate the reactor building response to the SRV and LOCA loads. Response spectra curves at various reactor building elevations are used to assess the adequacy of components in the reactor building.

2.2.2 Containment Submerged Structures Assessment Summary

Design assessment of the suppression chamber columns and downcomer pipes is being performed. Based upon an approximate, equivalent static analysis carried out to date, strengthening of these structures should not be required. This conclusion will be confirmed when the dynamic analysis is complete.

Preliminary results from the dynamic analysis of the suppression pool liner plate indicate that no structural modifications are required This conclusion will be confirmed when the final analysis is complete.

The original downcomer bracing has been redesigned with pipe sections to minimize bracing drag loads due to poolswell and fallback. The revised bracing system is designed using a simplified equivalent static approach.

2.2.3 Piping Systems Assessment Summary

Containment and reactor building piping systems are being designed to withstand the effects of LOCA and SRV induced dynamic loads. The load combinations for piping are defined in Table 6.1 of Ref. 10.

3.1 DESCRIPTION OF SAFETY RELIEF VALVE DISCHARGE

Susquehanna Units 1 and 2 are equipped with a safety relief system which condenses reactor steam in a suppression chamber pool. By this arrangement, reactor steam is conducted to the wetwell via fast acting safety relief valves and quencher equipped discharge lines. This section discusses the causes of SRV discharge, describes the SRV discharge process, and identifies the resultant SRV discharge actuation cases.

3.1.1 Causes of SRV Discharge

During certain reactor operating transients, the SRVs may be actuated (by pressure, by electrical signal, or by operator action) for rapid relief of pressure in the reactor pressure vessel. The following reactor operating transients have been identified as those which may result in SRV actuation:

a. Turbine generator trip (with bypass or without)

b. Main steam line isolation valve (MSIV) closure

c. Loss of condenser vacuum

d. Feedwater controller failure

e. Pressure regulator failure - open

f. Generator load rejection (with and without bypass)

g. Loss of ac power

h. Loss of feedwater flow

i. Trip of two recirculation pumps

j. Recirculation flow control failure - decreasing flow

k. Inadvertent safety relief valve opening

A detailed description of these transients is provided in Section 15.2 of the FSAR.

3.1.2 Description of the SRV Discharge Phenomena and SRV Loading Cases

Before an individual safety relief valve opens, the water level in the discharge line is approximately equal to the water level in the pool. As a valve opens, steam flows into the discharge line air space between the valve and the water column and mixes with the air (see detailed evaluation in Chapter 3 of Ref 1, pages 6-12 through 6-14). Since the downstream portion of the discharge line contains a water slug and does not allow an immediate steam discharge into the pool, the pressure inside the line increases. The increased pressure expels the water slug from the SRV discharge line and quencher. The magnitude of the water clearing pressure is primarily influenced by the steam flow rate through the valve, the degree to which entering steam is condensed along the discharge line walls, the volume of the discharge line airspace, and the length of the water slug to be accelerated.

The clearing of water is followed by an expulsion of the enclosed air-steam volume. The exhausted gas forms an oscillating system with the surrounding water, where the gas acts as the spring and the water acts as the mass. This oscillating system is the source of short term air clearing loads.

While the air-steam mixture oscillates in the pool it rises because of buoyancy and eventually breaks through the pool water surface at which time air clearing loads cease. When all the air leaves the safety relief system, steam flows into the suppression pool through the quencher holes and condenses. The SSES quencher design assures stable condensation even with elevated pool water temperature.

The SRV actuation cases resulting from the transients listed in Subsection 3.1.1 are classified, as being one of the following cases:

a. Symmetric (all valve, or AOT) discharge

b. Asymmetric discharge, including single valve discharge

c. Automatic Depressurization System (ADS) discharge

Also considered in the containment design is the effect of subsequent SRV actuations (second-pop), discussed in Subsection 4.1.3.6.

The symmetric discharge case (otherwise termed the all-valve, or AOT, case) is classified as the type of SRV discharge that would follow rapid isolation of the vessel from the turbine such as turbine trip, closure of all MSIVs, loss of condenser vacuum, etc. As pressure builds up following isolation of the vessel, the SRVs actuate sequentially according to the pressure set points of the valves. This may or may not result in actuation of all the SRVs, but for conservatism in loading considerations all valves are assumed to actuate. Refer to Subsection 4.1.3.1 for discussion of the loads resulting from this all-valve case.

Asymmetric discharge is defined as the firing of the SRVs for the three adjacent quencher devices which results in the greatest asymmetric pressure loading on the containment. This situation is hypothesized when, following a reactor scram and isolation of the vessel, decay heat raises vessel pressure so that low set point valves actuate. If, during this time of discharge of decay heat energy, manual actuation of the two other adjacent SRVs that comprise the asymmetric case is assumed, this actuation would result in the maximum symmetric pressure load on the containment. Subsection 4.1.3.2 gives a discussion of the loads resulting from the asymmetric discharge case.

The single valve discharge case is classified as the firing of the SRV which gives the single largest hydrodynamic load. Transients that could potentially initiate such a case are an inadvertent SRV discharge or Design Basis Accident (DBA). Refer to Subsection 3.2.3 for a discussion of the latter possibility. Subsection 4.1.3.2.1 provides a discussion of the loads resulting from the single valve case.

The ADS discharge is defined as the simultaneous actuation of the six SRVs associated with the ADS. See Figure 1-4 for the location of the quencher devices associated with the ADS valves. The ADS is assumed to actuate during an Intermediate Break Accident (IBA) or Small Break Accident (SBA). If an ADS discharge is hypothesized coincident to an IBA or SBA (described in Subsections 3.2.2 and 3.2.1, respectively), the effects of an increased suppression pool temperature (resulting from steam condensation during the LOCA transient) and increased suppression chamber pressure (resulting from clearing of the drywell air into the pool during the transient) are considered in the calculation of pressure loadings for the ADS discharge case. See Subsection 4.1.3.3 for further discussion of the loads resulting from the ADS case.

3.2 DESCRIPTION OF LOSS-OF-COOLANT ACCIDENT

This event involves the postulation of a spectrum of piping breaks inside the containment varying in size, type, and location of the break. For the analysis of hydrodynamic loadings on the containment, the postulated LOCA event is identified as a Small Break Accident (SBA), an Intermediate Break Accident (IBA), or aDesign Basis Accident (DBA).

3.2.1 Small Break Accident (SBA)

This subsection discusses the containment transient associated with small primary system blowdowns. The primary system ruptures in this category are those ruptures that will not result in reactor depressurization from either loss of reactor coolant or automatic operation of the ECCS equipment, ie, those ruptures with a break size less than 0.1 sq ft.

The following sequence of events is assumed to occur. With the reactor and containment operating at the maximum normal conditions, a small break occurs that allows blowdown of reactor steam or water to the drywell. The resulting pressure increase in the drywell leads to a high drywell pressure signal that scrams the reactor and activates the containment isolation system. The drywell pressure continues to increase at a rate dependent upon the size of the steam leak. The pressure increase lowers the water level in the downcomers. At this time, air and steam enter the suppression pool at a rate dependent upon the size of the leak. Once all the drywell air is carried over to the suppression chamber, pressurization of the suppression chamber ceases and the system reaches an equilibrium condition. The drywell contains only superheated steam, and continued blowdown of reactor steam condenses in the suppression pool. The principal loading condition in this case is the gradually increasing pressure in the drywell and suppression pool chamber and the loads related to the condensation of steam at the end of the vents.

3.2.2 Intermediate Break Accident (IBA)

This subsection discusses the containment transient associated with intermediate primary system blowdowns. This classification covers breaks for which the blowdown will result in limited reactor depressurization and operation of the ECCS, ie, the break size is equal to or slightly greater than 0.1 sq ft.

Following the break, the drywell pressure increases at approximately 1.0 psi/sec. This drywell pressure transient is sufficiently slow so that the dynamic effect of the water in the vents is negligible and the vents will clear when the drywell-to-suppression chamber differential pressure is equal to the hydrostatic pressure corresponding to the vent submergence. The

CHAPTER 4

LOAD DEFINITION

TABLE OF CONTENTS

CHAPTER 4

FIGURES

CHAPTER 4

TABLES

4.0 LOAD DEFINITION

4.1 SAFETY RELIEF VALVE (SRV) DISCHARGE LOAD DEFINITION

See the Proprietary Supplement for this section.

4.2 LOCA LOAD DEFINITION

Subsections 4.2.1, 4.2.2 and 4.2.3 will discuss the numerical definition of loads resulting from a LOCA in the SSES containment. The LOCA loads are divided into three groups.

(1) Short term LOCA loads associated with poolswell (Subsection 4.2.1).

(2) Condensation oscillations and chugging loads (Subsection 4.2.2).

(3) Long term LOCA loads (Subsection 4.2.3).

The application of these loads to the various components and structures in the SSES containment is discussed in Subsection 4.2.4.

4.2.1 LOCA LOADS ASSOCIATED WITH POOLSWELL

A description of the LOCA/Poolswell transient has been given in Section 3.2 of this Design Assessment Report. The LOCA loads associated with poolswell are listed in Table 4-16. The appropriate Mark II generic document from which SSES plant unique loads are calculated is also shown in Table 4-16. A discussion of these loads and their SSES unique values follows.

4.2.1.1 Wetwell/Drywell Pressures during Poolswell

The drywell pressure transient used for the poolswell portion of the LOCA transient ($\leq$ 2.0 seconds) is given in Table IV-D-3 of Ref 7. A portion of this table is reproduced herein as Table 4-17. This drywell pressure transient includes the blowdown effects of pipe inventory and reactor subcooling and is the highest possible drywell pressure case for poolswell.

The short term poolswell wetwell pressure transient resulting from this drywell pressure transient is calculated by applying the poolswell model contained in Ref 8. The equations and assumptions in the poolswell model were coded into a Bechtel computer program and verified against the Class 1, 2 and 3 test cases contained in Ref 9. This verification is documented in Appendix D to this report. Other inputs used for the calculation of the SSES plant unique poolswell transient are shown in Table 4-18. The short term suppression pool surface elevation and corresponding wetwell pressure transient calculated with the poolswell code are shown in Figures 4-38 and 4-39 respectively. The short term wetwell pressure peak is 56.1 psia (41.4 psig). The (drywell minus wetwell) pressure differential is also plotted on this curve. The minimum Δ P occurring during poolswell is -9.2 psid at 0.893 seconds after vent clearing (1.58 seconds after the break occurs).

4.2.1.2 Poolswell Impact Load

Any structure located between the initial suppression pool surface (el. 672') and the peak poolswell height (el. 690', see figure 4-38) is subject to the poolswell water impact load. There are only minor structures (such as miscellaneous wetwell piping) in this portion of the SSES wetwall. This load is calculated as specified in Ref 10, Subsection 4.4.6. A SSES plant-unique velocity vs elevation curve has been generated with the poolswell model (Figure 4-40). It is used in conjunction with impact pressure vs velocity curves for various size and shape components (Ref 10, Figures 4-34, 4-35 and 4-36) to develop a peak impact pressure at the component's elevation. The peak impact pressure is combined with a generalized impact pressure time history curve (Ref 10, Figure 4-37) to specify the structural load. All structures subject to poolswell impact loads in the SSES containment are classified as "small structures".

4.2.1.3 Poolswell Drag Load

The poolswell drag load applies to any structure located between the elevation of the vent exit (el. 660') and the peak pool swell height (el. 690'). The load is calculated for all components in the region based upon the maximum pool surface velocity (29.35 fps), regardless of elevation. The drag load pressure is calculated from Ref 10, Equation 4-24 using V_f = 29.35 fps for the velocity and ρ_f = 62.4 lbm/ft^3 for the density of water,

$$P_D = (1/2)C_D \rho_f V_f^2 \qquad (4-1)$$

$$P_D \text{ (psi)} = 5.8\ C_D. \qquad (4-2)$$

The appropriate drag coefficient for the structure involved is selected from Ref 10, Figure 4-29. The pool swell drag load is applied in either the horizontal or vertical direction (Subsection 4.4.5.2 of Ref 10).

For the case of a component oriented vertically with its axis parallel to the velocity of the pool surface, the skin friction coefficient, C_f, used in Ref 10, Subsection 4.4.8 is applied in place of C_D. This method would apply, for example, to the vertical loads on downcomers, columns, or safety relief lines in the wetwell. Using C_f = 0.0023, the vertical drag force on a vertically oriented component is recalculated using Equation 4-26 of Ref 10.

$$F_V \text{(lbf)} = 0.0133 A_f \text{ (in}^2\text{)}. \qquad (4-3)$$

Here A_f is the skin friction area (wetted surface area) subject to the vertical drag force.

LOCA loads on the downcomer bracing are described in Subsection 4.2.4.6.

4.2.1.4 Downcomer Clearing Loads

Vertical loads on the downcomers during downcomer clearing can be estimated by using a drag load formula similar to Equation 4-3. In this case the vent clearing velocity is 60 fps (Ref 10, Subsection 4.4.5.1) and A_f is the wetted inside area of the downcomer, conservatively calculated to be

$$A_f = (12 \text{ ft}) (\pi) (2 \text{ ft}) = 75.4 \text{ ft}^2.$$

From Equation 4-3 the vertical clearing load on the downcomer for SSES is,

$$F_v = 0.6 \text{ kips.}$$

This is of similar magnitude to the vertical thrust load of 0.7 kips on the downcomer during steam blowdown (Ref 10, Subsection 4.2.3).

Lateral loads on the downcomers during clearing are estimated from Ref 11, Table 3-4 to be less than 3 kips.

4.2.1.5 Downcomer Water Jet Load

The water clearing jet load is calculated based on the approach developed in the design guides (Refs 12 and 13). This load is experience as a drag load by structures located within the jet cone beneath the downcomers and as a jet impingement load by the basemat. The jet impingement load on the basemat is calculated from Ref 10, Equation 4-25, p. 4-43.

$$F_I = \rho_f \; A_r \; v_f^2 \qquad (4\text{-}4)$$

Here ρ_f is the density of water (taken to be 62.4 lbm/ft³), A is the total jet impingement area and v is the attenuated water velocity corresponding to the maximum vent clearing jet velocity (Ref 10). Figures 4-41 and 4-42 show elevation and plan views of the SSES downcomers and their associated jet cones. The radius of the jet cone at the basemat is 2.69 ft. and the total area intercepted by the 87 downcomers in the SSES wetwell is 1978 ft². As seen in Figure 4-42 there is no significant overlap of adjacent jets on the basemat.

The vent clearing velocity of 60 fps is attenuated by a factor of 0.68 using the method described in Ref. 10, Subsection 4.4.5.1 to yield a value of 40.8 fps at the basemat. The jet impingement pressure is calculated from Ref 10, Equation 4-26, p. 4-43 to be

$$P_I = \rho_f \; v_f^2 \qquad (4\text{-}5)$$

$$P_I = 22.4 \text{ psi.}$$

Using the value for A of 1978 ft² for the SSES design the total downcomer water jet impingement load on the basemat is

$F = 2848.3$ kips.

This load acts vertically downward on the basemat from the time the break occurs until the downcomers have cleared, at 0.6863 sec (Ref 7).

4.2.1.6 Poolswell Air Bubble Load

The poolswell air bubble pressure load as it applies to the containment walls is described in Ref 10, Subsection 4.4.5.3.

This load is viewed as an increase in the hydrostatic pressure on the suppression pool walls below the vent exit plane and is caused by the air bubble which has been purged from the drywell in the initial stages of the LOCA. The air bubble pressure transient calculated with the poolswell model (described in Subsection 4.2.1.2) is shown in Figure 4-43. Figure 4-44 shows the normalized total pressure distribution (hydrostatic plus air bubble) to be applied to the containment as a result of this load. The pressure on the wetwell walls between the vent exit and the water surface contains a linear decrease to 0.0 psig at the water surface (Ref 10, Subsection 4.4.5.3).

This load as it applies to submerged structures is described in Refs 13 and 14.

4.2.1.7 Poolswell Fallback Load

The poolswell fallback load is a drag load which applies to all structures between the peak poolswell height (el. 690') and the vent exit (el. 660'). This load is calculated for components in this region using the analysis of Subsection 4.4.5.4 of Ref 10.

Since the vertical structures are parallel to the fallback flow, they are subjected to negligible fallback loads. (For a fallback velocity of 30 fps the load is significantly less than 1 kip). The downcomer bracing structure at elevation 668'-0" is, however, perpendicular to the fallback flow and will undergo a fallback load applied vertically downward. The fallback drag velocity is calculated using the equation on page 4-45 of Ref 10.

$$V_{FB} = 9.82 \, (H_O)^{1/2}. \qquad (4\text{-}6)$$

For the SSES design, the maximum downcomer submergence, H_O, is 12 feet so the fallback velocity is 34.05 fps. The drag pressure due to this velocity is calculated from Ref 10, Equation 4-24 to be

$$P_{FB} \text{ (psi)} = 7.8 \, C_D, \qquad (4\text{-}7)$$

where C_D is the appropriate drag coefficient for the structure being loaded.

Fallback loads are calculated using Refs 12 and 13.

4.2.2 Condensation Oscillations and Chugging Loads

Condensation oscillation and chugging loads follow the poolswell loads in time. There are basically three loads in this time period, i.e., from about 4 to 60 seconds after the break. Condensation oscillation is broken down into two phenomena, a mixed flow regieme and a steam flow regieme. The mixed flow regieme is a relatively high mass flux phenomenon which occurs during the final period of air purging from the drywell to the wetwell. Thus, the mixed flow through the downcomer vents contains some air as well as steam. The steam flow portion of the condensation oscillation phenomena occurs after all the air has been carried over to the wetwell and a relatively high mass flux of pure steam flow is established.

Chugging is a pulsating condensation phenomenon which can occur either following the intermediate mass flux phase of a LOCA, or during the class of smaller postulated pipe breaks that result in steam flow through the vent system into the suppression pool. A necessary condition for chugging to occur is that pure steam flows from the LOCA vents. Chugging imparts a loading condition to the suppression pool boundary and all submerged structures.

4.2.2.1 Condensation Oscillation Load Definition

The load specification for the mixed and steam flow phases of condensation oscillation is taken from Appendix A to Ref 20.

The mixed flow portion of the condensation oscillation load is specified as a sinusoidal load at the containment's critical frequencies between 2 and 7 Hz with an amplitude of ± 1.75 psi. This load is to be applied uniformly to the wetted portion of the suppression pool boundary below the vent exit with a linear attenuation to the free surface of the suppression pool. The duration of this load is from 4 to 15 seconds after the break has occurred.

The steam flow portion of the condensation oscillation load is specified as a sinusoidal load at the containment's critical frequencies between 2 and 7 Hz with an amplitude of ± 5.0 psi. The load is to be applied uniformly to the wetted portion of the suppression pool boundary below the vent exit with a linear attenuation to the suppression pool free surface. Also a sinusoidal load of amplitude ± 0.5 psi is applied uniformly to the drywell boundary at critical frequencies between 2 and 7 Hz. The duration of both the drywell and suppression pool steam flow condensation oscillation load is the time period from 15 to 25 seconds following the initial break.

Condensation oscillation loads on submerged structures are calculated using Refs 12 and 13.

4.2.2.2 Chugging Load Definition

The pool boundary chugging load is specified in Ref 15. Two loading conditions are described: symmetric and asymmetric.

The symmetric loading condition is specified as +4.8 psig/-4.0 psig and is to be applied uniformly around the entire pool boundary as shown in Figure 4-45 (extracted from Ref 15).

The asymmetric loading condition has a specified maximum positive/negative pressure of +20 psig/-14 psig and has the circumferential spatial distribution depicted in Figure 4-45.

Chugging loads on submerged structures will be evaluated when the design guide dealing with these loads is completed.

The chugging load imparted to the downcomer will be specified when the appropriate dynamic forcing function becomes available.

4.2.3 LONG TERM LOCA LOAD DEFINITION

The loss-of-coolant accident causes pressure and temperature transients in the drywell and wetwell due to mass and energy released from the line break. The drywell and wetwell pressure and temperature time histories are required to establish the structural loading conditions in the containment because they are the basis for other containment hydrodynamic phenomena. The response must be determined for a range of parameters such as leak size, reactor pressure and containment initial conditions. The results of this analysis are documented in Ref 7.

4.2.3.1 Design Basis Accident (DBA) Transients

The DBA LOCA for SSES is conservatively estimated to be a 3.53 ft^2 break of the recirculation line (Ref 7). The SSES plant unique inputs for this analysis are shown in Table 4-19. Drywell and wetwell pressure responses are shown in Figures 4-46 and 4-47 (extracted from Ref 7). These transient descriptions do not, however, contain the effects of reactor subcooling. Suppression pool temperature response is shown in Figure 4-48 (Ref 7). This transient description also does not contain the effect of reactor subcooling. Drywell temperature response is shown in Figure 4-49 and similarly does not contain the effects of pipe inventory or reactor subcooling.

4.2.3.2 Intermediate Break Accident (IBA) Transients

The worst-case intermediate break for the Mark II plants is a main steam line break on the order of 0.05 to 0.1 ft^2. At this time plant unique IBA data for SSES is available only for the suppression pool temperature response to a 0.05 ft^2 break (Ref 7). This data is shown in Figure 4-50. Drywell temperature and wetwell and drywell pressures for the SSES IBA are estimated from curves for a typical Mark II containment shown in Figure 4-51 (extracted from Ref 10)

4.2.3.3 Small Break Accident (SBA) Transients

At this time plant-unique SBA data for SSES is not available. The wetwell and drywell pressure and temperature transients for a typical Mark II containment are used to estimate SSES containment response to these accidents. These curves are shown in Figure 4-52 (extracted from Ref 10).

4.2.4 LOCA LOADING HISTORIES FOR SSES CONTAINMENT COMPONENTS

The various components directly affected by LOCA loads are shown schematically in Figures 4-53 and 4-54. These components may in turn load other components as they respond to the LOCA loads. For example, lateral loads on the downcomer vents produce minor reaction loads in the drywell floor from which the downcomers are supported. The reaction load in the drywell floor is an indirect load resulting from the LOCA and is defined by the appropriate structural model of the downcomer/drywell floor system. Only the direct loading situations are described explicitly here. Table 4-20 is a LOCA load chart for SSES. This chart shows which LOCA loads directly affect the various structures in the SSES containment design. Details of the loading time histories are discussed in the following subsections.

4.2.4.1 LOCA Loads on the Containment Wall and Pedestal

Figure 4-55 shows the LOCA loading history for the SSES containment wall and the RPV pedestal. The wetwell pressure loads apply to the unwetted elevations in the wetwell; the appropriate hydrostatic pressure addition is made for loads on the wetted elevations. Condensation oscillation and chugging loads are applied to the wetted elevations in the wetwell only. The poolswell air bubble load applies to the wetwell boundaries as shown in Figure 4-44.

4.2.4.2 LOCA Loads on the Basemat and Liner Plate

Figure 4-56 shows the LOCA loading history for the SSES basemat and liner plate. Wetwell pressures are applied to the wetted and unwetted portions of the liner plate as discussed in Subsection 4.2.4.1. The downcomer water jet impacts the basemat liner plate as does the poolswell air bubble load. Chugging and condensation oscillation loads are applied to the wetted portion of the liner plate.

4.2.4.3 LOCA Loads on the Drywell and Drywell Floor

Figure 4-57 shows the LOCA loading history for the SSES drywell and drywell floor. The drywell floor undergoes a vertically applied, continuously varying differential pressure, the upward component of which is especially prominent during poolswell when the wetwell air space is highly compressed.

4.2.4.4 LOCA Loads on the Columns

Figure 4-58 shows the LOCA loading history for the SSES columns. Poolswell drag and fallback loads are very minor since the column surface is oriented parallel to the pool swell and fallback velocities. The poolswell air bubble, condensation oscillations and chugging will provide loads on the submerged (wetted) portion of the columns.

4.2.4.5 LOCA Loads on the Downcomers

Figure 4-59 shows the LOCA loading history for the SSES downcomers. The downcomer clearing load is a lateral load applied at the downcomer exit (in the same manner as the chugging lateral load) plus a vertical thrust load. Poolswell drag and fallback loads are very minor since the downcomer surfaces are oriented parallel to the pool swell and fallback velocities. The poolswell air bubble load is applied to the submerged portion of the downcomer as are the chugging and condensation oscillation loads.

4.2.4.6 LOCA Loads on the Downcomer Bracing

Figure 4-60 shows the LOCA loading history for the SSES downcomer bracing system. This system is not subject to impact loads since it is submerged at elevation 668'. As a submerged structure it is subject to poolswell drag, fallback and air bubble loads. Condensation oscillations and chugging at the vent exit will also load the bracing system both through downcomer reaction (indirect load) and directly through the hydrodynamic loading in the suppression pool.

4.2.4.7 LOCA Loads on Wetwell Piping

Figure 4-61 shows the LOCA loading history for piping in the SSES wetwell. Since the wetwell piping occurs at a variety of elevations in the SSES wetwell, sections may be completely submerged, partially submerged, or initially uncovered. Piping may occur parallel to poolswell and fallback velocities as with the main steam safety relief piping. For these reasons there are a number of potential loading situations which arise as shown in Table 4-21. In addition, the poolswell air bubble load applies to the submerged portion of the wetwell piping as do the condensation oscillation and chugging loads.

4.3 ANNULUS PRESSURIZATION

The RPV shield annulus has the recirculation pumps suction lines passing through it (for location in containment see Figure 1-1). The mass and energy release rates from a postulated recirculation line break constitute the most severe transient in the reactor shield annulus. Therefore, this pipe break is selected for analyzing loading of the shield wall and the reactor pressure vessel support skirt for pipe breaks inside the annulus. The reactor shield annulus differential pressure analysis and analytical techniques are presented in Appendices 6A and 6B of the SSES Final Safety Analysis Report (FSAR).

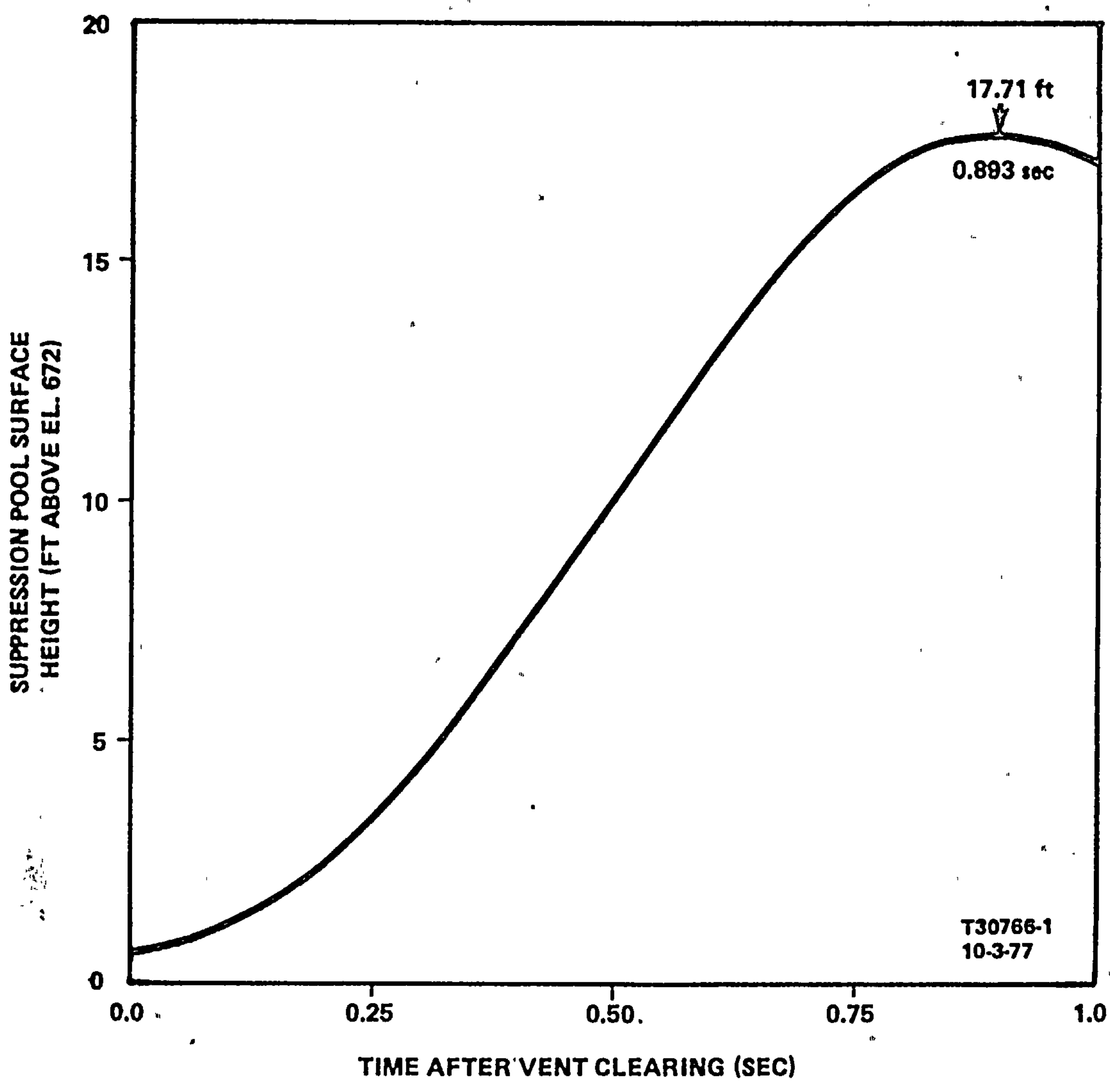

SUSQUEHANNA STEAM ELECTRIC STATION
UNITS 1 AND 2
DESIGN ASSESSMENT REPORT

SSES SHORT TERM SUPPRESSION POOL SURFACE HEIGHT

FIGURE 4-38

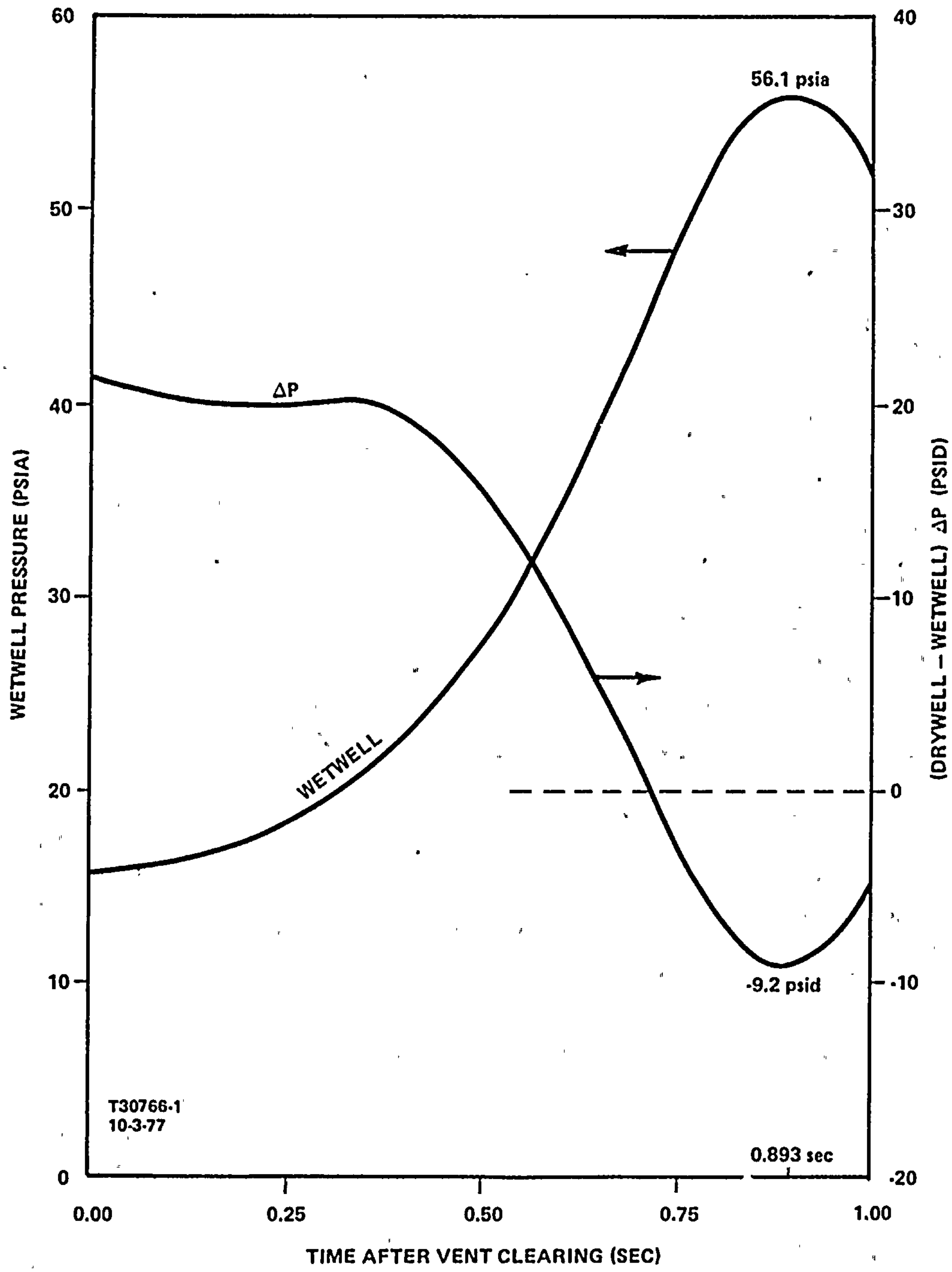

SUSQUEHANNA STEAM ELECTRIC STATION
UNITS 1 AND 2
DESIGN ASSESSMENT REPORT

SSES SHORT TERM
WETWELL PRESSURE

FIGURE 4-39

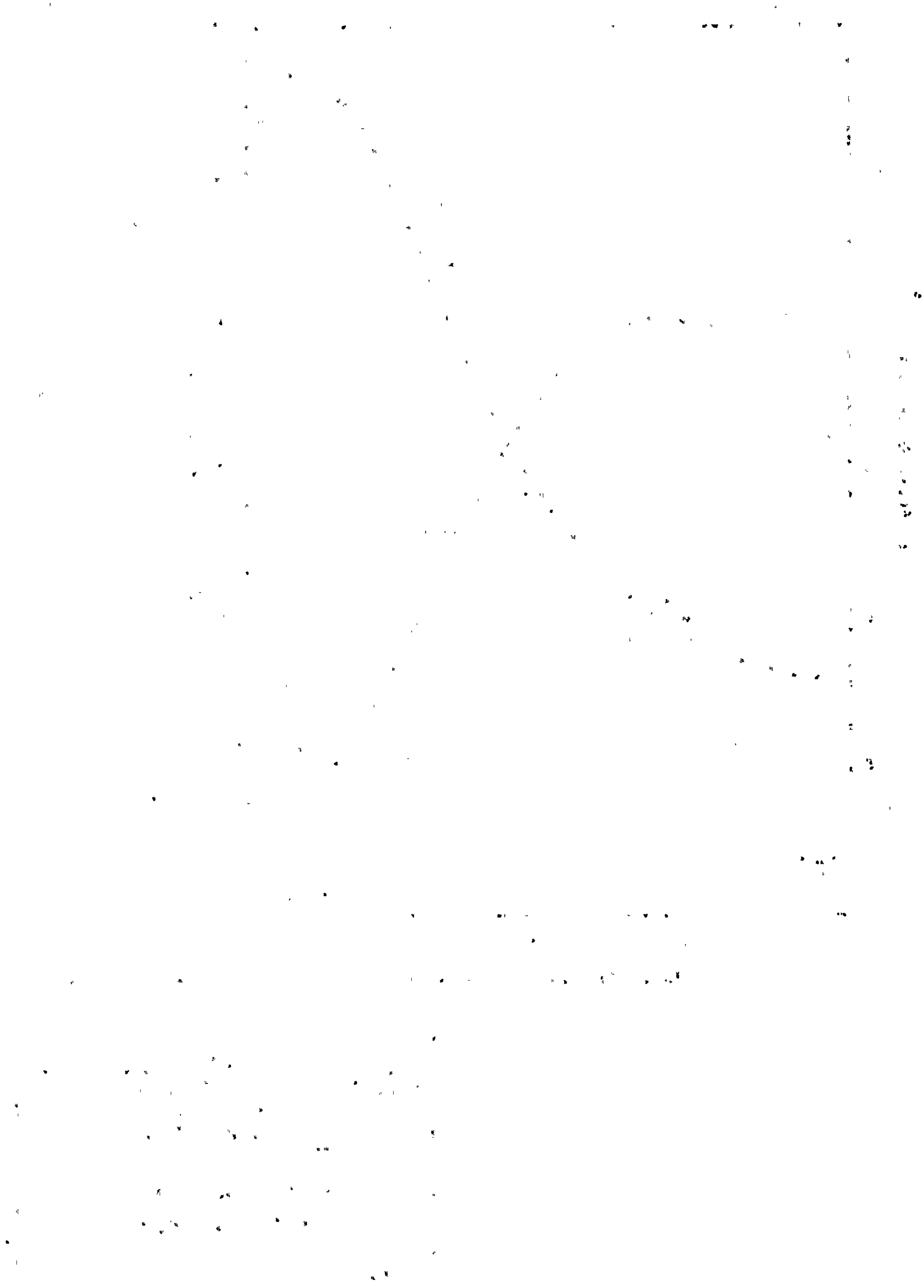

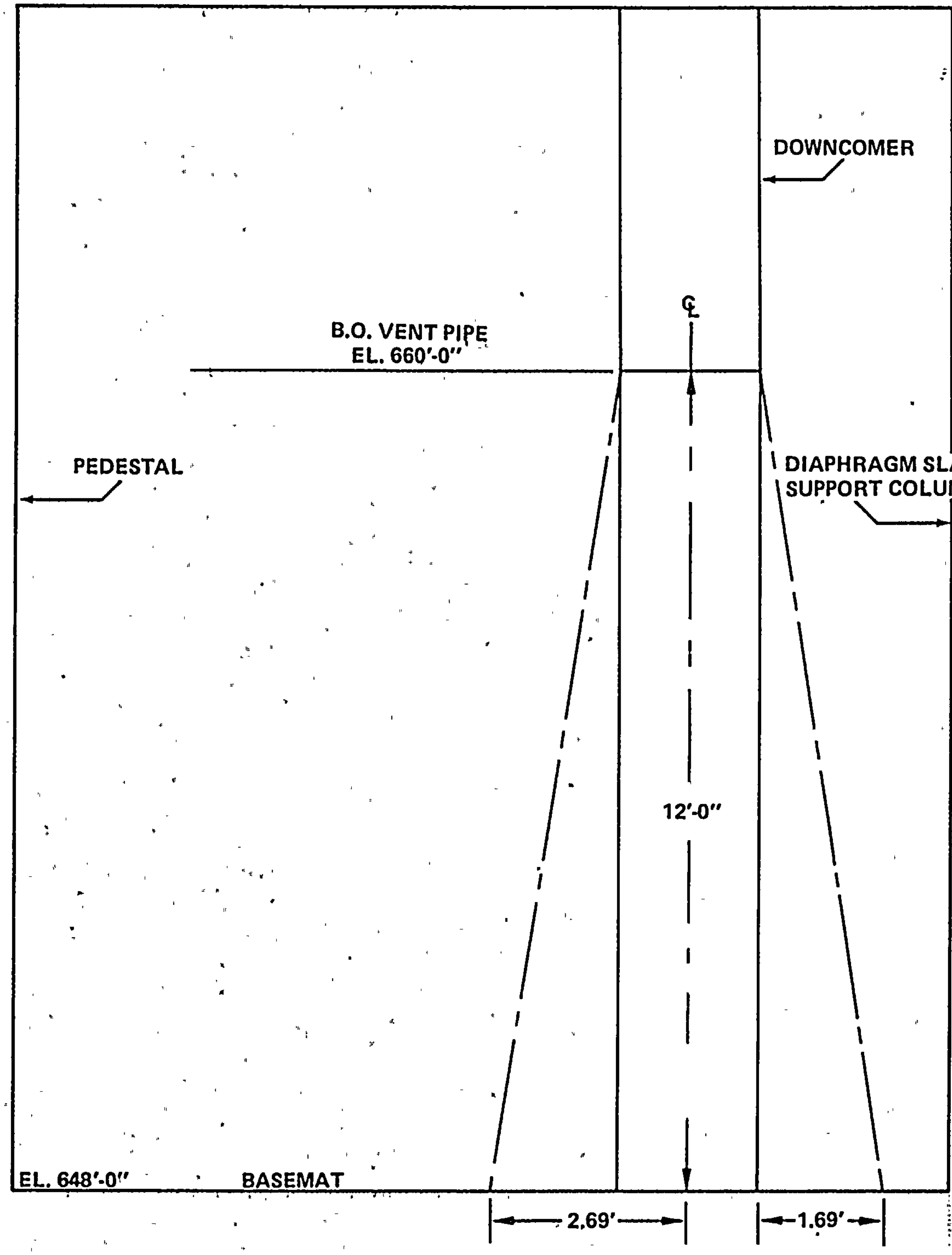

SUSQUEHANNA STEAM ELECTRIC STATION
UNITS 1 AND 2
DESIGN ASSESSMENT REPORT

BASEMAT
SSES WATER CLEARING JET

FIGURE 4-41

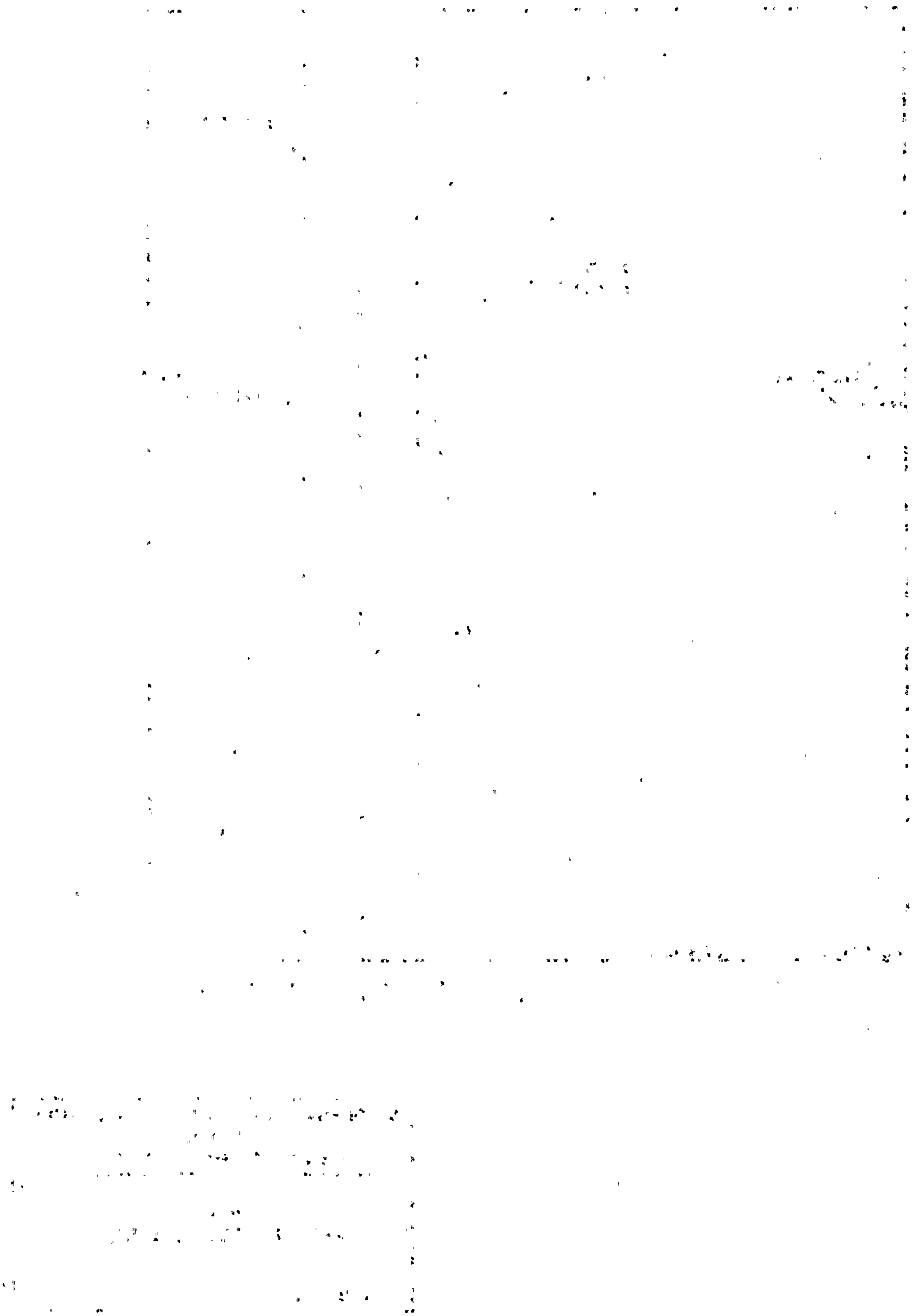

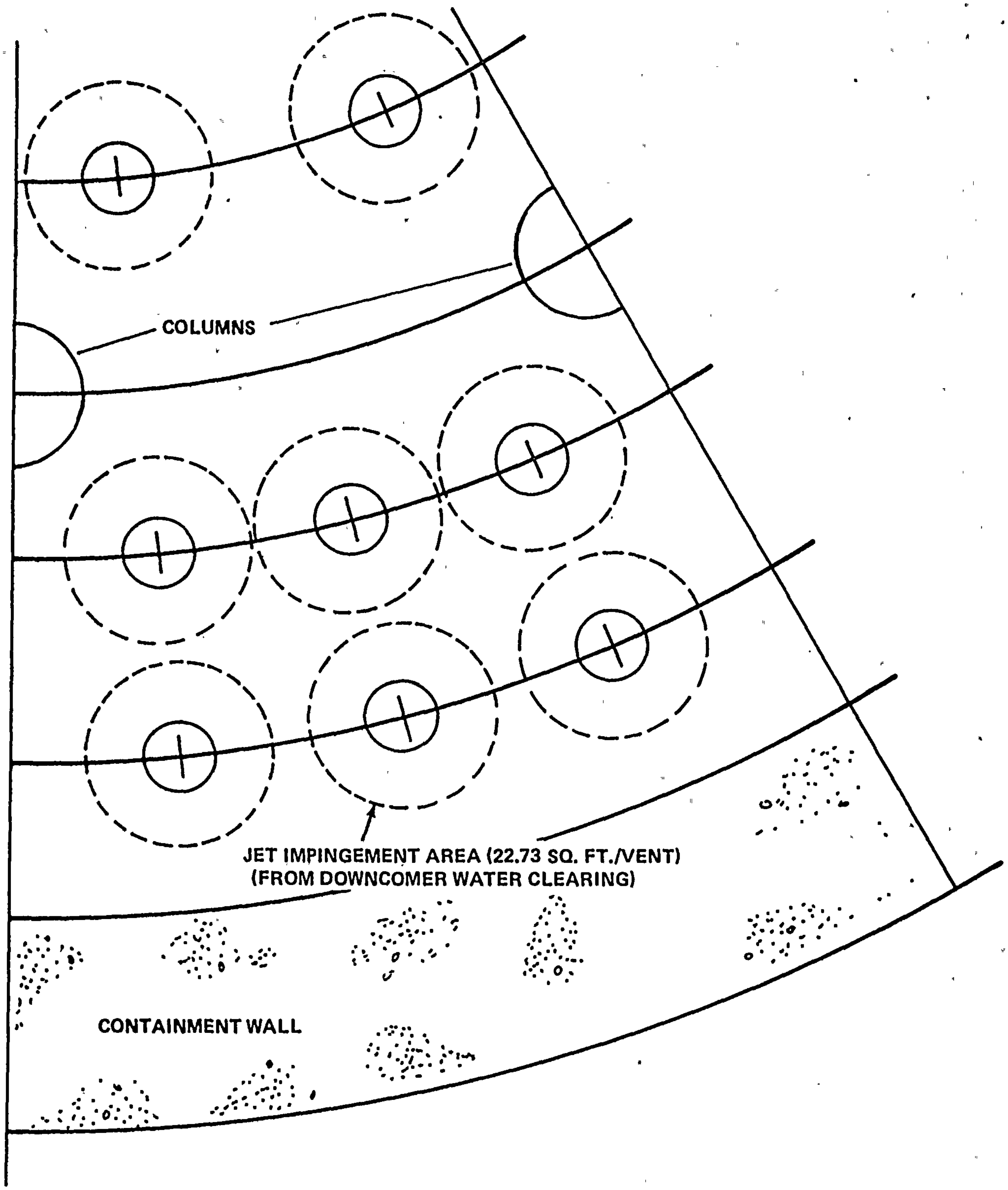

SUSQUEHANNA STEAM ELECTRIC STATION
UNITS 1 AND 2
DESIGN ASSESSMENT REPORT

SSES JET IMPINGEMENT AREA
(WATER CLEARING)

FIGURE 4-42

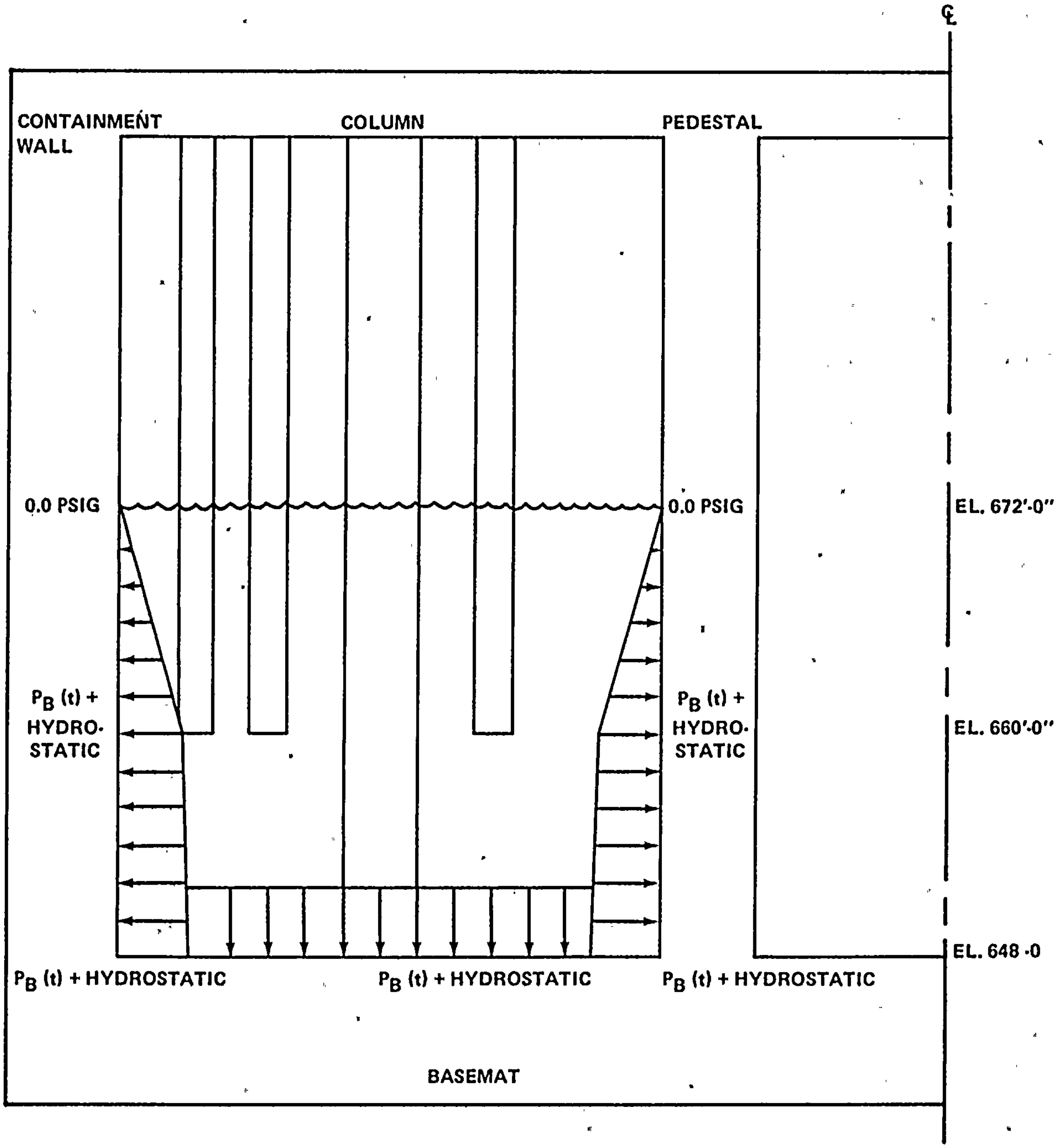

SUSQUEHANNA STEAM ELECTRIC STATION
UNITS 1 AND 2
DESIGN ASSESSMENT REPORT

AIR BUBBLE PRESSURE ON SUPPRESSION POOL WALLS

FIGURE 4-44

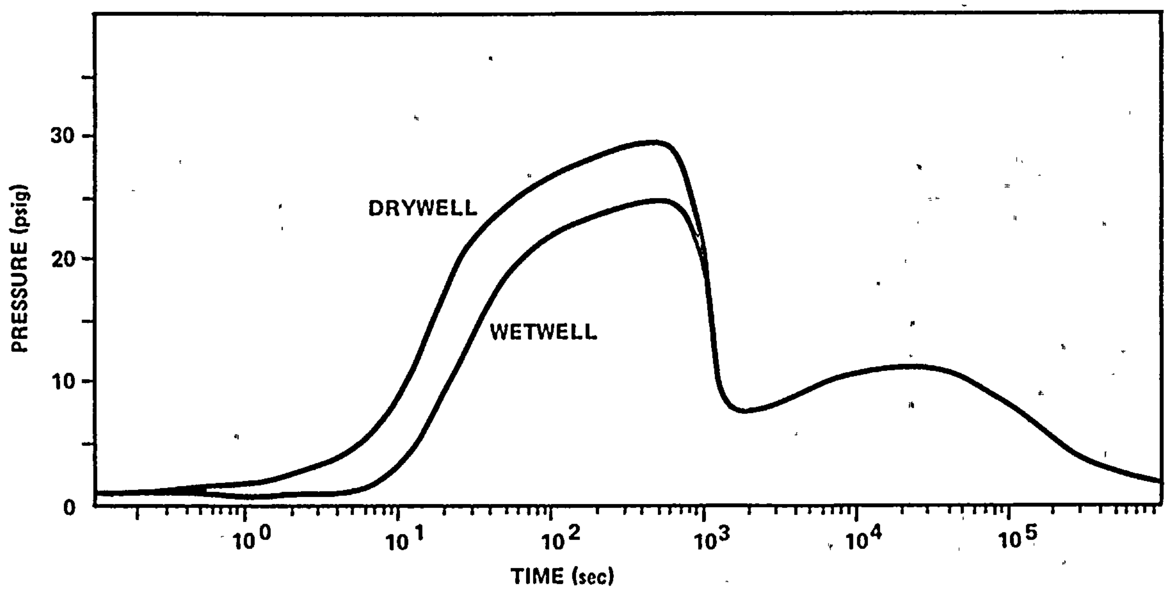

(a) CONTAINMENT PRESSURE RESPONSE FOR INTERMEDIATE BREAK AREA

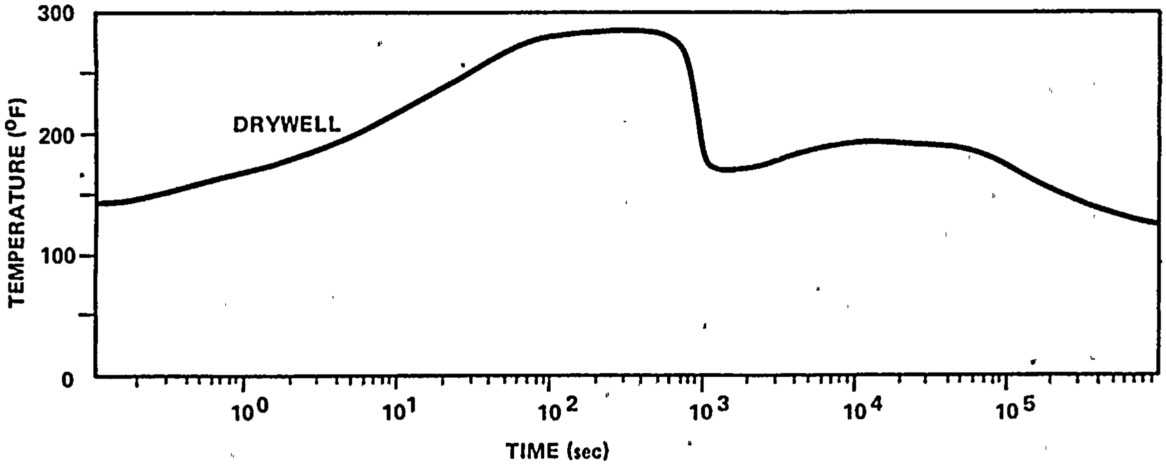

(b) DRYWELL TEMPERATURE RESPONSE FOR INTERMEDIATE BREAK AREA

SUSQUEHANNA STEAM ELECTRIC STATION
UNITS 1 AND 2
DESIGN ASSESSMENT REPORT

TYPICAL MARK II CONTAINMENT RESPONSE TO THE IBA

FIGURE 4-51

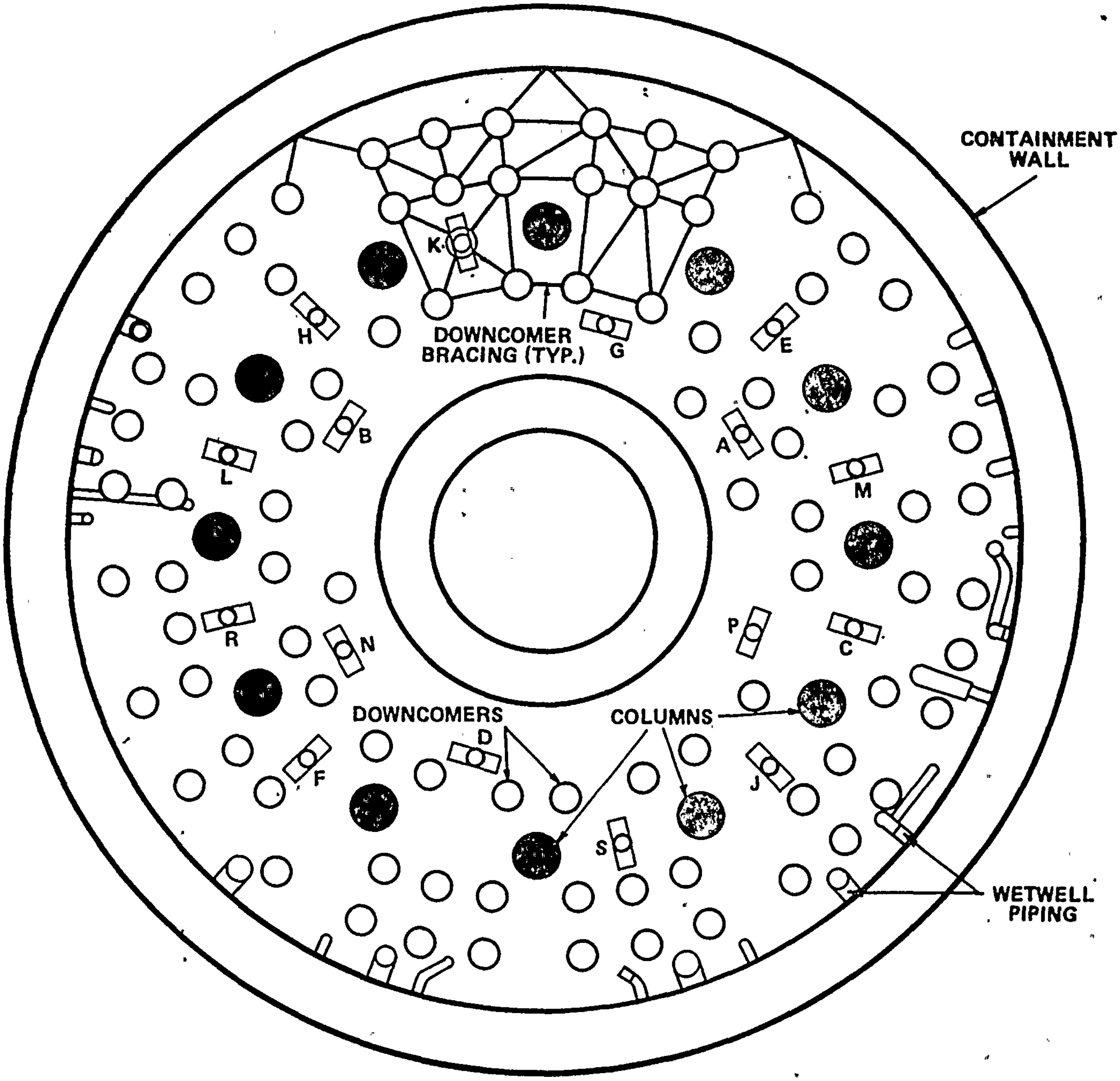

NOTE:
DOWNCOMER BRACING IS ONLY PARTIALLY SHOWN IN THE INTEREST OF CLARITY.
LETTERS INDICATE SRV QUENCHERS

SUSQUEHANNA STEAM ELECTRIC STATION UNITS 1 AND 2 DESIGN ASSESSMENT REPORT
SSES COMPONENTS AFFECTED BY LOCA LOADS FIGURE 4-53

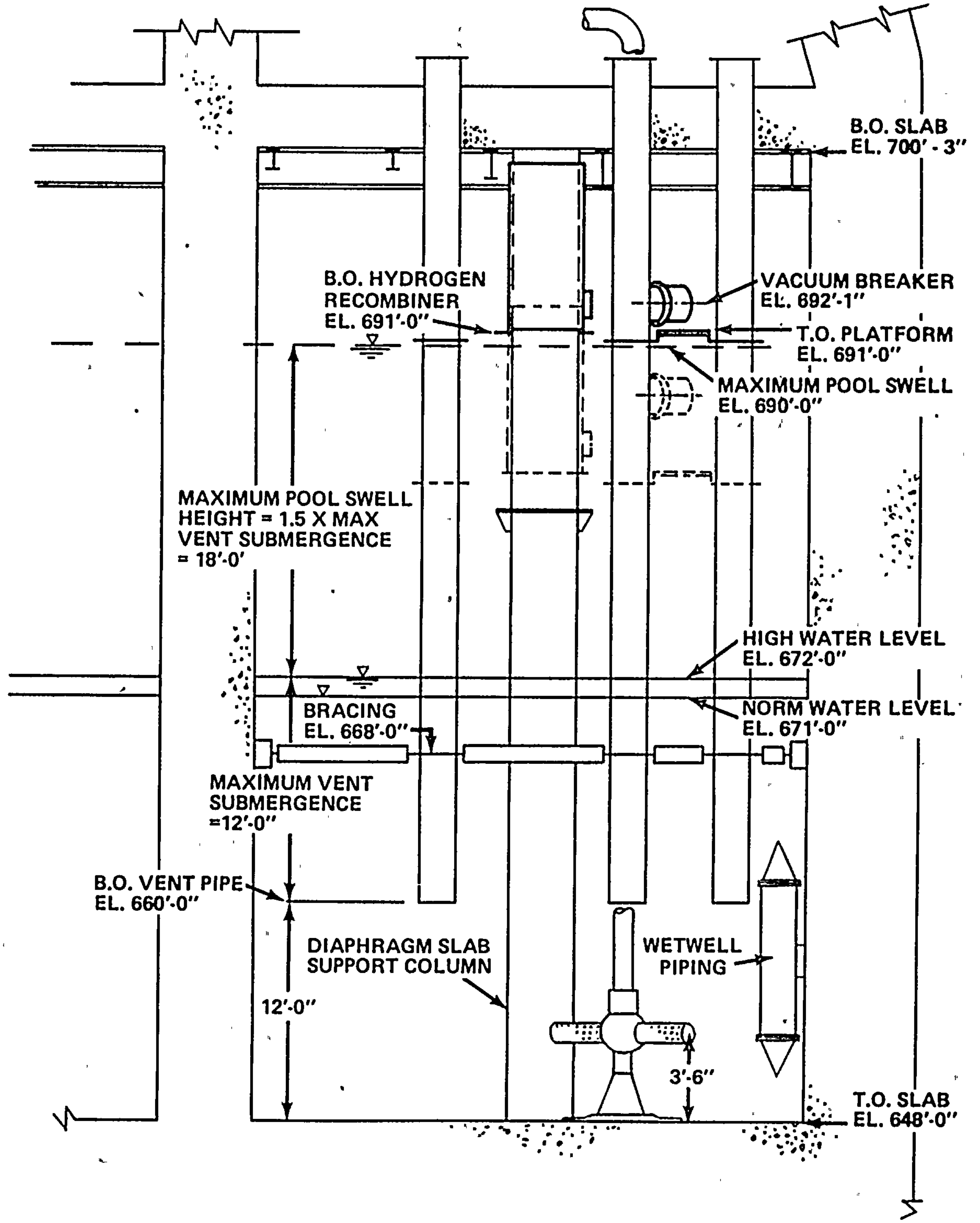

SUSQUEHANNA STEAM ELECTRIC STATION
UNITS 1 AND 2
DESIGN ASSESSMENT REPORT

SSES COMPONENTS
AFFECTED BY LOCA LOADS

FIGURE 4-54

TABLE 4-16

LOCA LOADS ASSOCIATED WITH POOLSWELL

	Load	Reference
1.	Wetwell/Drywell Pressures during Poolswell	Ref 7, Table IV-D-3; Ref 10, Subsection 4.4.1.5
2.	Poolswell Impact Loads	Ref 10, Subsection 4.4.6
3.	Poolswell Drag Loads	Ref 10, Subsections 4.4.5.2, 4.4.7, 4.4.8
4.	Downcomer Clearing Loads	Ref 10, Subsection 4.3.1, Reference 11, Subsection 3.3.1.2
5.	Downcomer Water Jet Load	Ref 10, Subsection 4.4.5.1
6.	Poolswell Air Bubble Load	Ref 10, Subsection 4.4.5.3
7.	Poolswell Fallback Load	Ref 10, Subsection 4.4.5.4

TABLE 4-18

SSES PLANT UNIQUE POOLSWELL CODE INPUT DATA

Downcomer Area (each)	2.96 ft^2
Suppression Pool Free Surface Area	5065.03 ft^2
Maximum Downcomer Submergence	12.00 ft
Downcomer Overall Loss Coefficient	2.5
Number of Downcomers	87
Initial Wetwell Pressure	15.45 psia
Wetwell Free Air Volume	149,000 ft^3
Vent Clearing Time	0.6863 sec
Pool Velocity at Vent Clearing	3.0 ft/sec
Initial Drywell Temperature	135°F
Initial Drywell Relative Humidity	0.20

TABLE 4-19

INPUT DATA FOR SSES LOCA TRANSIENTS

Drywell free air volume (including vents)	239,600 ft^3
Wetwell free air volume	149,000 ft^3
Maximum downcomer submergence	12.0 ft
Downcomer flow area (total)	256.7 ft
Downcomer loss coefficient	2.5
Initial drywell pressure	15.45 psia
Initial wetwell pressure	15.45 psia
Initial drywell humidity	20%
Initial pool temperature	90°F
Estimated DBA break size	3.53 ft^2
Number of vents	87
Initial mass of steam in vessel	24,500 lbm
Initial mass of saturated water in vessel	674,000 lbm
Minimum suppression pool mass	7.6×10^6 lbm
Initial vessel pressure	1,055 psia
Vessel & internals mass	2,940,300 lbm
Vessel & internals overall heat transfer coefficient	484.9 Btu/sec°F
Vessel and internals specific heat	0.123 Btu/lbm °F
Initial control rod drive flow	10.83 lbm/sec
Initial steam flow to main turbine	3931.5 lbm/sec
RCIC & HPCI (HPCS) flow initiation level, distance from vessel "0"	489.5 in

Table 4-19 (Continued)

RCIC & HPCI (HPCS) flow shutoff level (normal water level), distance from vessel "O"	564.0 in
Rated RCIC flow rate to vessel	83.4 lbm/sec
Rated HPCI (HPCS) flow rate to vessel	695 lbm/sec
RCIC shutoff pressure	165 psia
HPCI (HPCS) shutoff pressure	165 psia
Condensate storage tank enthalpy	48 Btu/lbm
CRD enthalpy	48 Btu/lbm
Initial power level	3.23×10^6 Btu/sec
Feedwater enthalpy	78 Btu/lbm
Cleanup system flow	36.94 lbm/sec
Cleanup system return enthalpy	413.2 Btu/lbm
Initial vessel fluid enthalpy	573.1 Btu/lbm
RHR heat exchanger "K" in pool cooling mode	306 Btu/sec °F
RHR heat exchanger steam flow in condensing mode	25 lbs/sec
RHR heat exchanger flow in pool cooling mode	1390 lbs/sec
RHR heat exchanger outlet enthalpy in condensing mode	108 Btu/lbm
Service water temperature	90 °F

CHAPTER 5
LOAD COMBINATIONS FOR STRUCTURES, PIPING, AND EQUIPMENT

TABLE OF CONTENTS

CHAPTER 5
FIGURES

CHAPTER 5

TABLES

5.0 LOAD COMBINATIONS FOR STRUCTURES, PIPING, AND EQUIPMENT

To verify the adequacy of mechanical and structural design, it is necessary first to define the load combinations to which structures, piping, and equipment may be subjected. In addition to the loads due to pressure, weight, thermal expansion, seismic, and fluid transients, hydrodynamic loads resulting from LOCA and SRV discharge are considered in the design of structures, piping, and equipment in the drywell and suppression pool. This chapter specifies how the LOCA and SRV discharge hydrodynamic loads will be combined with the other loading conditions. For the load combinations discussed in this chapter, seismic and hydrodynamic responses are combined by the methods specified in Ref. 10 Subsection 5.2.2 and Ref. 10 Section 6.3.

5.3 LINER PLATE LOAD COMBINATIONS

The liner plate and anchorage system are designed for the load combinations listed in Table 5-1 except that all load factors are taken as unity.

5.4 DOWNCOMER LOAD COMBINATIONS

Load combinations for the downcomers are given in Table 5-3. These load combinations are based on the load combinations given in Table 6-1 of Ref 10.

5.5 PIPING, QUENCHER, AND QUENCHER SUPPORT LOAD COMBINATIONS

LOCA loads considered on piping systems include poolswell impact loads, poolswell drag loads, downcomer water jet loads, poolswell air bubble loads, fallback drag loads, condensation oscillation loads, chugging loads, and inertial loading due to acceleration of the containment structure produced by LOCA loads. Loads due to SRV discharge on piping systems include water clearing loads, air clearing loads, fluid transient loads on SRV discharge piping, reaction forces at the quencher, and inertial loading due to the accleration of the containment structure produced by SRV discharge loads.

The load combinations and the acceptance criteria for piping systems are given in Table 6-1 of Ref 10.

5.5.1 Load Considerations for Piping Inside the Drywell

Piping systems inside the drywell are subjected to inertial loading due to the acceleration of the containment produced by LOCA and SRV discharge loads in the wetwell. The SRV discharge piping in the drywell is also subjected to fluid transient forces due to SRV discharge.

5.5.2 Load Considerations for Piping Inside the Wetwell

All piping in the wetwell is subject to the inertial loading due to LOCA and SRV discharge.

Drag and impact loads due to LOCA and SRV discharge on individual pipes in the wetwell depend on the physical location of the piping. Other SRV discharge and LOCA loads applicable to piping in the wetwell are discussed in the paragraphs that follow.

Piping systems located below the suppression chamber water level are shown on Figures 5-1 and 5-2. These lines are located outside of the jet impingement cone of the downcomer. In addition to the inertial loads, these piping systems are subject to air bubble loads, condensation oscillation loads, and chugging loads due to LOCA and SRV operation. The SRV piping, quencher, and quencher support are also subject to fluid transient forces due to SRV discharge.

Piping systems within the poolswell volume are shown on Figures 5-2, 5-3 and 5-4. All horizontal runs of these pipes are above the suppression chamber water level. The following loads, in addition to inertial loads, act on these systems:

a. The horizontal runs of pipe below elevation 690', experience poolswell impact , poolswell drag, and fallback drag loads.

b. The vertical portions of pipe in the water below elevation 690' experience poolswell drag and fallback drag loads.

5.5.3 Quencher and Quencher Support Load Considerations

The quencher and quencher supports are subjected to the following hydrodynamic loads in addition to the pressure, weight, thermal, and seismic loads:

a. Unbalanced loads on the quencher due to SRV water clearing and air clearing transients, irregular condensation, and steady state blowdown

b. Drag loads due to SRV discharge and LOCA

c. SRV piping end loads

d. Inertial loading due to the acceleration of the containment produced by SRV discharge and LOCA.

5.5.4 Load Considerations for Piping in the the Reactor Building

The effects of the inertial loading due to acceleration of the containment produced by SRV discharge and LOCA loads will be evaluated for this piping.

5.6 NSSS LOAD COMBINATIONS

To be provided later.

5.7 EQUIPMENT LOAD COMBINATIONS

Load combinations for safety-related equipment located within the reactor building and containment will be assessed and described in a revision to this Design Assessment Report ("Safety-related" is defined in Table 1.8-1 of the FSAR).

FIG. NO.	LINE NO.	QTY	SYSTEM	EL A
A	12"-GBC-101	6	M.S.R.V. DISCHARGE PIPING R.F.C.M.E.L.	651'-0"
B	12"-GBC-101	10	S.J.B.D.P.N.G.K.A.H.	651'-6"

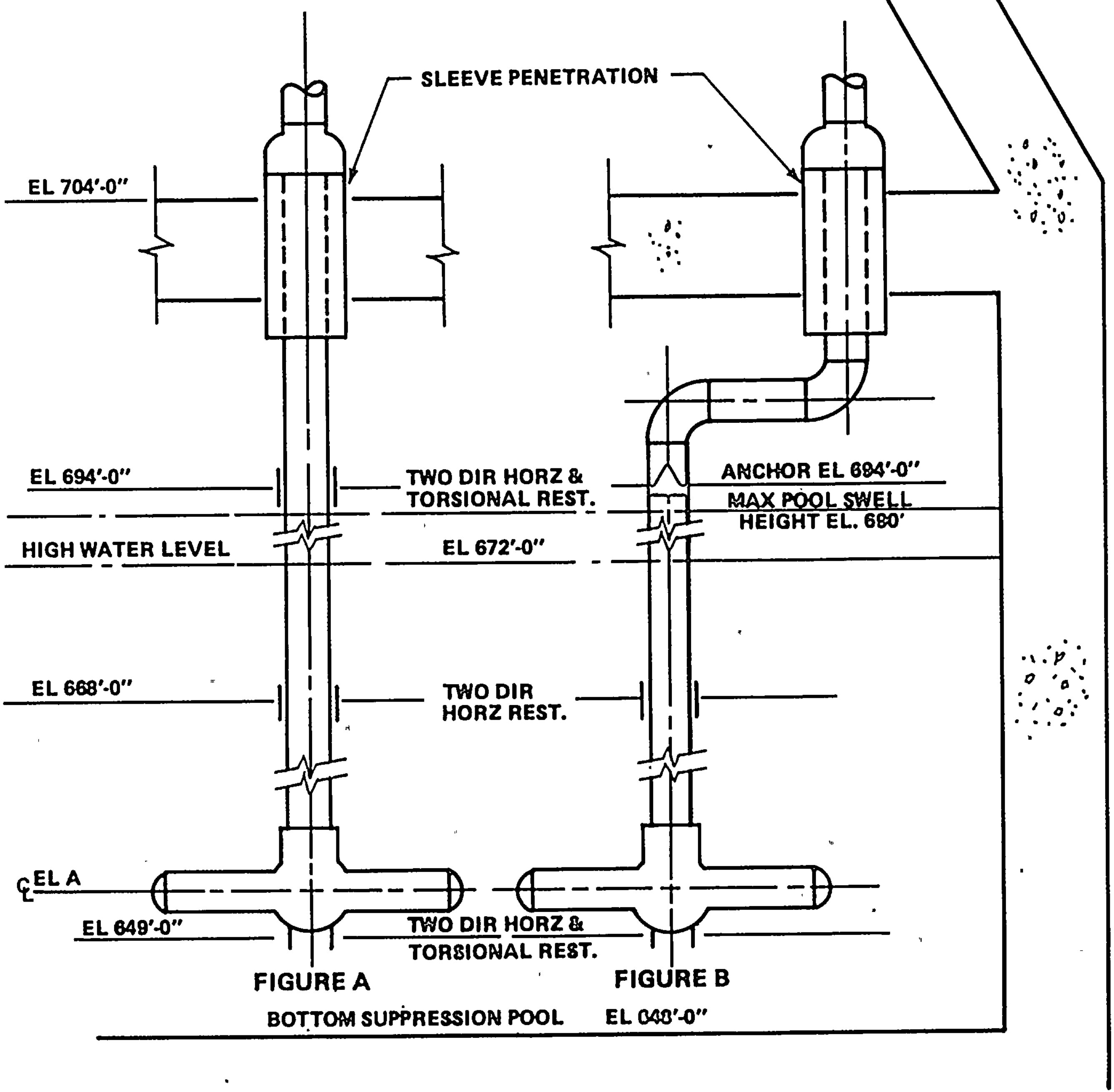

SUSQUEHANNA STEAM ELECTRIC STATION
UNITS 1 AND 2
DESIGN ASSESSMENT REPORT

PIPING STRESS
DIAGRAMS AND TABLES

FIGURE 5-3

FIG. NO.	QTY	LINE NO.	SYSTEM	EL A	EL B	EL C	RAD Y	DIM. X	REST. EL
		6"-GBB-120	RHR	668'-5 1/2"	695'-0"	697'-0"	42'-8 3/8"	15 5/8"	697'-0" 695'-0"

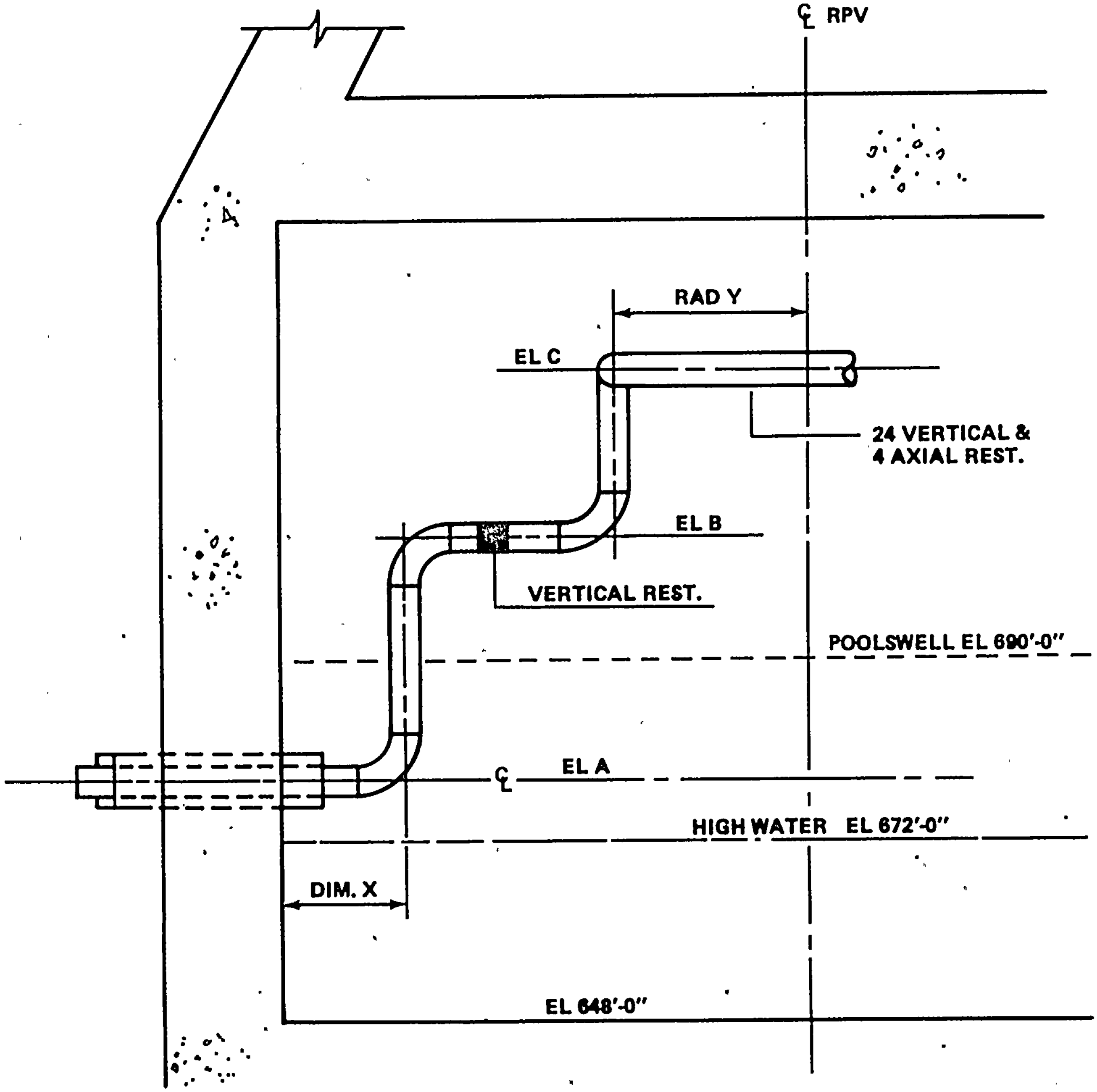

SUSQUEHANNA STEAM ELECTRIC STATION
UNITS 1 AND 2
DESIGN ASSESSMENT REPORT

PIPING STRESS
DIAGRAMS AND TABLES

FIGURE 5-4

TABLE 5-1

LOAD COMBINATIONS FOR CONTAINMENT AND REACTOR BUILDING CONCRETE STRUCTURES (CONSIDERING HYDRODYNAMIC) LOADS

Equation	Load Condition	D	L	P_o	T_o	R_o	E_o	E_{SS}	P_B	P_A	T_A	R_A	R_V	SRV(2)	AOT	ADS	ASYM	Single Valve	LOCA(3)
1	Normal w/o Temp.	1.4	1.7	1.0	–	–	–	–	–	–	–	–	–	1.5	X(1)	–	X	–	
2	Normal w/Temp.	1.0	1.3	1.0	1.0	1.0	–	–	–	–	–	–	–	1.3	X	–	X	–	
3	Normal Sev. Env.	1.0	1.0	1.0	1.0	1.0	1.25	–	–	–	–	–	–	1.25	X	–	X	–	
4	Abnormal	1.0	1.0	–	–	–	–	–	1.25	–	1.0	1.0	–	1.25	–	X	X	–	
4a	Abnormal	1.0	1.0	–	–	–	–	–	–	1.25	1.0	1.0	–	1.0	–	–	–	X	
5	Abnormal Sev. Env.	1.0	1.0	–	–	–	1.1	–	1.1	–	1.0	1.0	–	1.1	–	X	X	–	
5a	Abnormal Sev. Env.	1.0	1.0	–	–	–	1.1	–	–	1.1	1.0	1.0	–	1.0	–	–	–	X	
6	Normal Ext. Env.	1.0	1.0	1.0	1.0	1.0	–	1.0	–	–	–	–	–	1.0	X	–	X	–	
7	Abnormal Ext. Env.	1.0	1.0	–	–	–	–	1.0	1.0	–	1.0	1.0	1.0	1.0	–	X	X	–	
7a	Abnormal Ext. Env.	1.0	1.0	–	–	–	–	1.0	–	1.0	1.0	1.0	1.0	1.0	–	–	–	X	–

Load Description

D = Dead Loads

L = Live Loads

T_o = Operating Temperature Loads

R_o = Operating Pipe Reactions

P_o = Operating Pressure Loads

SRV = Safety Relief Valve Loads

E_o = Operating-Basis Earthquake

E_{SS} = Safe Shutdown Earthquake

P_B = SBA or IBA (LOCA) Pressure Load

P_A = DBA (LOCA) Pressure Load

T_A = Pipe Break Temperature Load

R_A = Pipe Break Temperatures Reaction Loads

R_V = Reaction and jet forces associated with the pipe break

Notes:

1) X indicates applicability for the designated load combination.

2) For the columns designated AOT, ADS, ASYM, and Single Valve, only one of the four possible columns may be included in the load combination for any one equation. For example, in equation 1 either AOT or ASYM may be considered with the other loads but not both AOT and ASYM simultaneously.

3) LOCA chugging and condensation oscillation loads will be included in a subsequent revision to this table

TABLE 5-2

LOAD COMBINATIONS AND ALLOWABLE STRESSES FOR STEEL STRUCTURAL COMPONENTS (Suppression Chamber Columns, Downcomer Bracing, and Reactor Building Structural Steel)

Equation	Condition	Load Combination	Stress Limit
1	Normal w/o Temp.	D+L+SRV	F_s
2	Normal w/Temp.	D+L+T_o+SRV	F_s
3	Normal/ Severe	D+L+T_o+E+SRV	1.5 F_s
4	Normal/ Extreme	D+L+T_o+E'+SRV	1.5 F_s
5	Abnormal	D+L+P+(T_o+T_a)+R +SRV	(Note 1)
6	Abnormal/ Severe	D+L+P+(T_o+T_a)+R+E +SRV	(Note 1)
7	Abnormal/ Extreme	D+L+P+(T_o+T_a)+R+E +SRV	(Note 1)

Note 1: In no case shall the allowable stress exceed $0.90F_y$ in bending, $0.85F_y$ in axial tension or compression, and $0.50F_y$ in shear. Where the design is governed by requirements of stability (local or lateral buckling), the actual stress shall not exceed $1.5F_s$.

TABLE 5-2 (Continued)

Notations:

F_s = Allowable stress according to the AISC, "Specification for the Design, Fabrication, and Erection of Structural Steel for Buildings", dated 1969, Part 1.

D = Dead load

L = Live load

T_o = Thermal effects during normal operating conditions including temperature gradients and equipment and pipe reactions.

T_a = Added thermal effects (over and above operating thermal effects) which occur during a design accident.

P = Design Basis Accident pressure load

R = Local force or pressure on structure due to postulated pipe rupture including the effects of steam/water jet impingement, pipe whip, and pipe reaction.

E = Load due to Operating Basis Earthquake.

E' = Load due to Safe Shutdown Earthquake.

SRV = Safety relief valve loads.

F_y = Minumum specified yield stength

TABLE 5-3

LOAD COMBINATIONS AND ALLOWABLE STRESSES FOR DOWNCOMERS

Equation	Condition	Load Combination	Primary Stress Limit
1	Upset	$D+P_o+SRV_{ALL}$	$1.5\ S_m$
2	Emergency	$D+P_o+SRV_{ALL}+E$	$2.25\ S_m$
3	Emergency	$D+P_{SBA}+SRV_{ADS}+E+SBA$	$2.25\ S_m$
4	Faulted	$D+P_o+SRV_{ALL}+E'$	$3\ S_m$
5	Faulted	$D+P_{IBA}+SRV_{ADS}+E+IBA$	$3\ S_m$
6	Faulted	$D+P_{SBA}$ (or P_{IBA}) $+SRV_{ADS}+E'+SBA$ (or IBA)	$3\ S_m$
7	Faulted	$D+P_A+E'+DBA_1$	$3\ S_m$
8	Faulted	$D+P_A+E'+DBA_2$	$3\ S_m$

Notations:

S_m = Maximum allowable stress according to Table I-10.1, Ref 28.

D = Dead weight of the downcomer

P_o = Pressure differential between drywell and suppression chamber during normal operating condition.

P_{SBA} = Pressure differential between drywell and suppression chamber during SBA.

P_{IBA} = Pressure differential between drywell and suppression chamber during IBA.

P_A = Pressure differential between drywell and suppression chamber during DBA.

SRV_{ALL} = Dynamic lateral pressure and inertia load due to the discharge of all 16 safety relief valves sequentially.

SRV_{ADS} = Dynamic lateral pressure and inertia load due to the discharge of all 6 ADS safety relief valves simultaneously.

E = Load due to Operating Basis Earthquake

TABLE 5-3 (Continued)

E'	=	Load due to Safe Shutdown Earthquake
SBA	=	Chugging loads due to SBA as follows:
		1. Horizontal load at bottom of downcomer, and
		2. Horizontal and vertical inertial loads.
IBA	=	Chugging loads due to IBA as follows:
		1. Horizontal load at bottom of downcomer, and
		2. Horizontal and vertical inertial loads.
DBA_1	=	Vertical loads due to:
		1. Viscous and pressure forces exerted by the flowing steam, and
		2. Inertial load due to DBA
DBA_2	=	Chugging loads due to DBA as follows:
		1. Horizontal load at bottom of downcomer, and
		2. Horizontal and vertical inertial loads.

CHAPTER 6

DESIGN CAPABILITY ASSESSMENT CRITERIA

TABLE OF CONTENTS

6.0 DESIGN CAPABILITY ASSESSMENT CRITERIA

The criteria by which the design capability is determined are discussed in this chapter. Design of the SSES is assessed as adequate when the design capability of the structures, piping, and equipment is greater than the loads (including LOCA and SRV discharge) to which the structures, piping, and equipment are subjected. Loading combinations are discussed in Chapter 5. The margins by which design capabilities exceed these loadings are discussed in Chapter 7, Design Assessment.

6.3 LINER PLATE CAPABILITY ASSESSMENT CRITERIA

The strains in the liner plate and anchorage system (welds and anchors) from self-limiting loads such as dead load, creep, shrinkage, and thermal effects are limited to the allowable values specified in Table CC-3720-1 of Ref. 29, and the displacements of the liner anchorage are limited to the displacement values of Table CC-3730-1 of Ref 29.

Primary membrane stresses in the liner plate and anchorage system (welds and anchors) from mechanical loads such as SRV discharge and chugging are checked according to Subsection NE-3221.1 of Ref 28. Primary plus secondary membrane plus bending stresses are checked according to Subsection NE-3222.2 of the same code. Fatigue strength evaluation is based on Subsection NE-3222.4. Allowable design stress intensity values, design fatigue curves, and material properties used conform to Subsection NA, Appendix I of Ref 28.

The capacity of the liner plate anchorage is limited by concrete pull-out to the service load allowables of concrete as specified in Ref 30.

6.4 DOWNCOMER CAPABILITY ASSESSMENT CRITERIA

The allowable stresses for the downcomers are given in Table 5-3. These allowable stresses are in accordance with Ref 28; Subsection NE. As permitted by Subsection NE-1120 for MC components, the downcomers are analyzed in accordance with Subsection NB-3650 of Ref 28; however, the lower allowable stresses, Sm, from Table I-10.1 for MC components are used when performing the analysis.

6.5 PIPING, QUENCHER, AND QUENCHER SUPPORT CAPABILITY ASSESSMENT CRITERIA

Piping in the containment and reactor building is analyzed in accordance with Ref 28 Subsections NB3600, NC3600, and ND3600 for the loading described in Section 5.5.

The quencher is designed in accordance with Ref 28, Subsection NC3200, for loading discussed in Subsection 5.5.3. The quencher support is designed in accordance with Subsection NF3000 of Ref 28.

6.6 NSSS CAPABILITY ASSESSMENT CRITERIA

To be provided later.

6.7 EQUIPMENT CAPABILITY ASSESSMENT CRITERIA

Assessment criteria for safety-related equipment subject to LOCA and SRV discharge loading which is located within the containment and reactor building will be described in a revision to this Design Assessment Report ("Safety-related" is defined in Table 1.8-1 of the FSAR).

CHAPTER 7

DESIGN ASSESSMENT

TABLE OF CONTENTS

CHAPTER 7

FIGURES

7.0 DESIGN ASSESSMENT

Loads on SSES structures, piping, and equipment are defined in Chapter 4. The methods by which these loads are combined are discussed in Chapter 5. The criteria for establishing design capability are stated in Chapter 6.

This chapter describes the assessment of the adequacy of the SSES design by comparing design capabilities with the loadings to which structures, piping, and components are subjected and demonstrating the extent of the design margin. The first section of this chapter discusses the methodology by which design capability and loads are compared. The second section indicates the results of these comparisons.

7.1 ASSESSMENT METHODOLOGY

7.1.1 Containment and Reactor Building Assessment Methodology

7.1.1.1 Containment Structure Assessment Methodology

The dynamic analysis for the structural response of the containment and internal structures due to the SRV discharge loads and LOCA related loads is performed using the finite element method. The ANSYS finite element computer program is chosen for the transient dynamic analysis. Figure 7-1 shows the ANSYS finite element model.

Flat shell elements are used to model the reinforced concrete containment structure and the reactor vessel. Pipe elements are used to model the columns supporting the diaphragm slab. The soil structure interaction is taken into consideration by modelling the soil using a series of discrete springs and dampers in three directions as shown on Figure 7-1. These discrete springs and dampers are specified based on the formulae for lumped parameter foundations found in Ref. 32.

The ANSYS program uses stiffness-proportional-damping, implying a structural damping matrix in the following form:

$$\{C\} = \beta\{K\},$$

where C = Damping Matrix
β = a stiffness-proportional - damping constant
K = Stiffness Matrix

Figure 7-2 shows the equivalent modal damping ratio versus the modal frequency for structural stiffness-proportional-damping. A value of β equaling 0.00063 is used in the ANSYS model which corresponds to a structural modal damping of approximately 4 percent of critical at 20 Hz.

Two computer programs have been developed, one as a preprocessor and the other as a postprocessor to the ANSYS computer program. The preprocessor transforms the pressure forcing functions acting on the suppression pool walls, base mat, and pedestal into a concentrated force acting at the associated nodes of the ANSYS model. The postprocessor calculates the acceleration time history from the displacement time history obtained by ANSYS and scans for the maximum displacements and accelerations.

Acceleration time histories, maximum structural displacements, accelerations, and broadened acceleration response spectra at selected nodes and directions are developed for the analysis of the piping, equipment, and NSSS systems. Response spectra curves are developed for all the previously mentioned SRV discharge and LOCA loads.

The response spectra are furnished for four different spectral damping values, ie, 0.5, 1, 2, and 5 percent of critical. Each spectrum has been broadened to account for the uncertainties in the structural modeling techniques and material properties. All spectral accelerations are expressed in units of g (the gravitational constant).

Appendix B contains examples of the broadened response spectra curves developed for the different loading cases of SRV discharge and LOCA related loads. (The pressure time history shown on Figure 4-29 is used as the basis for the examples given.)

The ANSYS program (stress pass) is also used to compute the forces and moments due to the SRV discharge and LOCA related loads. These forces and moments are then combined with the nonhydrodynamic loads in accordance with Table 5-1. Material stresses at the critical design sections in the primary containment and internal concrete structures are analyzed using the CECAP computer program (Refer to Appendix A to FSAR Section 3.8). Concrete cracking is considered in the analysis of reinforced concrete sections.

7.1.1.2 Reactor Building Assessment Methodology

The construction of the SSES reactor building is such that no direct coupling with the containment occurs. A 2 in. separation joint is kept between the containment structure and the reactor building at all points where the two structures abut, except at the base slabs where a cold joint exists. This arrangement minimizes the transfer of any direct dynamic response to the reactor building from the containment, where the SRV discharge and LOCA hydrodynamic loads originate.

The average horizontal and vertical base accelerations from the containment dynamic analysis are computed and used as input motions on the reactor building foundations. This results in two horizontal motions and one vertical motion. The input motions are used in the form of acceleration time histories at the base slab. Reactor building seismic models (horizontal north-south and east-west and vertical), as shown on FSAR Figures 3.7-9 through 3.7-11 and explained in detail in Subsection 3.7.2.1b of the FSAR, are used in the structural response analysis due to SRV discharge and LOCA loads.

Appendix C provides examples of the broadened response spectra curves for the reactor building due to SRV discharge loads for the abnormal operating transient (AOT) case at selected locations. The pressure time history shown in Figure 4-29 is used as the basis for the examples given). The response spectra curves are developed for use in the design of piping and NSSS systems. The response spectra are furnished for four different spectral damping values, ie, 0.5, 1, 2, and 5 percent of critical. Each spectrum has been broadened to account for the uncertainties in the structural modelling techniques and material propeties. All spectral accelerations are expressed in units of q (the gravitational constant). The forces and moments due to SRV discharge and LOCA loads are combined with the non-hydrodynamic loads in accordance with Table 5-1.

7.1.2 Structural Steel Assessment Methodology

7.1.2.1 Suppression Chamber Columns Assessment Methodology

The assessment methods used for non-hydrodynamic loads such as dead, live, pressure, temperature, seismic, and pipe rupture loads are described in the FSAR, Section 3.8.3.4.5.

For the analysis of the columns for hydrodynamic loads, the ANSYS computer program is used. A typical column is modelled as a fixed-ended beam as shown on Figure 7-3. The total length of the column is divided into beam finite elements joined at node points. An effective water mass due to submergence is considered. Dynamic horizontal forces are applied to the column at the node points below water level. Time-varying forces and moments in the column are calculated for each finite element. These results are combined with those for non-hydrodynamic loads to determine the total forces and moments in the column.

7.1.2.2 Downcomer Bracing Assessment Methodology

Axial loads are produced in the bracing due to lateral loading on the downcomers. See Subsection 7.1.4 for a description of the analysis of the downcomers for lateral loads. To determine the maximum axial load in the bracing, lateral loads are assumed to occur on all downcomers within a 90 degree influence zone in either the radial or tangential directions. Bracing for the 16 SRV discharge pipes is included with the downcomer bracing. A sliding support is provided at the connection of the bracing to the discharge pipe to allow the discharge pipe to move vertically without producing a reaction load on the bracing. Since these lateral loads on the downcomers due to seismic and hydrodynamic loads are randomly oriented, various combinations of load directions are considered in order to determine the maximum axial load in the bracing.

In addition to the axial load, there are lateral pressures applied along the length of the bracing members due to direct hydrodynamic loading. Since the bracing members are of varying lengths, several different lengths of bracing members are considered for the analysis. Stresses in the downcomer bracing due to equivalent static lateral pressures are calculated using classical beam theory equations. Stresses in the downcomer bracing due to dynamic lateral pressures are calculated using the ANSYS computer program. The total length of the bracing member is divided into beam finite elements joined at node points. An effective water mass due to submergence will be considered. Dynamic lateral forces are applied to the bracing at the node points. Time-varying forces and moments in the bracing member are calculated for each finite element. Maximum stresses are calculated from these results using classical beam theory equations.

7.1.3 Liner Plate Assessment Methodology

FSAR Subsection 3.8.1 provides a description of the liner plate and anchorage system for the containment.

The analysis of the liner plate and anchorages for non-hydrodynamic loads is in accordance with Ref 18.

For the analysis of the liner plate and anchorages for hydrodynamic suction pressure loads, the load on the liner is the net negative pressure load. The net negative pressure load equals the dynamic negative pressure due to SRV actuation or LOCA chugging minus the static positive pressure due to hydrostatic pressure or LOCA. Figures 7-4 and 7-5 describe the loads on the base mat and suppression chamber wall liner plate for the normal and abnormal load combinations respectively.

For the normal condition, the hydrostatic pressure on the base mat is 10.4 psi and the maximum negative pressure due to the actuation of all SRV's is 7.8 psi.

The distribution of these pressures on the suppression chamber wall is shown in Figure 7-4.

For the abnormal condition, the total positive pressure on the basemat is 35.4 psi which consists of 10.4 psi from hydrostatic pressure plus 25.0 from LOCA (small or intermediate break accident). The total maximum negative pressure on the base mat is 21.8 psi due to the asymmetric chugging load. The maximum negative pressures from SRV actuation and chugging are combined for conservatism. It is recognized that the probability of these two phenomena producing peak negative pressures at the same time is very low. The distribution of pressures on the suppression chamber wall is shown in Figure 7-5.

Since the negative pressure is more than balanced by the positive pressure, the liner plate does not experience any net negative pressure. Therefore, there are no flexural stresses induced in the liner plate.

7.1.4 Downcomer Assessment Methodology

Stresses in the downcomer pipes due to static loads, such as dead weight and pressure, are calculated using classical equations.

Stresses in the downcomer pipes due to inertial loads caused by seismic and hydrodynamic loads are calculated using the response spectrum method. The ANSYS computer program is used to solve for the mode shapes and frequencies of the downcomers and the downcomer bracing. A group of downcomer pipes and bracing members is represented by a lumped mass model. The inertia effect of the water surrounding the submerged portion of the downcomers is approximated by the addition of an effective water mass. The mass of water inside the downcomers is included in the model for all dynamic loadings except LOCA. For the LOCA conditions, the water has been vented from the downcomers and therefore it is not included in the model.

The ANSYS computer program is used to calculate the stresses in the downcomer pipes due to hydrodynamic lateral loads. A typical downcomer pipe is modelled as shown in Figure 7-6. Point A at the top of the downcomer is restrained to represent the fixity of the downcomer at the drywell floor. Point B is laterally restrained to represent the lateral support furnished by the downcomer bracing. The total length of the downcomer is divided into beam finite elements joined at node points. Dynamic horizontal forces are applied to the downcomer at the node points below water level. Time-varying forces and moments in the downcomer are calculated for each finite element. Maximum stresses are calculated from these results using classical beam theory equations.

7.1.5 Piping and SRV Systems Assessment Methodology

The piping and SRV systems will be analyzed for the loads discussed in Section 5.5 using Bechtel computer programs ME101 and ME632. These programs are described in FSAR Section 3.9. Static and dynamic analyses of the piping and SRV systems are performed as described in the paragraphs below.

Static analysis techniques are used to determine the stresses due to steady state loads and/or dynamic loads having equivalent static loads. The drag and impact loads are applied as equivalent static loads.

Response spectra at the piping anchors are obtained from the dynamic analysis of the containment subjected to LOCA and SRV loading. Piping systems are then analyzed for these response spectra following the method described in Ref 19.

Time history dynamic analysis of the SRV discharge piping subjected to fluid transient forces in the pipe due to relief valve opening is performed using Bechtel computer code ME632.

7.1.6 NSSS Assessment Methodology

To be provided later.

7.1.7 Equipment Assessment Methodology

Analysis methodologies for safety-related equipment within the containment and reactor building subject to LOCA and SRV discharge loading will be described in a revision to this DAR ("Safety related" is defined in Table 1.8-1 of the FSAR).

7.2 DESIGN CAPABILITY MARGINS

Stresses at the critical sections for each of the above structures, piping, and equipment will be evaluated for all the loading combinations presented in Chapter 5.

The results of the structural assessment of the containment and submerged structures will be summarized in Appendix A. (Figure A-2 shows the design sections in the basemat, containment walls, reactor pedestal, and the diaphragm slab considered in the structural assessment). The tables of Appendix A at present give the calculated design margins for load combination Equation 1 of Table 5-1 which applies to the previously mentioned structural components. Similar tables will be included in a future revision of this report in order to present the full assessment of the design capability margin for all the other load combinations.

The reinforcing steel and concrete quality control test results show that material strengths are higher than the minimum specified values used in computing these margins. This conservatism, along with the overload factors in the load combinations given in Table 5-1 and the material understrength factors built into the allowable stress criteria, results in actual safety margins greater that those given in the tables of Appendix A.

The results of the structural assessment of the reactor building will be summarized in Appendix E.

The results of the analysis of the piping systems will be summarized in Appendix F in the form of tables. These tables will provide the maximum stress for the critical load combination, the allowable stress, and the design margin.

The results of the assessment of the Nuclear Steam Supply System (NSSS) will be summarized in Appendix G.

The results of the assessment of equipment will be summarized in Appendix H.

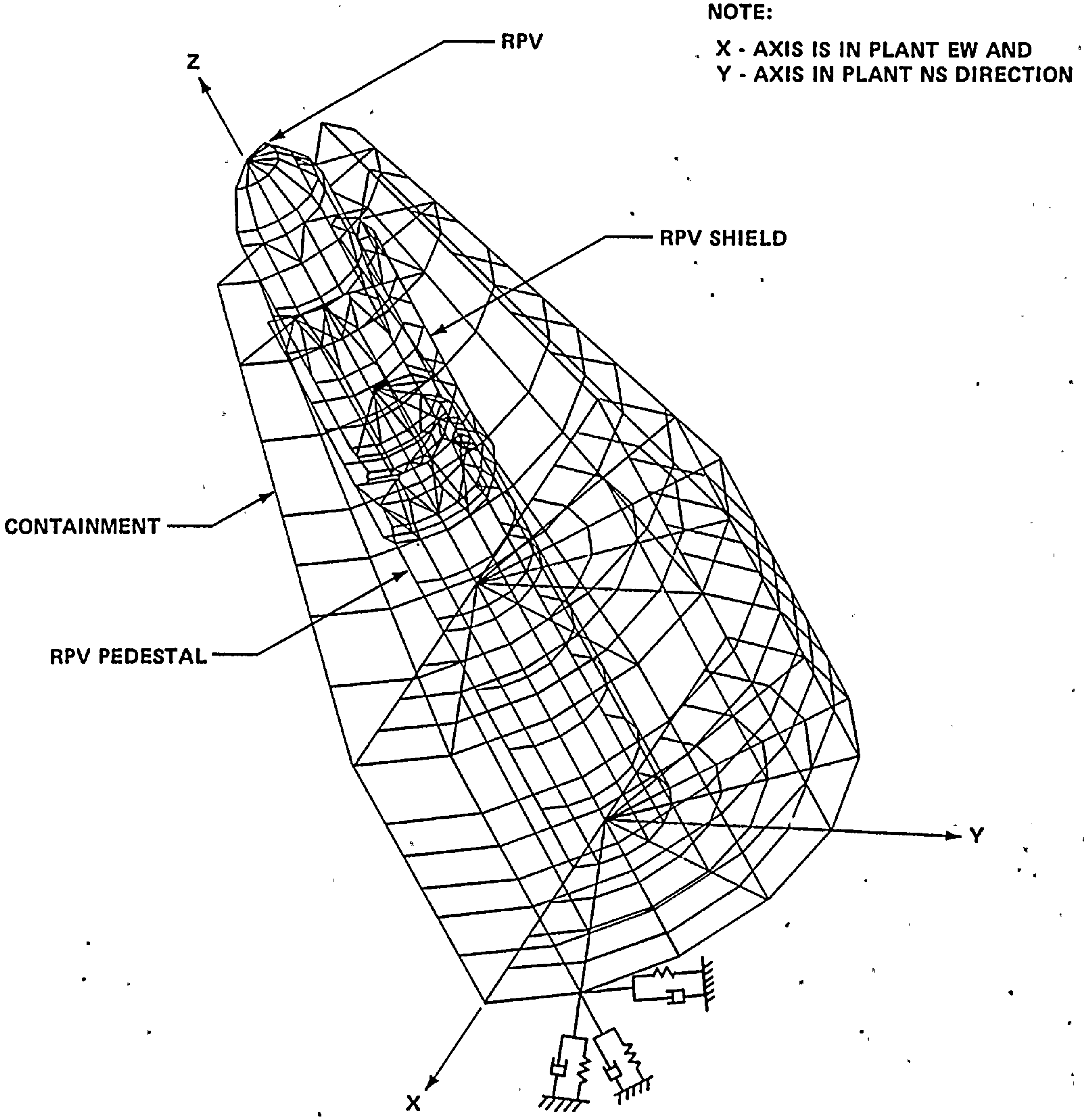

SUSQUEHANNA STEAM ELECTRIC STATION
UNITS 1 AND 2
DESIGN ASSESSMENT REPORT

GEOMETRY PLOT OF
CONTAINMENT STRUCTURE MODEL

FIGURE 7-1

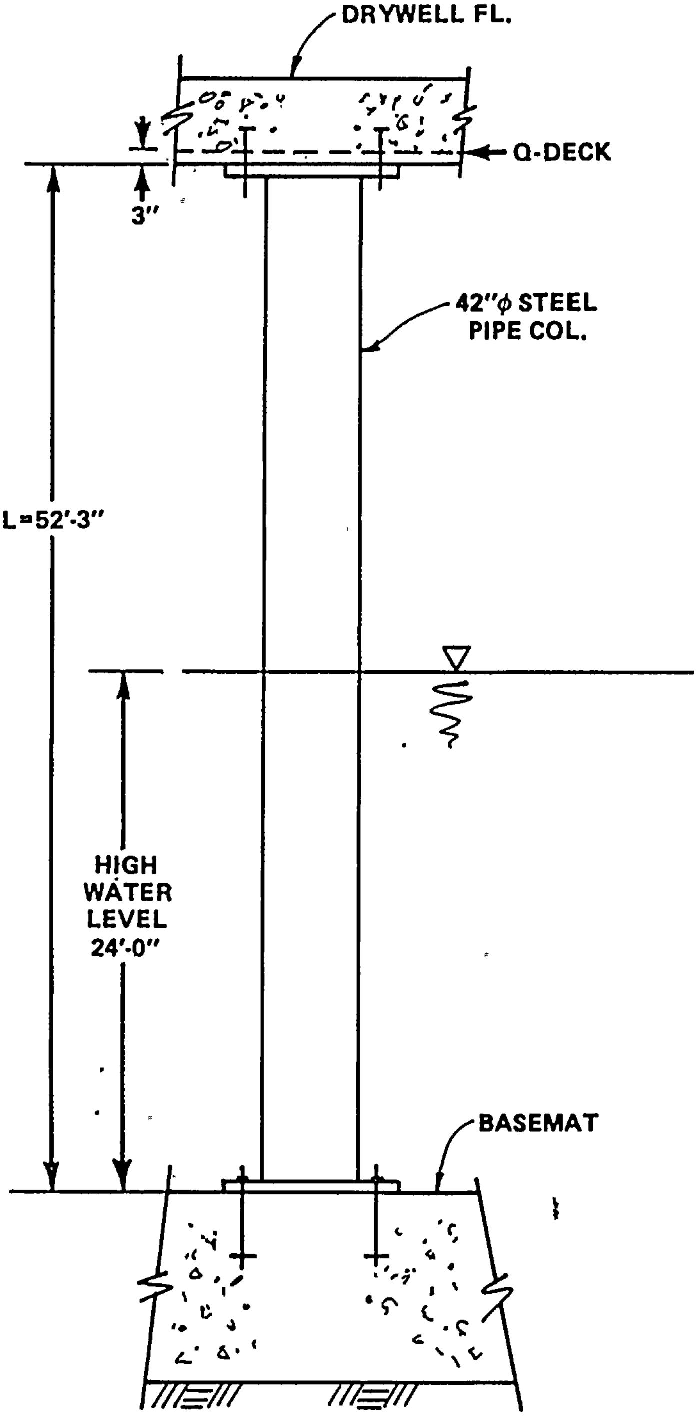

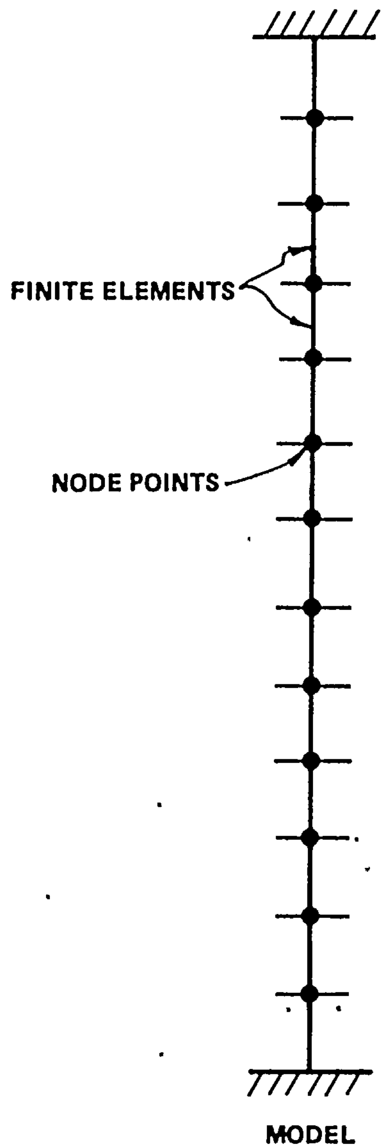

SUSQUEHANNA STEAM ELECTRIC STATION
UNITS 1 AND 2
DESIGN ASSESSMENT REPORT

FINITE ELEMENT MODEL OF COLUMN

FIGURE 7-3

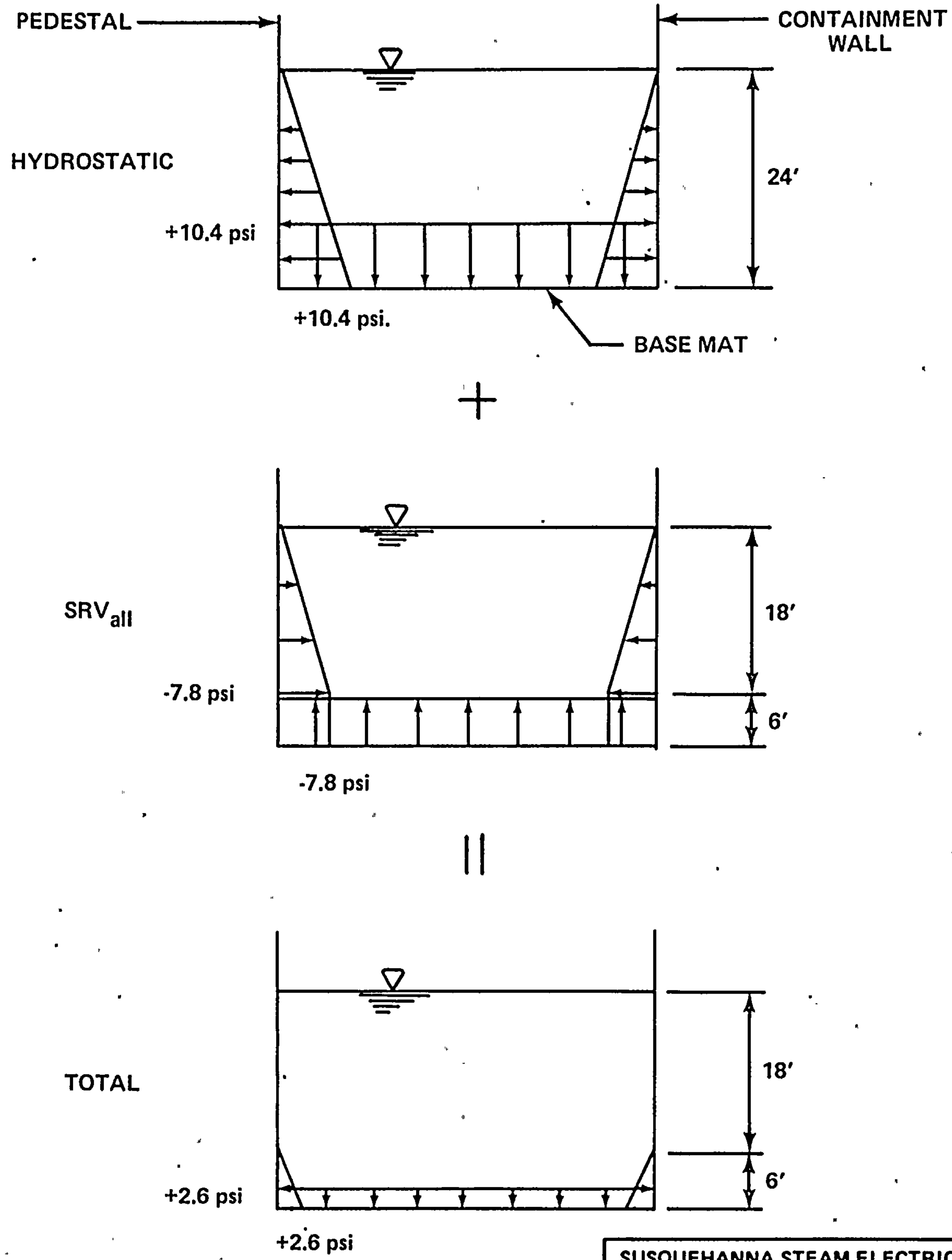

SUSQUEHANNA STEAM ELECTRIC STATION
UNITS 1 AND 2
DESIGN ASSESSMENT REPORT

LINER PLATE PRESSURES
NORMAL CONDITION

FIGURE 7-4

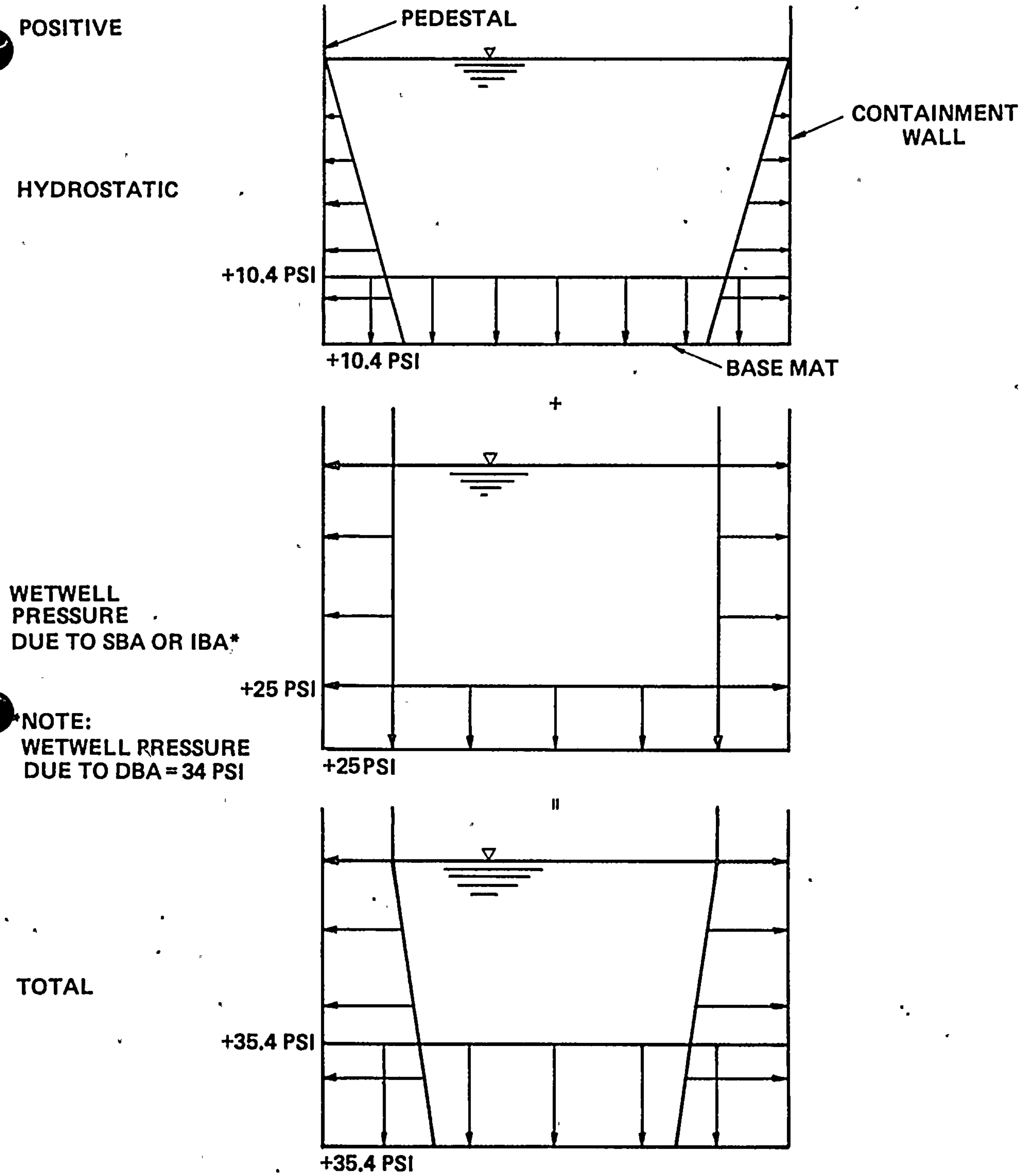

SUSQUEHANNA STEAM ELECTRIC STATION
UNITS 1 AND 2
DESIGN ASSESSMENT REPORT

LINER PLATE PRESSURES
ABNORMAL CONDITION

FIGURE 7-5 SHEET 1 OF 3

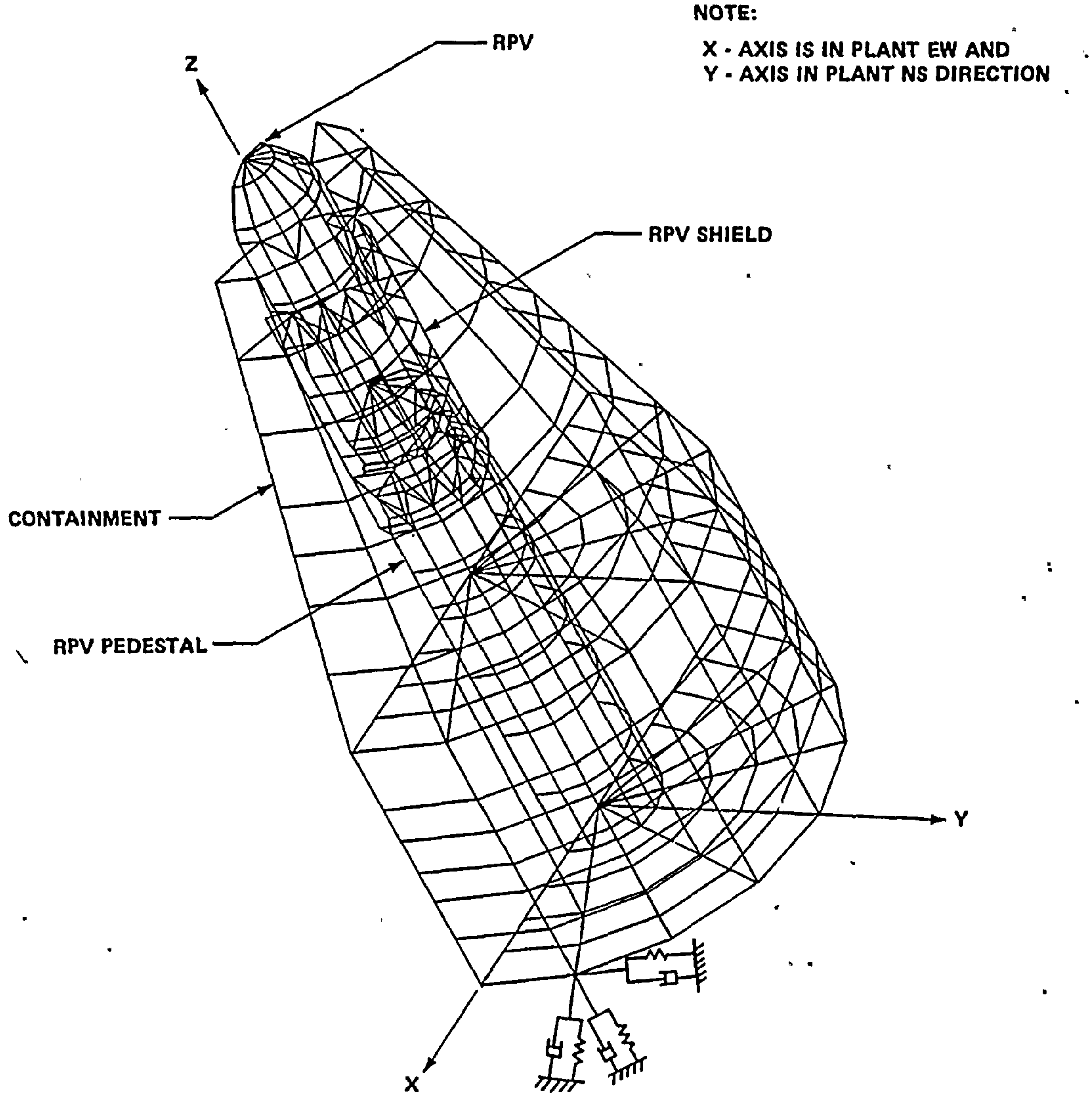

SUSQUEHANNA STEAM ELECTRIC STATION
UNITS 1 AND 2
DESIGN ASSESSMENT REPORT

3-D CONTAINMENT FINITE ELEMENT MODEL (ANSYS MODEL)

FIGURE 7-1

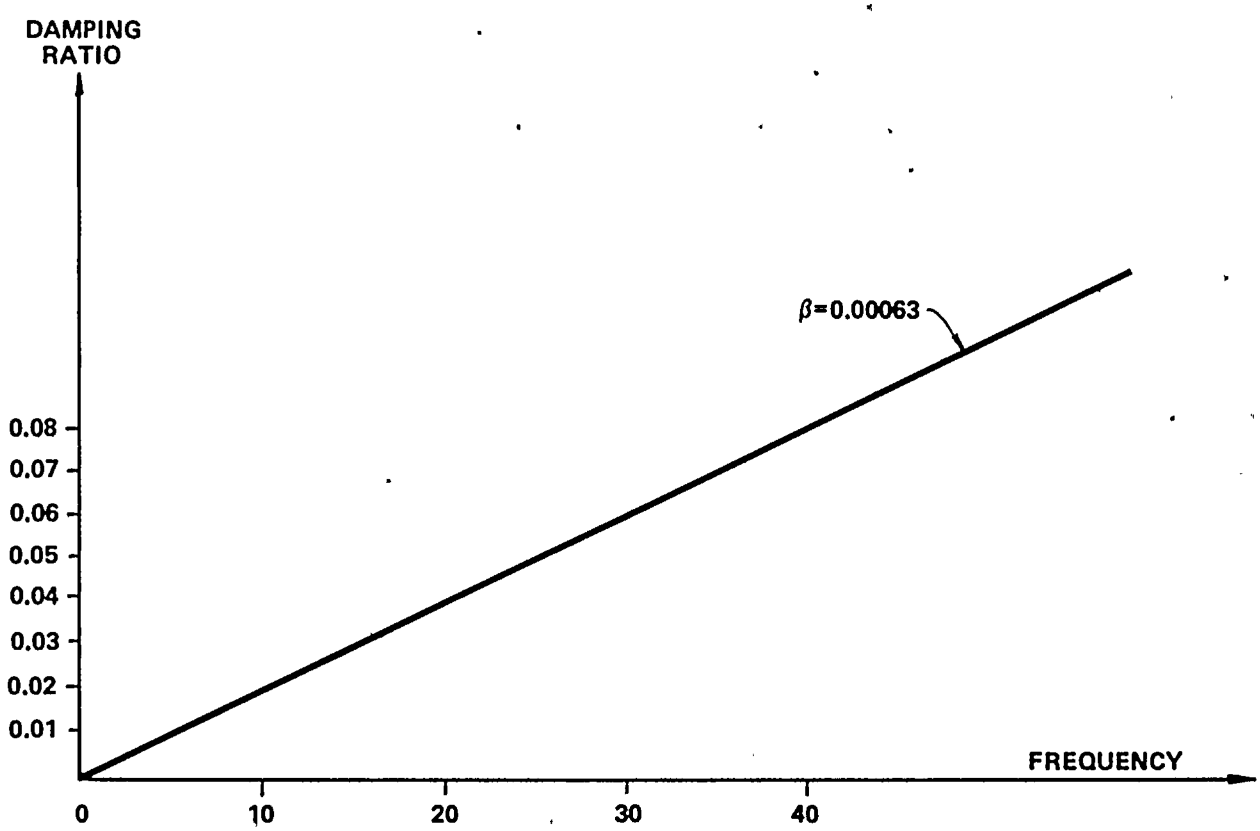

SUSQUEHANNA STEAM ELECTRIC STATION
UNITS 1 AND 2
DESIGN ASSESSMENT REPORT

EQUIVALENT MODAL DAMPING RATIO VS MODAL FREQ. FOR STRUCTURAL STIFFNESS PROPORTIONAL DAMPING

FIGURE 7-2

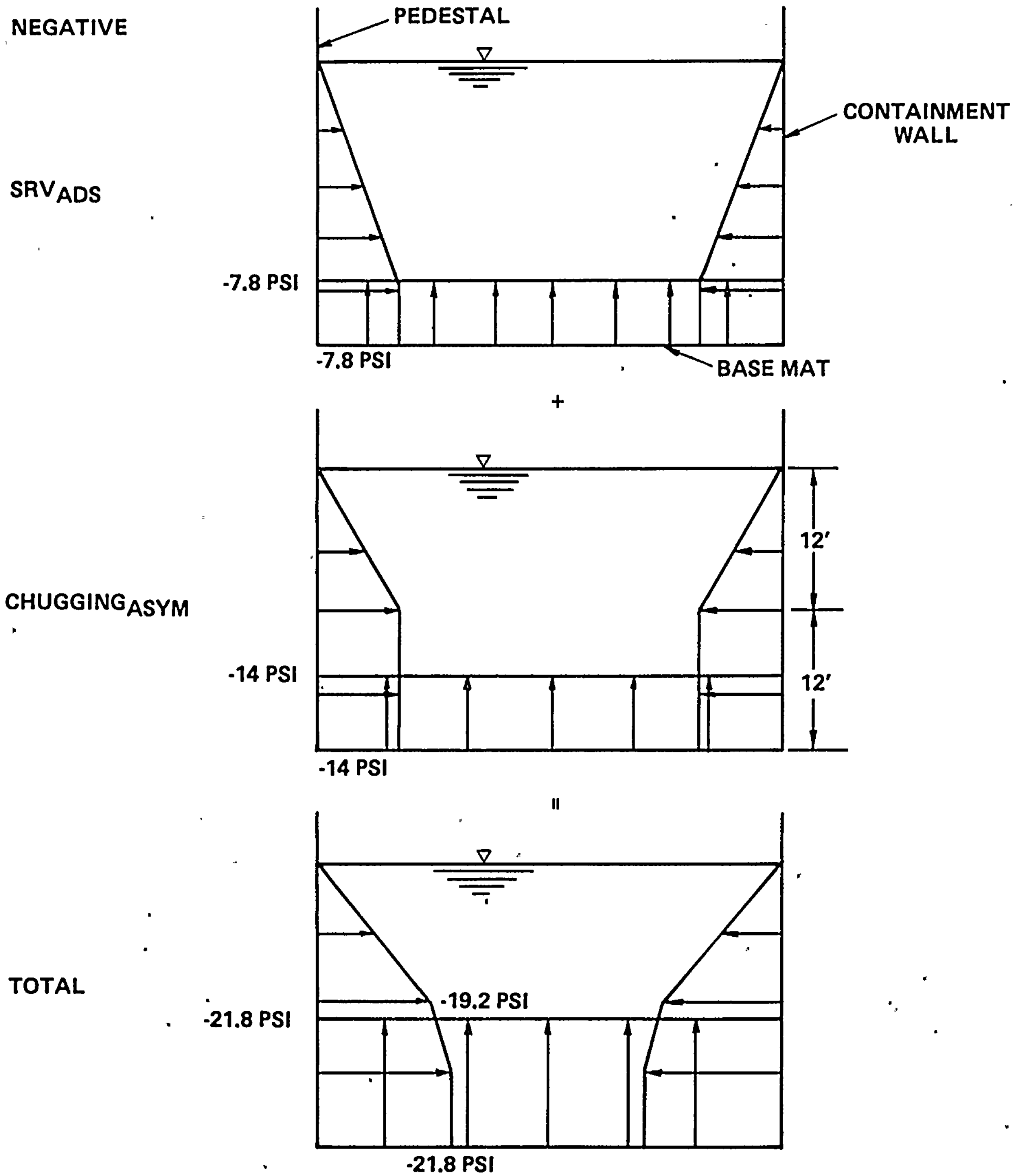

SUSQUEHANNA STEAM ELECTRIC STATION
UNITS 1 AND 2
DESIGN ASSESSMENT REPORT

LINER PLATE PRESSURES
ABNORMAL CONDITION

FIGURE 7-5 SHEET 2 OF 3

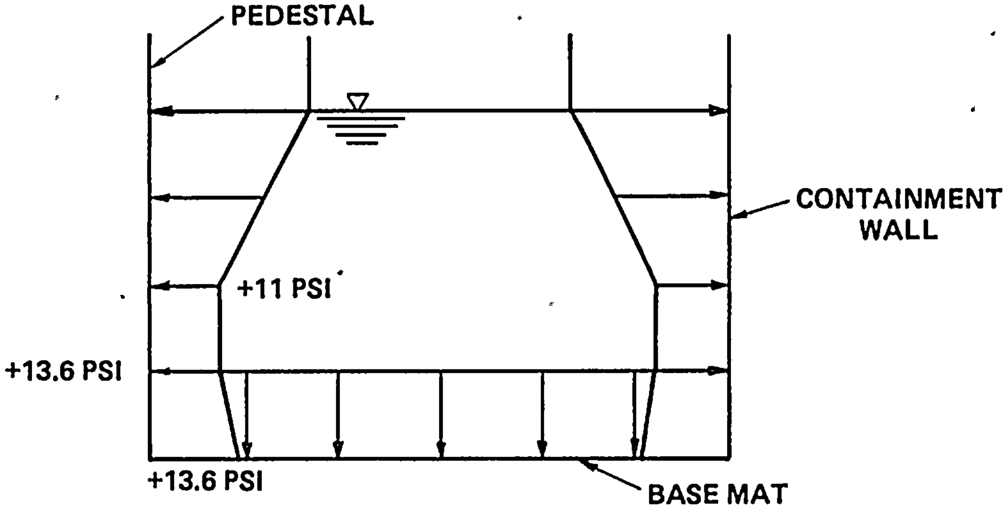

TOTAL = POSITIVE + NEGATIVE

SUSQUEHANNA STEAM ELECTRIC STATION
UNITS 1 AND 2
DESIGN ASSESSMENT REPORT

LINER PLATE PRESSURES
ABNORMAL CONDITION

FIGURE 7-5 SHEET 3 OF 3

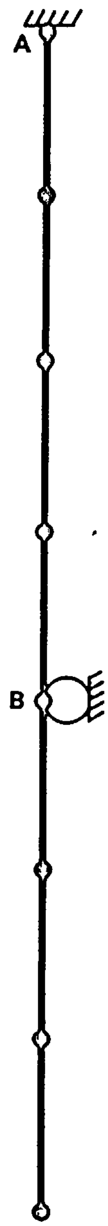

SUSQUEHANNA STEAM ELECTRIC STATION
UNITS 1 AND 2
DESIGN ASSESSMENT REPORT

DOWNCOMER ANALYTICAL MODEL

FIGURE 7-6

CHAPTER 9

RESPONSES TO NRC QUESTIONS

TABLE OF CONTENTS

9.0 RESPONSES TO NRC QUESTIONS

This chapter will provide responses to those Nuclear Regulatory Commission (NRC) questions whichhave been designated by Ref 10 (as amended) to be found in the plant-unique Design Assessment Report and to those questions for which the response in Ref 10 is inapplicable. The NRC questions for which responses will be provided are identified in Section 9.1, and detailed responses to the questions are found in Section 9.2.

9.1 IDENTIFICATION OF QUESTIONS UNIQUE TO SSES

The below listed questions address concerns unique to SSES. These questions are answered in detail in Section 9.2.

NRC Question Number	Question Topic
M020.26	Primary and Secondary LOCA Loads
M020.27	Inventory Effects on Blowdown
M020.44	Poolswell Waves and Seismic Slosh
M020.55	SRV Loads on Submerged Structures
M020.58(1),(2),(3)	Plant Unique Poolswell Calculations
M020.59(1),(3),(4)	Downcomer Lateral Braces
M020.60	Wetwell Pressure History
M020.61	Poolswell Inside Pedestal
M130.1	Pressure Loading Due to SRV Discharge
M130.2	Load Combination History
M130.4	Soil Modelling
M130.5	Liner and Anchorage Mathematical Model
M130.6	Containment Structural Model-Asymmetric Loads
M130.12	SRV Structural Response

9.2 QUESTIONS UNIQUE TO SSES AND RESPONSES THERETO

QUESTION M020.26

The DFFR presents a description of a number of LOCA related hydrodynamic loads without differentiating between primary and secondary loads. Provide this differentiation between the primary and secondary LOCA-related hydrodynamic loads. We recognize that this differentiation may vary from plant to plant. We would designate as a primary load any load that has or will result in a design modification in any Mark II containment since the pool dynamic concerns were identified in our April 1975 generic letters.

RESPONSE M020.26

The table below shows the LOCA-related hydrodynamic loads on the SSES containment. Those loads which have resulted in containment design modifications are designated as "Primary Loads." These primary loads result from the poolswell transient.

Drywell floor uplift pressures during the wetwell compression phase of poolswell lead to the decision to increase the SSES drywell floor design safety margin for uplift pressures by relocating drywell floor shear ties.

Poolswell impact, drag, and fallback loads resulted in the relocation of equipment in the SSES wetwell to a position above the peak poolswell height. Furthermore, the downcomer bracing system was redesigned.

All other LOCA-related hydrodynamic loads are designated as "Secondary Loads" since no design modification has resulted from their presence.

LOCA Load	"Primary Load"	Secondary Load"
1. Wetwell/Drywell Pressures (During Poolswell)	X(1)	
2. Poolswell Impact Load	X(2)	
3. Poolswell Drag Load	X(3)	
4. Downcomer Clearing Load		X
5. Downcomer Jet Load		X
6. Poolswell Air Bubble Load		X
7. Poolswell Fallback Load	X(4)	
8. Mixed Flow Condensation Oscillation Load		X

9. Pure Steam Condensation Oscillation Load	X
10. Chugging	X
11. Wetwell/Drywell Pressure and Temperature during DBA LOCA (Long Term)	X
12. Wetwell/Drywell Pressure and Temperature during IBA LOCA (Long Term)	X
13. Wetwell/Drywell Pressure and Temperature during SBA LOCA (Long Term)	X

Footnotes:

(1) Shear ties changed in drywell floor.

(2) Equipment moved in wetwell.

(3) Equipment moved in wetwell. Bracing system redesign.

(4) Equipment moved in wetwell.

QUESTION M020.27

The calculated drywell pressure transient typically assumes that the mass flow rate from the recirculation system or steamline is equal to the steady-state critical flow rate based on the critical flow area of the jet pump nozzle or steamline orifice. However, for approximately the first second after the break opening, the rate of mass flow from the break will be greater than the steady-state value. It has been estimated that for a Mark I containment this effect results in a temporary increase in the drywell pressurization rate of about 20 percent above the value based solely on the steady-state critical flow rate. The drywell pressure transient used for the LOCA pool dynamic load evaluation, for each Mark II plant, should include this initially higher blowdown rate due to the additional fluid inventory in the recirculation line.

RESPONSE M020.27

The drywell pressure transients have been recalculated by GE (Ref 7) with the additional blowdown flow rate produced by the inventory effects included in the analysis. The LOCA loads presented in Section 4.2 have been calculated using these recalculated drywell pressure transients. Specifically, the drywell pressure transient resulting from the DBA LOCA including the effects of pipe inventory has been used as input to the poolswell model.

QUESTION M020.44

Table 5-1 and Figures 5-1 through 5-16 in the DFFR provide a listing of the loads and the load combinations to be included in the assessment of specific Mark II plants. This table and these figures do not include loads resulting from pool swell waves following the pool swell process or seismic slosh. We require that an evaluation of these loads be provided for the Mark II containment design.

RESPONSE M020.44

This information will be supplied in a subsequent revision to this DAR.

QUESTION M020.55

The computational method described in DFFR Section 3.4 for calculating SRV loads on submerged structures is not acceptable. It is our position that the Mark II containment applications should commit to one of the following two approaches:

(1) Design the submerged structures for the full SRV pressure loads acting on one side of the structures; the pressure attenuation law described in Section 3.4.1 of NEDO-21061 for the ramshead and Section A10.3.1 of NEDO-11314-08 for the quencher can be applied for calculating the pressure loads.

(2) Follow the resolution of GESSAR-238 NI on this issue. The applicant for GESSAR-238 NI has proposed a method presented in the GE report, "Unsteady Drag on Submerged Structures," which is attached to the letter dated March 24, 1976 from G.L. Gyorey to R.L. Tedesco. This report is actively under review.

RESPONSE M020.55

Loads on submerged structures due to SRV actuation are discussed in Subsection 4.1.3.7.

QUESTION M020.58

Relating to the pool swell calculations, we require the following information for each Mark II plant:

(1) Provide a description of and justify all deviations from the DFFR pool swell model. Identify the party responsible for conducting the pool swell calculations (ie, GE or the A&E). Provide the program input and results of bench mark calculations to qualify the pool swell computer program.

(2) Provide the pool swell model input including all initial and boundary conditions. Show that the model input represents conservative values with respect to obtaining maximum pool swell loads. In the case of calculated input, (ie, drywell pressure response, vent clearing time), the calculational methods should be described and justified. In addition, the party responsible for the calculation (ie, GE or the A&E) should be identified.

(3) Pool swell calculations should be conducted for each Mark II plant. The following pool swell results should be provided in graphic form for each plant:

(a) Pool surface position versus time

(b) Pool surface velocity versus time

(c) Pool surface velocity versus position

(d) Pressure of the suppression pool air slug and the wetwell air versus time.

RESPONSE M020.58

(1) A specific response to this question can be found in Subsection 4.2.1.1. Verification of the SSES poolswell model is provided in Appendix Section D.1.

(2) Input and discussion of the poolswell model input can be found in Tables 4-17, 4-18, and Section 4.2.1.1.

(3) The requested graphic results of the SSES poolswell calculation can be found in Figures 4-38, 4-39, 4-40, and 4-43.

QUESTION M020.59

In the 4T test report NEDE-13442P-01 Section 3.3 the statement is made that for the various Mark II plants a wide diversity exists in the type and location of lateral bracing between downcomers and that the bracing in the 4T tests was designed to minimize the interference with upward flow. Provide the following information for each Mark II plant:

(1) A description of the downcomer lateral bracing system. This description should include the bracing dimensions, method of attachment to the downcomers and walls, elevation and location relative to the pool surface. A sketch of the bracing system should be provided.

(3) The basis for calculating the impact or drag load on the bracing system or downcomer flanges. The magnitude and duration of impact or drag forces on the bracing system or downcomer flanges should also be provided.

(4) An assessment of the effect of downcomer flanges on vent lateral loads.

RESPONSE M020.59

(1) A downcomer bracing system is furnished to resist lateral loads on the downcomers. The original downcomer bracing was designed to resist seismic inertia loads. A revised downcomer bracing system has been designed to resist hydrodynamic loads as well as seismic inertia loads. The revised bracing system consists of horizontal 6 in. diameter steel pipes spanning between the downcomers and embeds in the suppression chamber wall or the RPV pedestal. The pattern of bracing members forms a horizontal truss as shown on Figure 9-1. The bracing members are bolted or welded to the downcomers and embeds in the suppression chamber wall as shown on Figure 9-2. The bracing system is located 8 ft from the bottom end of the downcomer which is 3 ft below the normal water level.

(3) The basis for calculating the impact or drag loads on the downcomer bracing system (el. 668') and downcomer stiffener rings (el. 668' and el. 682') is given in Section 4.2. The magnitude and duration of impact or drag forces on the bracing system and downcomer stiffener rings is also given in Section 4.2 .

(4) This item is not applicable to the SSES design.

QUESTION M020.60

In the 4T test report NEDE-13442P-01 Section 5.4.3.2 the statement is made that an underpressure does occur with respect to the hydrostatic pressure prior to the chug. However, the pressurization of the air space above the pool is such that the overall pressure is still positive at all times during the chug. We require that each Mark II plant provide sufficient information regarding the boundary underpressure, the hydrostatic pressure, the air space and the SRV load pressure to confirm this statement or alternatively provide a bounding calculation applicable to all Mark II plants.

RESPONSE M020.60

This information will be supplied in a subsequent revision to this DAR.

QUESTION M020.61

Significant variations exist in the Mark II plants with regard to the design of the wetwell structures in the region enclosed by the reactor pedestal. These variations occur in the areas of (1) concrete backfill of the pedestal, (2) placement of downcomers, (3) wetwell air space volumes, and (4) location of the diaphragm relative to the pool surface. In addition to variation between plants, for a given plant, variations exist in some of these areas within a given plant. As a result, for a given plant, significant differences in the pool swell phenomena can occur in these two regions. We will require that each plant provide a separate evaluation of pool swell phenomena and loads inside of the reactor pedestal.

RESPONSE M020.61

The SSES pedestal and wetwell area is shown on Figures 1-1 and 9.3. Due to the absence of downcomers in the pedestal interior, no pool swell would be expected in this region. There are 12 holes in the pedestal, however, eight of which would allow the flow of water from the suppression pool to the pedestal during a LOCA. Some downcomers are near the pedestal flow holes, leading to the possibility that air could be blown through the pedestal holes, which would lead to a greater pedestal pool swell than would be experienced by incompressible water flow alone. One would expect the pedestal pool swell to be much reduced from the suppression pool swell due to its relative separation from the suppression pool and the lack of direct charging from downcomer vents. Indeed, 1/13.3 scale model tests of the SSES pedestal design conducted at the Stanford Research Institute under the sponsorship of EPRI show that the pedestal pool swell is less than 20 percent of the pool swell in the suppression pool (Ref 31). There is no piping or equipment inside the SSES pedestal and, since the pedestal pool swell is very small, the only load involved due to pedestal pool swell would be a small •P across the pedestal due to different water levels between the suppression pool and the pedestal. This load is considered in the design of the SSES pedestal.

QUESTION M130.1

Provide in Section 5 a description of the pressure loadings on the containment wall, pedestal wall, base mat, and other structural elements in the suppression pool, due to the various combinations of SRV discharges, including the time function and profile for each combination. If this information is not generic, each affected utility should submit the information as described above.

RESPONSE M130.1

Chapter 4 describes the pressure loadings and time histories due to SRV discharge and other hydrodynamic loads.

QUESTION M130.2

In DFFR Section 5.2 it is stated that the load combination histories are presented in the form of bar charts as shown on Figures 5-1 through 5-16. It is not indicated how these load combination histories are used. In particular, it is not clear whether only loads represented by concurrent bars will be combined, and it should be noted that depending on the dynamic properties of the structures and the rise time and duration of the loads, a structure may respond to two or more given loads at the same time even though these loads occur at different times. Also, although condensation oscillations are depicted as bars on the bar charts, the procedure for the analysis of structures due to these loads has not been presented. Accordingly, the description of the method should include consideration of such conditions. Also, for condensation oscillation loads and for SRV oscillatory loads, include low cycle fatigue analysis.

RESPONSE M130.2

The loads will be combined according to Tables 5-1 and 5-2 of this DAR to assess the containment structural components. Chapters 5 and 7 explain the load combination methods used in containment analysis. The structural analysis procedure to account for condensation oscillation load will be presented in a subsequent revision to this DAR.

QUESTION M130.4

Through the use of figures, describe in detail the soil modelling as indicated in DFFR Subsection 5.4.3 and describe the solid finite elements which you intend to use for the soil.

RESPONSE M130.4

Soil modelling is explained in Subsection 7.1.1.1 and Figure 7-1.

QUESTION M130.5

Describe the mathematical model which you will use for the liner and the anchorage system in the analysis as described in DFFR Subsection 5.6.3.

RESPONSE M130.5

The mathematical model which will be used for analysis of the liner and the anchorage for hydrodynamic suction pressures is described in Subsection 7.1.3.

QUESTION M130.6

In DFFR Subsection 5.1.1.1 it was stated that the SRV discharge could cause axisymmetric or asymmetric loads on the containment. In Subsection 5.4.1 an axisymmetric finite element computer program is recommended for dynamic analysis of structures due to SRV loads, and no mention is made of the analysis for asymmetric loads. Describe the structural analysis procedure used to consider asymmetric pool dynamic loads on structures and through the use of figures, describe in more detail the structural model which you intend to use.

RESPONSE M130.6

The dynamic analyses and models used are explained in Chapter 7 .

QUESTION M130.12

Reference is made in DFFR Subsection 5.4.3 to studies of structural response to SRV load. Provide citations for this reference and where such studies are not readily available, copies are requested.

RESPONSE M130.12

Studies mentioned in DFFR Subsection 5.4.3 are the results of analysis completed for a specific plant at the time of writing of the DFFR. Reference to the studies was intended to indicate the need for considering strain dependent soil properties. For the SSES analysis, Ref 32 is used to determine the soil constants in the analysis.

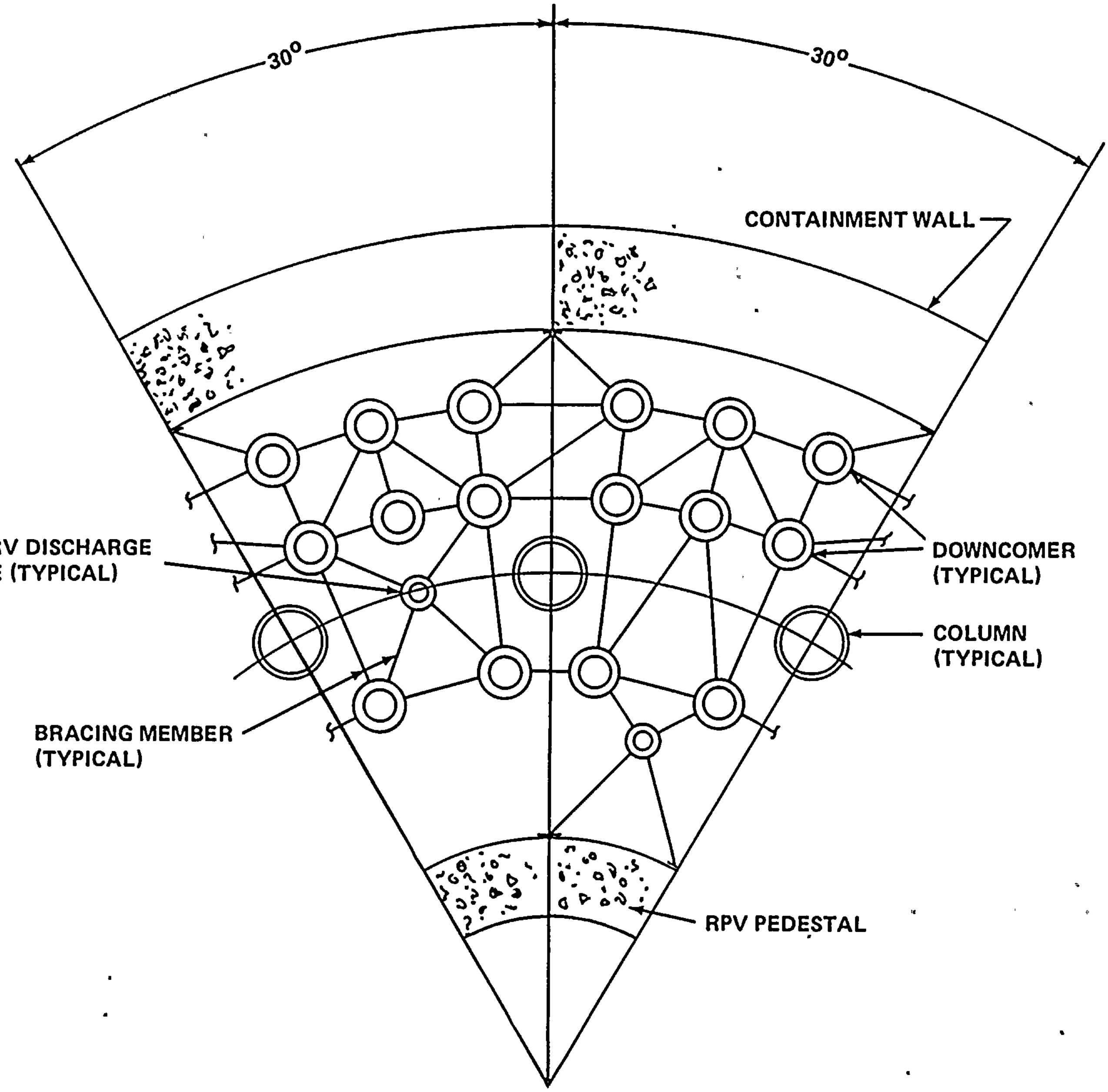

SUSQUEHANNA STEAM ELECTRIC STATION
UNITS 1 AND 2
DESIGN ASSESSMENT REPORT

DOWNCOMER
BRACING SYSTEM

FIGURE 9-1

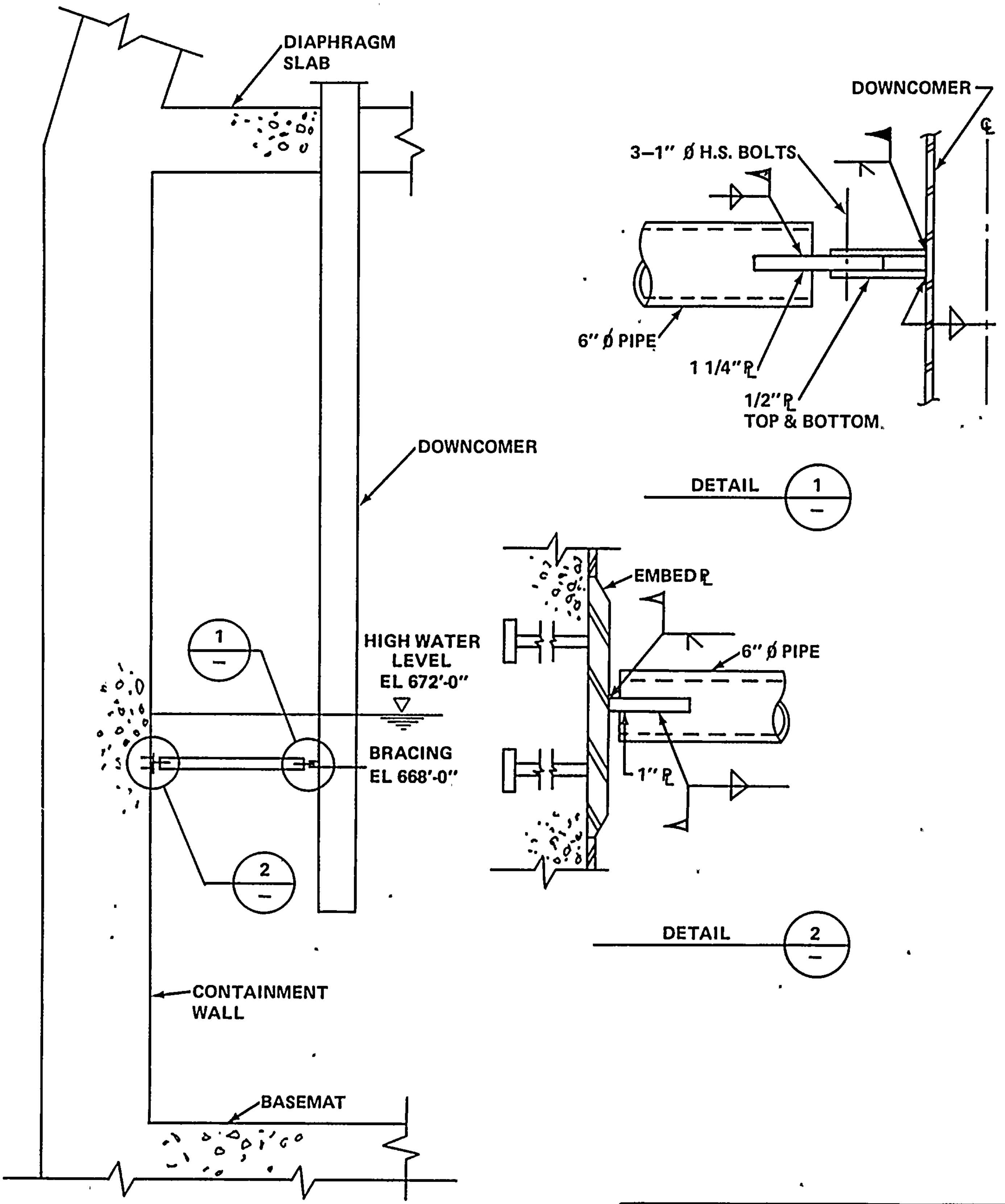

SUSQUEHANNA STEAM ELECTRIC STATION
UNITS 1 AND 2
DESIGN ASSESSMENT REPORT

DOWNCOMER
BRACING DETAILS

FIGURE 9-2

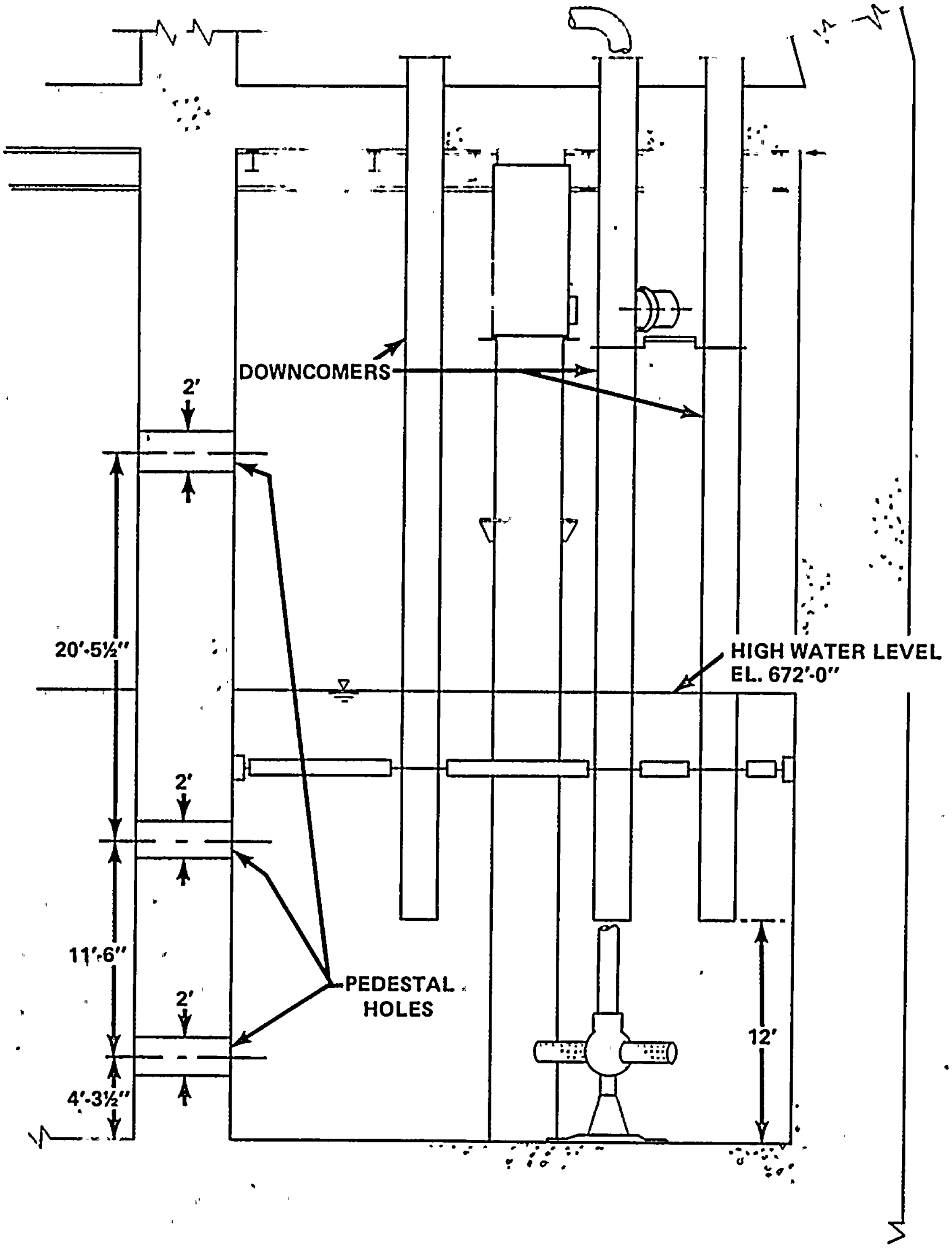

SUSQUEHANNA STEAM ELECTRIC STATION
UNITS 1 AND 2
DESIGN ASSESSMENT REPORT

SPATIAL RELATIONSHIP
OF DOWNCOMERS
AND PEDESTAL HOLES

FIGURE 9-3

10.0 REFERENCES

1. Dr. M. Becker and Dr. E. Koch, "KKB-Vent Clearing with the Perforated-Pipe Quencher" (translated by Ad-Ex, Watertown, Massachusetts), KWU/E3-2796, Kraftwerk Union, October 1973.

2. Dr. M. Becker and Dr. E. Koch, "Construction and Design of the Relief System with Perforated-Pipe Quencher" (translated by Ad-Ex), E3/E2-2703, Kraftwerk Union, July 1973.

3. Dr. M. Becker, "Results of the Non-Nuclear Hot Tests with the Relief System in the Brunsbuttel Nuclear Power Plant" (translated by Ad-Ex), KWU/R113-3267, Kraftwerk Union, December 1974.

4. Dr. H. Weisshaupl, "Formation and Oscillations of a Spherical Gas Bubble Under Water" (translated by Ad-Ex), AEG-Telefunken Report No. 2241, Kraftwerk Union, December 1972.

5. Dr. H. Weisshaupl and Schall, "Calculation Model to Clarify the Pressure Oscillations in the Suppression Chamber After Vent Clearing" (translated by Ad-Ex), AEG-Telefunken Report No. 2208, Kraftwerk Union, March 1972.

6. Dr. M. Becker, Feist and M. Burro, "Analysis of the Loads Measured on the Relief System During the Non-Nuclear Hot Test in KKB" (translated by Ad-Ex), R 113/R 213/R 314/R 521-3346, Kraftwerk Union, April 1975.

7. Letter, J. W. Millard to M. J. Lidl, "Susquehanna 1 & 2: Mass and Energy Release for Suppression Pool Temperature Analysis during Safety Relief Valve and LOCA Transients," GB-77-65, March 14, 1977.

8. R. J. Ernst and M. G. Ward, "Mark II Pressure Suppression Containment Systems: An Analytical Model of the Pool Swell Phenomenon," NEDE-21544P, General Electric Co., December 1976.

9. Letter, F. C. Rally to Mark II Technical Steering Committee Members, "Pool Swell Model Test Cases," MKII-301-E, August 22, 1977.

10. "Dynamic Forcing Functions Information report (DFFR)," Rev. 2, NEDO-21061, General Electric Co. and Sargent and Lundy Engineers, September 1976.

11. T. Y. Fukushima, et al., "Test Results Employed by GE for BWR Containment and Vertical Vent Loads," NEDE-21078-P, Table 3-4, General Electric Co., October 1975.

12. F. J. Moody, Analytical Model for Liquid Jet Properties for Predicting Forces on Rigid Submerged Structures, NEDE-21472, General Electric Co., (to be published).

13. R. J. Ernst, et al., Mark II Pressure Suppression Containment Systems: Loads on Submerged Structures - An Application Memorandum, NEDE-21730, General Electric Co., (to be published).

14. F. J. Moody, Analytical Model for Estimating Drag Forces on Rigid Submerged Structures Caused by LOCA and Safety Relief Valve Ramshead Air Discharges, NEDE-21471, General Electric Co., (to be published).

15. Mark II - Phase I, 4T Tests Applications Memorandum, Letter and Report to W. R. Butler (NRC) from J. F. Quirk (GE), June 14, 1976.

16. W. J. Bilanin, et. al., Mark II Lead Plant Topical Report: Pool Boundary and Main Vent Chugging Loads Justification, NEDE-23617P, July 1977.

17. Warmeatlas (Heat Transfer Data), VDI (Society of German Engineers), Dusseldorf, 1974.

18. T. E. Johnson, et al., "Containment Building Liner Plate Design Report," BC-TOP-1, Bechtel Corporation, San Francisco, December 1972.

19. "Seismic Analysis of Piping Systems," BP-TOP-1, Rev 2, Bechtel Power Corporation, San Francisco, January 1975.

20. Letter, J. R. Martin to Mark II Owners Group and TSC, MK II-250-E, Subject: Condensation Oscillation Excerpts to Applications Memorandum, July 1, 1977.

21. D. Hoffman and E. Schmid, "Brunsbuttel Nuclear Power Plant List of Test Parameters and Most Important Measurement Results of the Non-Nuclear Hot Tests with the Pressure Relief System" (translated by Ad-Ex), R 521/40/77, Kraftwerk Union, August 1977.

22. D. Gobel, "Results of the Non-Nuclear Hot Tests with the Relief System in the Philippsburg Nuclear Power plant" (translated by Ad-Ex), R 142-38/77, Kraftwerk Union, March 1977.

23. D. Hoffman and E. Schmid, "Philippsburg I Nuclear Power Plant List of Test Parameters and Most Important Measurement Results of the Non-Nuclear Hot Tests with the Pressure Relief System" (translated by Ad-Ex), R 521/41/77, Kraftwerk Union, August 1977.

24. Klans-D. Werner, "Experimental Studies of Vent Clearing in the Model Test Stand" (translated by Ad-Ex), KWU/R 521-3129, Kraftwerk Union, July 1975.

25. D. Gobel, "KKB - Nuclear Start-Up Results of the Tests with the Pressure Relief System" (translated by Ad-Ex), R 142-136/76, Kraftwerk Union, September 1976.

26. D. Hoffman and Dr. K. Melchior, "Condensation and Vent Clearing Tests in GKM with Perforated Pipes" (translated by Ad-Ex), KWU/E3-2594, Kraftwerk Union, May 1973.

27. GE Drawing 761E579, Bechtel No. 8856-M1-B11-89

28. ASME Boiler and Pressure Vessel Code, Section III, Division 1, 1974.

29. ASME Boiler and Pressure Vessel Code, Section III, Division 2, 1974.

30. ACI 318-71.

31. R.L. Kiang and B.J. Grossi, "Dynamic Modelling of a Mark II Pressure Suppression System," EPRI-NP-441, Palo Alto, April 1977.

32. "Seismic Analyses of Structures and Equipment for Nuclear Power Plants," BC-TOP-4A, Bechtel Power Corporation, November 1974.

APPENDIX A

CONTAINMENT DESIGN ASSESSMENT

TABLE OF CONTENTS

APPENDIX A

FIGURES

APPENDIX A

Containment Design Assessment

This appendix indicates the containment elements and cross-sections where stresses are to be determined and contains a tabulation of the predicted stresses, allowed stresses, and design margins for each loading combination considered. The structural assessment of the containment is covered in Section A.1; the submerged structures are assessed in Section A.2.

A.1 CONTAINMENT STRUCTURAL DESIGN ASSESSMENT

Typical examples of this material are included in the report (Figures A-1 through A-9); a complete Section A.1 will be included in a future revision to this report.

A.2 CONTAINMENT SUBMERGED STRUCTURES DESIGN ASSESSMENT

To be included in a future revision to this report.

CECAP OUTPUT

LOAD COMBINATION EQN. 1=1.4D+1.5 SRV(ASYM)

STRESSES IN KSI

STRUCTURAL COMPONENT	ANSYS ELEMENT NUMBER	SECTION NUMBER	INSIDE FACE REBAR*		OUTSIDE FACE REBAR*				SHEAR TIES	PRINCIPAL CONC. STRESS
			VERT.	HOOP	VERT.	HOOP	SPIRAL 1	SPIRAL 2		
DRYWELL WALL	86	1	-0.017	-0.067	-0.123	0.123	0.027	-0.027	-0.233	-0.039
	103	2	-0.099	-0.054	-0.145	0.052	-0.018	-0.076	-0.103	-0.026
	231	3	-0.264	-0.017	-0.373	0.080	-0.126	-0.166	-0.127	-0.063
	311	4	-0.350	0.409	-0.480	0.618	0.097	0.044	-0.140	-0.076
	315	5	-0.636	0.570	-0.595	0.586	0.007	-0.015	-0.304	-0.090

*ALLOWABLE REINFORCING STEEL STRESS = 54 KSI

SUSQUEHANNA STEAM ELECTRIC STATION
UNITS 1 AND 2
DESIGN ASSESSMENT REPORT

CONTAINMENT MARGINS
DRYWELL WALL

FIGURE A-4

CECAP OUTPUT

LOAD COMBINATION EQN. 1=1.4D+1.5 SRV(ASYM)

STRESSES IN KSI

STRUCTURAL COMPONENT	ANSYS ELEMENT NUMBER	SECTION NUMBER	INSIDE FACE REBAR*		OUTSIDE FACE REBAR*				SHEAR TIES	PRINCIPAL CONC. STRESS
			VERT.	HOOP	VERT.	HOOP	SPIRAL 1	SPIRAL 2		
SHIELD WALL	165	12					—	—		
	348	13					—	—		
							—	—		
RPV PEDESTAL	362	14					—	—		
	438	15					—	—		

*ALLOWABLE REINFORCING STEEL STRESS=54 KSI

SUSQUEHANNA STEAM ELECTRIC STATION
UNITS 1 AND 2
DESIGN ASSESSMENT REPORT

CONTAINMENT MARGINS
SHIELD WALL AND RPV PEDESTAL

FIGURE A-5

CECAP OUTPUT

LOAD COMBINATION EQN. 1=1.4D+1.5 SRV(ASYM)

STRESSES IN KSI

STRUCTURAL COMPONENT	ANSYS ELEMENT NUMBER	SECTION NUMBER	INSIDE FACE REBAR*		OUTSIDE FACE REBAR*				SHEAR TIES	PRINCIPAL CONC. STRESS
			VERT.	HOOP	VERT.	HOOP	SPIRAL 1	SPIRAL 2		
WETWELL WALL	441	7	-0.99	6.11		3.60	1.39	1.36	-0.080	-0.145
	455	8	-0.94	3.76	-0.95	2.52	0.99	0.59	-0.140	-0.140
	473	9	-0.92	2.91	-0.87	2.08	0.62	0.59	-0.078	-0.131
	475	10	-1.23	6.10	-0.703	4.04	1.69	1.65	-0.052	-0.191
	495	11	-1.24	4.09	-0.83	3.11	1.12	1.17	-0.32	-0.19
	385	6								

*ALLOWABLE REINFORCING STEEL STRESS=54 KSI

SUSQUEHANNA STEAM ELECTRIC STATION
UNITS 1 AND 2
DESIGN ASSESSMENT REPORT

CONTAINMENT MARGINS
WETWELL WALL

FIGURE A-6

CECAP OUTPUT

LOAD COMBINATION EQN. 1=1.4D+1.5 SRV(ASYM)

STRESSES IN KSI

STRUCTURAL COMPONENT	ANSYS ELEMENT NUMBER	SECTION NUMBER	INSIDE FACE REBAR*		OUTSIDE FACE REBAR*				SHEAR TIES	PRINCIPAL CONC. STRESS
			VERT.	HOOP	VERT.	HOOP	SPIRAL 1	SPIRAL 2		
RPV PEDESTAL	484	16	1.71	0.472	-3.15	0.687	0.0	0.0	1.68	-0.552
	550	17	-0.953	0.926	-1.78	2.57	0.0	0.0	0.160	-0.264
	595	18	-1.12	0.306	-1.73	0.48	0.0	0.0	-0.030	-0.257
	606	19	-1.07	-0.038	-2.19	0.238	0.0	0.0	0.234	-0.337
	644	20	-1.28	-0.031	-2.17	0.196	0.0	0.0	0.281	-0.330

*ALLOWABLE REINFORCING STEEL STRESS=54 KSI

SUSQUEHANNA STEAM ELECTRIC STATION
UNITS 1 AND 2
DESIGN ASSESSMENT REPORT

CONTAINMENT MARGINS
RPV PEDESTAL

FIGURE A-7

CECAP OUTPUT
LOAD COMBINATION EQN. 1=1.4D+1.5 SRV(ASYM)
STRESSES IN KSI

STRUCTURAL COMPONENT	ANSYS ELEMENT NUMBER	SECTION NUMBER	TOP FACE REBAR***		BOTTOM FACE REBAR***		SHEAR TIES	PRINCIPAL CONC. STRESS
			RADIAL	TANGENTIAL	RADIAL	TANGENTIAL		
BASE SLAB	551	30	8.51	2.10	2.43	0.92	0.501	-0.129
	607	26	0.431**	1.28*	-0.26	-0.13	-0.277	-0.082
	651	29	3.55	2.41	1.42	0.82	0.095	-0.075
	710	27	0.554*	0.680**	3.11	1.96	0.200	-0.102
	727	28	5.89*	6.44**	0.54	0.021	0.481	-0.105

* NORTH - SOUTH BARS
** EAST - WEST BARS
*** ALLOWABLE REINFORCING STEEL STRESS=54 KSI

SUSQUEHANNA STEAM ELECTRIC STATION
UNITS 1 AND 2
DESIGN ASSESSMENT REPORT

CONTAINMENT MARGINS
BASE SLAB

FIGURE A-8

CECAP OUTPUT
LOAD COMBINATION EQN. 1 = 1.4D+1.5 SRV(ASYM)
STRESSES IN KSI

STRUCTURAL COMPONENT	ANSYS ELEMENT NUMBER	SECTION NUMBER	TOP FACE REBAR*		BOTTOM FACE REBAR*		SHEAR TIES	PRINCIPAL CONC. STRESS
			RADIAL	TANGENTIAL	RADIAL	TANGENTIAL		
DIAPHRAGM SLAB	387	25	3.60	3.71	2.90	4.54	-0.321	-0.050
	411	24	1.93	3.40	3.23	5.55	-0.220	-0.044
	440	21	3.33	1.55	2.93	1.69	-0.350	-0.048
	452	22	0.844	3.62	1.92	4.42	4.61	-0.073
	470	23	0.392	3.87	2.18	5.68	4.56	-0.031

*ALLOWABLE REINFORCING STEEL STRESS=54 KSI

SUSQUEHANNA STEAM ELECTRIC STATION
UNITS 1 AND 2
DESIGN ASSESSMENT REPORT

CONTAINMENT MARGINS
DIAPHRAGM SLAB

FIGURE A-9

APPENDIX D

PROGRAM VERIFICATION

TABLE OF CONTENTS

APPENDIX D

FIGURES

APPENDIX D

TABLES

APPENDIX D

PROGRAM VERIFICATION

The purpose of this appendix is to provide information which verifies the accuracy of the computer programs used in conjunction with SSES design assessment.

D.1 POOLSWELL MODEL VERIFICATION

This subsection demonstrates the accuracy of the SSES DAR poolswell model by comparing it with the model developed by the General Electric Company. The latter model has predicted conservatively the results of the 4T poolswell tests (Ref 8).

To evaluate the agreement between the GE poolswell code and the poolswell code used for the SSES DAR, three test cases were selected. The test cases used were the Classes 1, 2, and 3 plants described in Ref 10. The input data for these three problems are given in Tables D-1 and D-2 (taken from Ref 9). (In the verification of the model, the boundary conditions assumed by GE in Ref 9 were used. These assumptions are shown in Table D-4.) These data are representative of typical U.S. Mark II BWRs. The poolswell code used in this DAR was revised until the results were in close agreement with GE's results as given in Ref 9. Agreement was judged by examining the peak swell velocity predicted, since this is one of the most important pool swell parameters and one that is fairly sensitive to how the phenomenon is modelled. The degree of agreement finally achieved between the poolswell code used in this DAR and the GE code is shown in Table D-3 where peak swell velocities are compared. Transient comparisons for Classes 1, 2, and 3 plants are shown on Figures D-1 through D-6 where the transient predictions of the two codes are shown to be essentially identical. From the good agreement shown in the check cases, the poolswell code used in this DAR is verified to be the same as the GE code for evaluation of pool swell.

APPENDIX E

REACTOR BUILDING STRUCTURAL DESIGN ASSESSMENT

The results of analysis of the reactor building structure will be summarized in this appendix. This appendix will be provided in a future revision to this report.